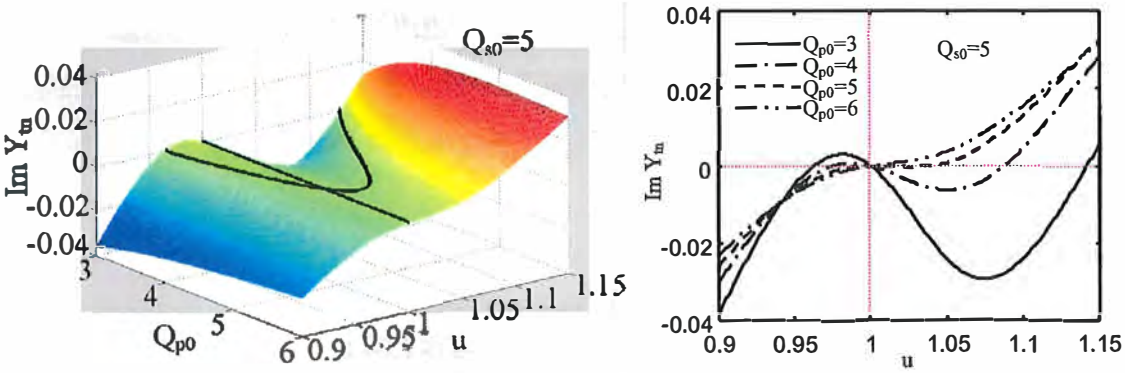

(i) Surface function. (ii) Cross sections of the surface.

(a) PP topology.

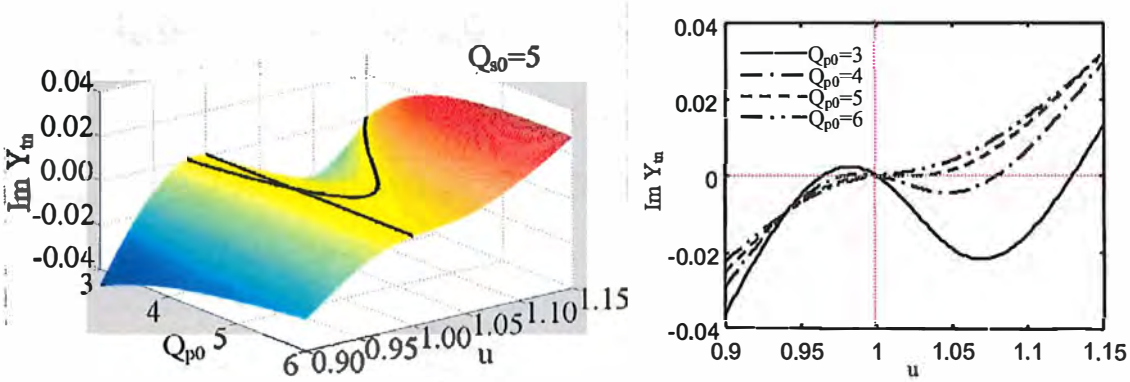

(i) Surface function. (ii) Cross sections of the surface.

(b) PS topology.

Fig. 5-11. Normalized load susceptance.

The normalized load reactance for the SS and SP topologies and the normalized load susceptance for the PP and PS topologies can be represented as:

$$\mathrm{Im}Z_{tn} or \mathrm{Im}Y_{tn} = \frac{(u^2-1)G(u,Q_{p0},Q_{s0})}{D(u,Q_{p0},Q_{s0})} \tag{5-11}$$

where the functions $G(u,Q_{p0},Q_{s0})$ and $D(u,Q_{p0},Q_{s0})$ are defined in Table 5-4 and (5-12) below for all basic topologies.

The factor (u^2-1) in (5-11) is zero at the secondary resonant frequency (u=1). This ensures system operation with zero-phase angle at the secondary resonant frequency. Since the factor (u^2-1) in (5-11) is negative when the operating frequency is below the secondary resonant frequency (u<1), and becomes positive when the operating frequency is above the secondary resonant frequency (u>1), it presents no bifurcation information. As shown in Table 5-4(a), the function $D(u,Q_{p0},Q_{s0})$ associated to each of the four basic topologies is always positive. It therefore carries no bifurcation information as well. Consequently, the bifurcation phenomenon, as shown in Fig. 5-10 and Fig. 5-11, will be inherent with the function $G(u,Q_{p0},Q_{s0})$.

For the four basic topologies, the function $G(u,Q_{p0},Q_{s0})$ is a polynomial of the form:

InductEV, Inc.
Exhibit 1010
Page 250

$$G(u,Q_{p0},Q_{s0}) = a_8u^8 + a_6u^6 + a_4u^4 + a_2u^2 + a_0 \tag{5-12}$$

The non-zero coefficients in (5-12) are given in Table 5-4(b). As shown, $G(u,Q_{p0},Q_{s0})$ is a bi-quadratic polynomial for the SS and SP topologies. For the PP and PS topologies, $G(u,Q_{p0},Q_{s0})$ is a bi-quartic polynomial.

TABLE 5-4
NORMALIZED FUNCTIONS IN (5-11)
(a) $D(u,Q_{p0},Q_{s0})$

SS&SP	$u(u^2-1)^2Q_{s0}^2 + u^3$
PP	$u\left\{u^2 + \left[(u^2-1)^2Q_{p0}Q_{s0}^2 + u^2Q_{p0} - (u^2-1)Q_{s0}\right]^2\right\}(1+Q_{p0}^2)$
PS	$u\left\{u^6 + \left[(u^2-1)^2Q_{p0}Q_{s0}^2 + u^2Q_{p0} - u^2(u^2-1)Q_{s0}\right]^2\right\}(1+Q_{p0}^2)$

(b) Coefficients of the polynomial $G(u, Q_{p0},Q_{s0})$ in (5-12)

SS	a_4	$Q_{p0}Q_{s0}^2 - Q_{s0}$
	a_2	$Q_{p0} - 2Q_{p0}Q_{s0}^2$
	a_0	$Q_{p0}Q_{s0}^2$
SP	a_4	$Q_{p0}Q_{s0}^2$
	a_2	$Q_{p0} - Q_{s0} - 2Q_{p0}Q_{s0}^2$
	a_0	$Q_{p0}Q_{s0}^2$
PP	a_8	$Q_{p0}^3Q_s^4$
	a_6	$-4Q_{p0}^3Q_{s0}^4 + 2Q_{p0}^3Q_{s0}^2 - 2Q_{p0}^2Q_{s0}^3 - Q_{p0}Q_{s0}^4$
	a_4	$6Q_{p0}^3Q_{s0}^4 - 4Q_{p0}^3Q_{s0}^2 + 5Q_{p0}^2Q_{s0}^3 + 3Q_{p0}Q_{s0}^4 - Q_{p0}Q_{s0}^2 - 2Q_{p0}^2Q_{s0} + Q_{p0}^3 + Q_{s0}^3$
	a_2	$-4Q_{p0}^3Q_{s0}^4 + 2Q_{p0}^3Q_{s0}^2 - 4Q_{p0}^2Q_{s0}^3 - 3Q_{p0}Q_{s0}^4 + Q_{p0}Q_{s0}^2 + Q_{p0}^2Q_{s0} - 2Q_{s0}^3 + Q_{s0}$
	a_0	$Q_{p0}^3Q_{s0}^4 + Q_{p0}^2Q_{s0}^3 + Q_{p0}Q_{s0}^4 + Q_{s0}^3$
PS	a_8	$Q_{p0}^3Q_{s0}^4 - 2Q_{p0}^2Q_{s0}^3 + Q_{p0}Q_{s0}^2$
	a_6	$-4Q_{p0}^3Q_{s0}^4 + Q_{p0} + 2Q_{p0}^3Q_{s0}^2 + 5Q_{p0}^2Q_{s0}^3 - Q_{p0}Q_{s0}^4 - Q_{p0}Q_{s0}^2 - 2Q_{p0}^2Q_{s0} + Q_{s0}^3$
	a_4	$6Q_{p0}^3Q_{s0}^4 + Q_{p0} - 4Q_{p0}^3Q_{s0}^2 - 4Q_{p0}^2Q_{s0}^3 + 3Q_{p0}Q_{s0}^4 - 2Q_{p0}Q_{s0}^2 + Q_{p0}^3 + Q_{p0}^2Q_{s0} - 2Q_{s0}^3 + Q_{s0}$
	a_2	$-4Q_{p0}^3Q_{s0}^4 + 2Q_{p0}^3Q_{s0}^2 + Q_{p0}^2Q_{s0}^3 - 3Q_{p0}Q_{s0}^4 + 2Q_{p0}Q_{s0}^2 + Q_{s0}^3$
	a_0	$Q_{p0}^3Q_{s0}^4 + Q_{p0}Q_{s0}^4$

The function $G(u,Q_{p0},Q_{s0})$ is shown in Fig. 5-12 for the four basic topologies (SS, SP, PP and PS). The white curves drawn on the surfaces of Fig. 5-12 represent zero values of the function $G(u,Q_{p0},Q_{s0})$. According to (5-11), these zero values correspond to either zero load reactance or susceptance. In consequence, two zero phase angle frequencies can be determined by these curves in addition to the secondary resonant frequency for each topology.

InductEV, Inc.
Exhibit 1010
Page 251

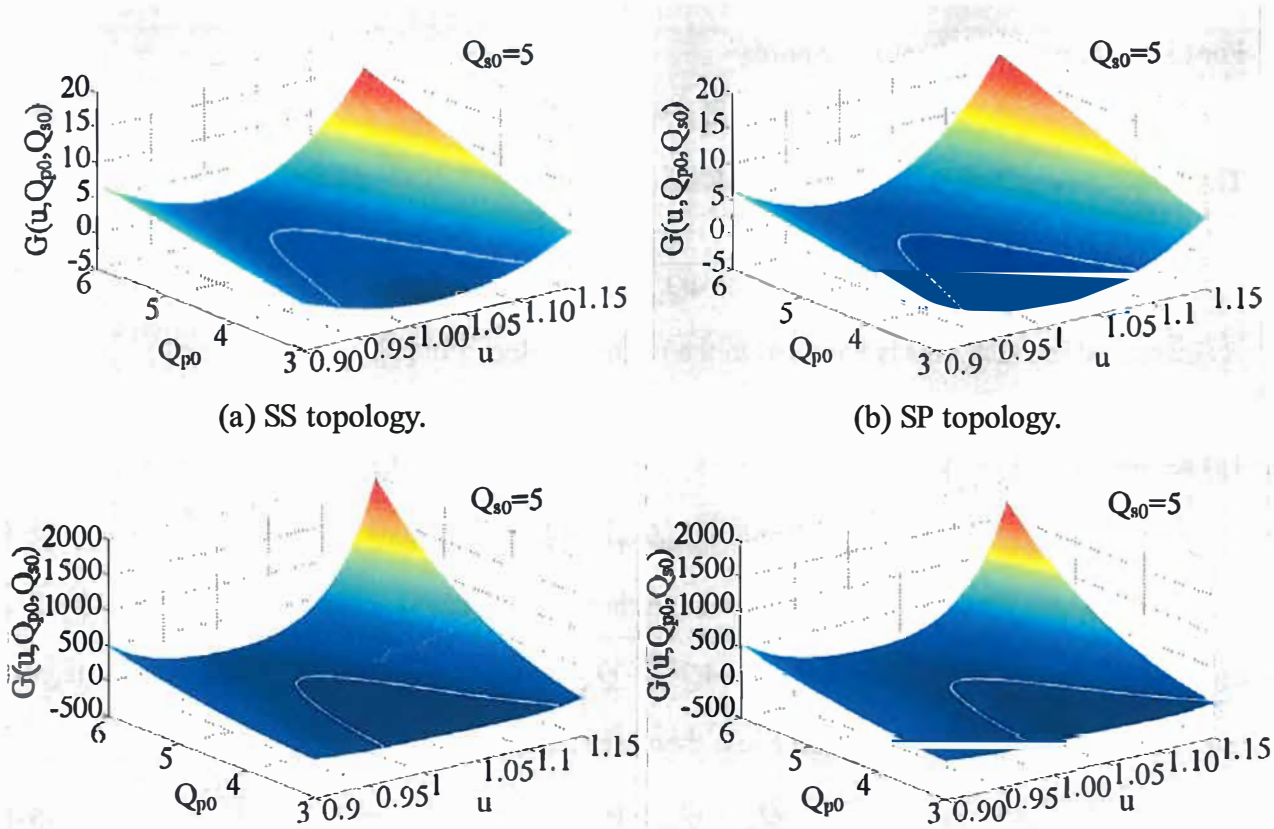

Fig. 5-12. Normalized function $G(u,Q_{p0},Q_{s0})$.

When the primary quality factor (Q_p) is much larger than the secondary quality factor (Q_s), the function $G(u,Q_{p0},Q_{s0})$ is positive across the frequency spectrum as shown in Fig. 5-12. However, the function $G(u,Q_{p0},Q_{s0})$ becomes negative around the secondary resonant frequency (u=1) if the primary quality factor is much lower than the secondary quality factor and as such two additional zero phase angle frequencies other than the secondary resonant frequency exist. To ensure the secondary resonant frequency is the only zero phase angle frequency, the function $G(u,Q_{p0},Q_{s0})$ must be greater than zero across the frequency spectrum. A general rule to avoid bifurcation is thus:

$$G(u,Q_{p0},Q_{s0}) > 0 \tag{5-13}$$

Normally both the primary and secondary quality factors are larger than unity. This makes the polynomial coefficient a_4 for SS and SP topologies positive so that if the bi-quadratic polynomial $G(u,Q_{p0},Q_{s0})$ is to be greater than zero, the discriminant:

$$\Delta = a_2^2 - 4a_4a_0 \tag{5-14}$$

must be less than zero.

Substituting the polynomial coefficients for the SS topology in Table 5-4 (b) into the discriminant (5-14) results in:

InductEV, Inc.
Exhibit 1010
Page 252

$$\Delta = \left(Q_{p0} - 2Q_{p0}Q_{s0}^2\right)^2 - 4Q_{p0}Q_{s0}^2\left(Q_{p0}Q_{s0}^2 - Q_{s0}\right) = Q_{p0}\left[Q_{p0}\left(1 - 4Q_{s0}^2\right) + 4Q_{s0}^3\right] \tag{5-15}$$

For (5-15) to become negative requires:

$$Q_{p0}\left(1 - 4Q_{s0}^2\right) + 4Q_{s0}^3 < 0 \tag{5-16}$$

The bifurcation criterion for the SS topology derived from (5-16) is then:

$$Q_{p0} > \frac{4Q_{s0}^3}{4Q_{s0}^2 - 1} \tag{5-17}$$

As discussed in 2-5.5, this is identical to the result developed in [9].

Substituting the polynomial coefficients for the SP topology in Table 5-4 (b) into the discriminant (5-14) results in:

$$\Delta = \left(Q_{p0} - Q_{s0} - 2Q_{p0}Q_{s0}^2\right)^2 - 4\left(Q_{p0}Q_{s0}^2\right)\left(Q_{p0}Q_{s0}^2\right) = \left(Q_{p0} - Q_{s0}\right)\left[Q_{p0}\left(1 - 4Q_{s0}^2\right) - Q_{s0}\right] \tag{5-18}$$

The secondary quality factor is normally larger than unity, and as such the term $(1 - 4Q_{s0}^2)$ in (5-18) is negative. As a result, the factor $Q_{p0}\left(1 - 4Q_{s0}^2\right) - Q_{s0}$ of the discriminat in (5-18) is also negative. Letting this discriminant (5-18) become less than zero results in:

$$Q_{p0} - Q_{s0} > 0 \tag{5-19}$$

The bifurcation criterion for the SP topology derived from (5-19) is thus:

$$Q_{p0} > Q_{s0} \tag{5-20}$$

The analytical bifurcation boundaries given by (5-17) and (5-20) respectively for the SS and SP topologies are shown in Fig. 5-13. The bifurcation boundary of the SS topology sits above the approximate bifurcation boundary given by $Q_{p0}>Q_{s0}$ in [6], [9-11] when the assumption of high Q_s is applied. In fact, the difference is negligible with high Q_s. With the SP topology, the analytical bifurcation boundary sits exactly at $Q_{p0}>Q_{s0}$.

The solutions of the general bifurcation rule (5-13) for the PP and PS topologies can be solved by the approach proposed by Ludovico Ferrari in 16th century [12], but is rather complicated and cumbersome. Alternatively, a numerical methodology can be used as shown in Fig. 5-14. Here, an iteration process is used over a practical range of Q_{s0} such as from 1 to 10 and a suitable frequency range of u around unity. In practical designs, Q_p is normally larger than Q_s to ensure bifurcation free operation [6], [10]. The numerical process starts from a significantly large Q_{p0} to make $G(u,Q_{p0},Q_{s0})$ positive across the frequency spectrum, and then reduces Q_{p0} by a small amount at each iteration step to verify whether $G(u,Q_{p0},Q_{s0})$ intersects with the axis $G(u,Q_{p0},Q_{s0})=0$, where bifurcation occurs. The iteration procedure stops when either the bifurcation boundary is found at a certain Q_{p0} or no bifurcation occurs for all Q_{p0} larger than zero.

InductEV, Inc.
Exhibit 1010
Page 253

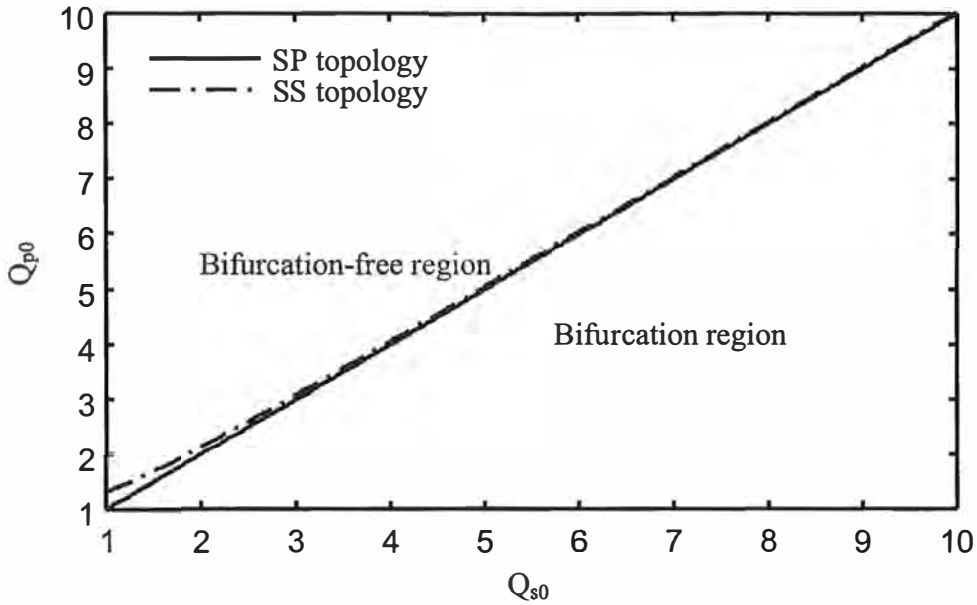

Fig. 5-13. Analytical bifurcation boundary for the SS and SP topologies.

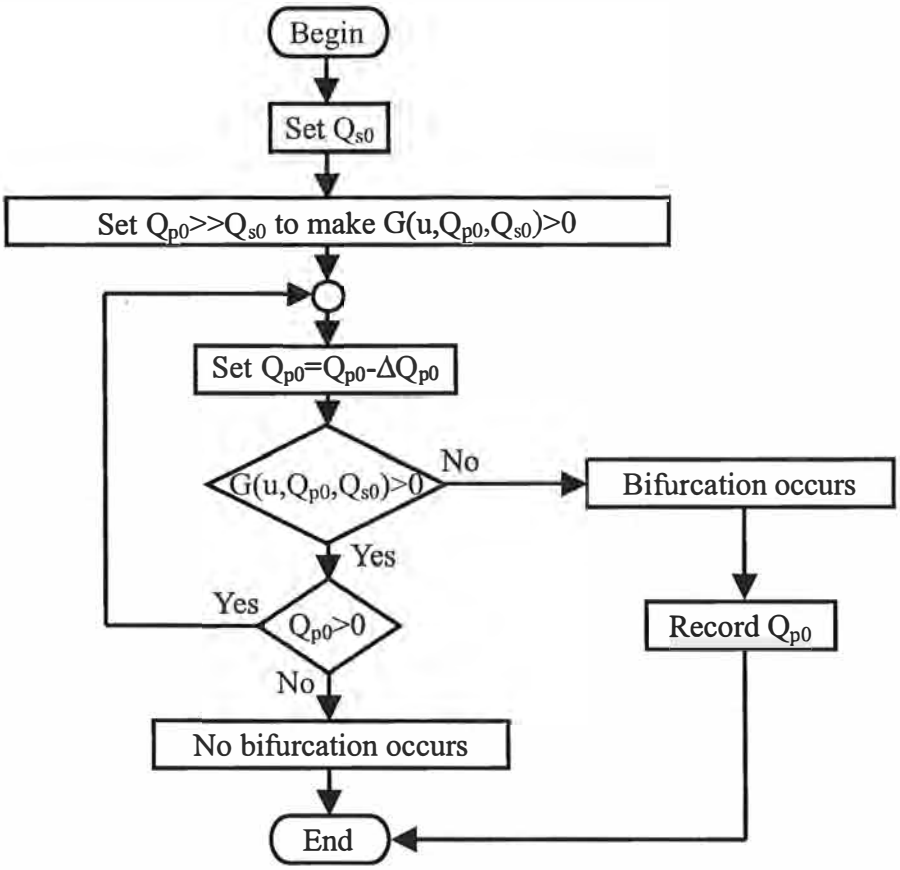

Fig. 5-14. Numerical algorithm for finding bifurcation boundary.

The numerical bifurcation boundaries are shown in Fig. 5-15 for the PP and PS topologies. It can be found that the numerical bifurcation boundary of the PP topology is identical to the analytical bifurcation boundary given by (5-20) for the SP topology and as such would be the exact analytical

InductEV, Inc.
Exhibit 1010
Page 254

bifurcation boundary. The numerical bifurcation boundary of the PS topology is below the approximate bifurcation boundary given by $Q_{p0}>Q_{s0}$. According to this numerical bifurcation boundary, if Q_{s0} is below 1.7 the system is free of bifurcation for any practical value of Q_{p0}. When Q_{s0} is above 1.7, the numerical bifurcation boundary of the PS topology is close to $Q_{p0}>Q_{s0}-1/Q_{s0}$.

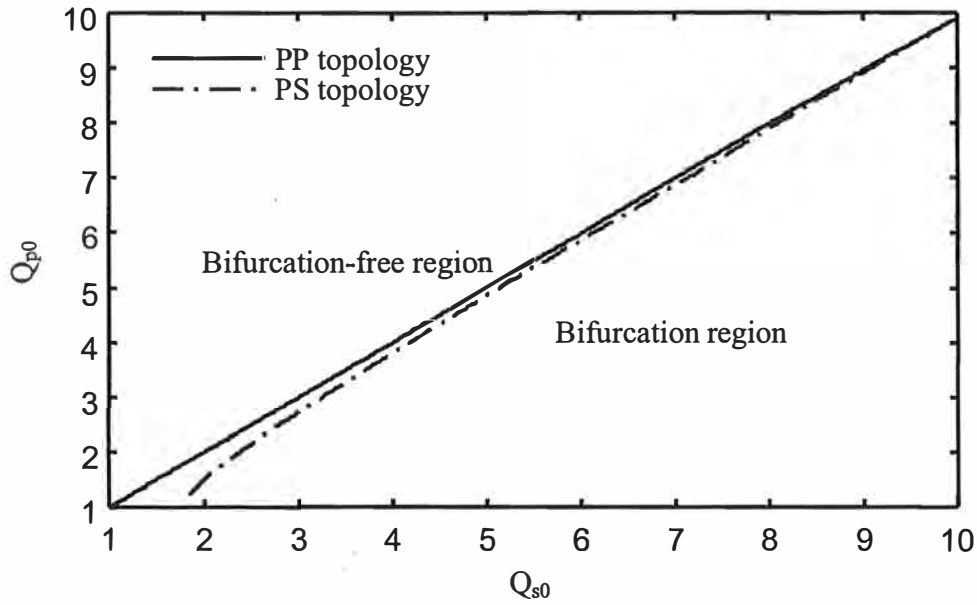

Fig. 5-15. Numerical bifurcation boundary for the PP and PS topologies.

A summary of the bifurcation criteria is given in Table 5-5 for four basic ICPT topologies. They are simple relations between the primary and secondary quality factors. According to above discussion, the bifurcation criteria given in this table for the SS, SP and PP topologies are exact analytical solutions, while that for the PS topology is an approximation.

Using (5-9), the bifurcation criteria can be expressed in terms k and Q_{s0} in Table 5-5.

If the magnetic coupling is very weak (k<<1), the bifurcation criteria given in Table 5-5 for the four basic topologies can be simplified to:

$$Q_{s0} < \frac{1}{k} \tag{5-21}$$

As noted in section 2-5.5, this result is identical to the analysis in [6], [9].

The bifurcation boundaries in terms of k and Q_{s0}, as given in Table 5-5, are compared in Fig. 5-16 for the four basic topologies. The maximum Q_{s0} for bifurcation-free operation decreases as k is improved. This boundary is topology dependent. For loosely coupled systems with a k of 0.1, the difference between the basic topologies is negligible, and bifurcation occurs in all topologies when Q_{s0} increases above 10. However, this difference increases with improved k. For example with a k of 0.6, bifurcation-free operation requires that Q_{s0} be below 1.3 for SP and PP topologies, 1.5 for the SS

InductEV, Inc.
Exhibit 1010
Page 255

topology, and 2 for the PS topology.

TABLE 5-5
BIFURCATION CRITERIA

	Standard derivation in terms of Q_{p0} and Q_{s0}	Re-expression in terms of k and Q_{s0}
SS	$Q_{p0} > \frac{4Q_{s0}^3}{4Q_{s0}^2 - 1}$	$Q_{s0} < \frac{\sqrt{1+\sqrt{1-k^2}}}{\sqrt{2}k}$
SP&PP	$Q_{p0} > Q_{s0}$	$Q_{s0} < \frac{\sqrt{1-k^2}}{k}$
PS	$\begin{cases} Q_{p0} > Q_{s0} - \frac{1}{Q_{s0}} & if\ Q_{s0} > 1.7 \\ No\ bifurcation & if\ Q_{s0} < 1.7 \end{cases}$	$\begin{cases} Q_{s0} < \frac{\sqrt{1+k^2}}{k} & if\ Q_{s0} > 1.7 \\ No\ bifurcation & if\ Q_{s0} < 1.7 \end{cases}$

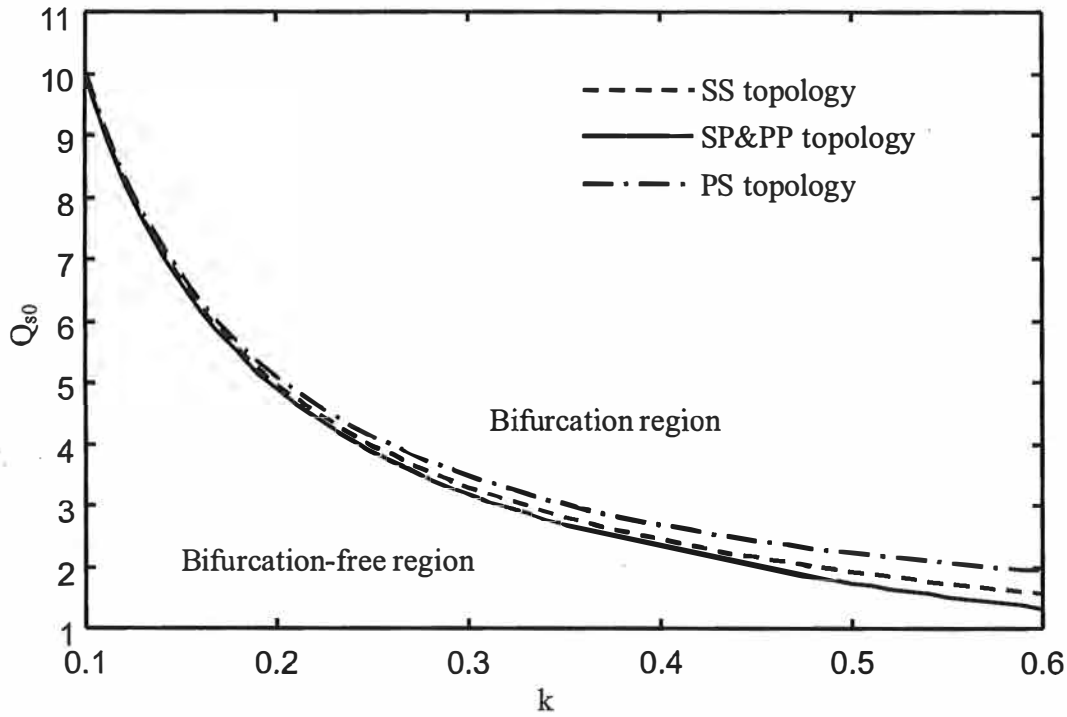

Fig. 5-16. Bifurcation boundary defined by k and Q_{s0} for the four basic topologies.

5-5 DISCUSSION

With k and $Q_{s0,rated}$ determined using the design methodology described in Chapter 4, the bifurcation criteria in Table 5-5 is used to evaluate the designed system under variable-frequency operation. This enables improvements in the power transfer capability (achieved as a result of modifying C_p to minimize pickup frequency detuning effects) to be determined. Here it is assumed that the power supply controller allows the operating frequency to vary such that unity DPF is achieved at

InductEV, Inc.
Exhibit 1010
Page 256

all times, thereby minimizing its required VA rating, size and cost. Consequently, in a single pickup system the required power supply VA rating equals the power transferred to the pickup.

The improvement in power transfer capability can be guaranteed with the modified tuning proposed in this chapter providing the bifurcation criterion is satisfied. If the designed system can not meet the bifurcation criterion, rated power is available only in the bifurcation region with both the original and modified tunings. Such a system is normally not desirable, and it is necessary to redesign the system to have lower k or $Q_{s0,rated}$ to force it to meet the bifurcation criterion.

The allowable $Q_{s0,rated}$ is strictly limited by k. In a loosely coupled system with k of 0.05, the maximum $Q_{s0,rated}$ is about 20 for all four basic topologies (SS, SP, PP and PS). With k improved to 0.2 for a middle coupled system, the maximum $Q_{s0,rated}$ reduces to about 5 for all topologies. In a well-coupled system with k of 0.4, the maximum $Q_{s0,rated}$ is close to 2.5 (2.5 for the SS topology, 2.3 for the SP and PP topologies, and 2.7 for the PS topology). Consequently, variable-frequency operation is not suitable for well-coupled (high k) systems with high $Q_{s0,rated}$. To avoid bifurcation, fixed-frequency operation may be considered. This is investigated in the following chapter.

The developed bifurcation criteria are valid for all loading conditions when the primary is series compensated, but are applicable only at rated load if the primary is parallel compensated. In this case, designing the system to meet the bifurcation criterion at rated load with a suitable safety margin assures bifurcation-free operation for all loading conditions up to and including rated load. This is a natural result as bifurcation only occurs with increasing load, as is verified in section 5-6 by a practical example.

Under the modified tuning scheme proposed in this chapter, when the primary is series-compensated (the SS and SP topologies), operation at ω_0 can theoretically be achieved independent of the load. In this case, pickup frequency detuning is minimized under all loading conditions. For parallel-compensated primary systems (the PP and PS topologies), operation at ω_0 is achieved only at rated operation. Consequently, pickup frequency detuning effects under lightly loading conditions cannot be avoided.

The improvement in the power transfer capability for selected examples are summarized in Table 5-6 to Table 5-8 for loosely coupled, middle coupled and well coupled systems respectively. The discussion focuses on the SP, PP and PS topologies, where modification of C_p is required. The improvement in the power transfer capability as expected depends on the compensation topology as well as k and $Q_{s0,rated}$. The required modification in C_p (as noted in section 5-2) for each case is given in these tables for comparison.

With loosely coupled systems, the original tuning works very well for all four basic topologies. Here the modified tuning and the original tuning are essentially identical since the required

InductEV, Inc.
Exhibit 1010
Page 257

modification of C_p is negligible as shown in Fig. 5-6. As expected, the improvement in the power transfer capability is very small or negligible.

For middle coupled systems, the original tuning also works well for the PP topology, and the SP and PS topologies with low $Q_{s0,rated}$. In these cases, the improvement in the power transfer capability with the modified tuning as shown in Table 5-7 is small. This improvement becomes more significant for the SP and PS topologies with higher $Q_{s0,rated}$. While it looks as if the modified tuning is useful here, the necessary change to C_p is small. To do this in practice requires good lifetime capacitance stability.

For well coupled systems as shown in Table 5-8, the improvement in the power transfer capability with the modified tuning can be up to about 15% for the PP topology, but again the required change in C_p is small and good lifetime capacitance stability is required. For the SP and PS topologies, the improvement in the power transfer capability can be more than 50% and the required change in C_p is significant.

The necessary C_p of this modified tuning depends on k, which may vary in practice due to misalignment of the electromagnetic structure. Moreover, the practical C_p selected may be different to the theoretical value due to manufacturing tolerances, aging or thermal effects. The influence of variations in capacitance and the misalignment in the electromagnetic structure are investigated in Chapter 7.

TABLE 5-6
IMPROVEMENT OF THE POWER TRANSFER CAPABILITY WITH THE MODIFIED TUNING FOR A LOOSELY COUPLED SYSTEM (k=0.05)

SP Topology.	Bifurcation criterion.	$Q_{s0}<20$		
	Rated load condition.	$Q_{s0,rated}=6$	$Q_{s0,rated}=12$	$Q_{s0,rated}=18$
	Modification in C_p.	$C_{pn}\sim1.00$		
	Improvement in power transfer.	0%	0%	4%
PP Topology.	Bifurcation criterion.	$Q_{s0}<20$		
	Rated load condition.	$Q_{s0,rated}=6$	$Q_{s0,rated}=12$	$Q_{s0,rated}=18$
	Modification in C_p.	$C_{pn}\sim1.00$		
	Improvement in power transfer.	0%	0%	0%
PS Topology.	Bifurcation criterion.	$Q_{s0}<20$		
	Rated load condition.	$Q_{s0,rated}=6$	$Q_{s0,rated}=12$	$Q_{s0,rated}=18$
	Modification in C_p.	$C_{pn}\sim1.00$		
	Improvement in power transfer.	0%	0%	3%

InductEV, Inc.
Exhibit 1010
Page 258

TABLE 5-7
IMPROVEMENT OF THE POWER TRANSFER CAPABILITY WITH THE MODIFIED TUNING FOR A MIDDLE COUPLED SYSTEM (k=0.2)

SP Topology.	Bifurcation criterion.	$Q_{s0}<4.9$		
	Rated load condition.	$Q_{s0,rated}=2$	$Q_{s0,rated}=3.5$	$Q_{s0,rated}=4.5$
	Modification in C_p.	$C_{pn}=1.04$		
	Improvement in power transfer.	1%	8%	28%
PP Topology.	Bifurcation criterion.	$Q_{s0}<4.9$		
	Rated load condition.	$Q_{s0,rated}=2$	$Q_{s0,rated}=3.5$	$Q_{s0,rated}=4.5$
	Modification in C_p.	$C_{pn}=1.04$	$C_{pn}=1.02$	$C_{pn}=1.01$
	Improvement in power transfer.	1%	2%	3%
PS Topology.	Bifurcation criterion.	$Q_{s0}<5.1$		
	Rated load condition.	$Q_{s0,rated}=2$	$Q_{s0,rated}=3.5$	$Q_{s0,rated}=4.5$
	Modification in C_p.	$C_{pn}=0.99$	$C_{pn}=0.98$	$C_{pn}=0.97$
	Improvement in power transfer.	1%	5%	18%

TABLE 5-8
IMPROVEMENT OF THE POWER TRANSFER CAPABILITY WITH THE MODIFIED TUNING FOR A WELL-COUPLED SYSTEM (k=0.4)

SP Topology.	Bifurcation criterion.	$Q_{s0}<2.3$		
	Rated load condition.	$Q_{s0,rated}=1.5$	$Q_{s0,rated}=2$	$Q_{s0,rated}=2.2$
	Modification in C_p.	$C_{pn}=1.19$		
	Improvement in power transfer.	16%	45%	64%
PP Topology.	Bifurcation criterion.	$Q_{s0}<2.3$		
	Rated load condition.	$Q_{s0,rated}=1.5$	$Q_{s0,rated}=2$	$Q_{s0,rated}=2.2$
	Modification in C_p.	$C_{pn}=1.10$	$C_{pn}=1.04$	$C_{pn}=1.01$
	Improvement in power transfer.	6%	12%	15%
PS Topology.	Bifurcation criterion.	$Q_{s0}<2.7$		
	Rated load condition.	$Q_{s0,rated}=1.5$	$Q_{s0,rated}=2$	$Q_{s0,rated}=2.6$
	Modification in C_p.	$C_{pn}=0.95$	$C_{pn}=0.91$	$C_{pn}=0.85$
	Improvement in power transfer.	9%	23%	59%

InductEV, Inc.
Exhibit 1010
Page 259

5-6 VERIFICATION

The design of the contact-less electric vehicle battery charger having a PP topology (previously described in section 3-11 and investigated in section 4-6) is now reconsidered using the modified tuning proposed in (5-2) for C_p. The controller is designed to operate with unity DPF. The operating frequency and power transfer capability are calculated for this operating condition, and then verified by experimental measurements.

With other design parameters unchanged, C_{pn} can be determined from the known k (of 0.45) and Q_{s0} (of 1.8) at rated load (of 6Ω). It is calculated to be 1.04. The modified tuning thus requires a C_p 4% higher than the original tuning. As a result, C_p needs to be increased from 2.20μF to 2.28μF.

Under variable frequency control where the controller is made to operate at the zero-phase angle of the power supply load impedance (at unity DPF as discussed in section 5-5), it is crucial with this modified tuning to ensure bifurcation-free operation for all loading conditions up to and including rated load. The primary quality factor (Q_{p0}) calculated using (5-9) is 2.19. The bifurcation criterion given by Table 5-5 (for the PP topology) is $Q_{p0}>Q_{s0}$. Since the calculated Q_{p0} satisfies this criterion, the system should not bifurcate for all normal operating loads, up to and including rated operation.

The bifurcation phenomenon and power transfer capability are shown in Fig. 5-17, where the operating frequency and power transfer curves are functions of the load extended into the bifurcation region. The measured operating frequencies and power transfers are shown in Fig. 5-17 as circles at each of the measured loads. As shown, the measured results closely follow theoretical curves.

Operation at ω_0 is achieved at rated load due to the modified tuning, and bifurcation is only apparent at higher loads, while the power transfer capability is equal to the desired power of 300W (30kW at rated primary current 150A) at rated load. With the original tuning, the power transfer at rated load condition is 266W. Here the change in C_p is only 4% and the improvement in power transfer capability is close to 13%.

At light loads, frequency detuning is unavoidable but it is less than that with the original tuning, where, as shown in Fig. 5-17 (b-i), the operating frequency is detuned more than 10% above ω_0 for all loads up to rated load. Because the pickup is better tuned, the power transfer capability at light loads is also higher than the original tuning.

The maximum power point of the re-tuned system under bifurcation-free operation is achieved at a slightly higher load than 'rated' despite the operating frequency being a little lower than ω_0. This maximum power transfer capability as shown is 322W (32.2kW at rated primary current 150A). Beyond this point (as the load is increased further), the power transfer capability decreases because the operating frequency drops away from ω_0.

InductEV, Inc.
Exhibit 1010
Page 260

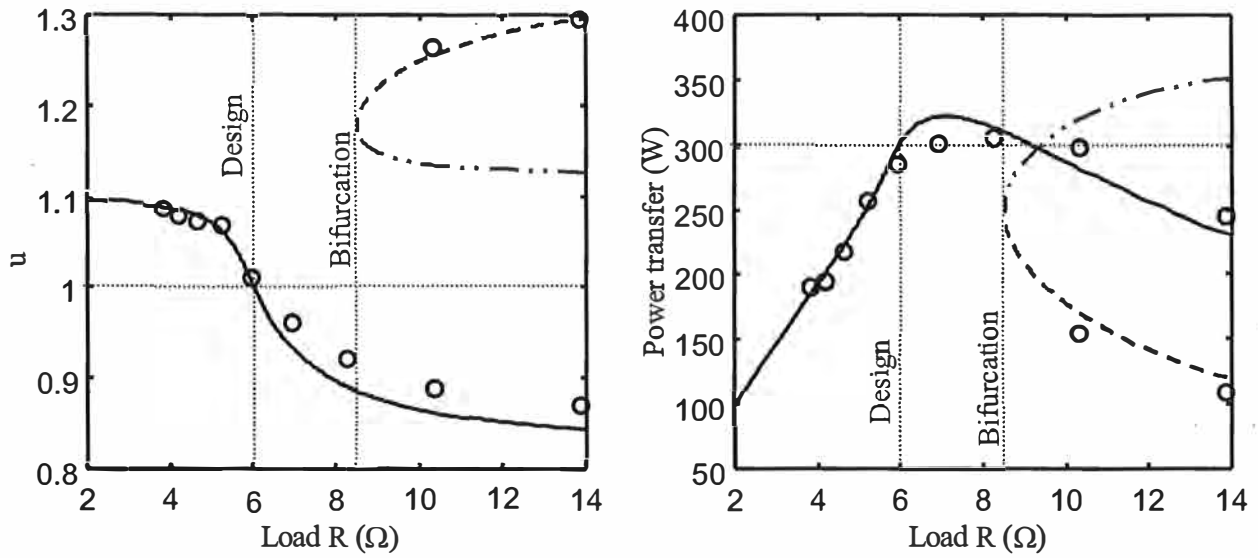

(i) Operational frequency. (ii) Power transfer capability (I_p=15A).

(a) Modified tuning.

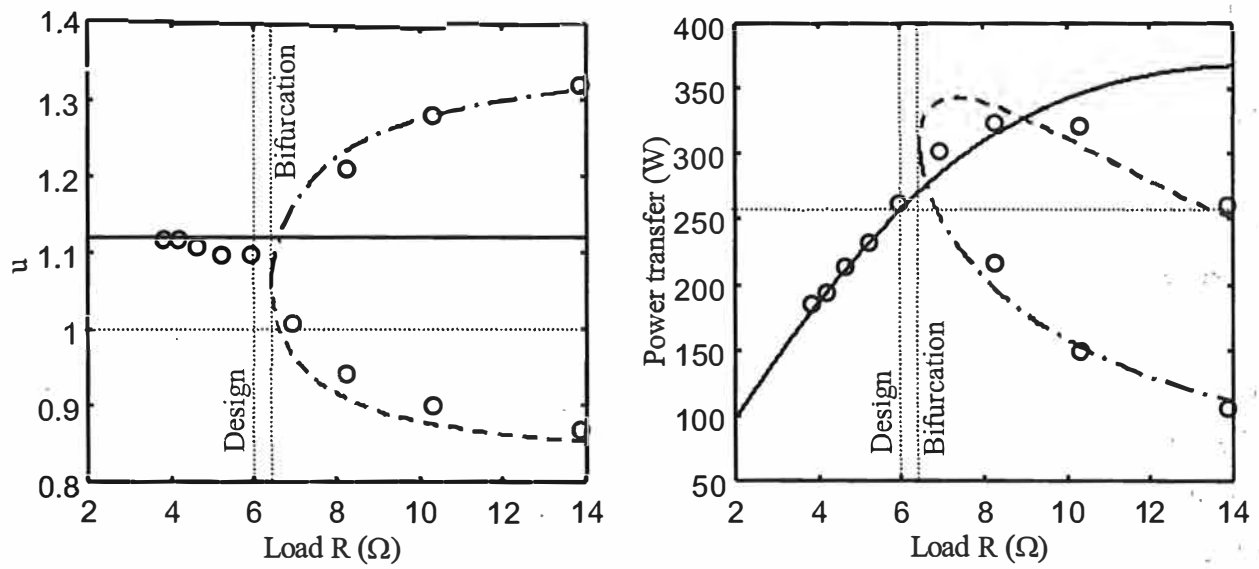

(i) Operational frequency. (ii) Power transfer capability (I_p=15A).

(b) Original tuning.

Fig. 5-17. A contact-less electric vehicle battery charger with PP topology – Operating frequency and power transfer capability under variable-frequency operation (a comparison of the original and modified tuning schemes).

As discussed in section 5-3, the modified tuning for this PP topology also increases the bifurcation boundary resulting in a larger safety margin before bifurcation. The onset of bifurcation occurs at 6.4Ω with the original tuning. It increases by 33% to 8.5Ω due to the modified tuning. Fig. 5-17 also clearly shows why a variable-frequency controller requires a suitable safety margin to ensure bifurcation-free operation over all practical power demands. Once such a controller begins to operate within the bifurcation region, the potential power delivery varies significantly if the controller moves in operation between the highest and lowest operational frequencies.

InductEV, Inc.
Exhibit 1010
Page 261

5-7 CONCLUSIONS

In this chapter the primary tuning capacitance (C_p) was modified to compensate not only the self-inductance of the primary coil but also the loading effects of the secondary resonant circuit on the primary. All other design parameters determined by the design methodology described in Chapter 4 were left unchanged. Under variable-frequency operation with unity DPF, this modified tuning minimizes frequency-detuning effects in the pickup when operating at rated load, resulting in improved power transfer capability.

The magnitude of the change in C_p depends on the choices of the primary and secondary compensation topologies (SS, SP, PP and PS) as well as the fundamental design parameters k and Q_s. An SS topology does not require any change to C_p, whereas the SP topology requires a larger C_p with improved k. When the primary is parallel-compensated (the PP and PS topologies), C_p is a function of both k and Q_s. In this case, C_p needs to be selected for rated load to achieve the required power. The required modification in C_p could be as high as 20% in a middle coupled high Q_s system, or 40% in a well coupled medium Q_s system.

Bifurcation criteria were developed for each of the basic ICPT topologies. As shown bifurcation -free operation is ensured if a design satisfies the bifurcation criteria. It was found that the SP and PP topologies have identical bifurcation criteria, while those of the SS and PS topologies are different. The bifurcation criteria were found to be simple equations dependent on Q_p and Q_s. When Q_s is high, the bifurcation criteria of each topology can be simply stated as $Q_p>Q_s$. Since Q_p and Q_s are inversely related, ICPT systems will always bifurcate with increased loading (Q_s).

The bifurcation criteria can also be expressed in terms of k and Q_s allowing subtly different interpretations. Here it was noted that the maximum allowable Q_s decreases as k improves. With a k of 0.1, the maximum Q_s is about 10 in all topologies. With an increased k of 0.6, the maximum allowable Q_s before bifurcation drops to less than 2, but varies between the topologies.

With k and Q_s determined using the design methodology described in Chapter 4, the bifurcation criteria can be used to evaluate the potential improvement in the power transfer capability by modifying C_p. This improvement is guaranteed providing the bifurcation criterion is satisfied. If the bifurcation criterion is violated, both the original tuning and the modified tuning cannot transfer the designed power and the system should be redesigned to reduce either k or Q_s.

With systems that meet the bifurcation criteria with a large safety margin, the difference between the modified tuning and the original tuning is small, and the improvement in the power transfer capability is negligible. This improvement becomes more significant in systems that satisfy the

InductEV, Inc.
Exhibit 1010
Page 262

bifurcation criteria with a small safety margin.

For the SP and PS topologies with good coupling, the modified tuning can increase the power transfer capability by more than 50%. Here the required modification in C_p is significant, and should be used in practical systems. For the PP topology with good coupling, or the SP and PS topologies with middle coupling, the potential improvement in the power transfer capability is about 10% to 25%. In these cases, the required modification in C_p is small. This is achievable in practice if good lifetime capacitance stability is available.

In loosely coupled systems, the modified tuning and the original tuning are essentially identical as the required modification in C_p is negligible. For middle coupled systems, the original tuning also works well for the PP topology and the SP and PS topologies with low Q_s.

Both the theoretical power transfer capability and bifurcation phenomenon predicted for the modified tuning were verified by a practical example using a contact-less electric vehicle battery charger. The measurements were found to follow the calculated values closely. When the system is designed to satisfy the bifurcation criterion with a suitable safety margin, it is able to ensure bifurcation-free operation for all loading conditions up to and including rated load.

REFERENCES

[1]. J. B. Turner, "Autotuned resonant power source," *US-Patent No. 5006973*, Apr. 9, 1991.

[2]. T. Bieler, M. Perrottet, V. Nguyen, Y. Perriard, "Contactless power and information transmission," in *Conf. Rec. IEEE-IAS Annual Meeting*, vol. 1, 2001, pp. 83-88.

[3]. R. Laouamer, M. Brunello, J. P. Ferrieux, O. Normand, N. Buchheit, "A multi-resonant converter for noncontact charging with electromagnetic coupling," in *Conf. Rec. IEEE-IES Annual Conference*, vol. 2, 1997, pp. 792-797.

[4]. H. Abe, H. Sakamoto, K. Harada, "A noncontact charger using a resonant converter with parallel capacitor of the secondary coil," *IEEE Transactions on Industry Applications*, vol. 36, pp. 444-451, Mar./Apr. 2000.

[5]. A. Okuno, L. Gamage, M. Nakaoka, "Performance evaluations of high-frequency inverter-linked DC/DC converter with noncontact pickup coil," *IEEE Transactions on Industrial Electronics*, vol. 48, pp. 475-477, Apr. 2001.

[6]. J. T. Boys, G. A. Covic, A. W. Green, "Stability and control of inductively coupled power transfer systems," *IEE Proceedings - Electric Power Applicaions*, vol. 147, pp. 37-43, Jan. 2000.

InductEV, Inc.
Exhibit 1010
Page 263

[7]. G. A. Covic, G. Elliott, O. H. Stielau, R. M. Green, J. T. Boys, "The design of a contact-less energy transfer system for a people mover system," in *Conf. Rec. International Conference on Power System Technology*, vol. 1, Dec. 2000, pp. 79-84.

[8]. Chwei-Sen Wang, G. A. Covic, O. H. Stielau, "General stability criterions for zero phase angle controlled loosely coupled inductive power transfer systems," in *Conf. Rec. IEEE-IES Annual Conference*, vol. 2, 2001, pp. 1049-1054.

[9]. A. P. Hu, *Selected resonant converters for IPT power supplies*, PhD thesis, The Electrical and Electronics Engineering Department, The University of Auckland, Auckland, New Zealand, 2001, pp. 68-79.

[10]. O. H. Stielau, G. A. Covic, "Design of loosely coupled inductive power transfer systems," in *Conf. Rec. International Conference on Power System Technology*, vol. 1, Dec. 2000, pp. 85-90.

[11]. A. W. Green, J. T. Boys, "An inductively coupled high-frequency power system for material handling applications," in *Conf. Rec. International Power Electronics*, vol. II, 1993, pp. 821-826.

[12]. J. Gullberg, *Mathematics: From the Birth of Numbers*, W.W. Norton&Company, New York, 1997, pp. 320-324.

InductEV, Inc.
Exhibit 1010
Page 264

InductEV, Inc.
Exhibit 1010
Page 265

CHAPTER 6

TUNING TO IMPROVE DPF FOR FIXED-FREQUENCY SYSTEMS

6-1 Introduction
6-2 System behaviour with primary tuning for unity DPF at rated load
6-3 Primary tuning for load independent unity DPF
6-4 Discussion
6-5 Design examples
6-6 Verification
6-7 Conclusions

6-1 INTRODUCTION

This chapter investigates a method by which the displacement power factor (DPF) of an ICPT power supply operating under fixed frequency operation can be improved. When the frequency of the power supply is fixed to the nominal frequency (ω_0), primary tuning does not affect the power transfer capability to the pickup loads providing the supply can maintain the primary current constant under all loading conditions. However the DPF of the power supply may be well below unity if its load resonant tank is not properly tuned. Consequently, this Chapter focuses on suitable variations to the primary tuning with the design methodology described in Chapter 4.

The modified primary tuning proposed in Chapter 5 for variable frequency systems is investigated first. Here the design ensures unity DPF at rated load. However many practical ICPT systems are found to operate for considerable periods of time under lightly load conditions, thus ideally DPF should be improved under all loading conditions (up to and including rated load). An alternative tuning option is therefore investigated that aims to achieve load independent unity DPF.

6-2 SYSTEM BEHAVIOUR WITH PRIMARY TUNING FOR UNITY DPF AT RATED LOAD

It is assumed in this section that the primary compensation capacitance (C_p) is modified using (5-2) so that unity DPF is assured at rated load for fixed-frequency systems operating at ω_0. As noted in section 5-2, the original tuning assumed with the design methodology described in Chapter 4 works

InductEV, Inc.
Exhibit 1010
Page 266

well for the SS topology. Here unity DPF is achieved independent of the load and there is no need to modify C_p. This section thus focuses on the SP, PP and PS topologies, where the original tuning does not have unity DPF and modification of C_p is required.

Similar to the analysis in section 4-5.1, the phase angle between the fundamental components of the output voltage and current of the power supply can be calculated using the normalized load impedance (Z_{tn}) as:

$$\tan\theta_1 = \frac{\mathrm{Im}Z_{tn}}{\mathrm{Re}Z_{tn}} \text{ or } \tan\theta_1 = \frac{-\mathrm{Im}Y_{tn}}{\mathrm{Re}Y_{tn}} \tag{6-1}$$

The DPF of the power supply can then be determined from this phase angle as:

$$\mathrm{DPF} = \cos\theta_1 \tag{6-2}$$

Thus under fixed frequency operation at ω_0 (u=1), equation (6-1) can be calculated (using the normalized load impedance given in Table 5-2 and Table 5-3) as:

$$\tan\theta_1(u=1) = \begin{cases} \left(\frac{1}{k^2 Q_{s0}}\right)\left(1-k^2-\frac{1}{C_{pn}}\right)=0 & \text{SP topology} \\ -k^2 Q_{s0} C_{pn} + \left(\frac{1-k^2}{Q_{s0}}\right)\left(\frac{1-C_{pn}+k^2 C_{pn}}{k^2}\right) & \text{PP topology} \\ -k^2 Q_{s0} C_{pn} + \left(\frac{1}{k^2 Q_{s0}}\right)\left(1-C_{pn}\right) & \text{PS topology} \end{cases} \tag{6-3}$$

where the normalized primary compensation capacitance C_{pn} is summarized in Table 6-1 for both the original tuning and the modified tuning. For the PP and PS topologies, the required C_{pn} with the modified tuning is a function of the load ($Q_{s0}=Q_s(\omega=\omega_0)$ equals "$\omega_0 C_s R$" for a parallel pickup and "$1/(\omega_0 C_s R)$" for a series pickup), and it is assumed here that C_{pn} is selected for rated operation ($Q_{s0,rated}$). It should be noted that as the operating frequency is fixed at ω_0 (u=1), the operating secondary quality factor Q_s equals Q_{s0} under all conditions.

With the phase angle determined by (6-3), the DPF of the power supply can be calculated using (6-2). They are functions of k, Q_{s0} and C_{pn}. As shown in Table 6-1, C_{pn} is a function of k for the SP topology, and depends on both k and $Q_{s0,rated}$ for the PP and PS topologies. Influences of this modified tuning on DPF are topology dependent as shown in Fig. 6-1 to Fig. 6-3. In these figures, the modified design is labelled "modified tuning", and the system designed using the methodology described in Chapter 4 is labelled "original tuning". The modified tuning and the original tuning are compared for loosely coupled (low k), mid-coupled (middle k), and well-coupled (high k) systems. For the PP and PS topologies, the difference between high and low $Q_{s0,rated}$ systems are identified.

InductEV, Inc.
Exhibit 1010
Page 267

TABLE 6-1
A SUMMARY OF C_{pn} FOR THE ORIGINAL TUNING AND THE MODIFIED TUNING FOR UNITY DPF AT RATED LOAD

Topologies	C_{pn}	
	Original tuning	Modified tuning
SS	1	1
SP	1	$\frac{1}{1-k^2}$
PP	1	$\frac{1-k^2}{Q_{s0,rated}^2 k^4 + (1-k^2)^2}$
PS	1	$\frac{1}{Q_{s0,rated}^2 k^4 + 1}$

SP Topology: In the SP topology, the DPF is independent of k under both the original and modified tuning. As shown in Fig. 6-1, the modified tuning has unity DPF at all loads (Q_s). The improvement in DPF under lightly loading conditions (low Q_s) is more significant. When Q_s is high, the DPF of the original system is very close to unity, and the difference between this system and that resulting from the modified tuning is negligible.

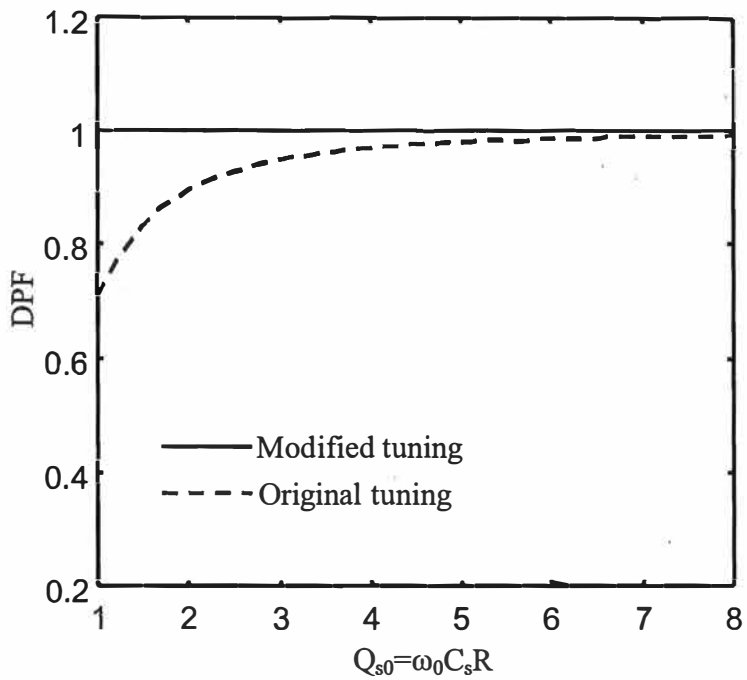

Fig. 6-1. SP topology - DPF under fixed-frequency operation at ω_0 assuming modified primary tuning to achieve unity DPF at rated load.

InductEV, Inc.
Exhibit 1010
Page 268

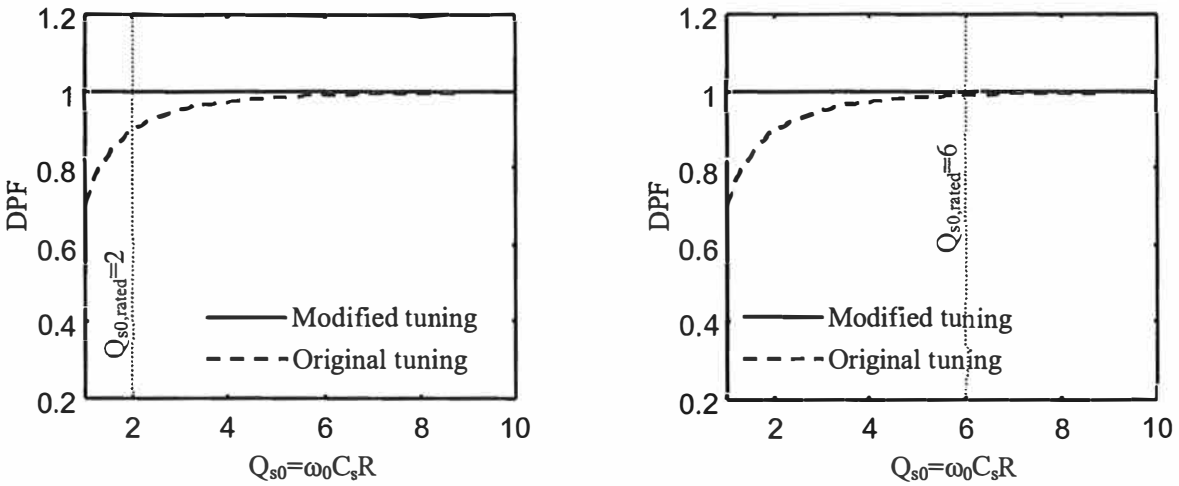

(i) Low $Q_{s0,rated}$ pickup. (ii) High $Q_{s0,rated}$ pickup.

(a) Loosely coupled systems (k=0.05).

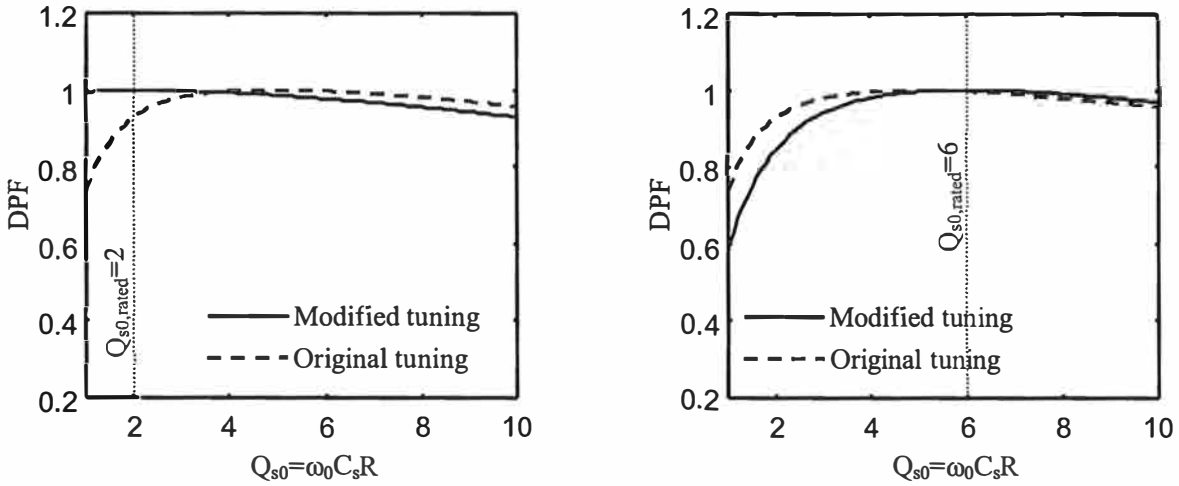

(i) Low $Q_{s0,rated}$ pickup. (ii) High $Q_{s0,rated}$ pickup.

(b) Mid-coupled systems (k=0.2).

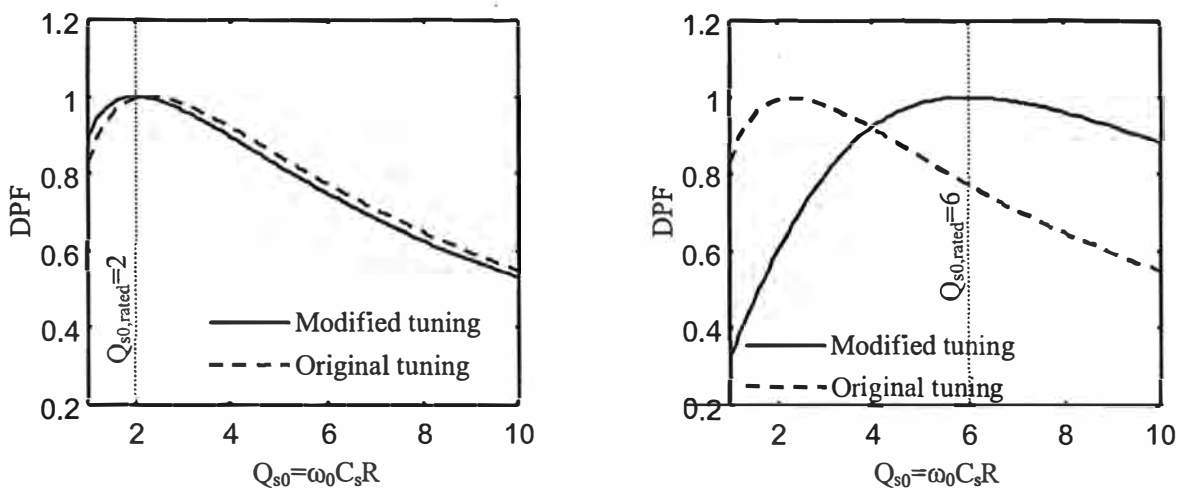

(i) Low $Q_{s0,rated}$ pickup. (ii) High $Q_{s0,rated}$ pickup.

(c) Well-coupled systems (k=0.4).

Fig. 6-2. PP topology - DPF under fixed-frequency operation at ω_0 assuming modified primary tuning to achieve unity DPF at rated load.

InductEV, Inc.
Exhibit 1010
Page 269

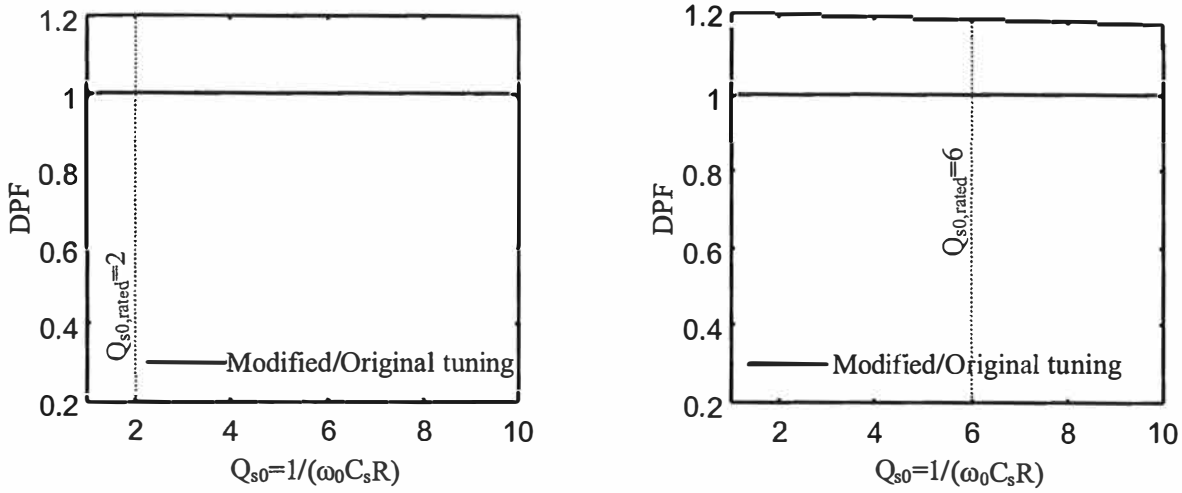

(i) Low $Q_{s0,rated}$ pickup. (ii) High $Q_{s0,rated}$ pickup.

(a) Loosely coupled systems (k=0.05).

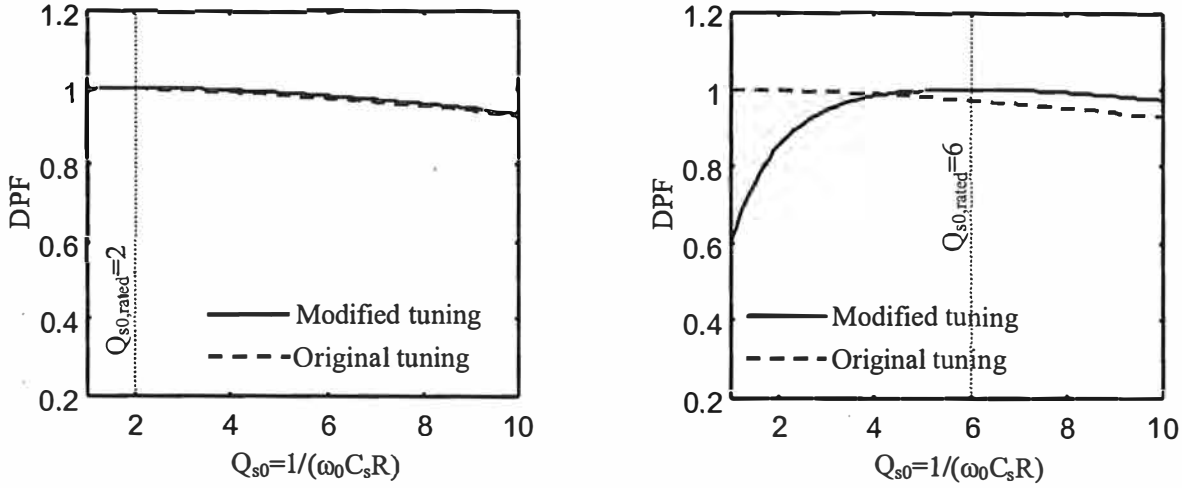

(i) Low $Q_{s0,rated}$ pickup. (ii) High $Q_{s0,rated}$ pickup.

(b) Mid-coupled systems (k=0.2).

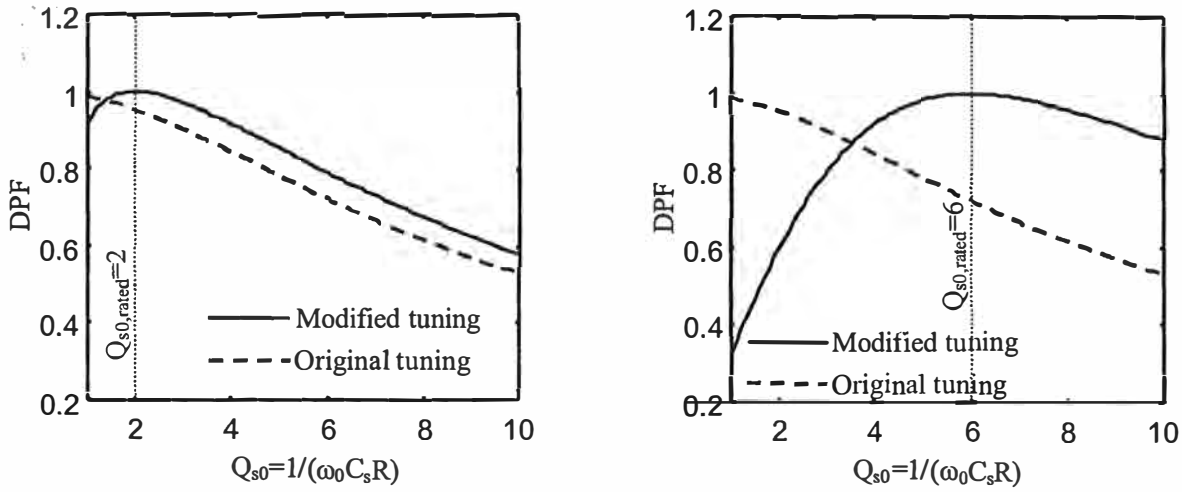

(i) Low $Q_{s0,rated}$ pickup. (ii) High $Q_{s0,rated}$ pickup.

(c) Well-coupled systems (k=0.4).

Fig. 6-3. PS topology - DPF under fixed-frequency operation at ω_0 assuming modified primary tuning to achieve unity DPF at rated load.

InductEV, Inc.
Exhibit 1010
Page 270

PP Topology: The original and modified tuning schemes are identical at the following condition:

$$Q_{s0,rated} = \frac{\sqrt{1-k^2}}{k} \tag{6-4}$$

Interestingly, this is the bifurcation boundary given in Table 5-5. It occurs at larger Q_s in loosely coupled systems. With a k of 0.05, 0.2 and 0.4, the original tuning achieves unity DPF at Q_s of 20, 4.9 and 2.3 respectively.

The degree of influence of the proposed modified tuning on DPF depends strongly on $Q_{s0,rated}$ as shown in Fig. 6-2. If $Q_{s0,rated}$ equals the value given in (6-4), the original tuning and the modified tuning are identical. With $Q_{s0,rated}$ below this value, the modified tuning improves the DPF for all loading conditions up to and including rated load. When $Q_{s0,rated}$ is above this value, the modified tuning improves the DPF only when Q_s is close to $Q_{s0,rated}$, but undesirably decreases the DPF at lower Q_s values.

PS Topology: With this topology, the original tuning has a DPF below unity for all normal Q_s, and the modified tuning achieves unity DPF only at $Q_{s0,rated}$ as shown in Fig. 6-3. The influences of k and Q_s on the DPF of the original tuning are quite different between the PP and PS topologies (as discussed in section 4-5.2). However, here with the suggested modified tuning the two topologies have similar characteristics. The DPF under lightly loading conditions (corresponding to lower Q_s) can however be poor when k is good and $Q_{s0,rated}$ is high. Overall the shift is desirable since the improvement in DPF at rated load minimizes the required VA rating of the power supply. The change is more significant in well-coupled systems with high $Q_{s0,rated}$. In order to improve the DPF for all loading conditions up to and including rated load, an alternative primary tuning option is proposed in the following section.

6-3 PRIMARY TUNING FOR LOAD INDEPENDENT UNITY DPF

In the previous section, it was noted that unity DPF could be achieved under all loading conditions only in series tuned primary systems using the tuning methodology described. In this section, a new primary tuning methodology is proposed that makes the load reactance (Im Z_t) equal to zero under all loading conditions in order to achieve load independent unity DPF for both series and parallel tuned primary systems. For parallel tuned primaries this is possible only with suitable modifications to the primary compensation capacitance and/or the operating frequency assumed with the design methodology described in Chapter 4. Influences of such modifications on the power transfer capability and the required secondary VA rating are investigated in order to identify the required operating conditions when using the modified systems to transfer rated power.

InductEV, Inc.
Exhibit 1010
Page 271

6-3.1 PRIMARY CAPACITANCE AND OPERATING FREQUENCY

The required primary compensation capacitance (C_{pn}) and the operating frequency (u) (derived in Appendix I) to achieve the above stated objectives are given in Table 6-2. In respect to the SP, PP and PS topologies, they are functions of k and independent of Q_{s0}. The latter independency ensures that unity DPF is possible under all load conditions.

As expected, there is no need to change either C_p or the operating frequency for the SS topology, while the SP topology requires a different C_p identical to the modified tuning proposed in section 5-2. The PP topology does not change C_p but requires a different operating frequency, while the PS topology needs to change both C_p and the operating frequency.

It should be noted that the required changes to the operating frequency for the PP and PS topologies will necessarily affect the power transfer capability and needs to be considered carefully when using the modified primary tuning methodology. This is investigated in section 6-3.2.

TABLE 6-2
NORMALIZED PRIMARY COMPENSATION CAPACITANCE AND OPERATING FREQUENCY REQUIRED TO ACHIEVE LOAD INDEPENDENT UNITY DPF

Topology	Normalized Primary Capacitance (C_{pn})	Normalized Operating Frequency (u)
SS	1	1
SP	$\frac{1}{1-k^2}$	1
PP	1	$\frac{1}{\sqrt{1-k^2}}$
PS	$1-k^2$	$\frac{1}{\sqrt{1-k^2}}$

The influence of k on the required change to C_p is shown in Fig. 6-4 for the SP and PS topologies (SS and PP topologies do not require a different C_p). The SP topology requires a larger C_p, while the PS topology needs a smaller C_p. The necessary change is small in loosely coupled systems, but becomes quite significant in well-coupled systems. With k of 0.6 the SP topology requires a 56% larger C_p value, while the PS topology needs a 36% smaller C_p value.

The required changes to the operating frequency are identical in both the PP and PS topologies as shown in Fig. 6-5. Here, it is necessary to deliberately operate at a frequency above ω_0 (u>1). The required change is small in loosely coupled (low k) systems, but becomes significant with improving k.

InductEV, Inc.
Exhibit 1010
Page 272

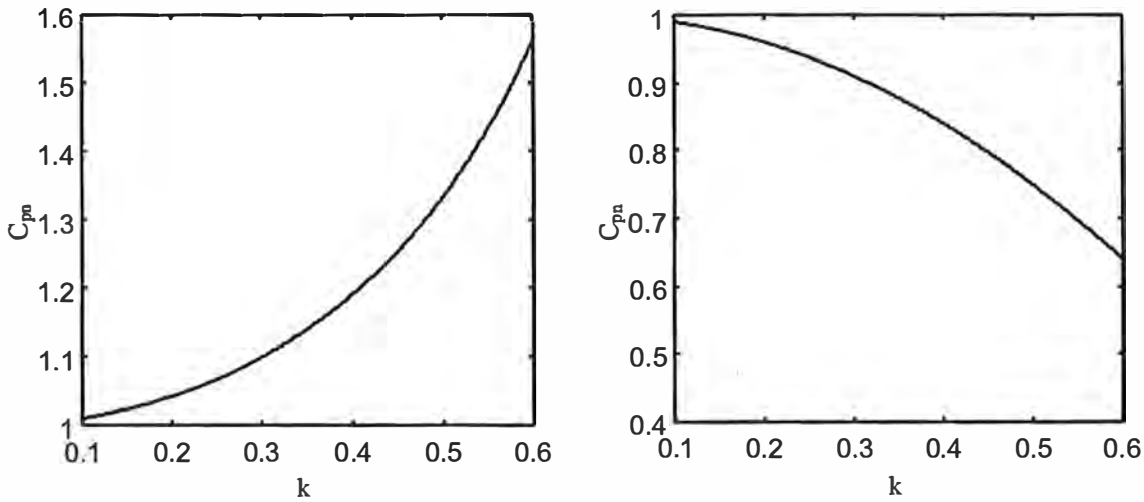

(a) SP topology. (b) PS topology.

Fig. 6-4. Influences of k to the required change in C_p to achieve load independent unity DPF.

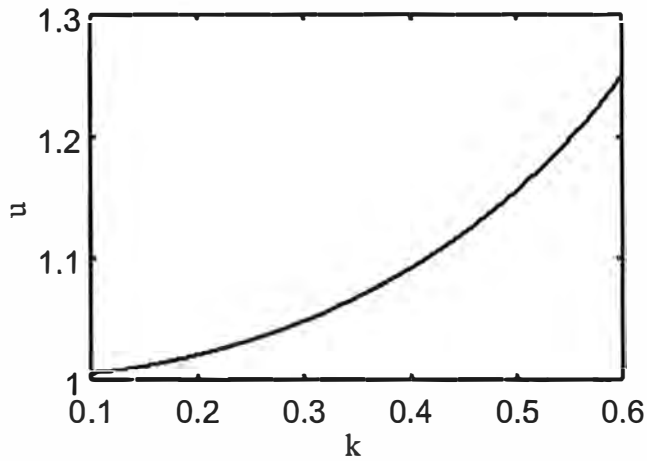

Fig. 6-5. Influence of k to the required change in ω to achieve load independent unity DPF (the PP and PS topologies).

6-3.2 POWER TRANSFER CAPABILITY AND SECONDARY VA RATING

The SS and SP topologies do not require a change to the operating frequency, and as such this tuning approach does not influence the power transfer capability or the required secondary VA rating. Furthermore, these tuning options are identical to those proposed in section 6-2 and have therefore been fully discussed already.

Consequently, this section focuses only on the PP and PS topologies, where operating above ω_0 is required. The behaviours of these systems are shown in Fig. 6-6 and 6-7. Here each system using the design methodology described in Chapter 4 is shown using dashed lines (labelled as "original tuning"), while all systems using the primary compensation capacitance and operating frequency given in Table 6-2 are shown as solid lines (labelled as "modified tuning").

InductEV, Inc.
Exhibit 1010
Page 273

Under the modified tuning suggested, the operating frequency shifts above ω_0 by increasing amounts as the coupling increases. With k of 0.2, 0.3 and 0.4, this shift in ω_0 is about 2%, 5% and 9% respectively. These percentage changes in ω_0 reflects the percentage changes in Q_s under all loading conditions, since for the PP topology "$Q_s=uQ_{s0}$" while in the PS topology "$Q_s=Q_{s0}/u$".

The need to deliberately detune the operating frequency above ω_0 for the PP and PS topologies in order to achieve load independent unity DPF affects the power transfer capability of the pickup. If the primary current is assumed constant, such influences can be quantified using the normalized power (P_n) defined in (5-7) using the rated power determined at rated load ($Q_{s0,rated}$) and ω_0 (u=1). Here P_n is determined to be a function of k, Q_{s0} and the specified rated load ($Q_{s0,rated}$) given by:

$$P_n = \begin{cases} \dfrac{1-k^2}{1-k^2+k^4Q_{s0}^2}\left(\dfrac{Q_{s0}}{Q_{s0,rated}}\right) & \text{PP topology} \\ \dfrac{1}{1-k^2+k^4Q_{s0}^2}\left(\dfrac{Q_{s0}}{Q_{s0,rated}}\right) & \text{PS topology} \end{cases} \tag{6-5}$$

For a general analysis, the secondary current, secondary voltage and required secondary VA rating are normalized here using the rated values determined at rated load and ω_0. The normalized secondary current and voltage can be calculated using Table 3-1 as:

$$I_{sn} = \frac{I_s}{I_{s0,rated}} = \begin{cases} \dfrac{\sqrt{\left(1-k^2+k^2Q_{s0}^2\right)^2+\left(1-k^2\right)^3Q_{s0}^2}}{\left(1-k^2+k^4Q_{s0}^2\right)\sqrt{1+Q_{s0,rated}^2}} & \text{PP topology} \\ \dfrac{Q_{s0}\sqrt{1-k^2+k^4Q_{s0}^2}}{\left(1-k^2+k^4Q_{s0}^2\right)Q_{s0,rated}} & \text{PS topology} \end{cases} \tag{6-6}$$

and

$$V_{sn} = \frac{V_s}{V_{s0,rated}} = \begin{cases} \dfrac{Q_{s0}\sqrt{\left(1-k^2\right)\left(1-k^2+k^4Q_{s0}^2\right)}}{\left(1-k^2+k^4Q_{s0}^2\right)Q_{s0,rated}} & \text{PP topology} \\ \dfrac{\sqrt{Q_{s0}^2+\left(1-k^2\right)\left(1-k^2Q_{s0}^2\right)^2}}{\left(1-k^2+k^4Q_{s0}^2\right)\sqrt{1+Q_{s0,rated}^2}} & \text{PS topology} \end{cases} \tag{6-7}$$

The normalized VA rating required for the pickup coil (VA_{sn}) is then:

$$VA_{sn} = \frac{VA_s}{VA_{s0,rated}} = I_{sn}V_{sn} \tag{6-8}$$

The normalized power (P_n), secondary current (I_{sn}), secondary voltage (V_{sn}) and required secondary VA rating (VA_{sn}) are shown in Fig. 6-6 and 6-7 by arbitrarily selecting $Q_{s0,rated}$ as 5. In loosely coupled

InductEV, Inc.
Exhibit 1010
Page 274

(low k) systems, the original tuning works well and the required change to C_p and the operating frequency is negligible. For such systems, there is essentially no difference between the original and modified tuning. For mid-coupled systems with k of about 0.2, rated power is achieved with the modified tuning but at a Q_{s0} slightly above $Q_{s0,rated}$. In well-coupled systems with k of about 0.4, the modified tuning cannot achieve rated power, and the system should be redesigned to have lower $Q_{s0,rated}$. A practical well-coupled low Q_s system (k=0.45, $Q_{s0,rated}$=1.8) for contact-less electric vehicle battery charging is discussed later in section 6-5.

With k of 0.3, rated power is achieved with the modified tuning at Q_{s0} of about 7.5 in the PP topology. At this operating condition, the secondary current and voltage increase by 27% and 22%, requiring a secondary VA rating increase of 55%. For the PS topology, rated power is achieved at Q_{s0} of about 6, and here the secondary current and voltage increases by 9% and 4% respectively, so that the required secondary VA rating increases by 14%. Generally, the PP topology requires a larger secondary VA rating than the PS topology when this modified tuning methodology is applied.

The power transfer capability of the original tuned system increases linearly with Q_{s0}, while that of the modified tuning increases but at a decreasing rate with Q_{s0} until it reaches a maximum point after which it drops. This maximum power point can be determined by:

$$\frac{dP_n}{dQ_{s0}} = 0 \qquad \text{PP and PS topologies} \qquad (6\text{-}9)$$

Substituting (6-5) into (6-9), the maximum power point is found to be:

$$Q_{s0} = \frac{\sqrt{1-k^2}}{k^2} \qquad \text{PP and PS topologies} \qquad (6\text{-}10)$$

and

$$P_n = \begin{cases} \left(\dfrac{\sqrt{1-k^2}}{2k^2}\right)\left(\dfrac{1}{Q_{s0,rated}}\right) & \text{PP topology} \\ \left(\dfrac{1}{2k^2\sqrt{1-k^2}}\right)\left(\dfrac{1}{Q_{s0,rated}}\right) & \text{PS topology} \end{cases} \qquad (6\text{-}11)$$

Assuming rated power can just be achieved with the modified tuning at the maximum power point, then replacing P_n with unity, $Q_{s0,rated}$ can be determined using (6-11) to be:

$$Q_{s0,rated} = \begin{cases} \dfrac{\sqrt{1-k^2}}{2k^2} & \text{PP topology} \\ \dfrac{1}{2k^2\sqrt{1-k^2}} & \text{PS topology} \end{cases} \qquad (6\text{-}12)$$

InductEV, Inc.
Exhibit 1010
Page 275

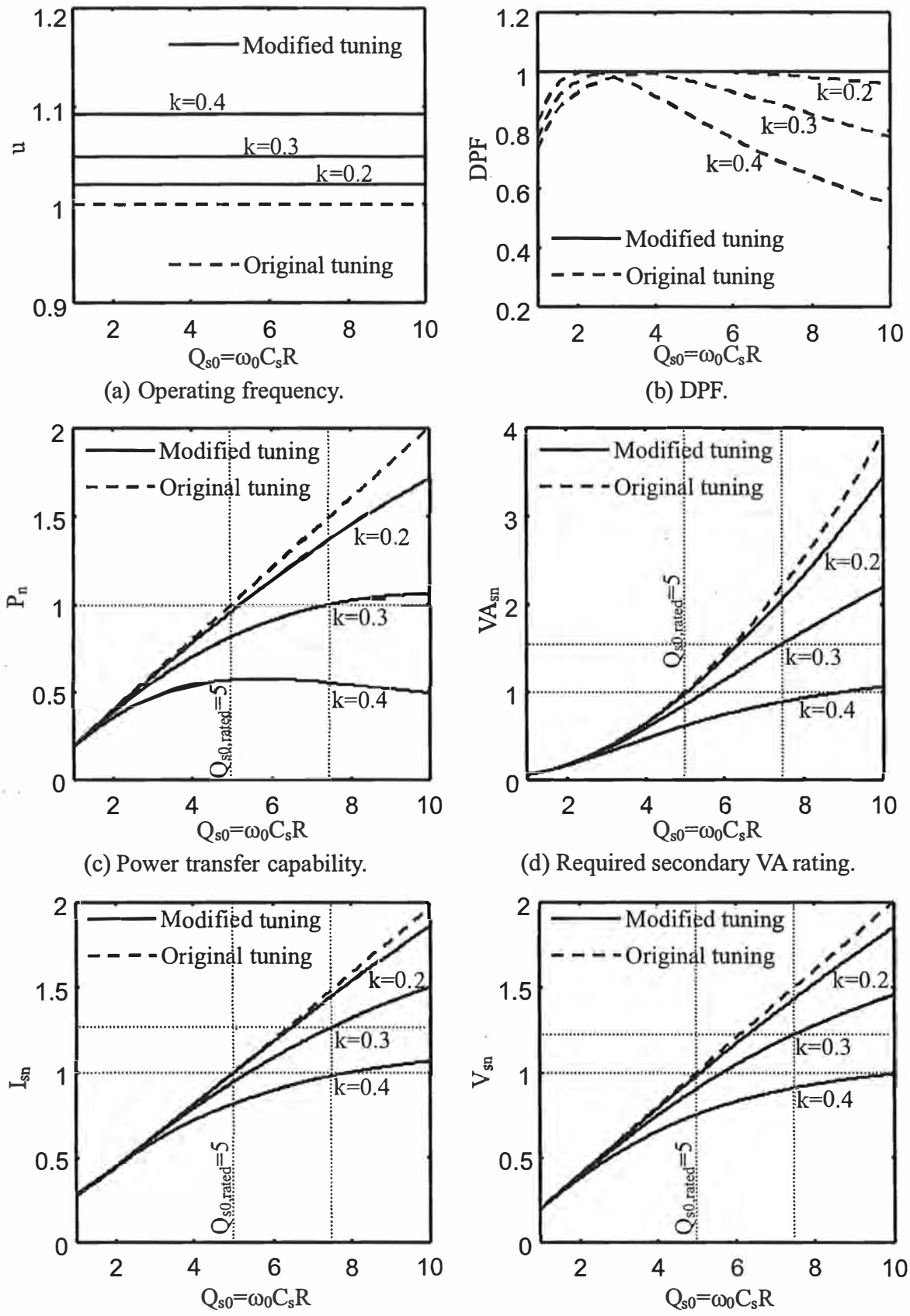

(a) Operating frequency.

(b) DPF.

(c) Power transfer capability.

(d) Required secondary VA rating.

(e) Secondary current.

(f) Secondary voltage.

Fig. 6-6. PP topology – System behaviour under fixed-frequency operation ($Q_{s0,rated}$=5).

InductEV, Inc.
Exhibit 1010
Page 276

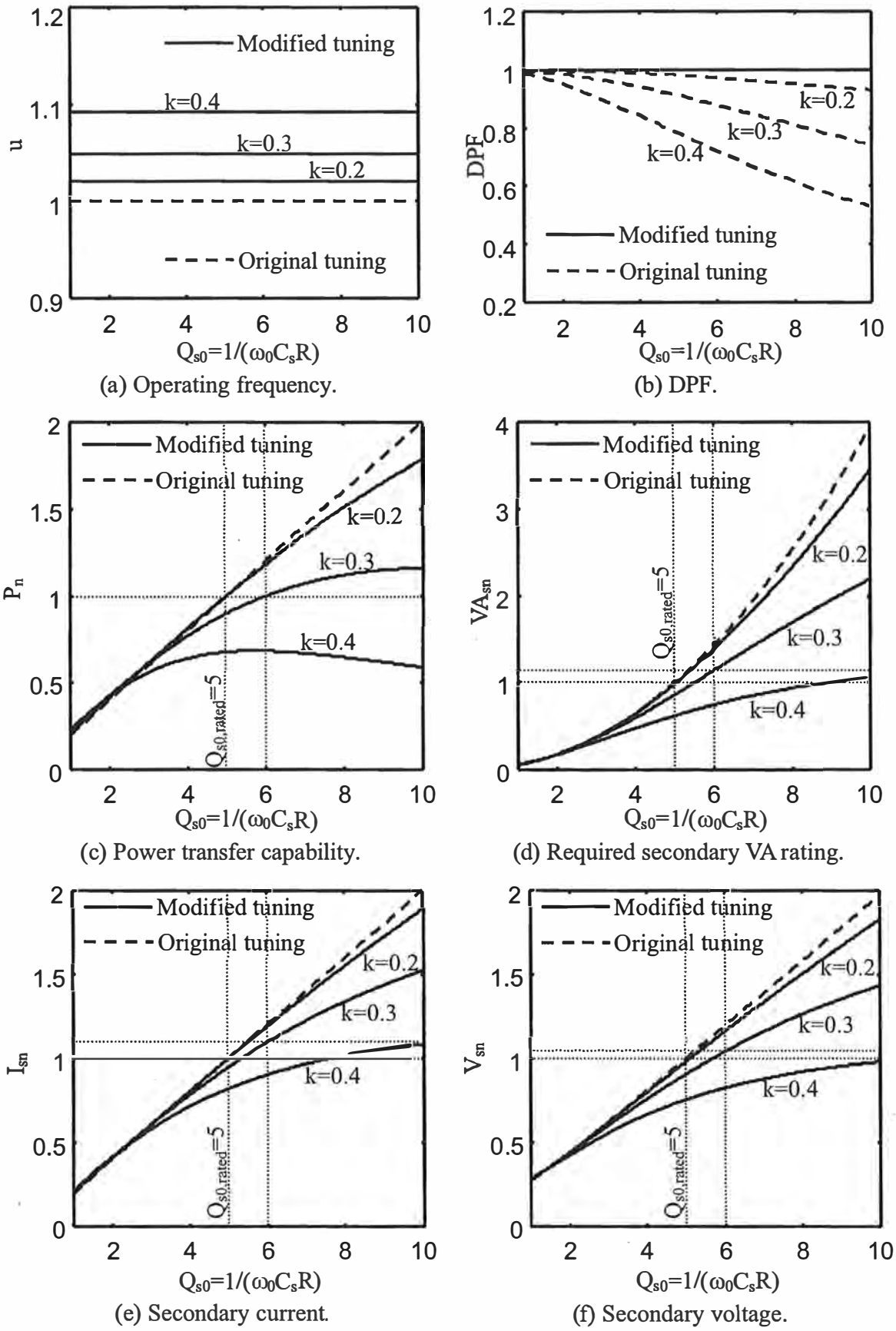

(a) Operating frequency. (b) DPF.

(c) Power transfer capability. (d) Required secondary VA rating.

(e) Secondary current. (f) Secondary voltage.

Fig. 6-7. PS topology – System behaviour under fixed-frequency operation ($Q_{s0,rated}$=5).

InductEV, Inc.
Exhibit 1010
Page 277

Equation (6-12) determines the maximum $Q_{s0,rated}$ for a given coupling k when using the modified tuning methodology to achieve load independent unity DPF for both the PP and PS topologies. This is shown in Fig. 6-8. For a given coupling k, it is necessary to ensure $Q_{s0,rated}$ is within the shaded region to ensure rated power can be achieved. The PS topology allows slightly larger $Q_{s0,rated}$ than the PP topology. For both topologies, a trade-off between k and $Q_{s0,rated}$ is necessary. In a mid-coupled system with k of 0.2, the maximum $Q_{s0,rated}$ is more than 10. The maximum $Q_{s0,rated}$ in a well-coupled system with k of 0.4 is much lower at about 3. Track-type systems are normally loosely-middle coupled with medium-high Q_s, while coil-type systems are normally middle-well coupled with low-medium Q_s, as such this characteristic suits practical ICPT systems since a well coupled high Q_s system would rarely if ever exist in practice.

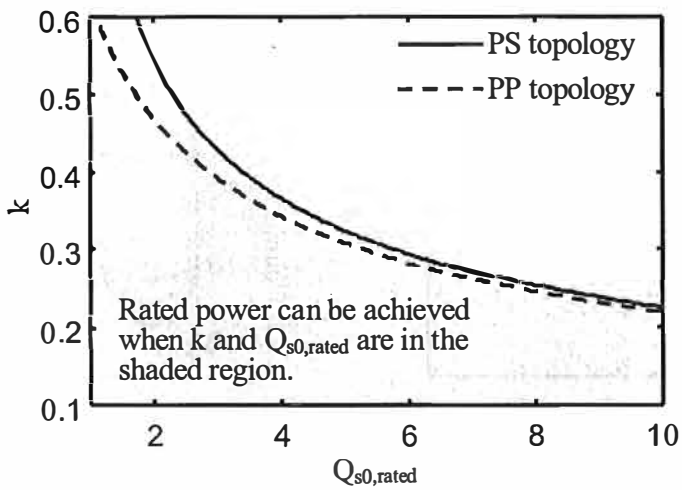

Fig. 6-8. Limit of k and $Q_{s0,rated}$ when using the modified tuning to achieve load independent unity DPF.

With the modified tuning applied, the changes in the secondary current, secondary voltage, required secondary VA rating when operating at rated power are shown in Fig. 6-9 for the PP and PS topologies. Here k is arbitrarily selected as 0.2, 0.3 and 0.4. In each case, the changes are calculated for all possible values of $Q_{s0,rated}$ within the shaded region in Fig. 6-8. For each value of k, the required Q_{s0} to achieve rated power (P_n=1) is calculated using (6-5). The secondary current, secondary voltage and required secondary VA rating at this new operating condition are then determined using (6-6), (6-7) and (6-8). These changes strongly depend on k and $Q_{s0,rated}$. For systems using a PP topology, the required secondary VA rating with the modified tuning is always higher than the original tuning. This increase is small for loosely coupled systems with reasonable $Q_{s0,rated}$, or well-coupled systems with low $Q_{s0,rated}$, but can be more than 50% for well-coupled systems with high $Q_{s0,rated}$. It is also found that the increase in the secondary voltage is less than the secondary current.

InductEV, Inc.
Exhibit 1010
Page 278

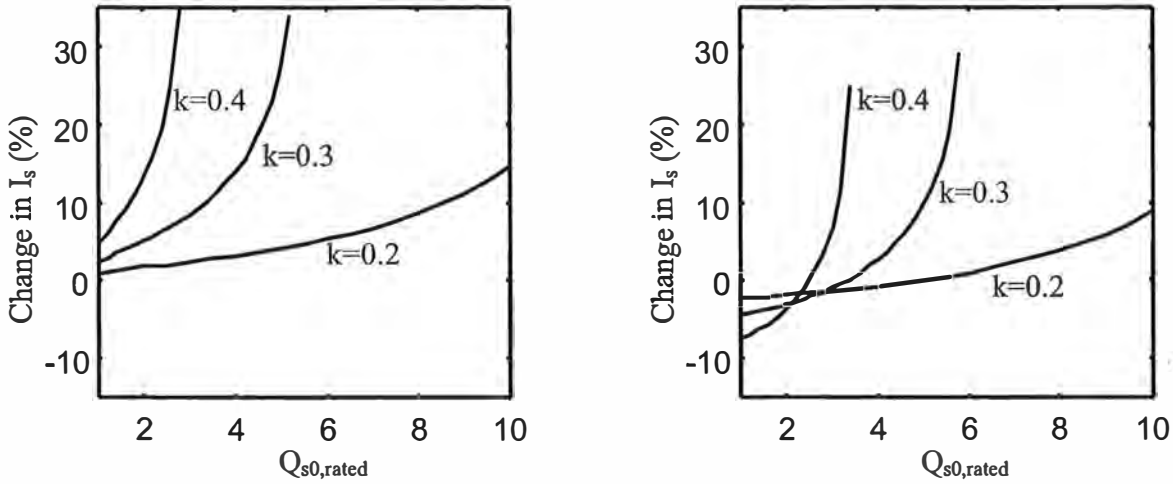

(i) PP topology. (ii) PS topology.

(a) Change in the secondary current.

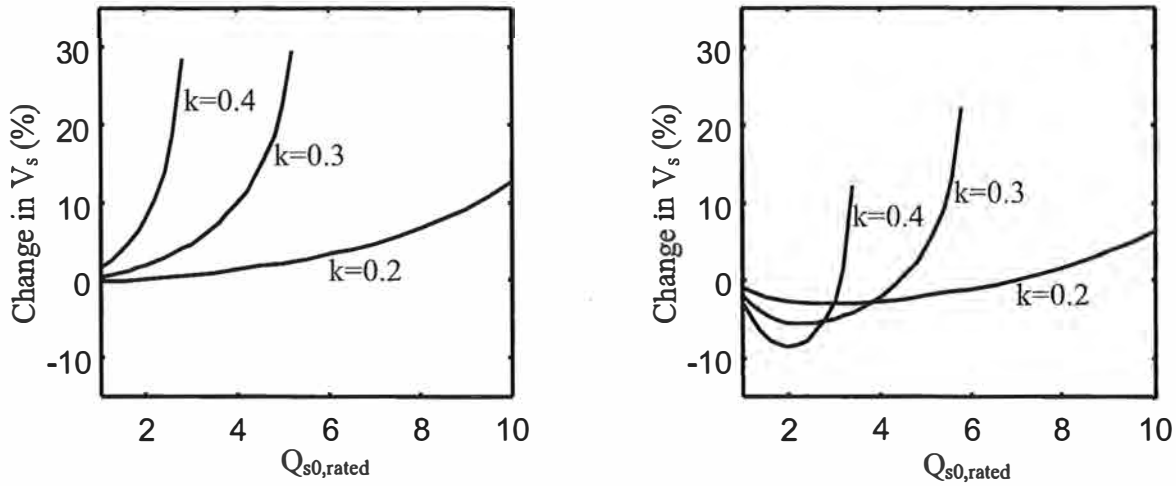

(i) PP topology. (ii) PS topology.

(b) Change in the secondary voltage.

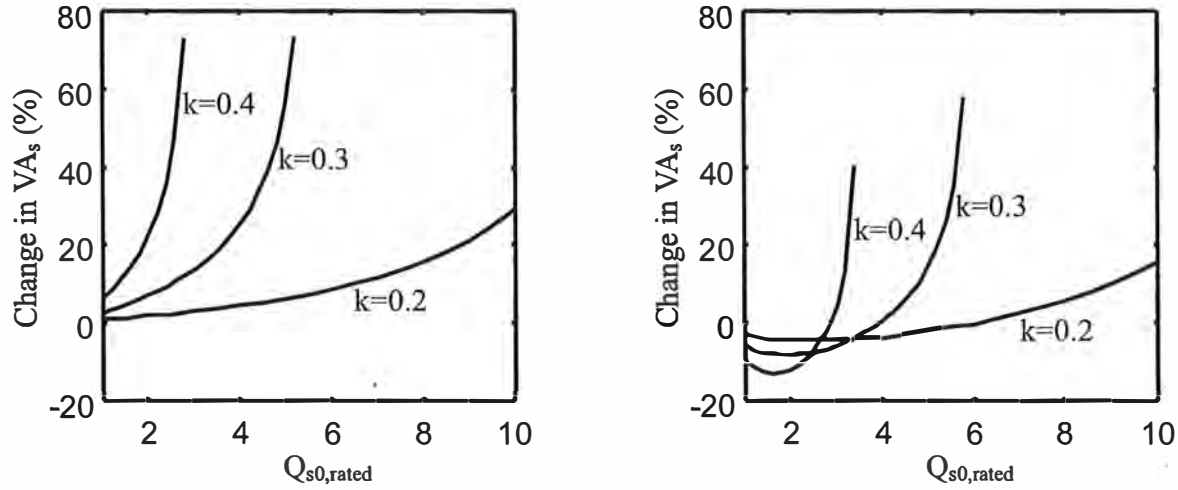

(i) PP topology. (ii) PS topology.

(b) Change in the required secondary VA rating.

Fig. 6-9. Changes in the secondary current, secondary voltage, and required secondary VA rating under rated power operation when using the modified tuning to achieve load independent unity DPF.

InductEV, Inc.
Exhibit 1010
Page 279

For systems using a PS topology, the required secondary VA rating with the modified tuning is less than the PP topology, and can be lower than the original tuning in loosely coupled systems with reasonable $Q_{s0,rated}$, or well-coupled systems with low $Q_{s0,rated}$. The decrease in the required secondary VA rating can be more than 10% for well-coupled systems with low $Q_{s0,rated}$. It is also noted that the decrease in the secondary voltage is more than the decreases shown in the secondary current.

The power transfer capability of systems with low $Q_{s0,rated}$ is illustrated in Fig. 6-10 where $Q_{s0,rated}$ is assumed to be 2. As can be seen, rated power is achieved with the modified tuning at a Q_{s0} higher than $Q_{s0,rated}$ for the PP topology, but for the PS topology interestingly it is at a Q_{s0} lower than $Q_{s0,rated}$. Consequently, the required secondary VA rating of the PS topology with the modified tuning is reduced.

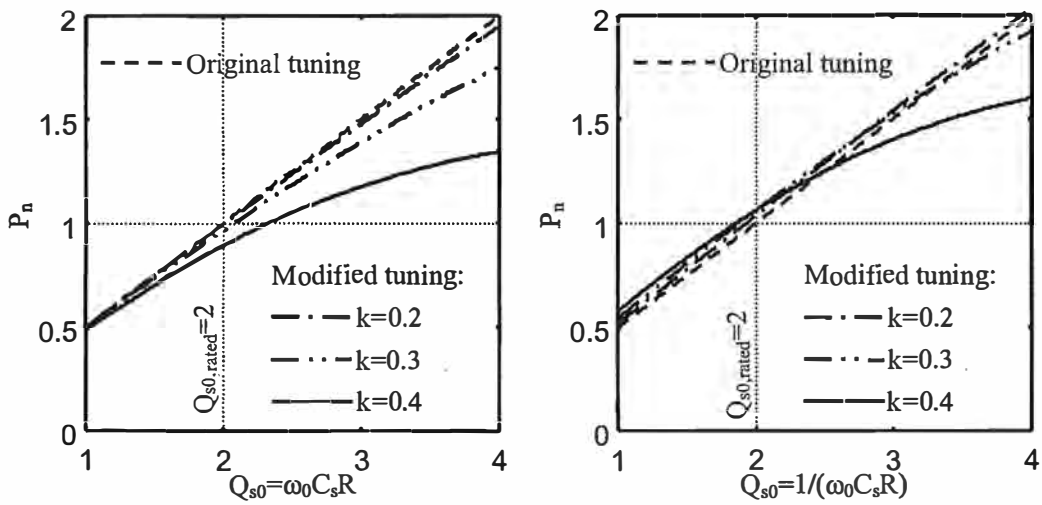

(a) PP topology. (b) PS topology.

Fig. 6-10. Power transfer capability under fixed-frequency operation ($Q_{s0,rated}$=2).

6-4 DISCUSSION

In order to ensure maximum power transfer capability is achievable in a pickup, it is desirable to operate the system at or near the tuned frequency (ω_0). It is also desirable to operate the power supply with a DPF close to unity in order to minimize the required VA rating while maximizing the efficiency. As shown, load independent unity DPF is achievable at ω_0 for the SS topology using the original tuning (assumed with the design methodology described in Chapter 4). Load independent unity DPF is also achievable at ω_0 for the SP topology providing the original tuning is modified using the approach proposed in Chapter 5. Consequently, series-compensated primary systems (the SS and SP topologies) are good topologies for fixed-frequency systems.

Parallel-compensated primary systems (PP and PS topologies) may be required in an application for practical reasons. In such systems, the modified tuning proposed in section 6-2 achieves unity DPF at

InductEV, Inc.
Exhibit 1010
Page 280

ω_0 at rated load only. Since the DPF is less than unity at light load, the efficiency of the power supply is also lower. In order to improve this efficiency, it is desirable to have unity DPF under all loading conditions. This is achievable using the modified tuning proposed in section 6-3, but then it is necessary to deliberately raise the operating frequency above ω_0. Both the power transfer capability and the required secondary VA rating are affected, as the pickup is not operating at the designed frequency. Rated power can still be delivered in the majority of ICPT systems, however there is now a trade-off between the system k and the maximum allowable Q_s when using this tuning scheme. Typical track-type ICPT systems are loosely coupled with reasonable Q_s, while coil-type ICPT systems are well coupled with low Q_s. In such systems, the required secondary VA rating increases slightly in a PP topology, but favourably decreases in a PS topology. In well-coupled systems with low Q_s, the PS topology ensures unity DPF under all load conditions with pickup VA requirement reduced by more than 10%. With this modified tuning, the required secondary VA rating for the PS topology is always less than the PP topology, and as such would be the preferred choice.

The above analysis assumes constant resonant parameters (C_p, C_s, L_p, L_s and M). In practice, the capacitance values (C_p and C_s) are affected by aging, thermal effects and manufacturing tolerance, while the coupling parameters (L_p, L_s and M) vary due to misalignment of the electromagnetic structure. Influences of such variations on the sensitivity of systems using the modified tuning approaches proposed here are investigated further in Chapter 7.

6-5 DESIGN EXAMPLES

The options proposed above for improving DPF under fixed-frequency operation are considered in this section for the design of the contact-less electric vehicle battery charger (described in sections 3-11 and 4-6). Both PP and PS topologies are investigated.

PP topology: Under fixed-frequency operation at ω_0 (f_0=19.7kHz), unity DPF is achieved with the original tuning when Q_{s0} is 1.98 (6.6Ω) determined using (6-4) from the known k (of 0.45). Here the DPF at rated load (6Ω, $Q_{s0,rated}$=1.8) is slightly lower than unity. To achieve unity DPF at rated load as described in section 6-2, the required C_{pn} calculated using Table 6-1 is 1.04 requiring C_p to be 4% larger than the original tuning. The improvement in the DPF with the modified tuning is shown in Fig. 6-11 compared to the original tuned system. At rated operation, the improvement with this modification is not significant, because the DPF of the original system is close to unity due to the values of k and $Q_{s0,rated}$. However, under lightly loaded conditions, the improvement in DPF is more significant but still remains well below unity.

The tuning approach suggested in section 6-3 for achieving load independent unity DPF can also be

InductEV, Inc.
Exhibit 1010
Page 281

used here without compromising the rated power delivery because the system k of 0.45 and $Q_{s0,rated}$ of 1.8 are within the shaded region in Fig. 6-8 for the PP topology. The required C_{pn} determined using Table 6-2 is unity thus C_p does not need to change. However the normalized operating frequency ($u=\omega/\omega_0$) is 1.12 and the operating frequency needs to be raised 12% above ω_0 at 22.1kHz. While the overall power transfer capability is affected (as shown in Fig. 6-12(a) due to pickup frequency detuning effects), rated power transfer of 300W now occurs at Q_{s0} of 2.3 (R=7.6Ω) rather than 1.8 (R=6Ω). The required secondary VA rating (shown in Fig. 6-12(b)) increases by 33% from 620 VA to 825VA as a result of the increased Q_{s0} for rated power delivery (labelled as $Q'_{s0,rated}$).

PS topology: Under fixed-frequency operation at ω_0, the DPF with the original tuning at $Q_{s0,rated}$ (shown in Fig. 6-13) is less than unity. To achieve unity DPF at $Q_{s0,rated}$ as proposed in section 6-2, the required C_{pn} calculated using Table 6-1 is 0.88, and C_p needs to be reduced from 2.20μF by 12% to 1.94μF. With this scheme, however, the DPF under lightly loaded operation is sacrificed, and is notably worse than the original system.

As the system k and $Q_{s0,rated}$ are within the shaded region in Fig. 6-8, the tuning approach suggested in section 6-3 can be applied to achieve load independent unity DPF while ensuring rated power transfer. The required C_{pn} calculated using Table 6-2 is 0.80 and a 20% smaller C_p of 1.76μF is required. Similar to the PP topology, the operating frequency needs to be raised 12% above ω_0 to 22.1kHz. The resulting DPF is shown in Fig. 6-13. The power transfer capability with this modified tuning is compared with the original tuning in Fig. 6-14(a). Under the original tuning rated power is achieved at $Q_{s0,rated}$ of 1.8 (R=1.8Ω), while under the modified tuning rated power is achieved at a smaller Q_{s0} of 1.64 (R=2Ω), labelled as $Q'_{s0,rated}$. Consequently, the required secondary VA rating reduces by 14% from 620VA to 533VA (as shown in Fig. 6-14(b)).

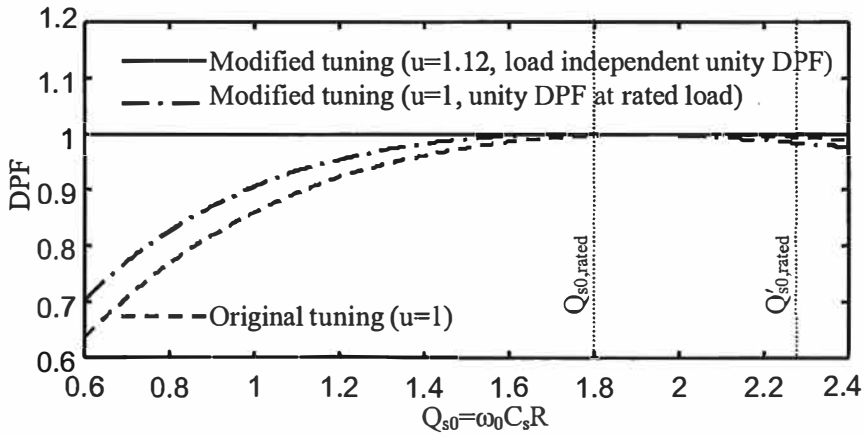

Fig. 6-11. A contact-less electric vehicle battery charger with PP topology – DPF under fixed-frequency operation (a comparison of the original and modified tuning schemes).

InductEV, Inc.
Exhibit 1010
Page 282

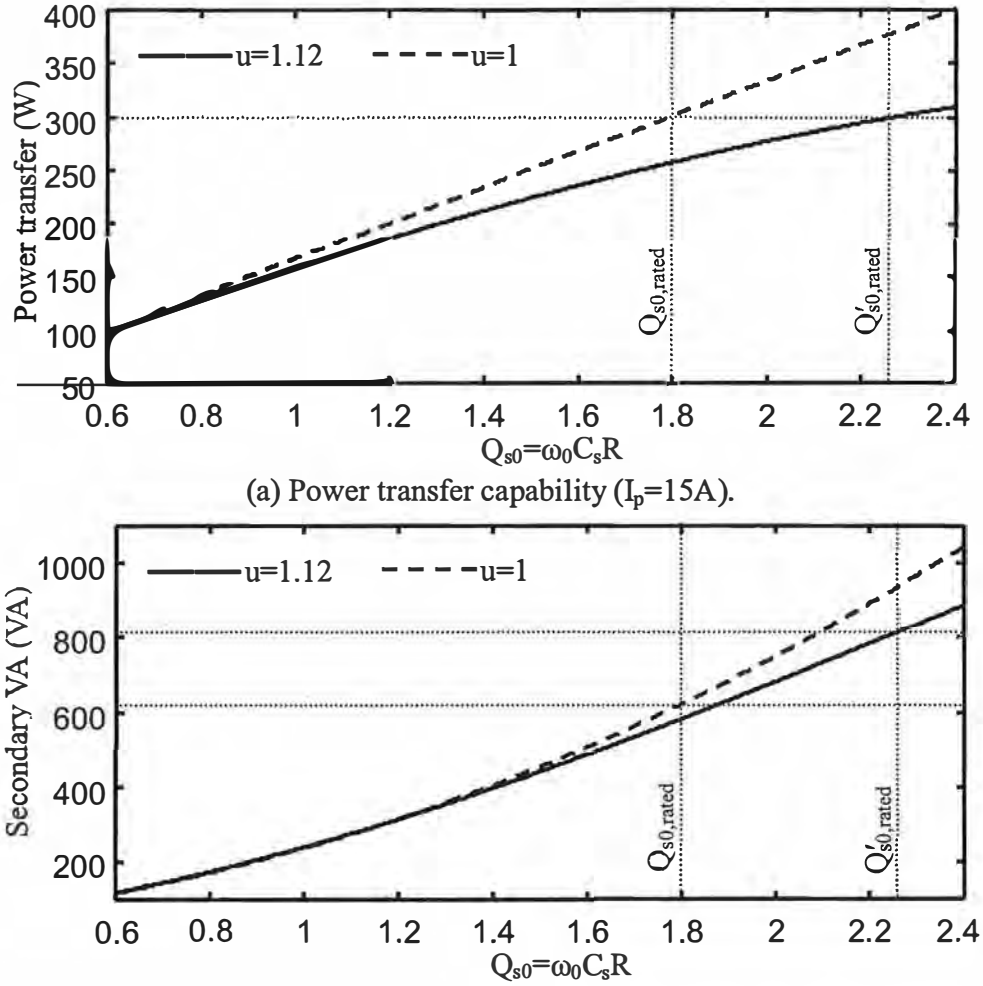

(a) Power transfer capability (I_p=15A).

(b) Required secondary VA rating (I_p=15A).

Fig. 6-12. A contact-less electric vehicle battery charger with PP topology – Power transfer capability and required secondary VA rating under fixed-frequency operation (a comparison of the original and modified tuning schemes).

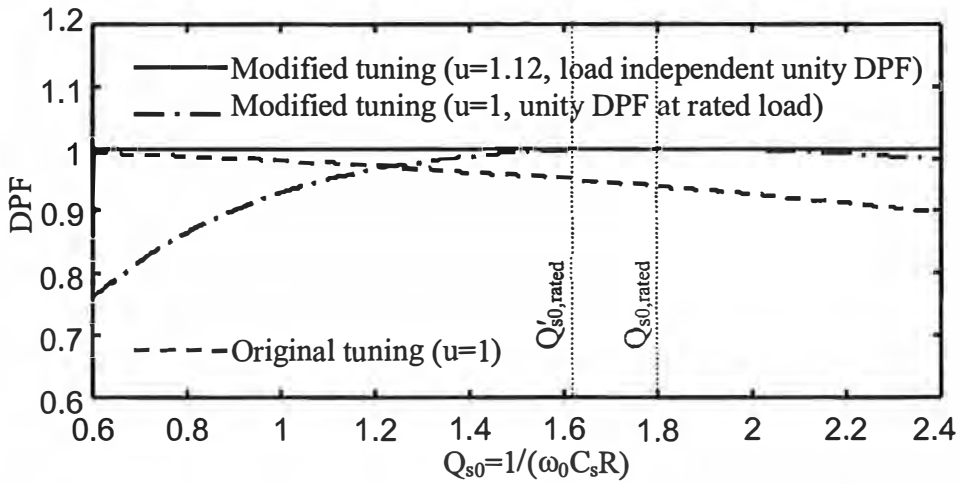

Fig. 6-13. A contact-less electric vehicle battery charger with PS topology – DPF under fixed-frequency operation (a comparison of the original and modified tuning schemes).

InductEV, Inc.
Exhibit 1010
Page 283

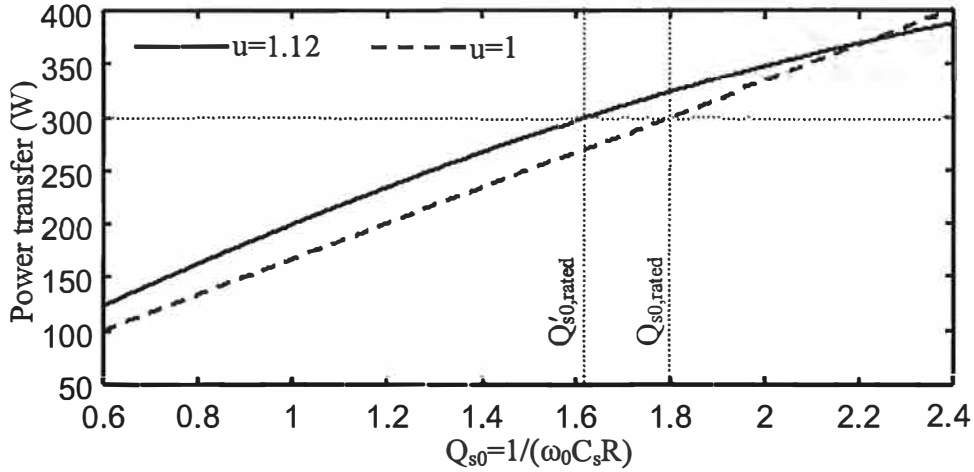

(b) Power transfer capability (I_p=15A).

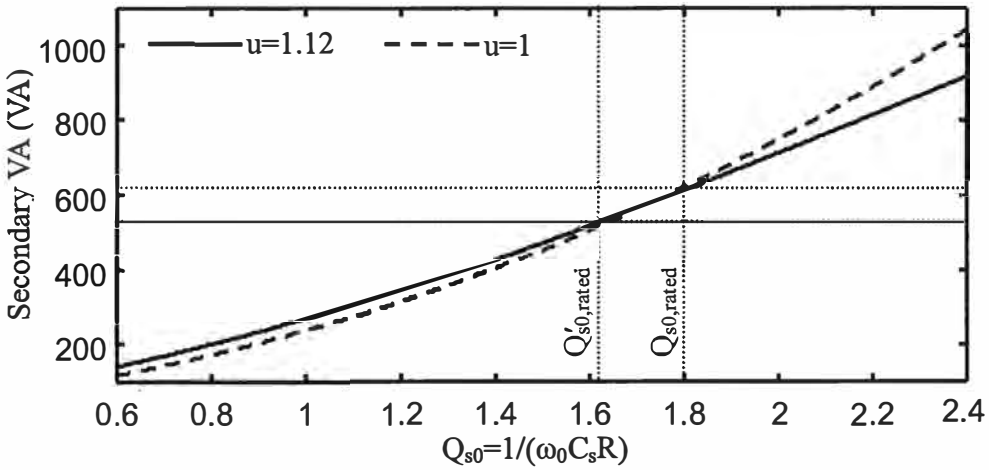

(c) Required secondary VA rating (I_p=15A).

Fig. 6-14. A contact-less electric vehicle battery charger with PS topology – Power transfer capability and required secondary VA rating under fixed-frequency operation (a comparison of the original and modified tuning schemes).

6-6 VERIFICATION

The test system (described in section 4-6) was used to verify the design examples with the modified tuning to achieve load independent unity DPF applied (as discussed above).

The DPF of the power supply was determined by measuring the phase relationship between the discontinuous inverter current (i_i) and the resonant tank voltage (v_p). The measured waveforms of i_i and v_p at the measured loads are shown in Fig. 6-15 (for the PP topology) and Fig. 6-17 (for the PS topology). The fundamental inverter current is closely in phase with the resonant tank voltage for all loads. The measured and predicted power and secondary VA are illustrated in Fig. 6-16 (for the PP topology) and Fig. 6-18 (for the PS topology). Measurements are shown as circles, while the calculated values are shown as solid lines. These results verify the theoretical analysis.

InductEV, Inc.
Exhibit 1010
Page 284

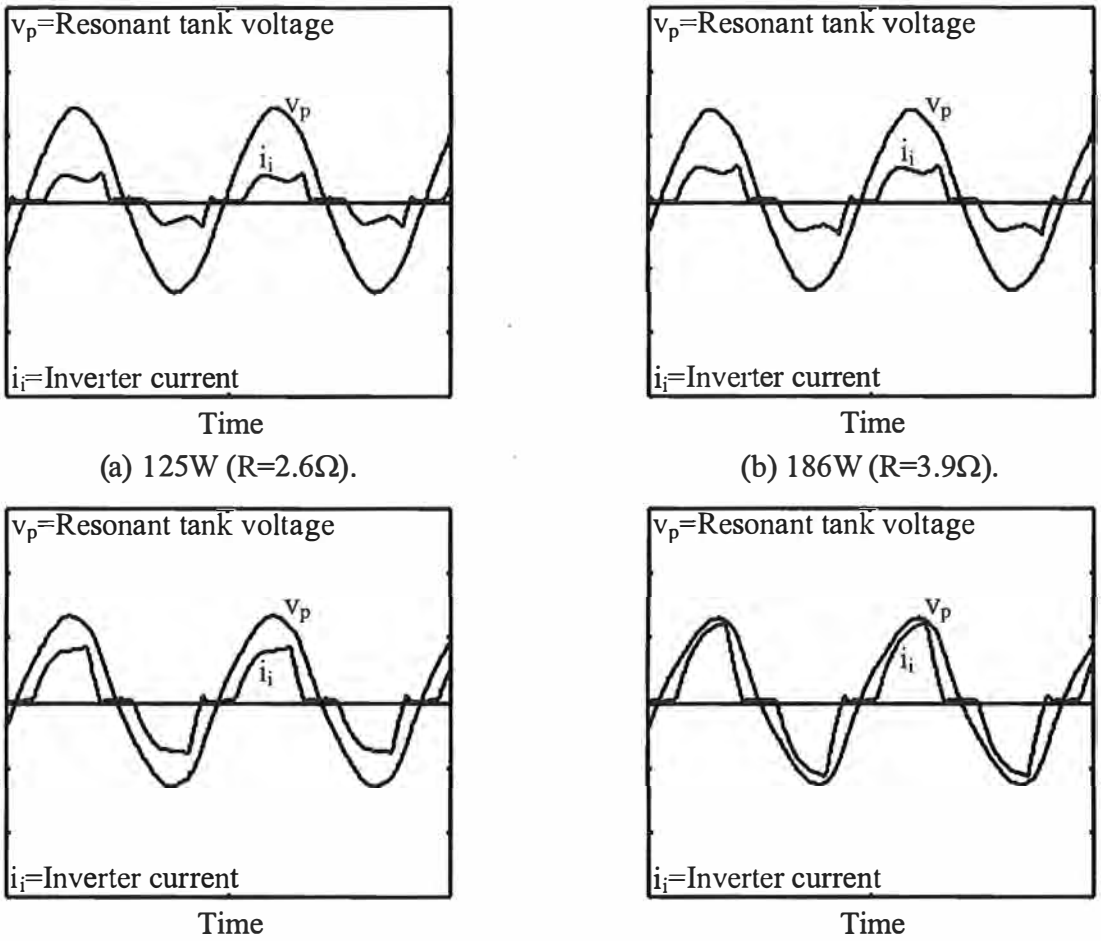

Fig. 6-15. A contact-less electric vehicle battery charger with PP topology, using the modified tuning to achieve load independent unity DPF (C_{pn}=1, u=1.12) - Measured waveforms of the inverter current (i_i) and the resonant tank voltage (v_p).

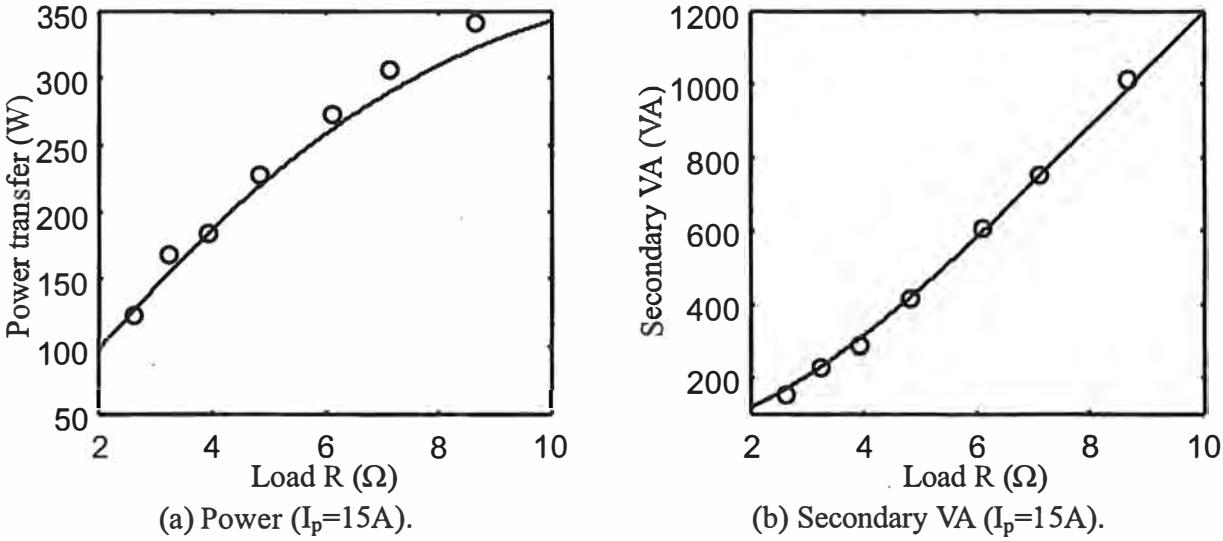

Fig. 6-16. A contact-less electric vehicle battery charger with PP topology, using the modified tuning to achieve load independent unity DPF (C_{pn}=1, u=1.12) - Measured and calculated power and secondary VA.

InductEV, Inc.
Exhibit 1010
Page 285

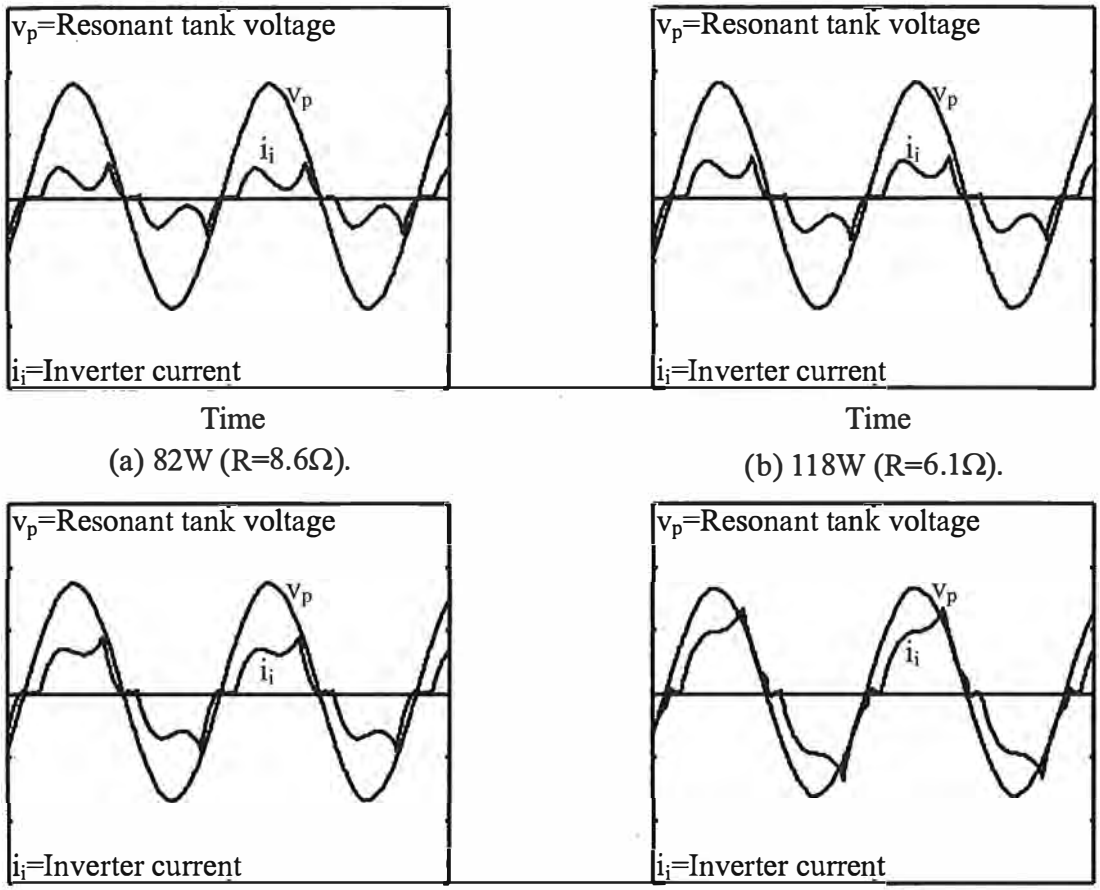

(a) 82W (R=8.6Ω).

(b) 118W (R=6.1Ω).

(c) 175W (R=3.9Ω).

(d) 246W (R=2.6Ω).

Fig. 6-17. A contact-less electric vehicle battery charger with PS topology, using the modified tuning to achieve load independent unity DPF (C_{pn}=0.8, u=1.12) - Measured waveforms of the inverter current (i_i) and the resonant tank voltage (v_p).

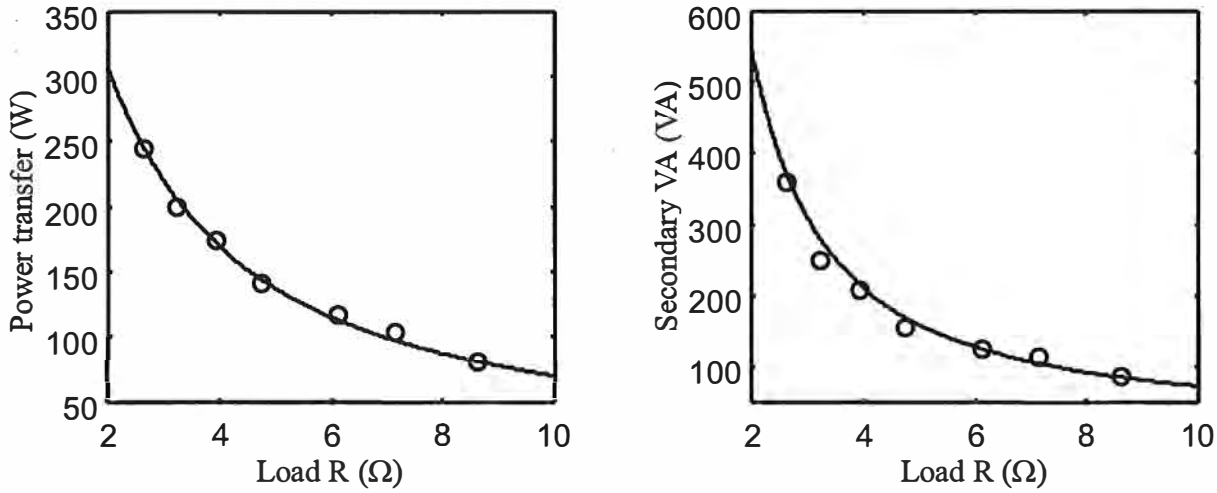

(a) Power (I_p=15A).

(b) Secondary VA (I_p=15A).

Fig. 6-18. A contact-less electric vehicle battery charger with PS topology, using the modified tuning to achieve load independent unity DPF (C_{pn}=0.8, u=1.12) - Measured and calculated power and secondary VA.

InductEV, Inc.
Exhibit 1010
Page 286

6-7 CONCLUSIONS

In this chapter, the primary tuning was modified to improve the displacement power factor (DPF) of the power supply under fixed-frequency operation. With series-compensated primary systems (the SS and SP topologies), load independent unity DPF was found to be achievable at ω_0 ensuring maximum power transfer capability to the pickup. Therefore they are desirable choices for fixed-frequency systems. Due to practical considerations, parallel-compensated primary systems (the PP and PS topologies) may be required and here if the system is constrained to operate at ω_0 unity DPF is achievable only at rated load.

Load independent unity DPF can be achieved in parallel-tuned primary systems providing the operation frequency is deliberately increased above ω_0. This affects the power transfer capability of the pickups and the required secondary VA rating but does not necessarily impact on rated power delivery. Rated power can still be achieved in the majority of ICPT systems that are either loosely coupled systems with reasonable Q_s, or well-coupled systems with low Q_s.

The theory was verified on a practical contact-less electric vehicle battery charging system. The measurements closely follow the predictions.

InductEV, Inc.
Exhibit 1010
Page 287

CHAPTER 7

A SENSITIVITY ANALYSIS OF SYSTEMS USING THE PROPOSED PRIMARY TUNING SCHEMES

7-1 Introduction
7-2 Fundamentals of the sensitivity analysis
7-3 Compensation capacitor selection
7-4 The influence of variations in primary capacitance
7-5 The influence of variations in secondary capacitance
7-6 The influence of misalignment in the electromagnetic structure
7-7 Discussion
7-8 Conclusions

7-1 INTRODUCTION

The design approaches proposed in chapters 4, 5 and 6 assume all components are ideal. This is not true in the real world where real components have losses, parasitics, tolerances and operating variations. This chapter investigates the influence of variations in the primary and secondary compensation capacitances (C_p and C_s) as well as misalignment of the electromagnetic structure (variations in the coupling parameters L_p, L_s and M) in order to determine the relative sensitivity of the various tuning schemes described, while at the same time indicate practical design considerations that should minimize the influence of such variations on the power transfer capability to the pickup and the displacement power factor (DPF) of the power supply.

In order to determine the extent of practical variations that should be considered, this chapter considers the choice of suitable compensation capacitors based on typical high frequency power capability in addition to thermal and lifetime stability. The degree of misalignment and the resulting variations in coupling parameters between the primary and secondary depends on the configuration of the electromagnetic structure and the ICPT application. Typical misalignment and the resulting variations of the coupling parameters are discussed in this context.

The sensitivity of the DPF, the operating frequency and the power transfer capability to variations in C_p, C_s, L_p, L_s and M are compared for systems designed using the original tuning (assumed with the design methodology described in Chapter 4), the modified tuning to achieve unity DPF at rated load (Chapter 5 for variable-frequency systems, and section 6-2 for fixed-frequency systems), and the modified tuning to achieve load independent unity DPF (section 6-3).

As previously shown, the behaviour of an ICPT system depends strongly on the sensitivity of the

InductEV, Inc.
Exhibit 1010
Page 288

load resonant tank (seen by the power supply), which can be characterised by the fundamental design parameters k (the magnetic coupling coefficient) and Q_s (the secondary quality factor). Practical ICPT systems are normally well coupled (high k) with low Q_s or loosely coupled (low k) with reasonable Q_s. In this chapter, a well-coupled electric vehicle battery charger and a loosely coupled monorail material handling system are used for the sensitivity analysis. Both fixed and variable-frequency operations are investigated.

7-2 FUNDAMENTALS OF THE SENSITIVITY ANALYSIS

The sensitivity analysis in this chapter focuses on variations in C_p, L_p, M, C_s and L_s. The fundamental influences of such variations on the power transfer capability and the DPF are discussed in this section for both fixed and variable frequency systems.

As described in earlier chapters, the power transferred from the primary to the secondary is the reflected resistance multiplied by the square of the primary current as given by:

$$P = (\mathrm{Re}\, Z_r) I_p^2 \tag{7-1}$$

where the reflected impedance (Z_r) is given by:

$$Z_r = \frac{\omega^2 M^2}{Z_s} \tag{7-2}$$

with the secondary impedance (Z_s) given by:

$$Z_s = \begin{cases} j\omega L_s + \dfrac{1}{j\omega C_s} + R & \text{series secondary} \\ j\omega L_s + \dfrac{1}{j\omega C_s + \dfrac{1}{R}} & \text{parallel secondary} \end{cases} \tag{7-3}$$

The DPF of the power supply can be determined as:

$$\mathrm{DPF} = \cos(\tan^{-1} \frac{\mathrm{Im} Z_t}{\mathrm{Re}\, Z_t}) \tag{7-4}$$

where the load impedance (Z_t) is given by:

$$Z_t = \begin{cases} \dfrac{1}{j\omega C_p} + j\omega L_p + Z_r & \text{series primary} \\ \dfrac{1}{j\omega C_p + \dfrac{1}{j\omega L_p + Z_r}} & \text{parallel primary} \end{cases} \tag{7-5}$$

InductEV, Inc.
Exhibit 1010
Page 289

As shown, the power transfer capability depends on ω, M, C_s L_s and R, but is independent of C_p and L_p. It is proportional to the square of M and ω, and therefore changes in either of these parameters will have a significant impact on power transfer. The influence that C_s and L_s have on the power transfer capability needs to be considered by investigating their influence on Z_s. In particular, an increase in L_s directly increases Z_s while also detuning the pickup, resulting in reduced power transfer capability, and vice versa. Variations in C_s, however, have a similar but less direct impact. This sensitivity analysis is further complicated by the fact that Z_s depends on the compensation topology of the pickup and is a complex variable depending on ω and R.

DPF depends on L_p, C_p, M, C_s and L_s. The influence of these parameters on DPF needs to be considered by investigating their influence on Z_t which is dependent on both the primary and secondary compensation topologies, and is also a function of ω and R.

According to above, in fixed-frequency systems, variations in C_p and L_p in fixed-frequency systems do not affect the power transfer capability of the pickup providing the primary current (I_p) is controlled constant. The main influence is on the DPF of the power supply. However, variations in ω, M, C_s and L_s affect both the DPF and the power transfer. Thus for the tuning scheme suggested in section 6-3 where ω has been increased to achieve load independent unity DPF, its sensitivity to M, C_s and L_s relative to other schemes is of particular interest.

Under variable-frequency operation, the operating frequency is allowed to vary so that the power supply operates with unity DPF. Variations in C_p, L_p, M, C_s and L_s therefore affect both the operating frequency and the power transfer.

A complete sensitivity analysis is out of the scope of this thesis. This chapter instead focuses on comparing the various tuning schemes discussed in this thesis to determine their relative sensitivities to those component variations.

7-3 COMPENSATION CAPACITOR SELECTION

In an ICPT system, the compensation capacitors must work with high frequency alternating voltage and current. A major consideration when choosing these capacitors is their high frequency power capability, since the apparent power in the compensation networks is usually large. Good capacitance stability is also often required as the system is usually highly sensitive to capacitance variations.

There are three basic types of capacitors: the electrolytic (aluminium and tantalum), the plastic film, and the ceramic. Electrolytic capacitors are normally polarized. The dielectric layers of polar electrolytic capacitors are arranged so that the current is blocked in only one direction, and as such these cannot be used as compensation capacitors in an ICPT system. As such, the following discussion

InductEV, Inc.
Exhibit 1010
Page 290

focuses on plastic film and ceramic types.

The ability of a capacitor to withstand alternating voltage and current is dependent on the operating frequency. This is discussed following by separating the voltage and current limits into three frequency ranges labelled as 'I', 'II' and 'III' in Fig. 7-1, where f_1 and f_2 can be characterised for any particular capacitor as shown in Appendix J.

Below f_1 (Region I), the allowable alternating voltage and current are limited by the dielectric strength of the capacitor. The applied alternating voltage should not exceed the rated ac voltage ($V_{ac,rated}$) and the maximum allowable alternating current is less than the rated ac current ($V_{ac,rated}$). Between f_1 and f_2 (Region II), the allowable alternating voltage and current are less than rated values due to the limitation of the thermal dissipation capability of the capacitor. Above f_2 (Region III), the resistances of the leads, the metal layers, and the soldered and welded joints limit the allowable alternating voltage and current. The applied alternating current should not exceed $I_{ac,rated}$, and the maximum permissible alternating voltage is less than $V_{ac,rated}$.

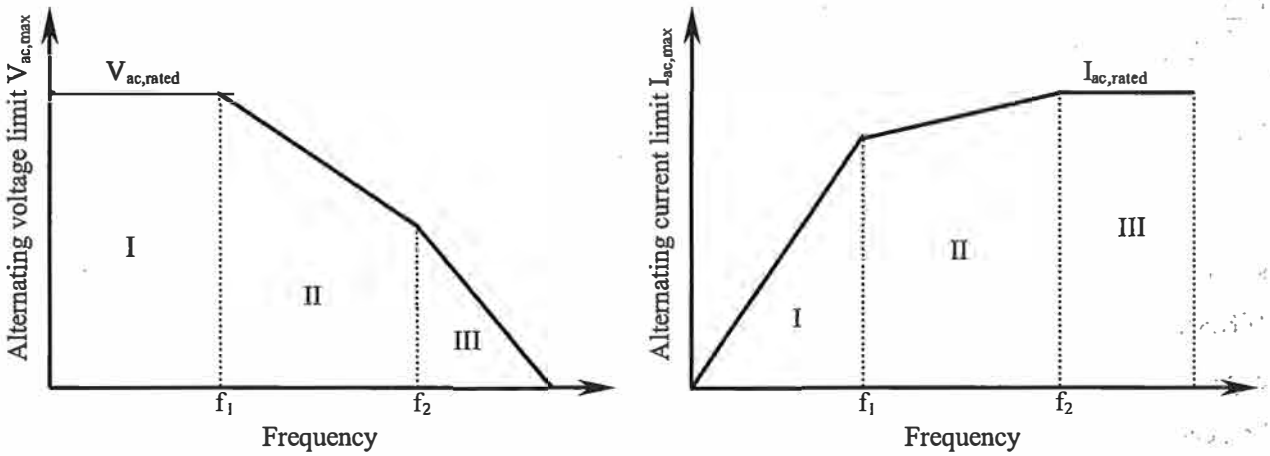

(a) Alternating voltage limit. (b) Alternating current limit.

Fig. 7-1. High frequency power capability of capacitors.

Typical frequency dependences of the dissipation factor of ceramic and plastic film capacitors are shown in Fig. 7-2. The dissipation factor of both capacitor types increases with frequency. Below 100kHz, Class I ceramic capacitors and polypropylene plastic film capacitors have the lowest dissipation factors.

Typical capacitance tolerances of the plastic film and ceramic capacitors are compared in Table 7-1 for selected manufacturers. Generally, better tolerance can be achieved for ceramic capacitors.

InductEV, Inc.
Exhibit 1010
Page 291

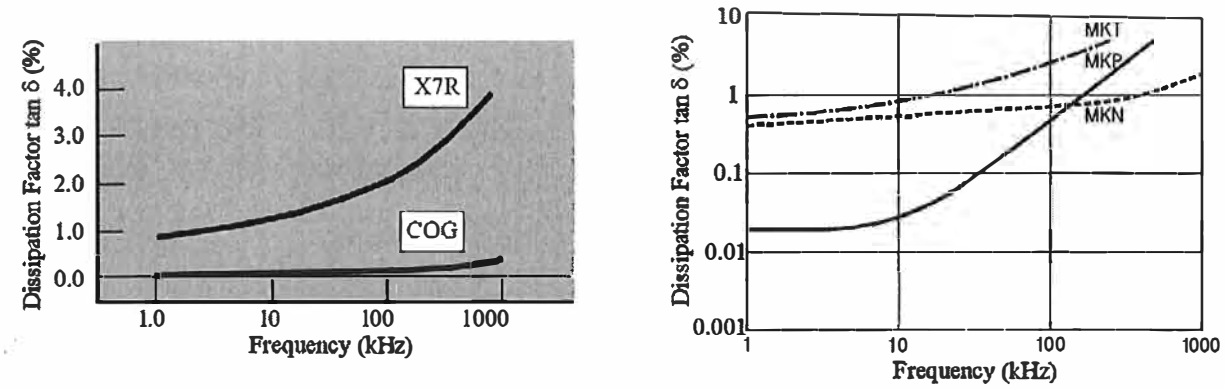

(a) Ceramic capacitors (Source: NOVACAP) – Class I (COG), Class II (X7R).

(b) Plastic film capacitors (Source: EPCOS) – Polyester (MKT/MKN), Polypropylene (MKP).

Fig. 7-2. Typical frequency dependence of the dissipation factor (tan δ) of capacitors.

TABLE 7-1

TYPICAL CAPACITANCE TOLERANCE OF PLASTIC FILM AND CERAMIC CAPACITORS

Manufacturer	Capacitance Tolerance	
	Plastic Film Capacitors	Ceramic Capacitors
EPCOS (Siemens Matsushita)	±5%,±10%,±20%	±1%,±5%,±10%
NIPPON (Marcon)	±3%,±5%,±10%	±20%
WIMA	±5%,±10%,±20%	N.A.
NOVACAP	N.A.	±1%,±5%,±10%

Typical temperature dependences of the capacitance of plastic film and ceramic capacitors are shown in Fig. 7-3. Polyester film capacitors have positive temperature coefficients (MKT, MFT and MKN), such that their capacitance increases with increasing temperature, while polypropylene film capacitors have negative temperature coefficients (MKP and MFP). Class II ceramic capacitors have bad capacitance stability with changing temperature, while Class I ceramic capacitors are comparable to the plastic film capacitor.

Typical long-term capacitance changes in plastic film capacitors are shown in Table 7-2. These are close to the manufacturing tolerances.

Class I ceramic capacitors use non-ferroelectric (paraelectric) materials and virtually have no significant aging characteristics. The aging phenomenon occurs predominantly in Class II ceramic capacitors that use ferroelectric materials especially with a high dielectric constant. Typical capacitance aging characteristics are shown in Fig. 7-4 for Class II ceramic capacitors.

The voltage dependences of the capacitance of typical polyester plastic film capacitors and Class II ceramic capacitors are compared in Fig. 7-5. The polyester capacitor has good capacitance stability with changing voltage, while that of the Class II ceramic capacitor is worse. High voltage dependence results in large non-linear distortion in the alternating voltage and current associated with the capacitor.

InductEV, Inc.
Exhibit 1010
Page 292

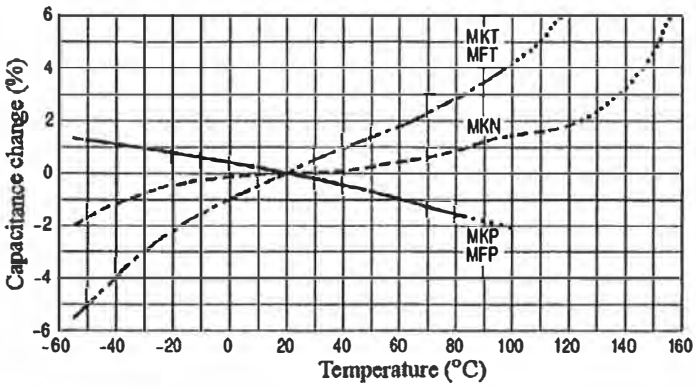

(a) Plastic film capacitors (Source: EPCOS) – Polyester (MKT/MFT/MKN), Polypropylene (MKP/MFP).

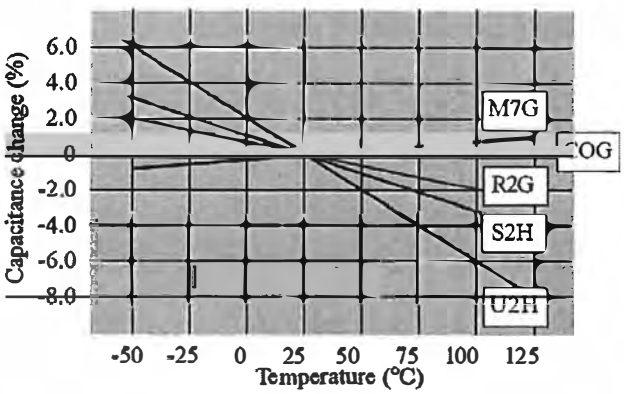

(i) Class I.

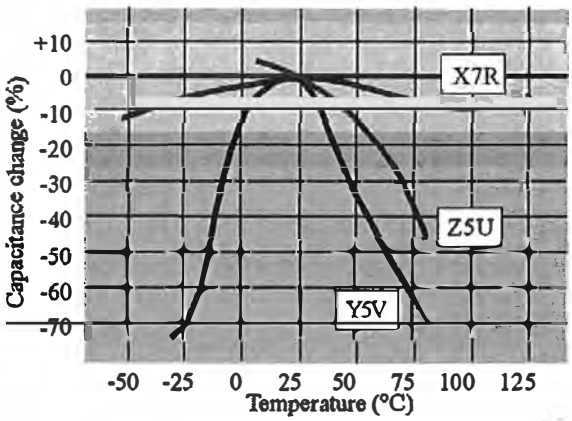

(ii) Class II.

(b) Ceramic capacitors (Source: NOVACAP).

Fig. 7-3. Typical temperature dependence of the capacitance.

TABLE 7-2

LONG TERM CAPACITANCE CHANGE OF PLASTIC FILM CAPACITORS

Manufacturer	Plastic film capacitors
EPCOS (Siemens Matsushita)	±3%
NIPPON (Marcon)	±5%
WIMA	±3%

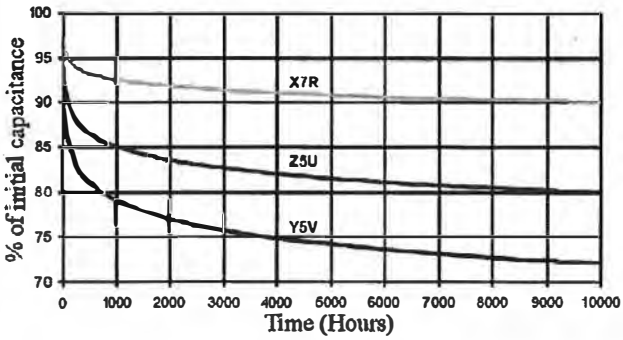

Fig. 7-4. Typical aging (time dependence of the capacitance) – Class II ceramic capacitors (Source: American Technical Ceramics).

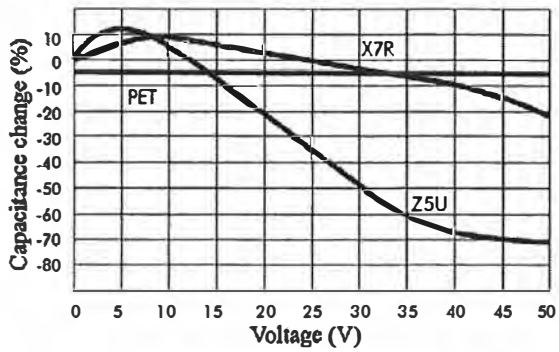

Fig. 7-5. Typical voltage dependence of the capacitance (Source: WIMA) – Polyester plastic film capacitors (PET), Class II ceramic capacitors (X7R/Z5U).

InductEV, Inc.
Exhibit 1010
Page 293

Additional characteristics of plastic film and ceramic capacitors are compared in Table 7-3. The ceramic capacitor has a significantly larger dielectric constant and as such can achieve a higher capacitance per unit volume. However, the plastic film capacitor has a larger range of available capacitance values. The plastic film capacitor also has less dielectric absorption, equivalent series resistance (ESR), and non-linear distortion. Low ESR is a desirable characteristic for capacitors used for high-frequency/high-current ac applications.

According to above discussion, plastic film capacitors are well suited for compensation capacitors in an ICPT system. The polypropylene capacitor in particular has good power capability and lifetime capacitance stability.

TABLE 7-3

TYPICAL CHARACTERISTICS OF PLASTIC FILM AND CERAMIC CAPACITORS (SOURCE: WIMA)

	Plastic film capacitors		Ceramic capacitors	
	Polyester	Polypropylene	NPO (Class I)	X7R (Class II)
Dielectric constant (1kHz, 23°C)	3.3	2.2	12 to 40	700 to 2000
Capacitance range	1000pF to 10μF	100pF to 10μF	1pF to 0.01μF	100pF to 2.2μF
Dielectric absorption (%)	0.5	0.05 to 0.1	0.6	2.5
ESR	low	very low	low	moderate to high
Non-linear distortion	very low	very low	low	high

7-4 THE INFLUENCE OF VARIATIONS IN PRIMARY CAPACITANCE

7-4.1 FIXED-FREQUENCY SYSTEMS

A well-coupled system (electric vehicle battery charging) – This example is described in sections 3-11, 4-6, 5-6 and 6-6. The influence of variations in C_p, when using the tuning scheme proposed in Chapter 4 (here after noted as "original tuning"), is illustrated in Fig. 7-6.

With the frequency fixed at ω_0 (u=1) and the primary current controlled at 15A, the power transfer capability of the system is independent of variations in C_p. The loading condition to achieve rated power of 300W is about 6Ω as shown in Fig. 7-6(a). Percentage variations in DPF as a result of variations in C_p can be determined from Fig. 7-6(b), and for rated load are shown in Fig. 7-6(c). For comparison, the sensitivity of the DPF at a reduced power (150W) is shown in Fig. 7-6(d). At rated power DPF remains close to unity having a small sensitivity to variations in C_p. At reduced power, it is well below unity and has a much higher sensitivity due to increased primary quality factor (Q_p).

InductEV, Inc.
Exhibit 1010
Page 294

Interestingly, the DPF is more sensitive to decreases than increases in C_p.

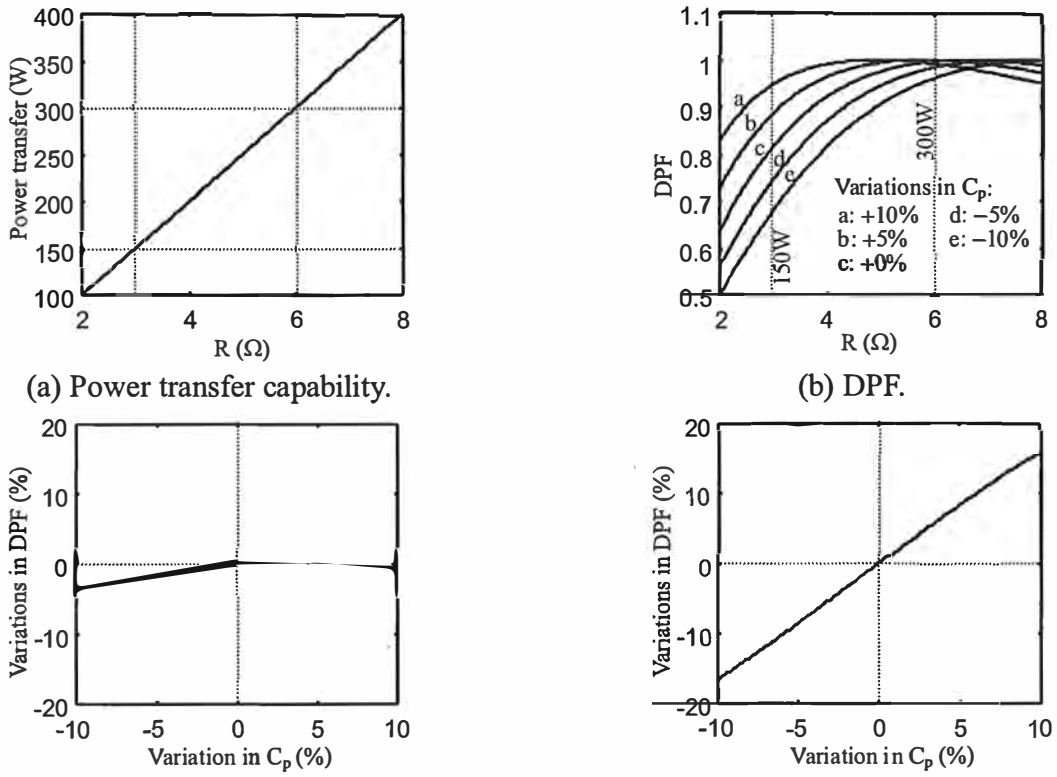

(a) Power transfer capability. (b) DPF.

(c) Sensitivity of the DPF at 300W. (d) Sensitivity of the DPF at 150W.

Fig. 7-6. Original tuning (C_{pn}=1, u=1) – The influence of variations in C_p for an electric vehicle battery charger under fixed-frequency operation (k=0.45, $Q_{s0,rated}$=1.8, PP topology, I_p=15A).

The influence of variations in C_p when using the tuning scheme proposed in section 6-2 (here after noted as "modified tuning for unity DPF at rated load") is illustrated in Fig. 7-7. The operating frequency is also fixed at ω_0. The power transfer capability is therefore identical to the original tuned system. The sensitivity of the DPF to variations in C_p is similar to the original system operating at both rated and light load.

The influence of variations in C_p when using the tuning scheme proposed in section 6-3 (here after noted as "modified tuning for load independent unity DPF") is illustrated in Fig. 7-8. Here the operating frequency is deliberately increased above ω_0 (u=1.12) resulting in reduced power transfer capability to the pickup as described in Chapter 6 and shown in Fig. 7-8(a). Relative to Fig. 7-6(a) and 7-7(a), the loading condition at which rated power (300W) is achieved is 7.6Ω since a higher operating Q_s is necessary. The influence on the DPF can be determined from Fig. 7-8(b). The sensitivity when operating at 300W is once again similar to the original tuning scheme as shown in Fig. 7-8(c). However, the system is less sensitive at light load. Increases and decreases in C_p have identical influences on the DPF at all loading conditions as shown in Fig. 7-8(d).

InductEV, Inc.
Exhibit 1010
Page 295

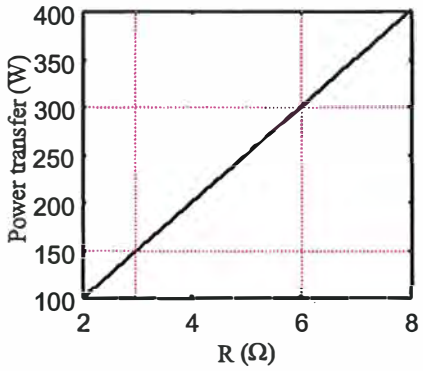

(a) Power transfer capability.

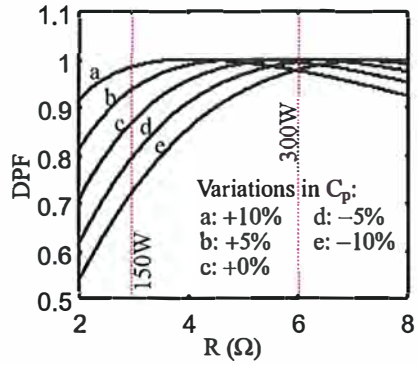

(b) DPF.

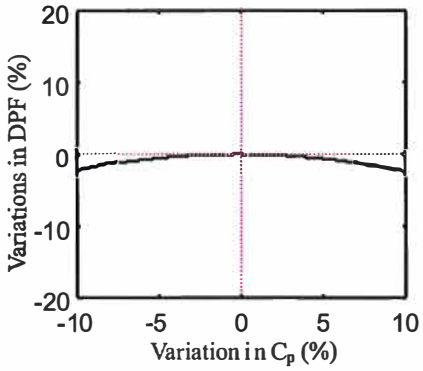

(c) Sensitivity of the DPF at 300W.

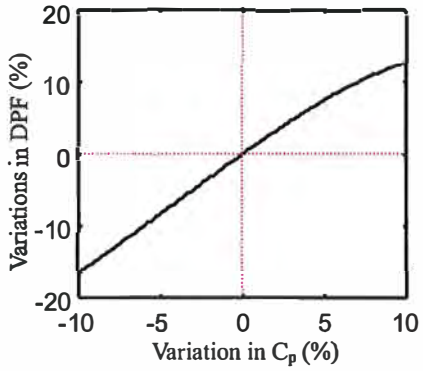

(d) Sensitivity of the DPF at150W.

Fig. 7-7. Modified tuning for unity DPF at rated load (C_{pn}=1.04, u=1) – The influence of variations in C_p for an electric vehicle battery charger under fixed-frequency operation.

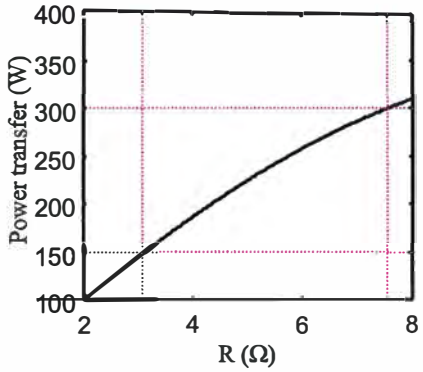

(a) Power transfer capability.

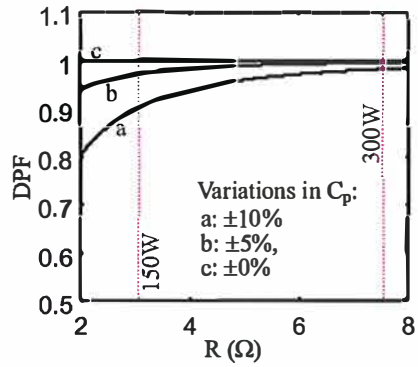

(b) DPF.

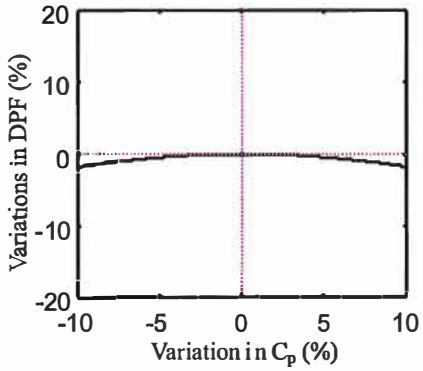

(c) Sensitivity of the DPF at 300W.

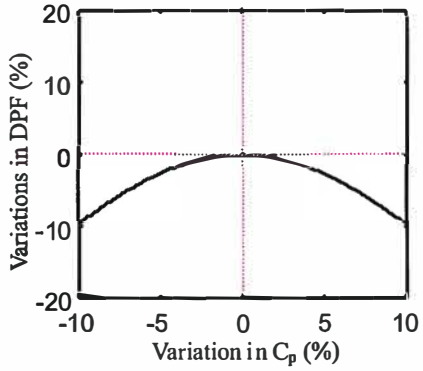

(d) Sensitivity of the DPF at150W.

Fig. 7-8. Modified tuning for load independent unity DPF (C_{pn}=1, u=1.12) – The influence of variations in C_p for an electric vehicle battery charger under fixed-frequency operation.

InductEV, Inc.
Exhibit 1010
Page 296

A loosely coupled system (monorail material handling) – This example is described in [1,2]. The power supply generates a 10-kHz current in the track magnetic circuit. The magnetic circuit is coupled to multiple secondary vehicles and the power transferred to these vehicles is then conditioned to produce a stable supply on the vehicle capable of driving travelling motors. In this example only one vehicle is considered.

The electromagnetic structure is shown in Fig. 7-9. In this system, a single turn primary winding without magnetic material is constructed using parallel cables extending along the track. The secondary winding uses several turns of coil wound on a ferrite core that concentrates the flux generated by the primary current flowing in the track.

Both the primary and secondary of the monorail material handling system are parallel compensated (PP topology). A summary of the system parameters [1,2] is given in Table 7-4. With the selected secondary capacitance of 0.38μF, the secondary resonant frequency is calculated as 10.2kHz. As the pickup winding is magnetically coupled with only a small portion of the extended primary coil, the magnetic coefficient (k) is only 0.086. The primary current is controlled constant at 54A, and the rated power is 800W ($Q_{s0,rated}$=4.7, R=192Ω).

When using the tuning scheme proposed in section 6-2 to achieve unity DPF at rated load while operating at ω_0 (u=1), the required C_{pn} calculated using Table 6-1 is 1.007. As such the required change to the original tuning is negligible.

When using the tuning scheme proposed in section 6-3 to achieve load independent unity DPF, the required C_{pn} is unity and the operating frequency calculated using Table 6-2 is 1.004. Again the necessary change to the original tuning is negligible. The following sensitivity analysis therefore focuses only on the original tuned system (C_{pn}=1, u=1), as this is representative of all tuning schemes.

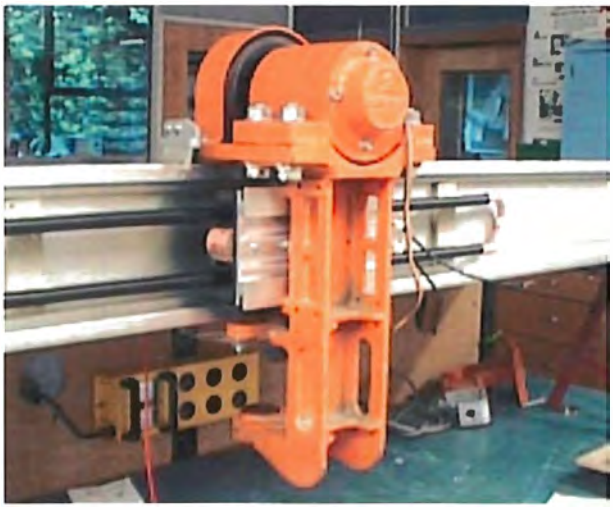

Fig. 7-9. Electromagnetic structure of the monorail material handling system.

InductEV, Inc.
Exhibit 1010
Page 297

TABLE 7-4
PARAMETERS OF THE MONORAIL MATERIAL HANDLING SYSTEM

Nominal frequency (f_0, secondary resonant frequency)	10.2kHz
Primary track current (I_p)	54A
Primary track inductance (L_p)	123μH
Primary track compensation capacitance (C_p)	1.96μF
Pickup mutual inductance (M)	24μH
Secondary pickup self-inductance (L_s)	634μH
Secondary pickup compensation capacitance (C_s)	0.38μF
Secondary pickup rated load (R)	192Ω
Secondary quality factor ($Q_{s0,rated}$)	4.7
Secondary pickup rated power (P)	800W
Magnetic coefficient (k)	0.086

The influence of variations in C_p is illustrated in Fig. 7-10. Here both increases and decreases in C_p have similar influences on the DPF. Because of higher Q_p, the sensitivity of the DPF to variations in C_p is much higher compared to the well-coupled system noted earlier. Similarly, this sensitivity increases under lightly loaded conditions. For reliable operation C_p should not change by more than about 2%. This is difficult to achieve as noted in section 7-3.

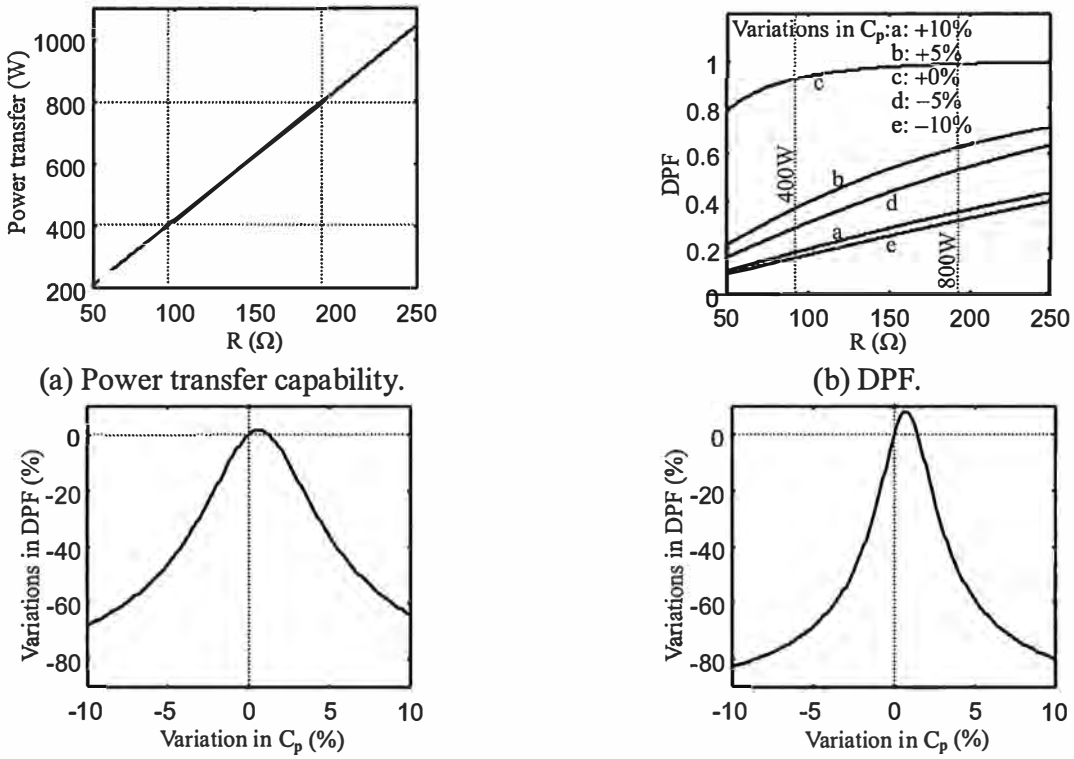

(a) Power transfer capability. (b) DPF.

(c) Sensitivity of the DPF at 800W. (d) Sensitivity of the DPF at 400W.

Fig. 7-10. The influence of variations in C_p for a monorail material handling system under fixed-frequency operation (k=0.086, $Q_{s0,rated}$=4.7, PP topology, C_{pn}=1, u=1).

InductEV, Inc.
Exhibit 1010
Page 298

7-4.2 VARIABLE-FREQUENCY SYSTEMS

A well-coupled system (electric vehicle battery charging) – The influence of variations in C_p for the original system (C_{pn}=1) is illustrated in Fig. 7-11. The operating frequency and power transfer capability when C_{pn} is unity are shown as solid lines. In this design case, bifurcation occurs slightly above rated load. The operating frequency is independent of load providing the operation is restricted within the bifurcation-free area. This load independent frequency (u=1.12) is above ω_0 and as such the pickup does not operate at the maximum power point.

An increase of C_{pn} above unity has two major effects. Firstly, the emergence of bifurcation is at a higher load. Secondly, the operating frequency at light loads becomes closer to ω_0 resulting in higher power transfer capability. The operating frequency at rated load equals ω_0 when C_{pn} is 1.04.

A decrease of C_{pn} below unity also results in the occurrence of bifurcation at higher load. However, the operating frequency for all loading conditions up to rated load shifts further away from ω_0 resulting in lower power transfer capability, which is undesirable.

Assuming operation is restricted within the bifurcation-free region, the loading conditions to achieve rated power (300W) can be determined from the power curves. The operating frequencies at these loading conditions calculated from the frequency curve are shown in Fig. 7-11(c-i). For comparison, the sensitivity of the operating frequency at a reduced power (150W) to variations in C_p is shown in Fig. 7-11(c-ii). This sensitivity is significant at rated power, and becomes slightly lower at reduced power because of reduced secondary quality factor (Q_s).

Fig. 7-12 shows the influence of variations in C_p when using the modified tuning scheme for unity DPF at rated load as described in Chapter 5 for variable-frequency systems. Here the designed C_p using (5-4) is 4% larger than the original tuning. Similar characteristics to the original system (noted in Fig. 7-11) are found.

A loosely coupled system (monorail material handling) – As described in section 7-4.1, the difference between the original tuning and the modified tuning for unity DPF at rated load is negligible as the required change to C_p calculated using (5-4) is very small. As such, the analysis here only focuses on the original system (C_{pn}=1), since the trends are representative of both tuning schemes. Fig. 7-13 shows the influence of variations in C_p.

With a k of 0.086, the maximum Q_{s0} for bifurcation-free operation determined using the bifurcation criterion (Table 5-5 for the PP topology) is 11.6. Since the monorail material handling system with $Q_{s0,rated}$ of 4.7 is well within the bifurcation boundary, it does not bifurcate within normal operating conditions.

With the theoretical C_p, the operating frequency is close to ω_0 (u=1) for all loading conditions. An

InductEV, Inc.
Exhibit 1010
Page 299

increase in C_p results in a shift in the operating frequency below ω_0 (u<1), while decreasing C_p shifts the operating frequency above ω_0 (u>1). The change in operating frequency is similar at all loading conditions and causes the pickup to become detuned. Consequently the power transfer capability to the pickup reduces. In comparison to well-coupled systems (noted in Fig. 7-11 and 7-12), this sensitivity to variations in C_p is lower.

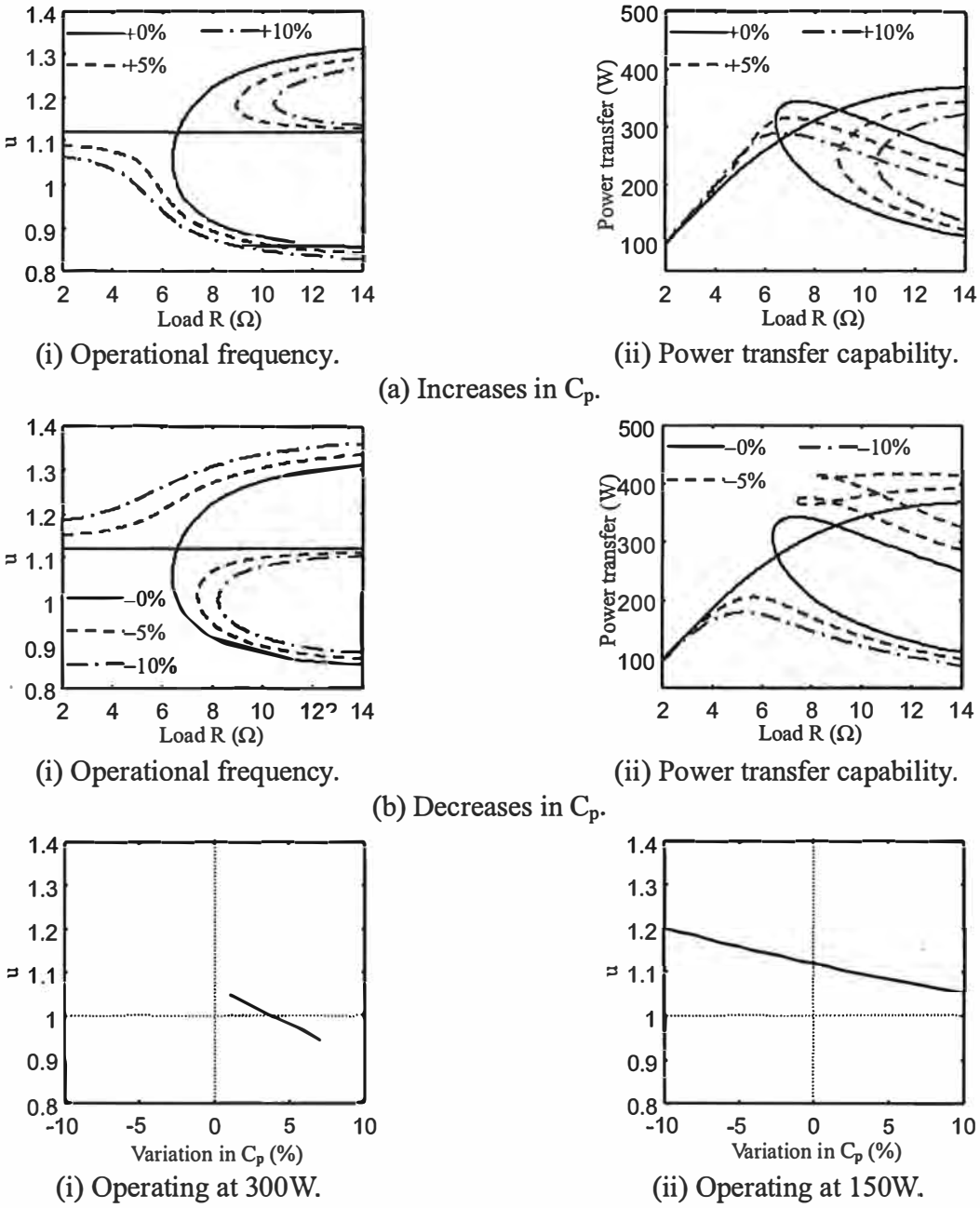

(i) Operational frequency. (ii) Power transfer capability.

(a) Increases in C_p.

(i) Operational frequency. (ii) Power transfer capability.

(b) Decreases in C_p.

(i) Operating at 300W. (ii) Operating at 150W.

(c) Sensitivity of the operating frequency.

Fig. 7-11. Original tuning (C_{pn}=1) – The influence of variations in C_p for an electric vehicle battery charger under variable-frequency operation (k=0.45, $Q_{s0,rated}$=1.8, PP topology, I_p=15A).

InductEV, Inc.
Exhibit 1010
Page 300

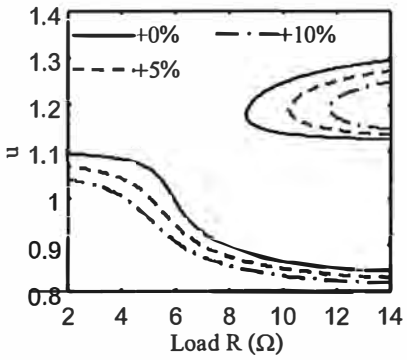

(i) Operational frequency.

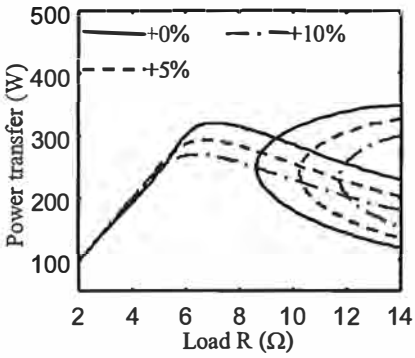

(ii) Power transfer capability.

(a) Increases in C_p.

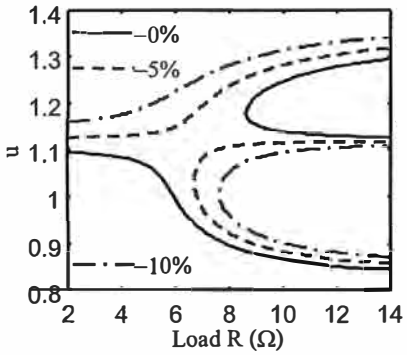

(i) Operational frequency.

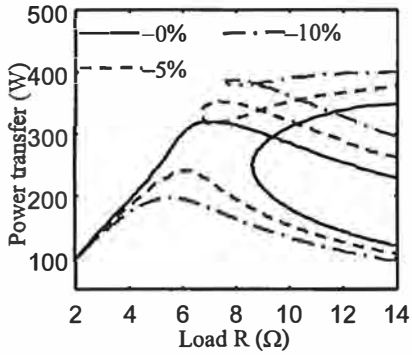

(ii) Power transfer capability.

(b) Decreases in C_p.

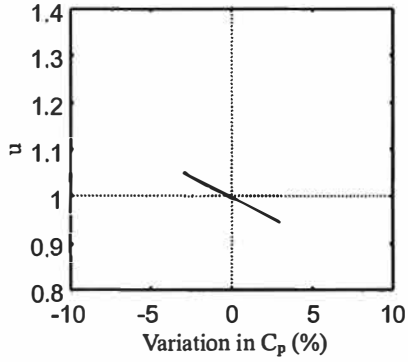

(i) Operating at 300W.

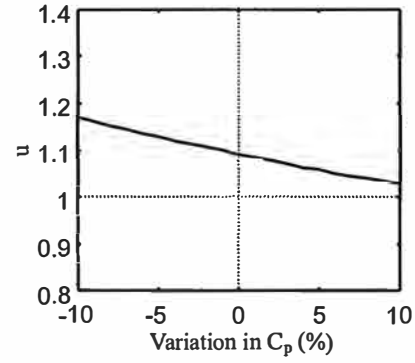

(ii) Operating at 150W.

(c) Sensitivity of the operating frequency.

Fig. 7-12. Modified tuning for unity DPF at rated load (C_{pn}=1.04) – The influence of variations in C_p for an electric vehicle battery charger under variable-frequency operation.

7-5 THE INFLUENCE OF VARIATIONS IN SECONDARY CAPACITANCE

7-5.1 FIXED-FREQUENCY SYSTEMS

A well-coupled system (electric vehicle battery charging) – The influence of variations in C_s are illustrated in Fig. 7-14 for the original tuned system. As discussed in section 7-2, variations in C_s affect

InductEV, Inc.
Exhibit 1010
Page 301

both the DPF and the power transfer capability, but here the influences are found to be small over all loading conditions. Fig. 7-15 shows the influence of variations in C_s when using the modified tuning scheme for unity DPF at rated load. Similar to the original tuned system, both the DPF and the power transfer have low sensitivity to variations in C_s under all loading conditions. Fig. 7-16 shows the influence of variations in C_s when using the modified tuning for load independent unity DPF. In this case, the influence on the power transfer capability is significant. An increase in C_s results in lower power transfer capability as the pickup resonant frequency moves further away from the operating frequency (u), while decreases in C_s improve the power transfer capability since the secondary tuned frequency moves closer to u. The influence on the DPF is however small, especially at light load. Interestingly, increases and decreases in C_s have an identical influence on the DPF. Overall, the sensitivity of the DPF to variations in C_s is small irrespective of load.

A loosely coupled system (monorail material handling) – As shown in Fig. 7-17, variations in C_s have significant influence on both the DPF and the power transfer capability because of higher Q_p and Q_s.

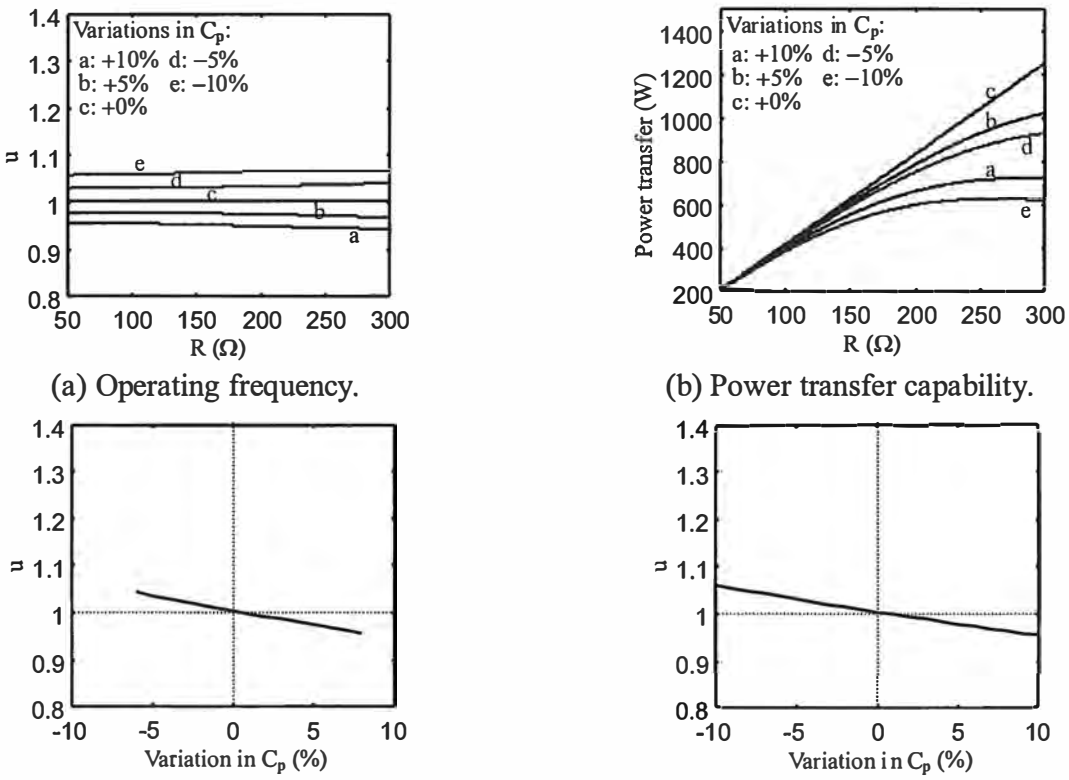

(a) Operating frequency. (b) Power transfer capability.

(c) Sensitivity of u at 800W. (d) Sensitivity of u at 400W.

Fig. 7-13. The influence of variations in C_p for a monorail material handling system under variable-frequency operation (k=0.086, $Q_{s0,rated}$=4.7, PP topology, C_{pn}=1, I_p=54A).

InductEV, Inc.
Exhibit 1010
Page 302

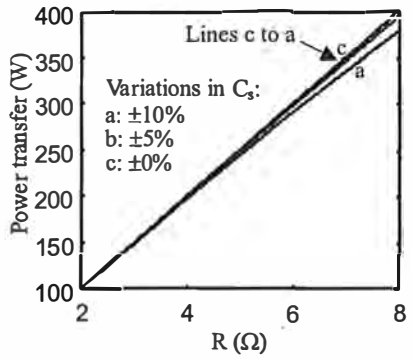

(a) Power transfer capability.

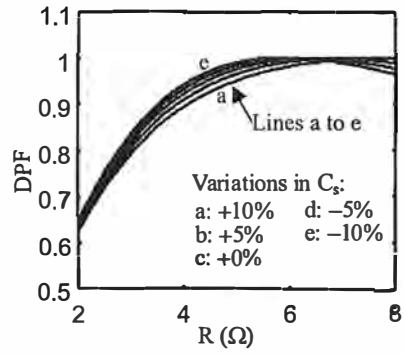

(b) DPF.

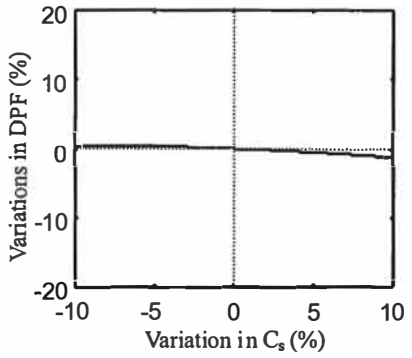

(c) Sensitivity of the DPF at 300W.

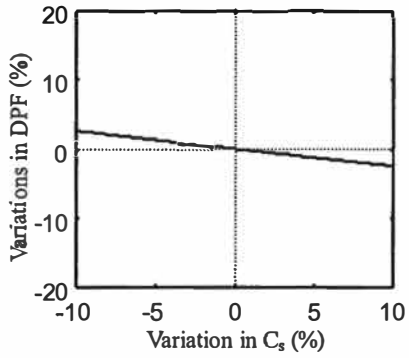

(d) Sensitivity of the DPF at 150W.

Fig. 7-14. Original tuning (C_{pn}=1, u=1) – The influence of variations in C_s for an electric vehicle battery charger under fixed-frequency operation (k=0.45, $Q_{s0,rated}$=1.8, PP topology, I_p=15A).

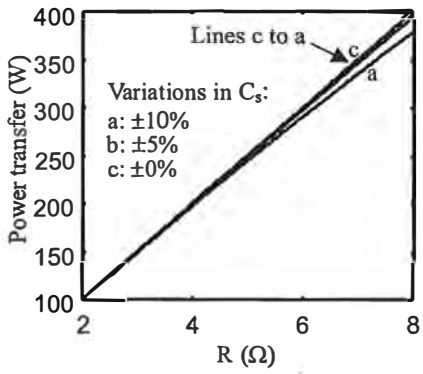

(a) Power transfer capability.

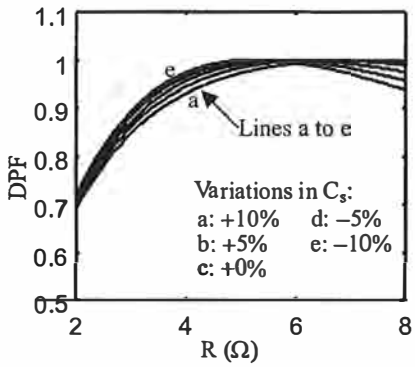

(b) DPF.

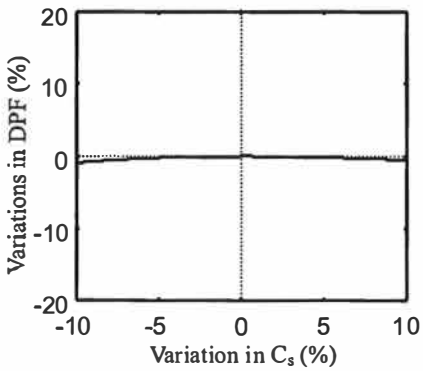

(c) Sensitivity of the DPF at 300W.

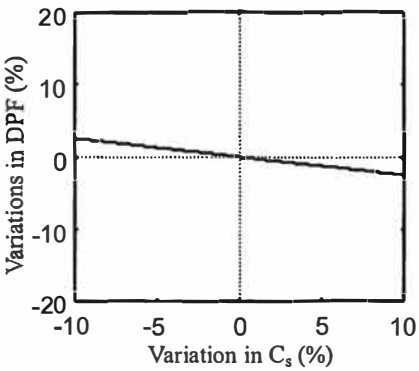

(d) Sensitivity of the DPF at150W.

Fig. 7-15. Modified tuning for unity DPF at rated load (C_{pn}=1.04, u=1) – The influence of variations in C_s for an electric vehicle battery charger under fixed-frequency operation.

InductEV, Inc.
Exhibit 1010
Page 303

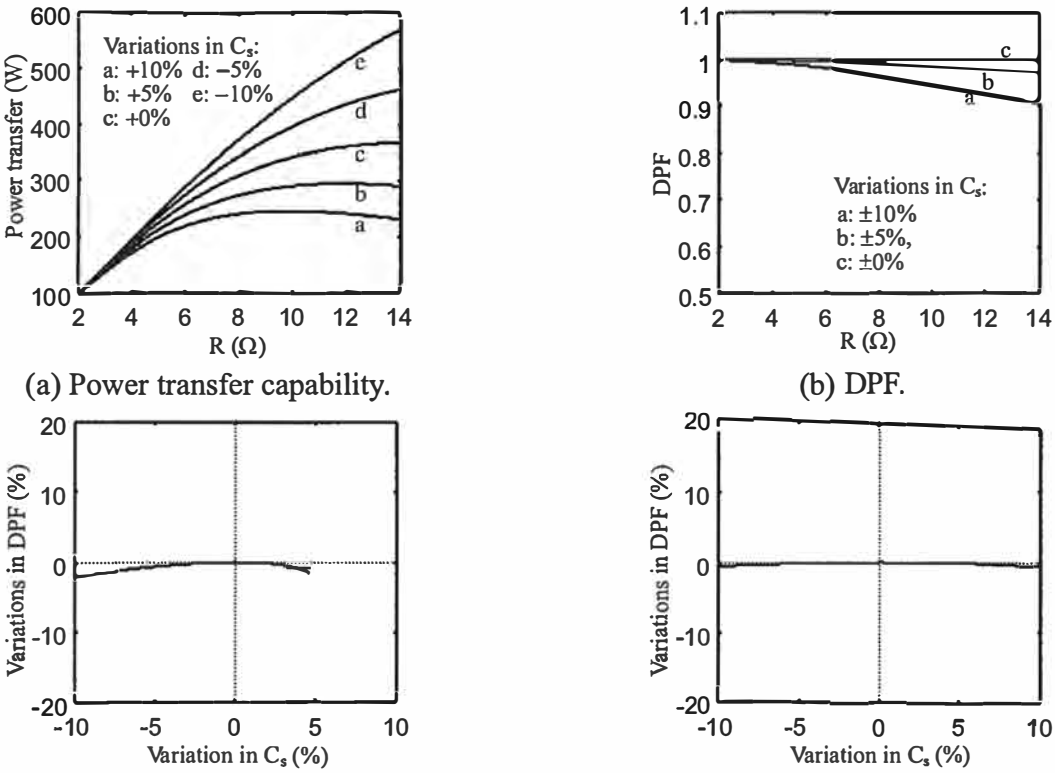

(a) Power transfer capability. (b) DPF.

(c) Sensitivity of the DPF at 300W. (d) Sensitivity of the DPF at150W.

Fig. 7-16. Modified tuning for load independent unity DPF (C_{pn}=1, u=1.12) – The influence of variations in C_s for an electric vehicle battery charger under fixed-frequency operation.

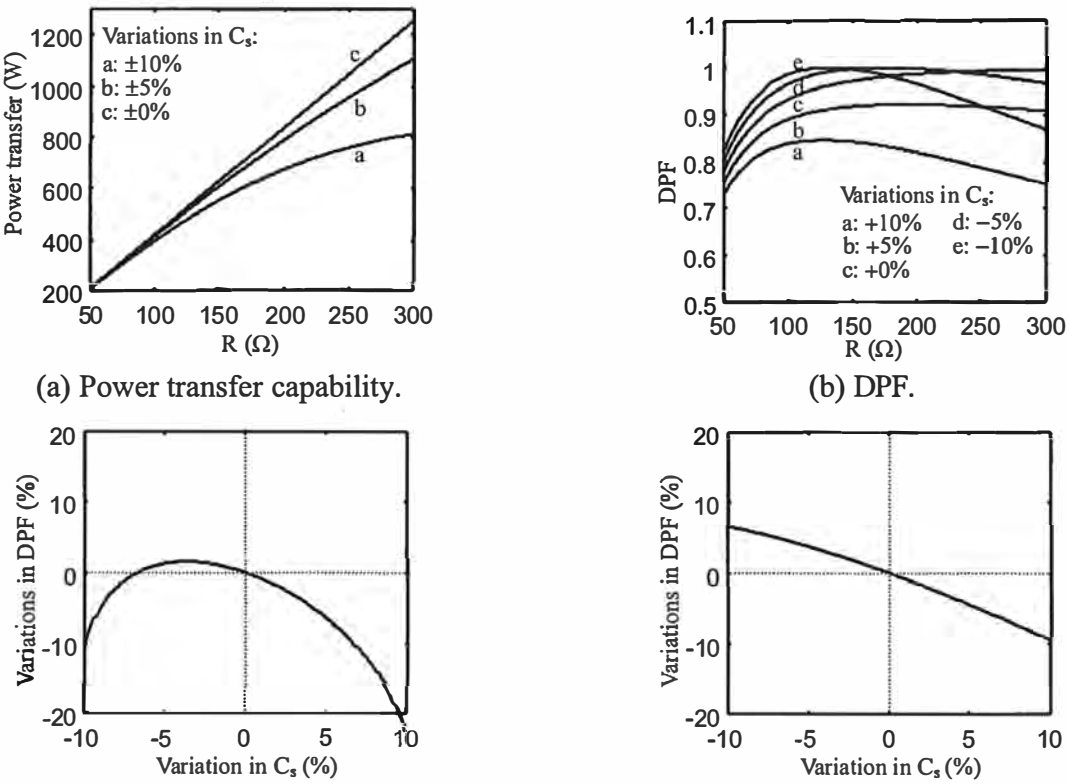

(a) Power transfer capability. (b) DPF.

(c) Sensitivity of the DPF at 800W. (d) Sensitivity of the DPF at 400W.

Fig. 7-17. The influence of variations in C_s for a monorail material handling system under fixed-frequency operation (k=0.086, $Q_{s0,rated}$=4.7, PP topology, C_{pn}=1, u=1).

InductEV, Inc.
Exhibit 1010
Page 304

7-5.2 VARIABLE-FREQUENCY SYSTEMS

A well-coupled system (electric vehicle battery charging) – The influence of variations in C_s are shown in Fig. 7-18 for the original tuned system. The effects of decreasing C_s are similar to those found when C_p is increased, and vice versa. However, the actual sensitivity of the operating frequency to variations in C_s is lower than that found with variations in C_p.

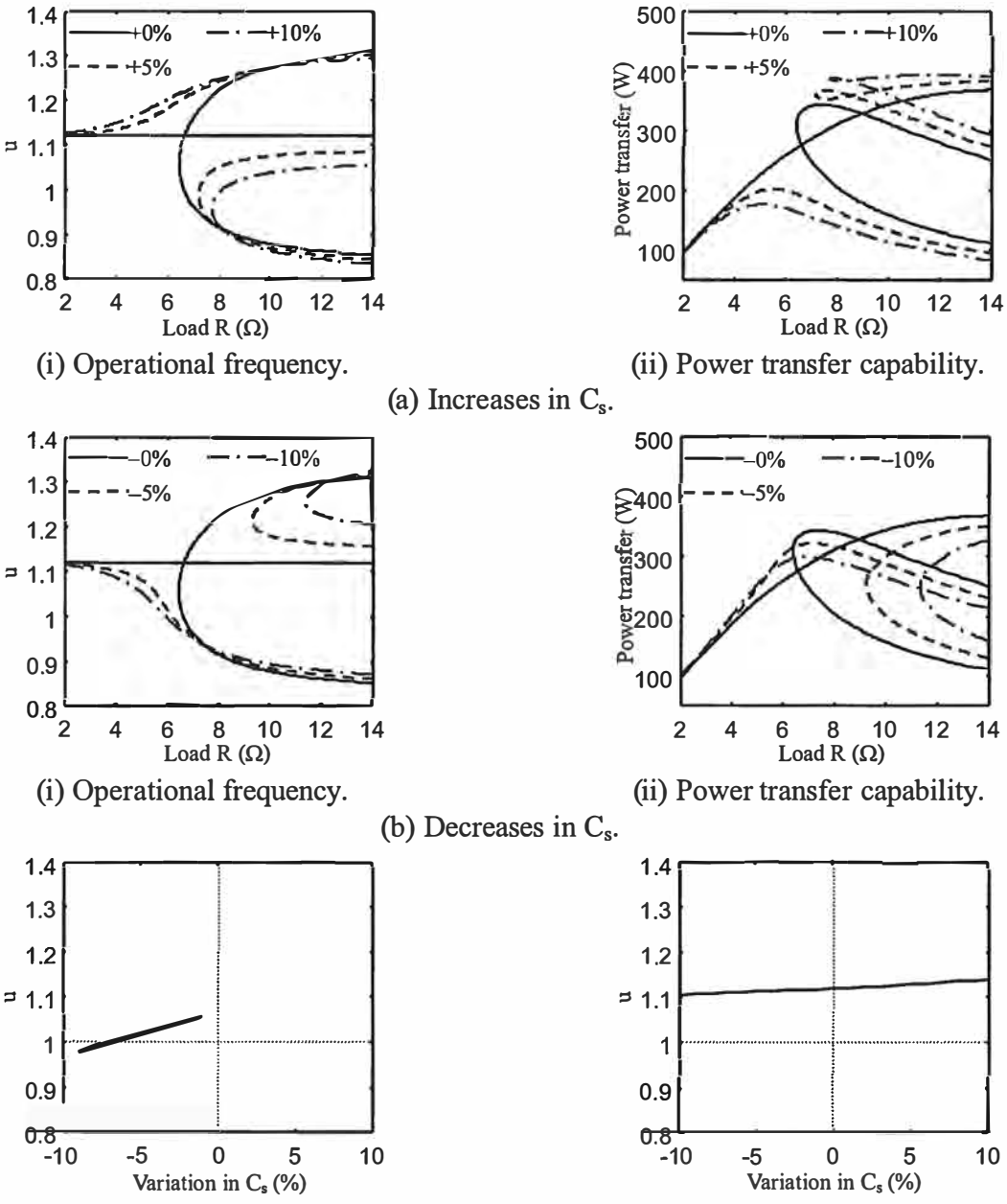

(i) Operational frequency. (ii) Power transfer capability.

(a) Increases in C_s.

(i) Operational frequency. (ii) Power transfer capability.

(b) Decreases in C_s.

(i) Operating at 300W. (ii) Operating at 150W.

(c) Sensitivity of the operating frequency.

Fig. 7-18. Original tuning (C_{pn}=1) – The influence of variations in C_s for an electric vehicle battery charger under variable-frequency operation (k=0.45, $Q_{s0,rated}$=1.8, PP topology, I_p=15A).

InductEV, Inc.
Exhibit 1010
Page 305

Fig. 7-19 shows the influence of variations in C_s when using the modified tuning scheme for unity DPF at rated load. Once again, similar characteristics to the original tuned system are found.

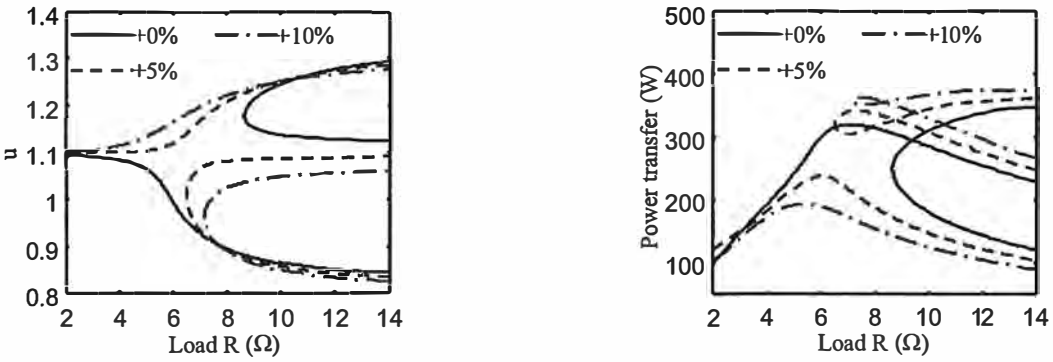

(i) Operational frequency. (ii) Power transfer capability.

(a) Increases in C_s.

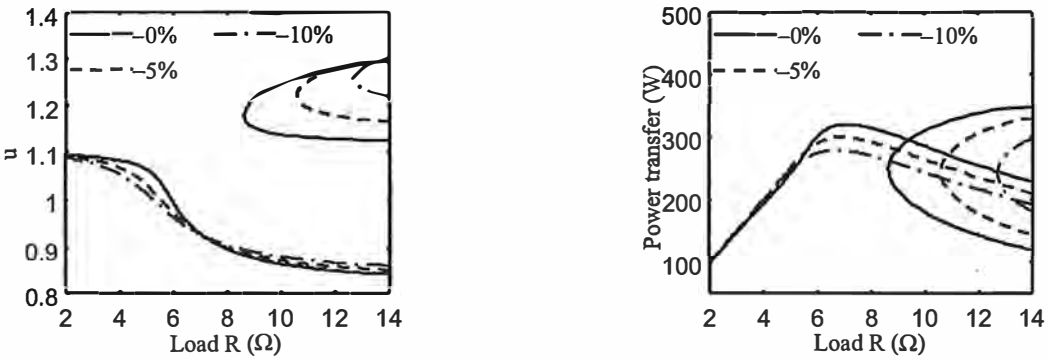

(i) Operational frequency. (ii) Power transfer capability.

(b) Decreases in C_s.

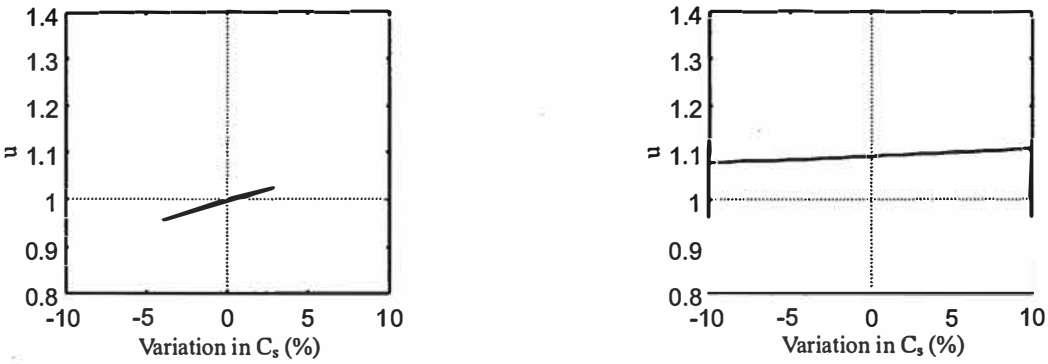

(i) Operating at 300W. (ii) Operating at 150W.

(c) Sensitivity of the operating frequency.

Fig. 7-19. Modified tuning for unity DPF at rated load (C_{pn}=1.04) – The influence of variations in C_s for an electric vehicle battery charger under variable-frequency operation (k=0.45, $Q_{s0,rated}$=1.8, PP topology, I_p=15A).

A loosely coupled system (monorail material handling) – Fig. 7-20 shows the influence of variations in C_s. The influence on the operating frequency is negligible since the loading effects of the pickup on the primary can be neglected. However, the influence on the power transfer capability is significant as the operating Q_s is high and is therefore highly sensitive to pickup tuning.

InductEV, Inc.
Exhibit 1010
Page 306

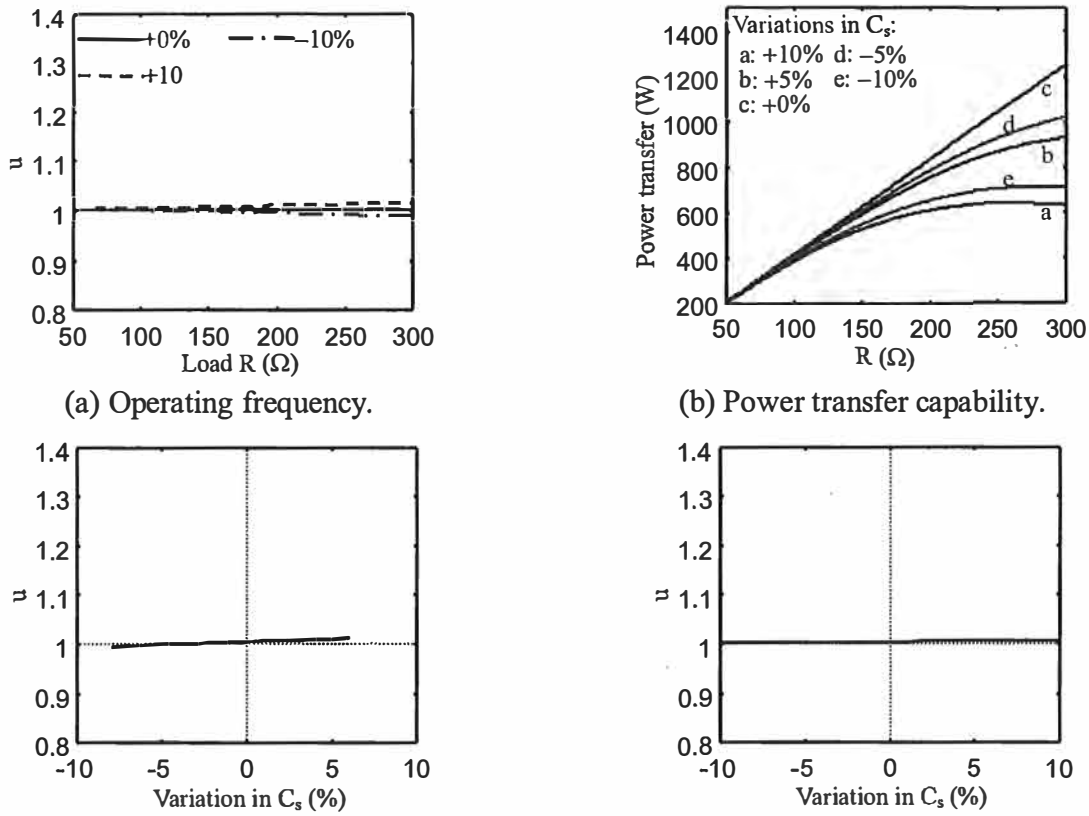

(a) Operating frequency. (b) Power transfer capability.

(c) Sensitivity of the operating frequency at 800W. (d) Sensitivity of the operating frequency at 400W.

Fig. 7-20. The influence of variations in C_s for a monorail material handling system under variable-frequency operation (k=0.086, $Q_{s0,rated}$=4.7, PP topology, C_{pn}=1, I_p=54A).

7-6 THE INFLUENCE OF MISALIGNMENT IN THE ELECTROMAGNETIC STRUCTURE

The amount of misalignment in the electromagnetic structure depends on how the primary and secondary are aligned. Both mechanical and electrical guiding methodologies can be used. For contact-less battery charging of portable consumer products, the product can be designed to sit in a pocket of the battery charger and as such to minimize the misalignment. For the monorail material handling system discussed above, the primary coil is fixed on a rail while the secondary pickup is fixed to a bogie that is guided on the same rail to minimize misalignment. In automatic guided vehicle applications and in contact-less electric vehicle battery charging systems (such as that discussed earlier), vehicles are normally electrically guided in position and may have "significant" misalignment.

The misalignment of the electromagnetic structure results in variations to the coupling parameters (L_p, L_s and M). In fixed-frequency systems, such variations affect the DPF and the power transfer capability. In variable-frequency systems, the main influences of this misalignment are on the operating frequency and the power transfer capability. These influences are investigated in this

InductEV, Inc.
Exhibit 1010
Page 307

section.

7-6.1 COUPLING PARAMETER VARIATIONS IN AN ELECTRIC VEHICLE BATTERY CHARGER

For the contact-less electric vehicle battery charger used in examples throughout this thesis and designed earlier in section 4-6, misalignment of the electromagnetic structure can be defined as variations in air gap, offset and skew angle as shown in Fig. 7-21. A vehicle with a flat tire results in smaller air gap. As the vehicle stops at the charging station, offset and skew angle between the primary and secondary while limited are in practice unavoidable.

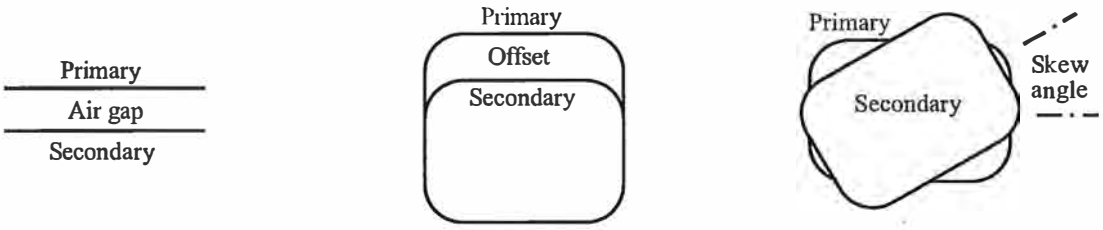

(a) Air gap. (b) Offset. (c) Skew angle.

Fig. 7-21. Misalignment of the contact-less electric vehicle battery charging system.

The primary and secondary self-inductances as well as the mutual inductance were measured for selected air gap, offset and skew angle (measurements are shown in Fig. 7-22 as circles). Increases in all of these factors result in a drop in the coupling parameters. Variations in the air gap are the most significant in comparison to the offset and skew angle as a result of the magnetic design in this system (as shown in Fig. 7-23). As the air gap increases from 10mm to 85mm, the mutual inductance drops to less than a third. The drop of the primary and secondary self-inductance is relatively smaller. Due to the symmetry of the primary and secondary electromagnetic structure, the effects of the skew angle are small.

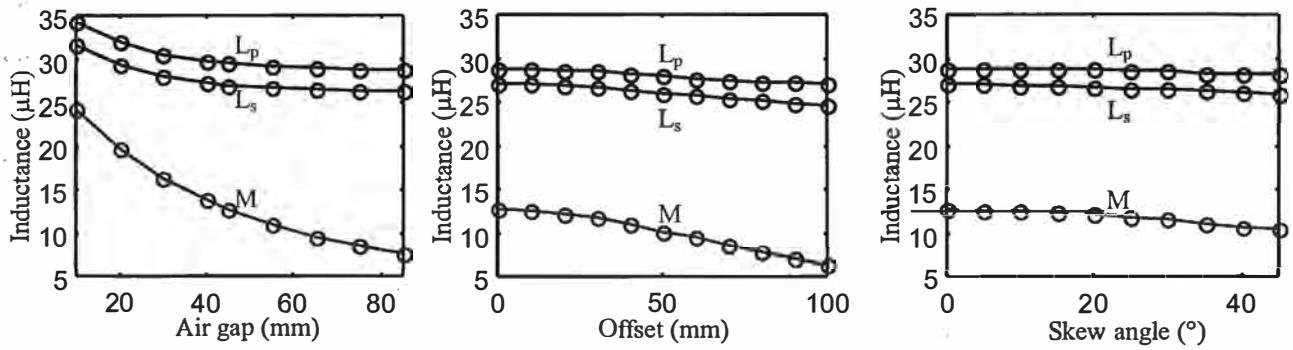

(a) Air gap. (b) Offset. (c) Skew angle.

Fig. 7-22. Measurement of the effects of misalignment on coupling parameters for the contact-less electric vehicle battery charger.

InductEV, Inc.
Exhibit 1010
Page 308

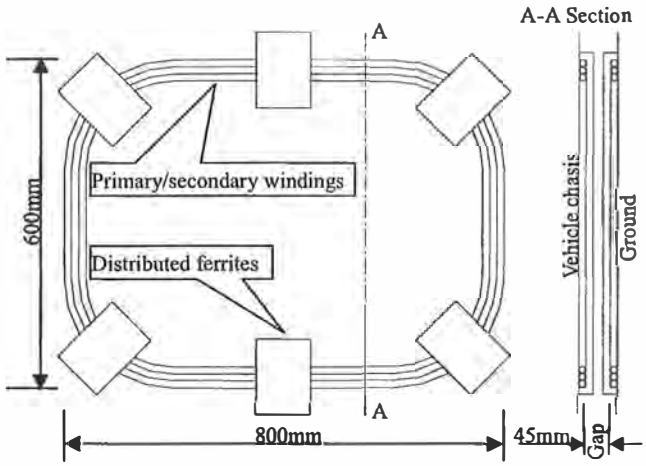

Fig. 7-23. Symmetry of the electromagnetic structure of the battery charger.

7-6.2 FIXED-FREQUENCY SYSTEMS

A well-coupled system (electric vehicle battery charging) – The influence on power and DPF of variations in the coupling parameters (L_p, L_s and M) are illustrated in Fig. 7-24 to 7-32 for each tuning scheme discussed in this thesis. The DPF has a small sensitivity to variations in L_p at rated load for all tuning schemes, but becomes more sensitive at light load due to increased Q_p. Here, systems using the modified tuning for load independent unity DPF have the lowest sensitivity.

The variation in L_s has moderate influences on both the DPF and the power transfer capability in all tuning schemes. Overall, the sensitivity of the DPF to variations in L_s is small under all loading conditions. An increase in L_s results in lower power transfer capability, and as such a higher operating Q_s is required for the same power transfer. In practice, increases in L_s are almost always accompanied by increases in M that are more than enough to compensate for this power drop.

As expected, variations in M influence both the DPF and the power transfer capability in all tuning schemes. In percentage terms, this influence is moderate, however M can change significantly with misalignment so that the influence on DPF and power can be quite large. A decrease in M results in lower power transfer capability and therefore a higher operating Q_s is required for the same power transfer. The sensitivity of the DPF to variations in M is small at rated load, but becomes more sensitive at light load due to increased Q_p. Systems using the modified tuning for load independent unity DPF have the lowest sensitivity at light load.

A loosely coupled system (monorail material handling) – The influence of variations in the coupling parameters are shown in Fig. 7-33 to 7-35. The DPF is highly sensitive to variations in L_p because Q_p is high. The sensitivity of DPF to variations in L_s is significant at rated load, and becomes lower at light load due to reduced influence of the pickup on the primary. The sensitivity of DPF to variations in M is small. Variations in M and L_s have significant influences on the power transfer

InductEV, Inc.
Exhibit 1010
Page 309

capability because of Q_s.

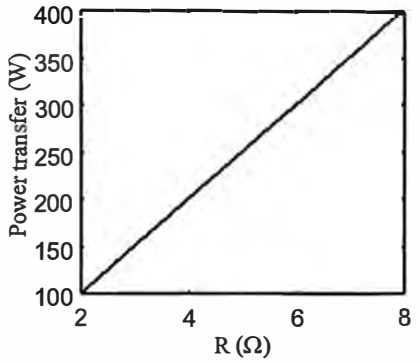

(a) Power transfer capability.

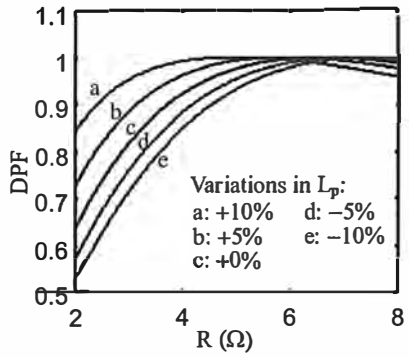

(b) DPF.

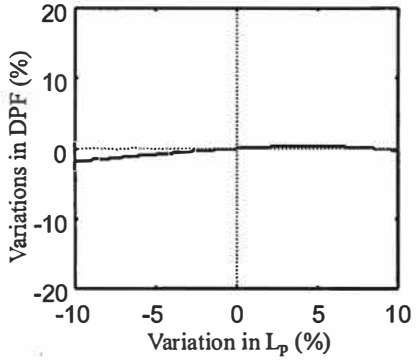

(c) Sensitivity of the DPF at 300W.

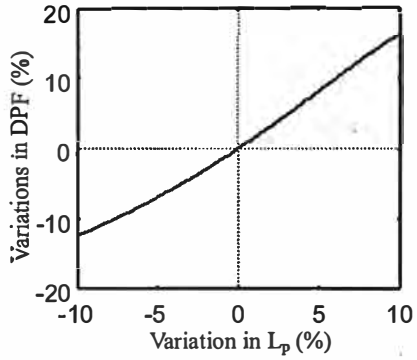

(d) Sensitivity of the DPF at 150W.

Fig. 7-24. Original tuning (C_{pn}=1, u=1) – The influence of variations in L_p for an electric vehicle battery charger under fixed-frequency operation (k=0.45, $Q_{s0,rated}$=1.8, PP topology, I_p=15A).

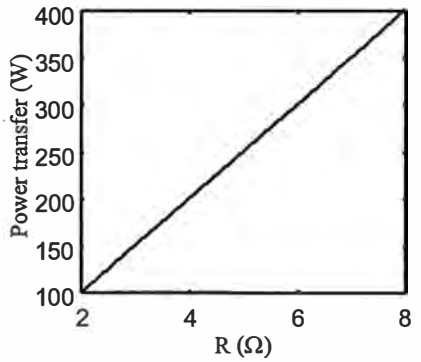

(a) Power transfer capability.

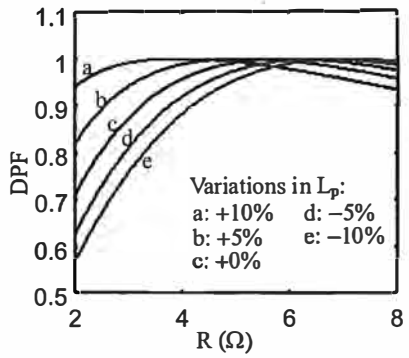

(b) DPF.

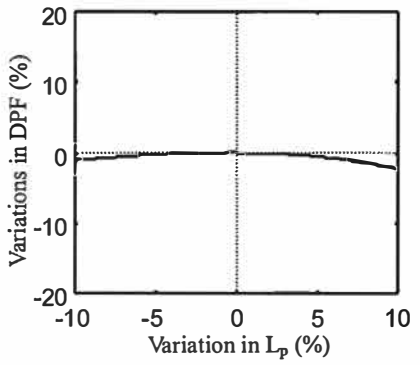

(c) Sensitivity of the DPF at 300W.

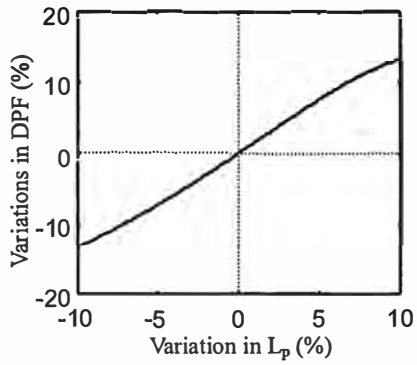

(d) Sensitivity of the DPF at150W.

Fig. 7-25. Modified tuning for unity DPF at rated load (C_{pn}=1.04, u=1) – The influence of variations in L_p for an electric vehicle battery charger under fixed-frequency operation.

InductEV, Inc.
Exhibit 1010
Page 310

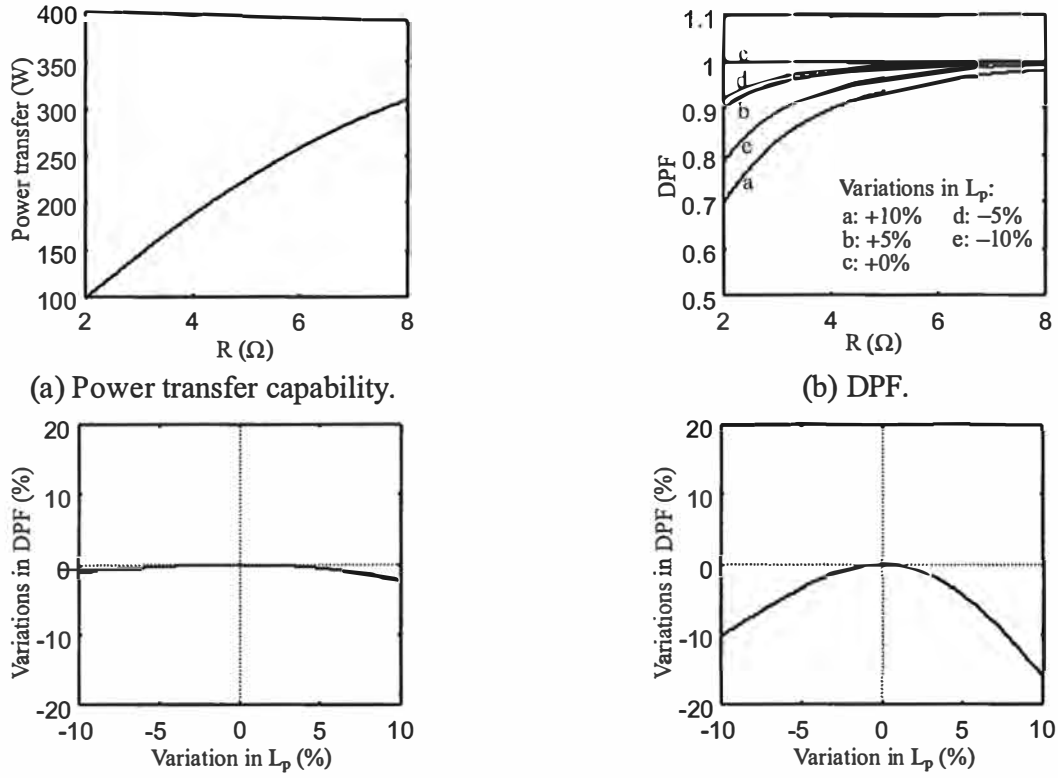

(a) Power transfer capability. (b) DPF.

(c) Sensitivity of the DPF at 300W. (d) Sensitivity of the DPF at150W.

Fig. 7-26. Modified tuning for load independent unity DPF (C_{pn}=1, u=1.12) – The influence of variations in L_p for an electric vehicle battery charger under fixed-frequency operation.

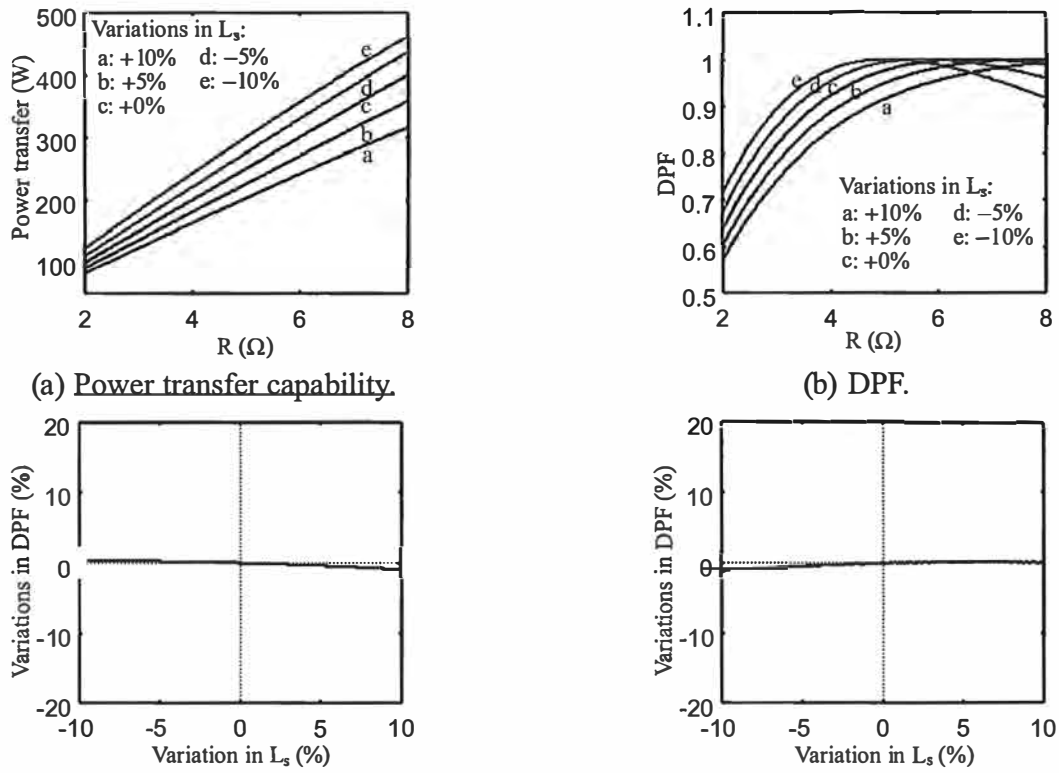

(a) Power transfer capability. (b) DPF.

(c) Sensitivity of the DPF at 300W. (d) Sensitivity of the DPF at 150W.

Fig. 7-27. Original tuning (C_{pn}=1, u=1) – The influence of variations in L_s for an electric vehicle battery charger under fixed-frequency operation (k=0.45, $Q_{s0,rated}$=1.8, PP topology, I_p=15A).

InductEV, Inc.
Exhibit 1010
Page 311

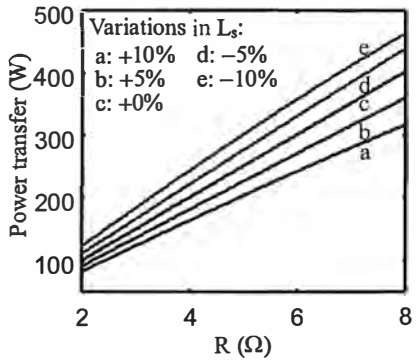

(a) Power transfer capability.

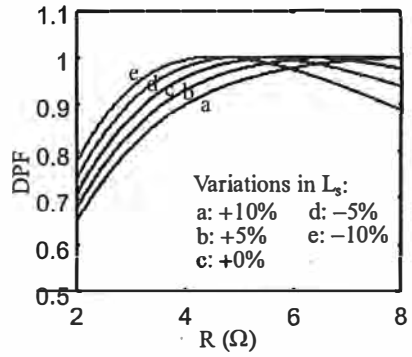

(b) DPF.

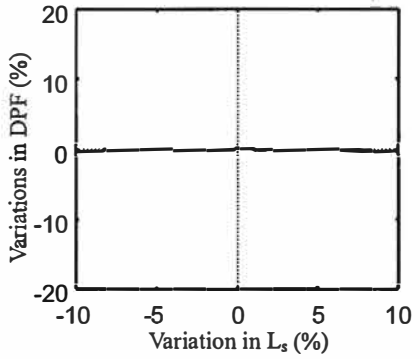

(c) Sensitivity of the DPF at 300W.

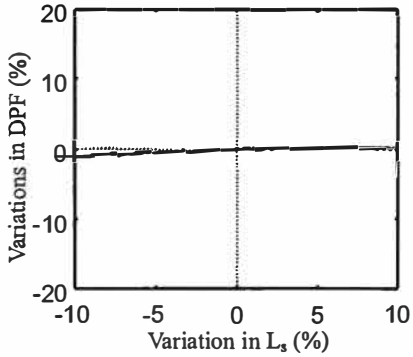

(d) Sensitivity of the DPF at150W.

Fig. 7-28. Modified tuning for unity DPF at rated load (C_{pn}=1.04, u=1) – The influence of variations in L_s for an electric vehicle battery charger under fixed-frequency operation.

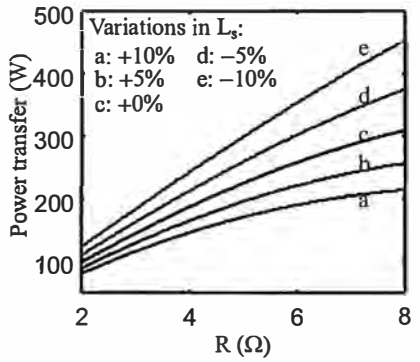

(a) Power transfer capability.

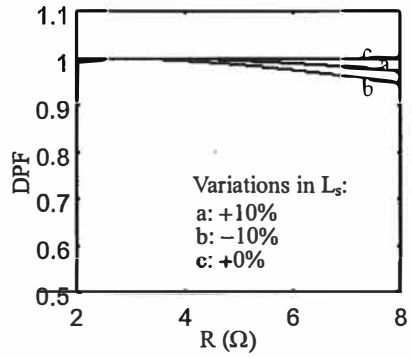

(b) DPF.

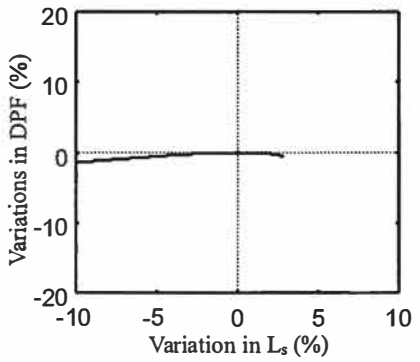

(c) Sensitivity of the DPF at 300W.

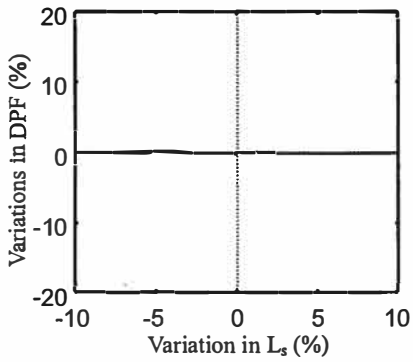

(d) Sensitivity of the DPF at150W.

Fig. 7-29. Modified tuning for load independent unity DPF (C_{pn}=1, u=1.12) – The influence of variations in L_s for an electric vehicle battery charger under fixed-frequency operation.

InductEV, Inc.
Exhibit 1010
Page 312

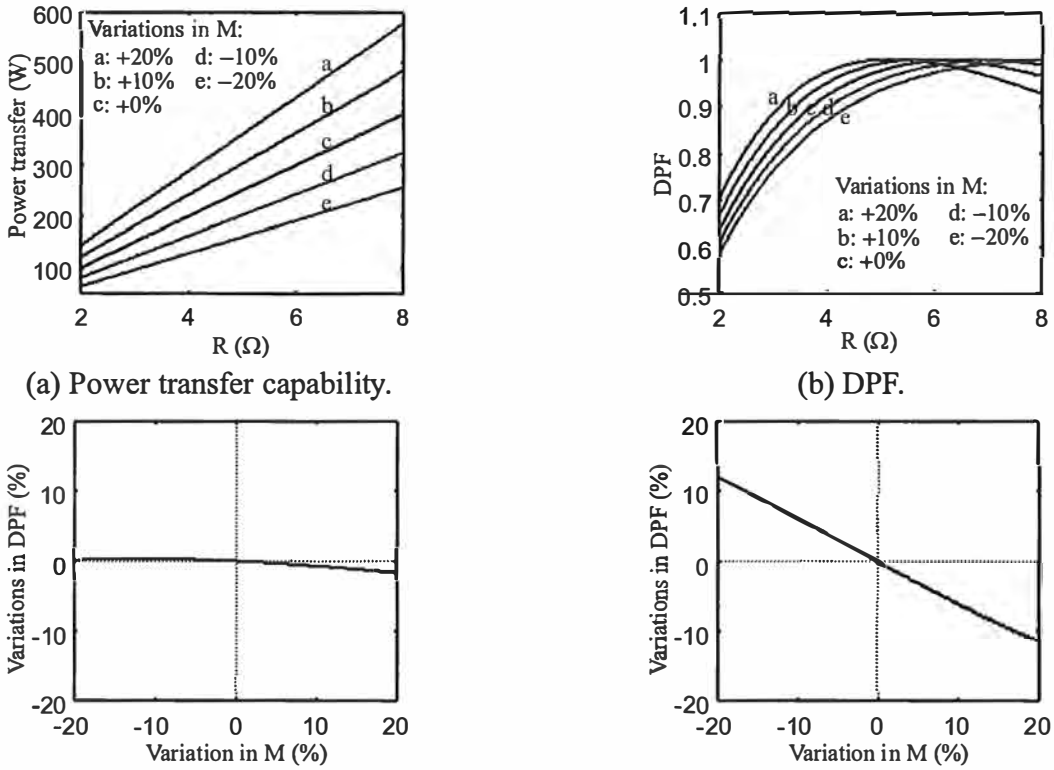

(a) Power transfer capability. (b) DPF.

(c) Sensitivity of the DPF at 300W. (d) Sensitivity of the DPF at 150W.

Fig. 7-30. Original tuning (C_{pn}=1, u=1) – The influence of variations in M for an electric vehicle battery charger under fixed-frequency operation (k=0.45, $Q_{s0,rated}$=1.8, PP topology, I_p=15A).

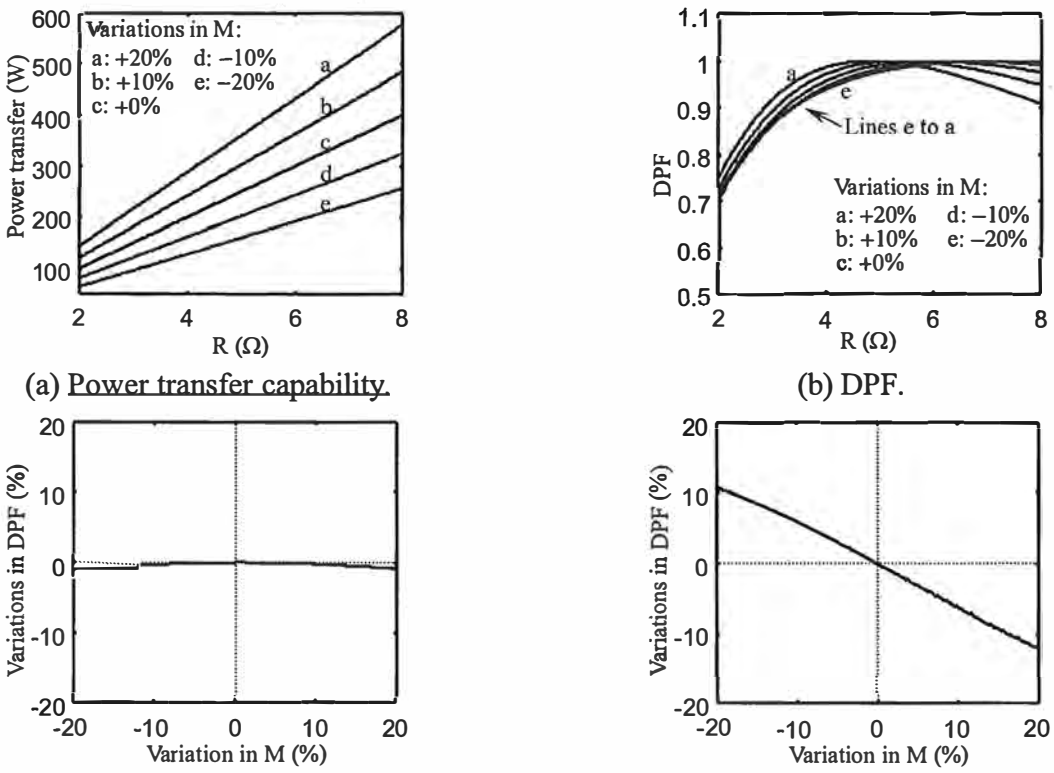

(a) Power transfer capability. (b) DPF.

(c) Sensitivity of the DPF at 300W. (d) Sensitivity of the DPF at150W.

Fig. 7-31. Modified tuning for unity DPF at rated load (C_{pn}=1.04, u=1) – The influence of variations in M for an electric vehicle battery charger under fixed-frequency operation.

InductEV, Inc.
Exhibit 1010
Page 313

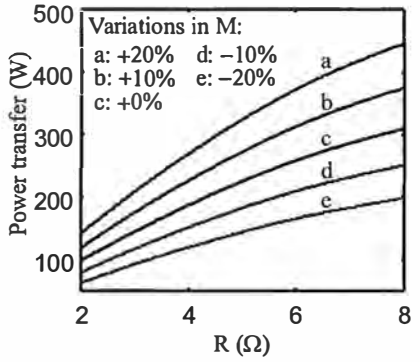

(a) Power transfer capability.

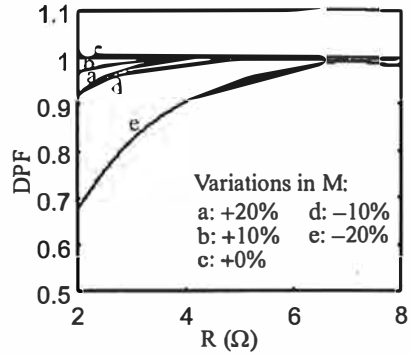

(b) DPF.

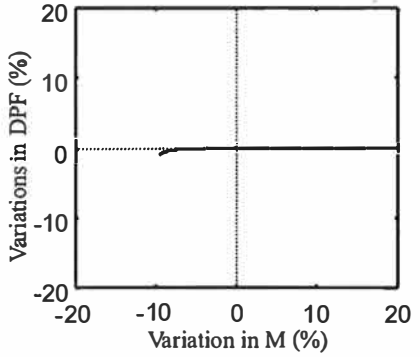

(c) Sensitivity of the DPF at 300W.

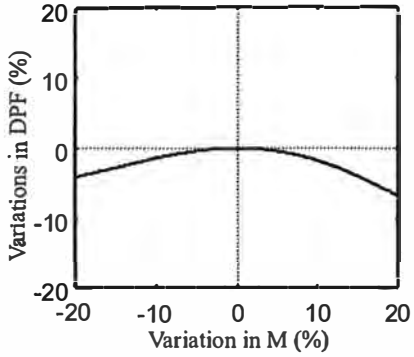

(d) Sensitivity of the DPF at150W.

Fig. 7-32. Modified tuning for load independent unity DPF (C_{pn}=1, u=1.12) – The influence of variations in M for an electric vehicle battery charger under fixed-frequency operation.

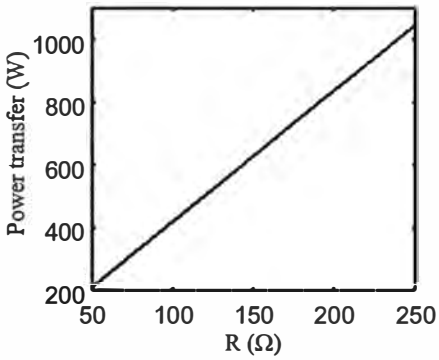

(a) Power transfer capability.

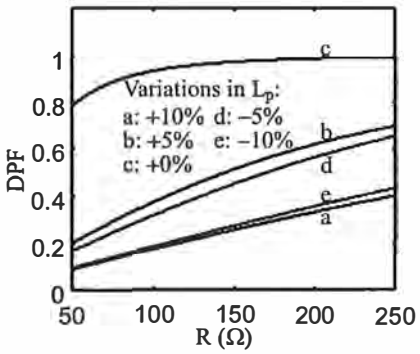

(b) DPF.

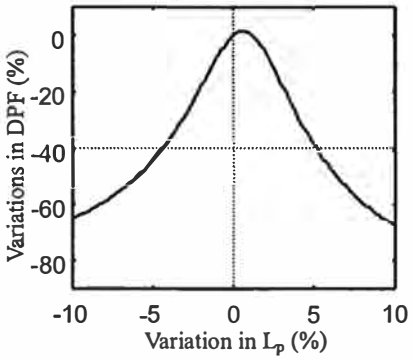

(c) Sensitivity of the DPF at 800W.

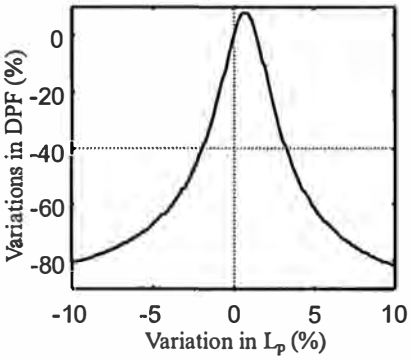

(d) Sensitivity of the DPF at 400W.

Fig. 7-33. The influence of variations in L_p for a monorail material handling system under fixed-frequency operation (k=0.086, $Q_{s0,rated}$=4.7, PP topology, C_{pn}=1, u=1).

InductEV, Inc.
Exhibit 1010
Page 314

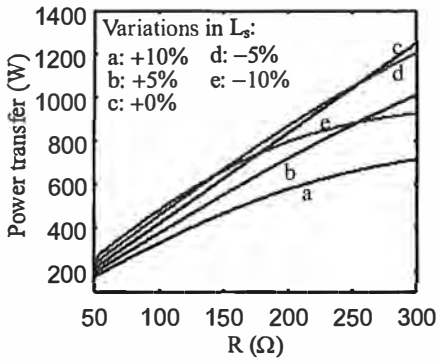

(a) Power transfer capability.

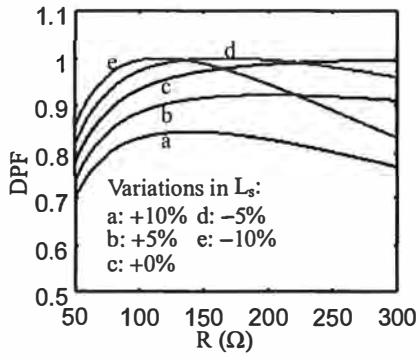

(b) DPF.

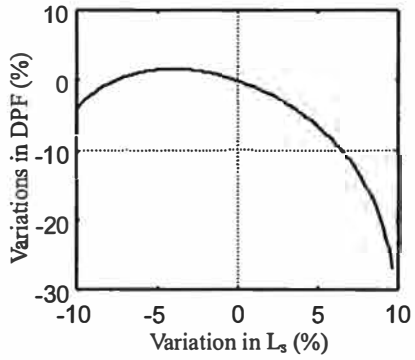

(c) Sensitivity of the DPF at 800W.

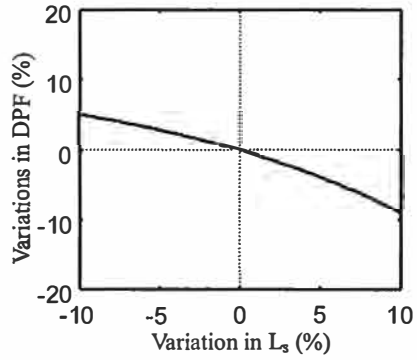

(d) Sensitivity of the DPF at 400W.

Fig. 7-34. The influence of variations in L_s for a monorail material handling system under fixed-frequency operation (k=0.086, $Q_{s0,rated}$=4.7, PP topology, C_{pn}=1, u=1).

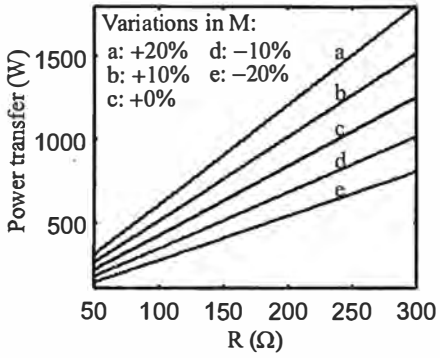

(a) Power transfer capability.

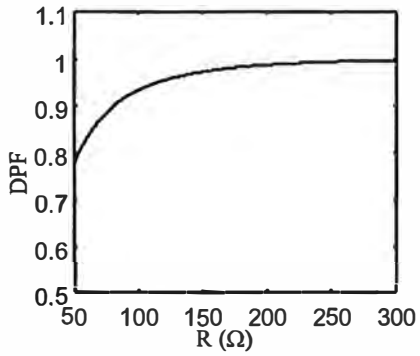

(b) DPF.

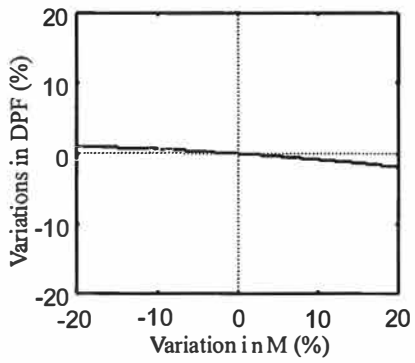

(c) Sensitivity of the DPF at 800W.

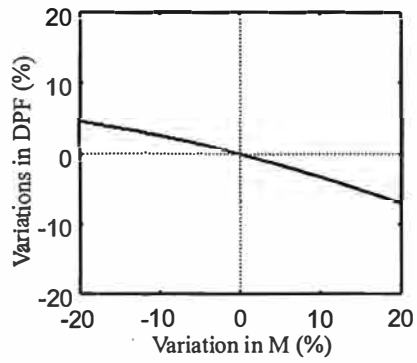

(d) Sensitivity of the DPF at 400W.

Fig. 7-35. The influence of variations in M for a monorail material handling system under fixed-frequency operation (k=0.086, $Q_{s0,rated}$=4.7, PP topology, C_{pn}=1, u=1).

InductEV, Inc.
Exhibit 1010
Page 315

7-6.3 VARIABLE-FREQUENCY SYSTEMS

A well-coupled system (electric vehicle battery charging) – The influence on operating frequency and power of variations in the coupling parameters are shown in Fig. 7-36 to 7-41. The original and modified tuning schemes exhibit similar sensitivities. Variations in L_p have a similar influence to that seen with variations in C_p. Here, the power transfer capability is highly sensitive to decreases in L_p. The sensitivity of the operating frequency to variations in L_p is significant at rated power, and becomes slightly lower at reduced load because of lower Q_s.

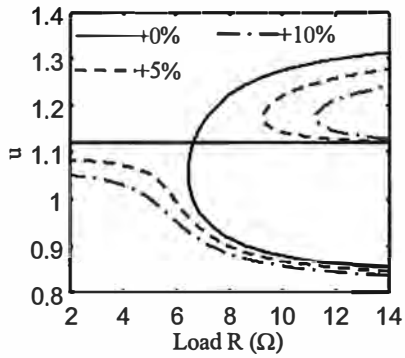

(i) Operational frequency.

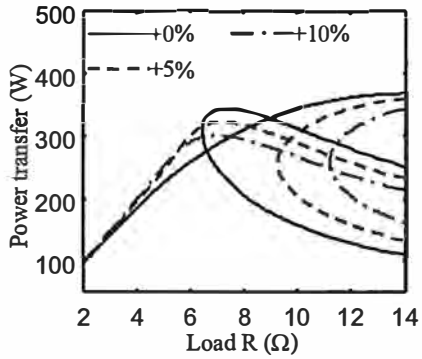

(ii) Power transfer capability.

(a) Increases in L_p.

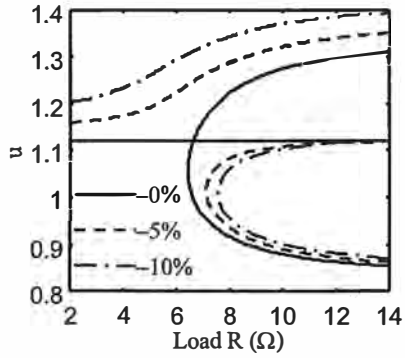

(i) Operational frequency.

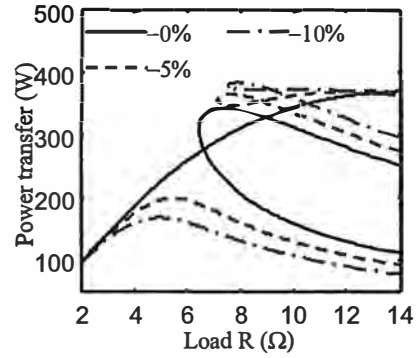

(ii) Power transfer capability.

(b) Decreases in L_p.

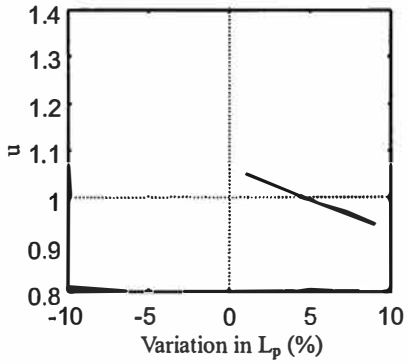

(i) Operating at 300W.

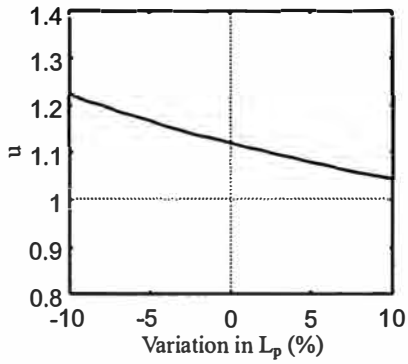

(ii) Operating at 150W.

(c) Sensitivity of the operating frequency.

Fig. 7-36. Original tuning (C_{pn}=1) – The influence of variations in L_p for an electric vehicle battery charger under variable-frequency operation (k=0.45, $Q_{s0,rated}$=1.8, PP topology, I_p=15A).

InductEV, Inc.
Exhibit 1010
Page 316

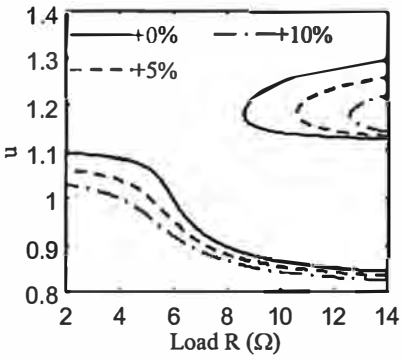

(i) Operational frequency.

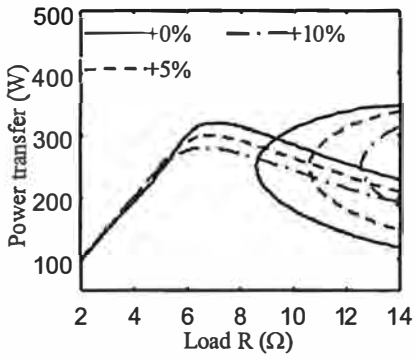

(ii) Power transfer capability.

(a) Increases in L_p.

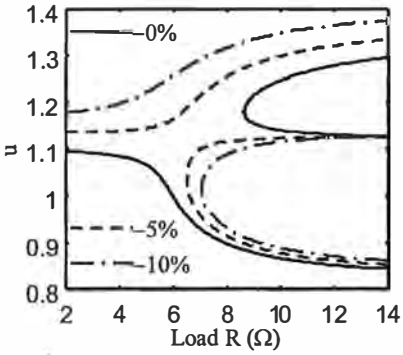

(i) Operational frequency.

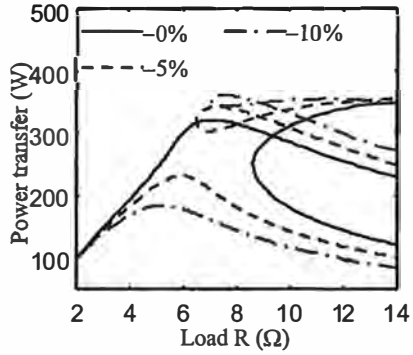

(ii) Power transfer capability.

(b) Decreases in L_p.

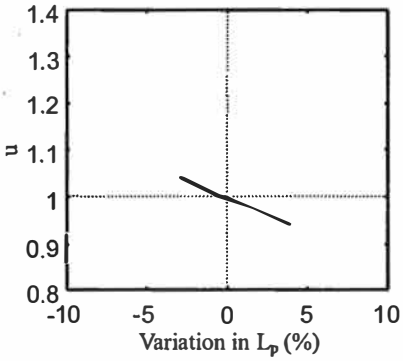

(i) Operating at 300W.

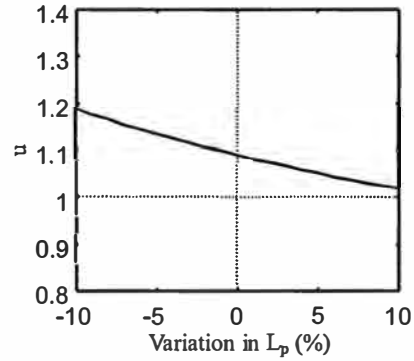

(ii) Operating at 150W.

(c) Sensitivity of the operating frequency.

Fig. 7-37. Modified tuning for unity DPF at rated load (C_{pn}=1.04) – The influence of variations in L_p for an electric vehicle battery charger under variable-frequency operation (k=0.45, $Q_{s0,rated}$=1.8, PP topology, I_p=15A).

InductEV, Inc.
Exhibit 1010
Page 317

Variations in L_s have similar effects to that seen with variations in C_s. Here, the power transfer capability is highly sensitive to increases in L_s. The sensitivity of the operating frequency to variations in L_s is less than that seen with variations in L_p, especially at light load where the sensitivity is negligible because the frequency shift can be neglected.

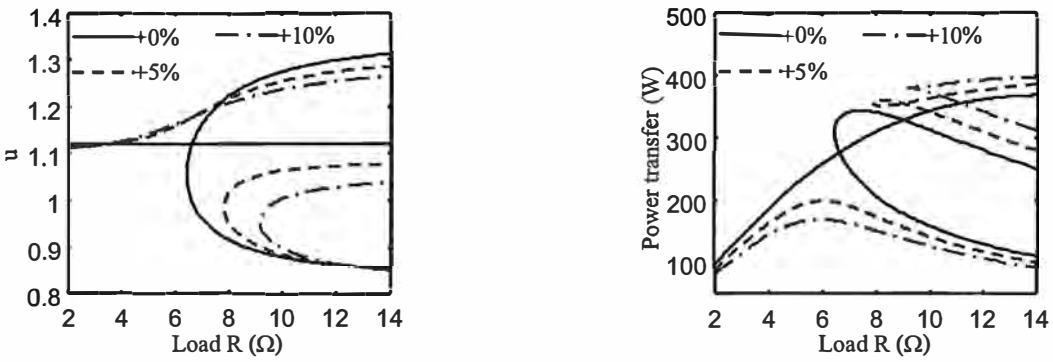

(i) Operational frequency. (ii) Power transfer capability.

(a) Increases in L_s.

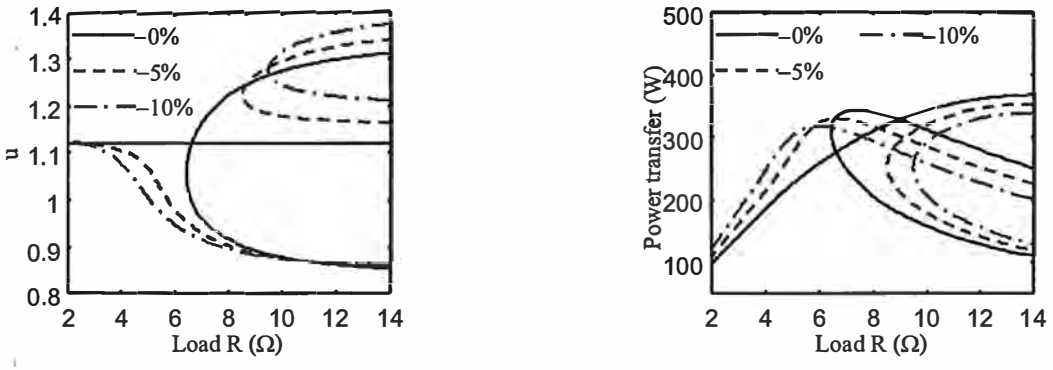

(i) Operational frequency. (ii) Power transfer capability.

(b) Decreases in L_s.

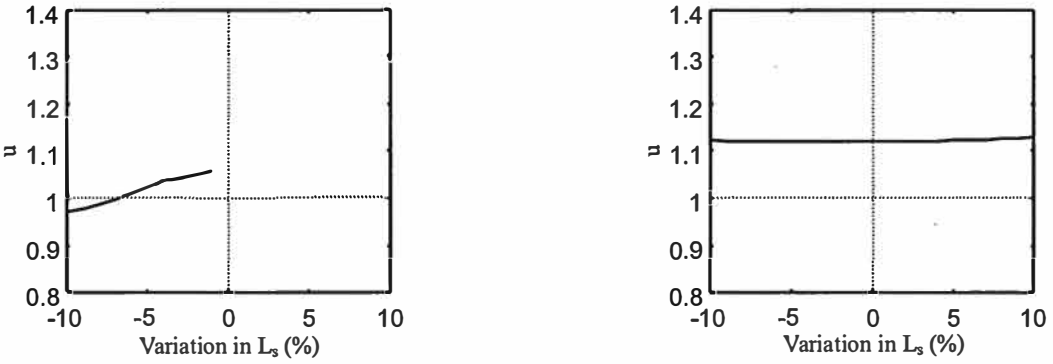

(i) Operating at 300W. (ii) Operating at 150W.

(c) Sensitivity of the operating frequency.

Fig. 7-38. Original tuning (C_{pn}=1) – The influence of variations in L_s for an electric vehicle battery charger under variable-frequency operation (k=0.45, $Q_{s0,rated}$=1.8, PP topology, I_p=15A).

InductEV, Inc.
Exhibit 1010
Page 318

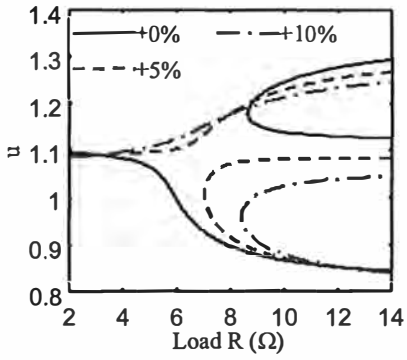

(i) Operational frequency.

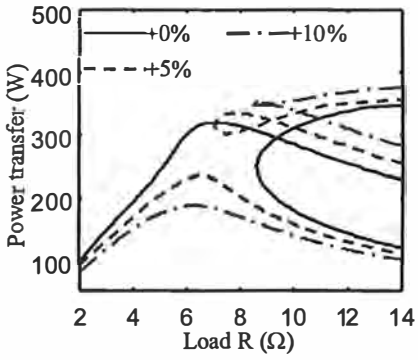

(ii) Power transfer capability.

(a) Increases in L_s.

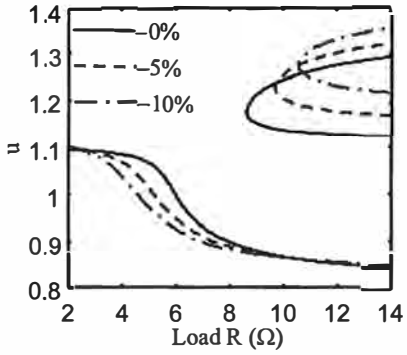

(i) Operational frequency.

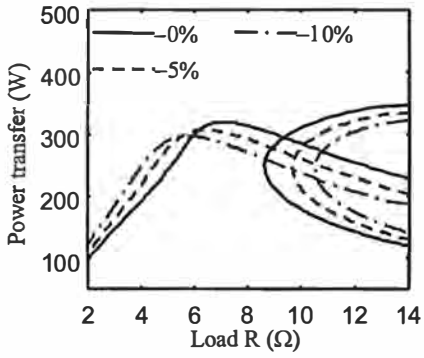

(ii) Power transfer capability.

(b) Decreases in L_s.

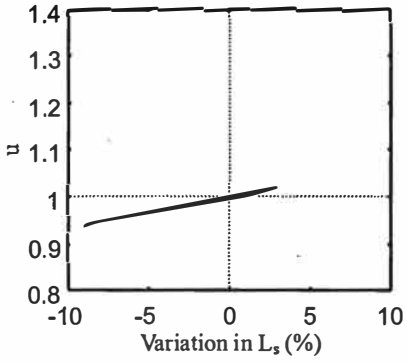

(i) Operating at 300W.

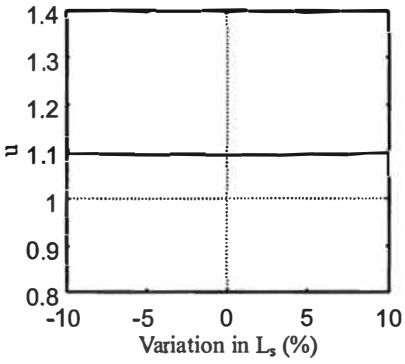

(ii) Operating at 150W.

(c) Sensitivity of the operating frequency.

Fig. 7-39. Modified tuning for unity DPF at rated load (C_{pn}=1.04) – The influence of variations in L_s for an electric vehicle battery charger under variable-frequency operation (k=0.45, $Q_{s0,rated}$=1.8, PP topology, I_p=15A).

InductEV, Inc.
Exhibit 1010
Page 319

As expected, variations in M have a significant influence on the power transfer capability. An increase in M results in improved power transfer capability as well as the occurrence of bifurcation at a light load. Decreasing M results in reduced power transfer capability and the appearance of bifurcation at higher load. Because of changes in the loading effects of the pickup, the sensitivity of the operating frequency to variations in M is higher than that seen with variations in L_s for all loading conditions.

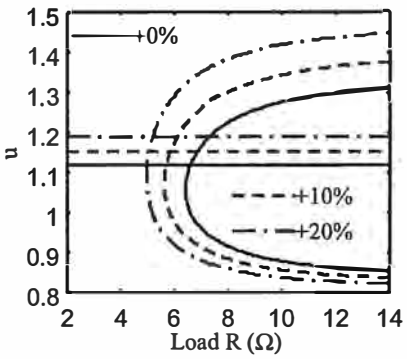

(i) Operational frequency.

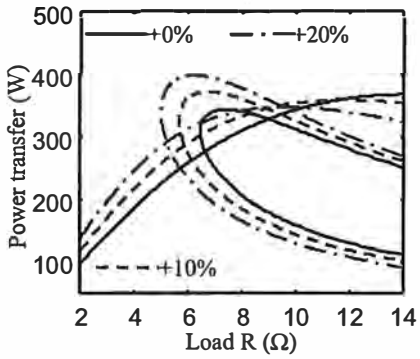

(ii) Power transfer capability.

(a) Increases in M.

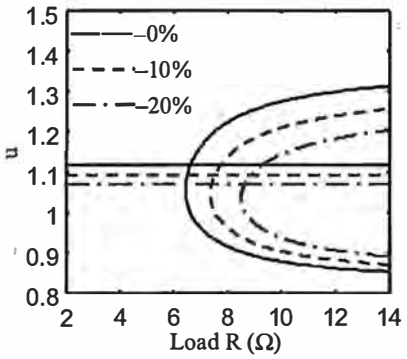

(i) Operational frequency.

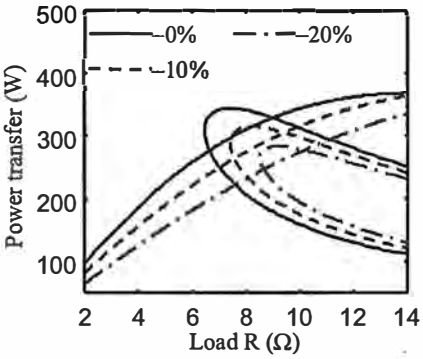

(ii) Power transfer capability.

(b) Decreases in M.

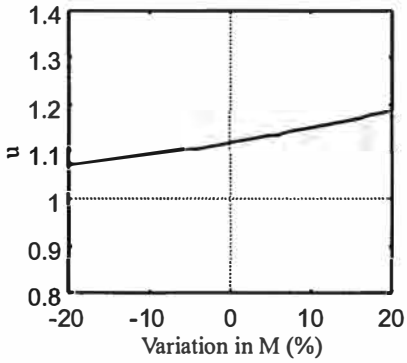

(c) Sensitivity of the operating frequency operating at 150W.

Fig. 7-40. Original tuning (C_{pn}=1) – The influence of variations in M for an electric vehicle battery charger under variable-frequency operation (k=0.45, $Q_{s0,rated}$=1.8, PP topology, I_p=15A).

InductEV, Inc.
Exhibit 1010
Page 320

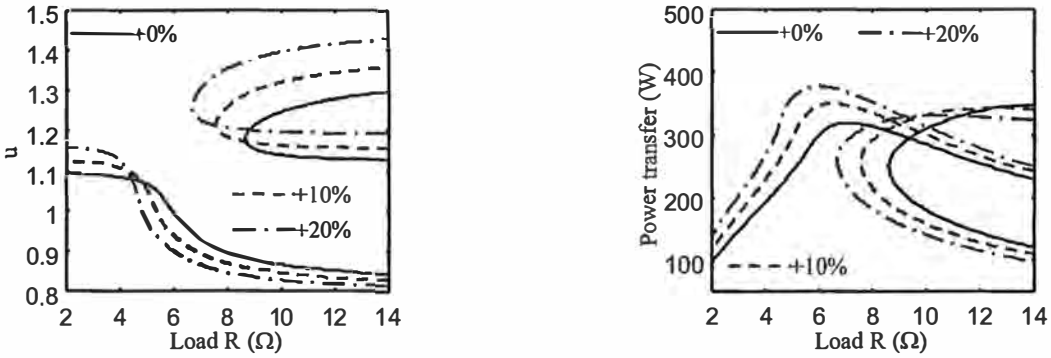

(i) Operational frequency. (ii) Power transfer capability.

(a) Increases in M.

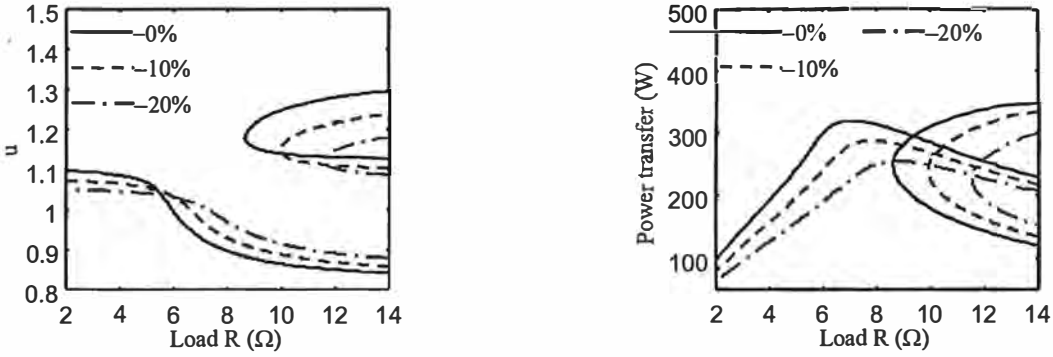

(i) Operational frequency. (ii) Power transfer capability.

(b) Decreases in M.

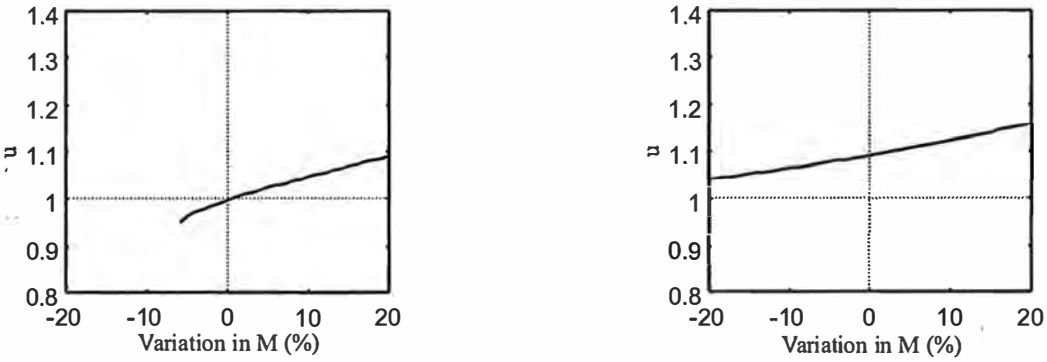

(i) Operating at 300W. (ii) Operating at 150W.

(c) Sensitivity of the operating frequency.

Fig. 7-41. Modified tuning for unity DPF at rated load (C_{pn}=1.04) – The influence of variations in M for an electric vehicle battery charger under variable-frequency operation (k=0.45, $Q_{s0,rated}$=1.8, PP topology, I_p=15A).

A loosely coupled system (monorail material handling) –The influence on operating frequency and power of variations in the coupling parameters are shown in Fig. 7-42 to 7-44. The operating frequency is sensitive to variations in L_p, while its insensitivity to variations in L_s and M is small as the loading effects of the pickup are insignificant. The power transfer capability is quite sensitive to variations in each coupling parameter since Q_s is high.

InductEV, Inc.
Exhibit 1010
Page 321

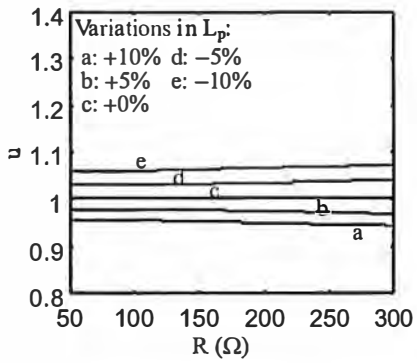

(a) Operating frequency.

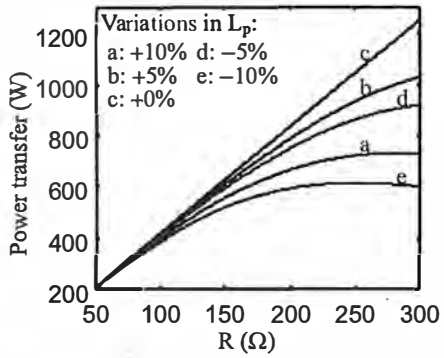

(b) Power transfer capability.

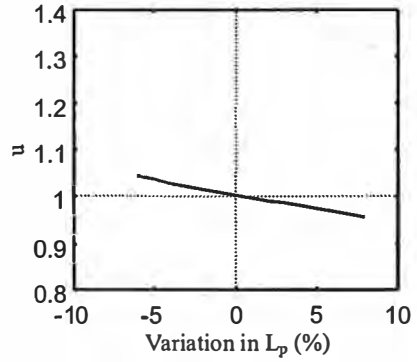

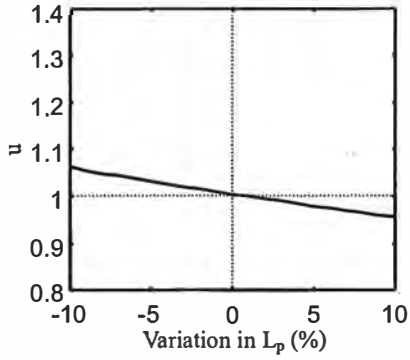

(c) Sensitivity of the operating frequency at 800W. (d) Sensitivity of the operating frequency at 400W.

Fig. 7-42. The influence of variations in L_p for a monorail material handling system under variable-frequency operation (k=0.086, $Q_{s0,rated}$=4.7, PP topology, C_{pn}=1, I_p=54A).

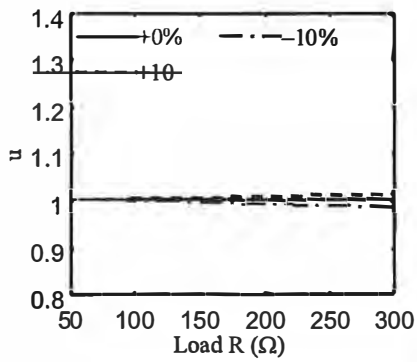

(a) Operating frequency.

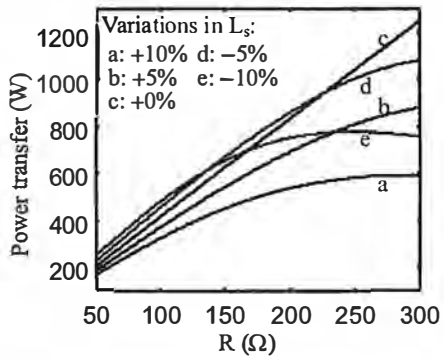

(b) Power transfer capability.

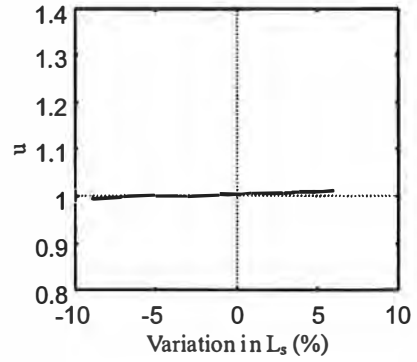

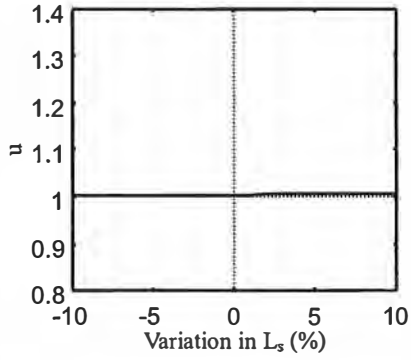

(c) Sensitivity of the operating frequency at 800W. (d) Sensitivity of the operating frequency at 400W.

Fig. 7-43. The influence of variations in L_s for a monorail material handling system under variable-frequency operation (k=0.086, $Q_{s0,rated}$=4.7, PP topology, C_{pn}=1, I_p=54A).

InductEV, Inc.
Exhibit 1010
Page 322

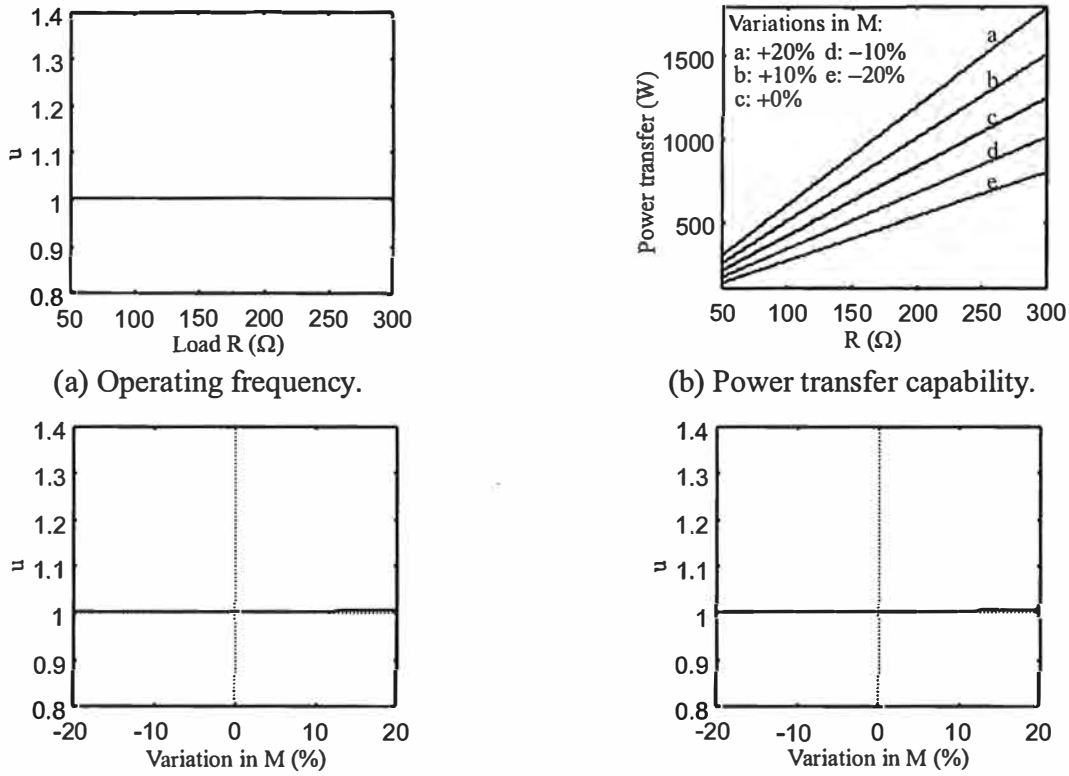

(a) Operating frequency. (b) Power transfer capability.

(c) Sensitivity of the operating frequency at 800W. (d) Sensitivity of the operating frequency at 400W.

Fig. 7-44. The influence of variations in M for a monorail material handling system under variable-frequency operation (k=0.086, $Q_{s0,rated}$=4.7, PP topology, C_{pn}=1, I_p=54A).

7-7 DISCUSSION

A comparison of the various sensitivity analyses for variations in C_p, C_s, L_p, L_s and M are summarized in Table 7-5 to 7-8. Here, all of the tuning schemes discussed in this thesis are compared. Influences on the DPF, the power transfer capability and the operating frequency are classified here into: "Very High (>50%)", "High (<50%)", "Moderate (<30%)", "Low (<15%)" and "Very Low (<5%)" according to the percentage changes found when each of the parameters of interest is varied by ±10%. In all cases, the original tuning and the modified tunings are essentially identical and therefore are not separated.

For loosely coupled systems under fixed-frequency operation, the DPF is highly sensitive to variations in C_p and L_p. This can result in very poor DPF requiring a larger VA rating for the power supply. In consequence, fixed-frequency operation is not a good choice when variations in C_p or L_p are large. With variable-frequency control, the operating frequency is also sensitive to variations in C_p and L_p. This has moderate influences on the power transfer capability. Variations in C_s, L_s and M also have moderate influences on the power transfer capability in both fixed and variable-frequency systems. Overall, in order to minimize the VA rating of the power supply, variable-frequency operation is a good choice for loosely coupled systems.

InductEV, Inc.
Exhibit 1010
Page 323

For well-coupled systems under fixed-frequency operation, the sensitivity of DPF to variations in C_s, C_p, L_p, L_s and M is small at rated power in all three tuning schemes. The sensitivity becomes higher under lightly loading conditions. Here, the modified tuning for load independent unity DPF has lower sensitivity, but the sensitivity of the power transfer capability to variations in C_s becomes higher, requiring a careful choice of the type and grade of capacitor used here. Variations in L_s have a significant impact on the power transfer capability for all tuning schemes. However, as noted in Fig. 7-22, if L_s increases M increases faster to compensate its influence on power transfer.

TABLE 7-5
SENSITIVITY OF DPF TO VARIATIONS IN C_P, C_S, L_P, L_S AND M
UNDER FIXED-FREQUENCY OPERATION (PP TOPOLOGY)

		Well-coupled systems			Loosely coupled systems
		Original tuning	Modified tuning for unity DPF at rated load	Modified tuning for load independent unity DPF	
C_p	Rated power	Very Low	Very Low	Very Low	Very High
	Light power	Moderate	Moderate	Low	Very High
C_s	Rated power	Very Low	Very Low	Very Low	Moderate
	Light power	Very Low	Very Low	Very Low	Moderate
L_p	Rated power	Very Low	Very Low	Very Low	Very High
	Light power	Moderate	Moderate	Low	Very High
L_s	Rated power	Very Low	Very Low	Very Low	Moderate
	Light power	Very Low	Very Low	Very Low	Low
M	Rated power	Very Low	Very Low	Very Low	Very Low
	Light power	Moderate	Moderate	Low	Low

TABLE 7-6
THE INFLUENCE OF VARIATIONS IN C_S, L_S AND M ON THE POWER TRANSFER
CAPABILITY UNDER FIXED-FREQUENCY OPERATION (PP TOPOLOGY)

		Well-coupled systems			Loosely coupled systems
		Original tuning	Modified tuning for unity DPF at rated load	Modified tuning for load independent unity DPF	
C_s	Rated power	Low	Low	High	Moderate
	Light power	Low	Low	Low	Low
L_s	Rated power	High	High	High	Moderate
	Light power	Moderate	Moderate	Moderate	Moderate
M	Rated power	Moderate	Moderate	Moderate	Moderate
	Light power	Moderate	Moderate	Moderate	Moderate

InductEV, Inc.
Exhibit 1010
Page 324

TABLE 7-7
SENSITIVITY OF THE OPERATING FREQUENCY TO VARIATIONS IN C_P, C_S, L_P, L_S AND M UNDER VARIABLE-FREQUENCY OPERATION (PP TOPOLOGY)

		Well-coupled systems		Loosely coupled systems
		Original tuning	Modified tuning for unity DPF at rated load	
C_p	Rated power	High	High	Moderate
	Light power	Moderate	Moderate	Low
C_s	Rated power	Moderate	Moderate	Very Low
	Light power	Very Low	Very Low	Very Low
L_p	Rated power	High	High	Moderate
	Light power	Moderate	Moderate	Low
L_s	Rated power	Moderate	Moderate	Very Low
	Light power	Very Low	Very Low	Very Low
M	Rated power	Moderate	Moderate	Very Low
	Light power	Low	Low	Very Low

TABLE 7-8
THE INFLUENCE OF VARIATIONS IN C_P, C_S, L_P, L_S AND M ON THE POWER TRANSFER CAPABILITY UNDER VARIABLE-FREQUENCY OPERATION (PP TOPOLOGY)

		Well-coupled systems		Loosely coupled systems
		Original tuning	Modified tuning for unity DPF at rated load	
C_p	Increase	Low	Low	Moderate
	Decrease	High	High	Moderate
C_s	Increase	High	High	Moderate
	Decrease	Low	Low	Moderate
L_p	Increase	Low	Low	Moderate
	Decrease	High	High	Moderate
L_s	Increase	High	High	Moderate
	Decrease	Low	Low	Moderate
M	Increase	Moderate	Moderate	Moderate
	Decrease	Moderate	Moderate	Moderate

For well-coupled systems under variable-frequency operation, the original and modified tuning schemes have similar sensitivity. The operating frequency is sensitive to variations in C_p and L_p, particularly with increased output power. Such variations in the operating frequency result in reduced

InductEV, Inc.
Exhibit 1010
Page 325

power transfer capability, and as such rated power may be unavailable. Importantly, the power transfer capability is particularly sensitive to decreases in C_p and L_p as well as increases in C_s and L_s. If it were possible to have positive variations in C_p and L_p and negative variations in C_s and L_s, the impact on system operation would be minimized.

The sensitivity analysis in this chapter focused on two typical systems, one of which was a well-coupled contact-less electric vehicle battery charger and the other a loosely coupled monorail material handling system. Both examples use PP topologies. Similar sensitivities can be found using other topologies (SS, SP and PS), but such an extended analysis is beyond the scope of this thesis.

7-8 CONCLUSIONS

The sensitivity of the displacement power factor (DPF), the operating frequency and the power transfer capability to variations in the primary and secondary compensation capacitances (C_p and C_s) as well as the misalignment of the electromagnetic structure (variations in the coupling parameters M, L_p and L_s) were investigated in this chapter for both fixed and variable-frequency systems. It was found that systems designed using the tuning schemes proposed in Chapter 5 (for variable-frequency systems) and Chapter 6 (for fixed-frequency systems) have similar sensitivities to that found with those tuned using the approach described in Chapter 4. The exception is the tuning scheme for load independent unity DPF proposed in section 6-3 (for fixed-frequency systems). Here, the sensitivity of its DPF at light load is lower than all other tuning schemes, however, its power transfer is particularly sensitive to increases in C_s, and therefore requires this capacitor to be carefully selected for temperature and lifetime stability.

REFERENCES

[1]. J. T. Boys, G. A. Covic, A. W. Green, "Stability and control of inductively coupled power transfer systems," *IEE Proceedings-Electric Power Applications*, vol. 147, pp. 37-43, Jan. 2000.

[2]. A. W. Green, J. T. Boys, "10 kHz inductively coupled power transfer-concept and control," in *Conf. Rec. Power Electronics and Variable-Speed Drives*, 1994, pp. 694-699.

InductEV, Inc.
Exhibit 1010
Page 326

InductEV, Inc.
Exhibit 1010
Page 327

CHAPTER 8

INVESTIGATING AN LCL RESONANT INVERTER FOR ICPT APPLICATIOMS

8-1 Introduction
8-2 Overview of the system
8-3 Capability of the inverter
8-4 Capability of the resonant tank
8-5 Steady state power flow analysis
8-6 Verification
8-7 Conclusions

8-1 INTRODUCTION

Throughout this thesis, an LCL resonant inverter has been used to verify the proposed theory. This chapter investigates the suitability of this LCL resonant inverter for ICPT applications.

Resonant inverters are popular for applications such as induction heating [1]. Induction heating inverters in the 10 to 100 kHz frequency range can be used for ICPT applications, but the design considerations are very different due to the difference in load characteristics. When analysing such inverters, the load is normally represented as a resistor in series with the primary inductance, but in many practical ICPT systems the reflected reactance due to secondary resonance is comparable to the primary inductance [2-5]. Consequently, in order to analyse ICPT systems accurately, the secondary resonant circuit needs to be solved simultaneously with the primary resonant network.

Sinusoidal ac analysis (fundamental mode analysis) is commonly used to analyse resonant inverters [1][3][5][6]. This approach is suitable for determining steady state characteristics, but is unable to identify the transient response or non-linear features. Alternatively, time domain analysis using differential equations can be used [7]. However, this approach becomes too complex to be solved analytically when combining the primary and secondary resonant circuits of an ICPT system.

In this chapter, the inverter is modelled using time domain differential equations, while sinusoidal ac analysis is used to model the resonant tank (the impedance model developed in Chapter 3). A power flow balance between the inverter and the resonant tank determines the steady state operation, enabling the inverter to be designed to achieve maximum power transfer to the load. The analysis is verified using a design example for contact-less electric vehicle battery charging.

InductEV, Inc.
Exhibit 1010
Page 328

8-2 OVERVIEW OF THE SYSTEM

This section introduces the fundamental operation of the LCL resonant inverter, and summarizes the proposed analytical procedure used in the following sections to match the inverter to the resonant tank for maximum power transfer to the load.

8-2.1 OPERATING MODES OF THE LCL RESONANT INVERTER

The schematic in Fig. 8-1 shows an ICPT system using an LCL resonant inverter. The switching power supply used here is a full-bridge inverter fed by a dc voltage (V_d). The inductance of the primary winding (L_p), its primary parallel compensation capacitor (C_p), together with the series inductor L_m form the LCL resonant circuit. Either series or parallel compensation can be used for the secondary, with the advantages of each topology discussed in section 2-3. In this system, a parallel topology was chosen for the secondary compensation.

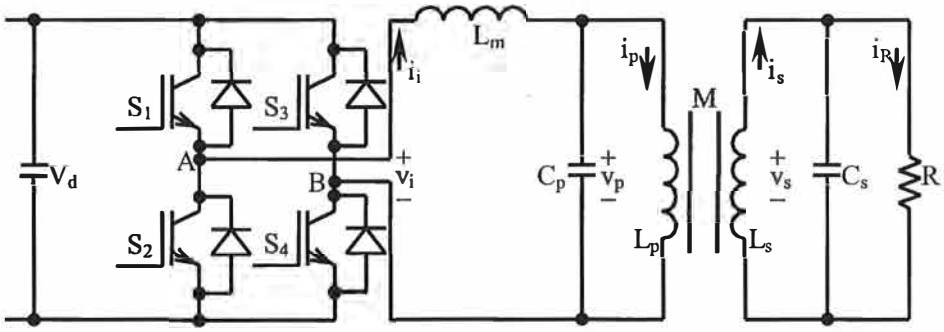

Fig. 8-1. Circuit diagram of an ICPT system driven by an LCL resonant inverter.

The inverter can be controlled using either a fixed or a variable-frequency controller. The advantages and disadvantages of fixed and variable-frequency operations have been discussed in section 2-5.

LCL resonant inverters can be operated with either continuous or discontinuous current. Continuous current operation has been reported in detail for induction heating applications under variable- frequency operation [1], and for ICPT applications under fixed-frequency operation [8]. Discontinuous current operation, however, has not been investigated thoroughly in the literature. Consequently, this chapter investigates a variable frequency controlled LCL resonant inverter operating with discontinuous current.

In continuous current mode, the inverter is controlled to always ensure a path for the inverter current. This can be achieved by using the voltage amplification effect described in [1]. With this design the resonant tank voltage is much larger than the output inverter voltage, and the inverter

InductEV, Inc.
Exhibit 1010
Page 329

current becomes nearly sinusoidal as shown in Fig. 8-2 (a). For optimal inverter efficiency, the frequency is controlled so that the inverter current is in phase with the inverter output voltage. Switching losses are virtually non-existent, and very high operating frequencies can be achieved. Power regulation can be achieved by varying the frequency as described in [1], but the resulting switching losses need to be considered carefully.

In discontinuous current mode the inverter is switched so that the inverter current drops to zero and stays there for a finite period during each half cycle as shown in Fig. 8-2 (b). The biggest advantage is that turn-on losses are eliminated, and only conduction and turn-off losses need to be considered.

(a) Continuous current mode. (b) Discontinuous current mode.

Fig. 8-2. Inverter voltage and current waveforms for the LCL resonant inverter.

It is further possible to control the switches so that inverter current is minimised. This is achieved by ensuring the inverter voltage always has the same polarity as the resonant tank voltage. With v_p positive, only S_1 and S_4 are allowed to turn on, while S_2 and S_3 will only be turned on if v_p is negative. Figure 8-3 shows current and voltage waveforms for half a cycle.

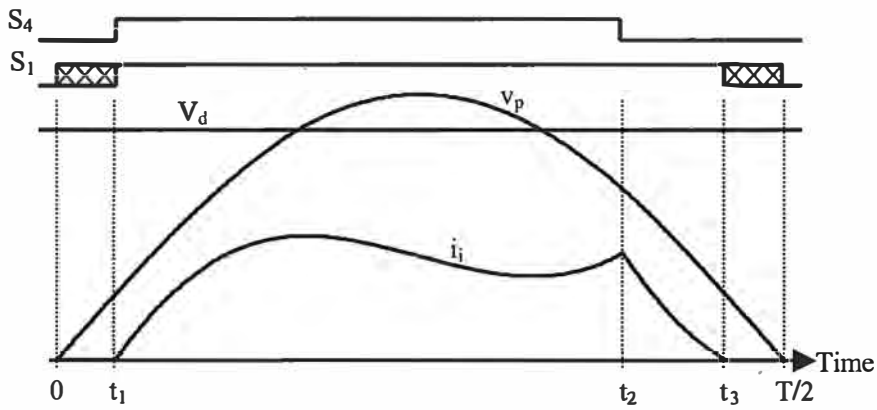

Fig. 8-3. Switching control of the LCL resonant inverter in discontinuous current mode.

To ensure discontinuous current, t_2 has to be early enough to ensure that the current will drop back to zero before the end of the half cycle. Since the resonant tank voltage v_p provides the voltage to drive the inverter current back to zero, t_2 is a strong function of v_p (t_2 must reduce as v_p reduces).

Power control is mainly achieved by varying t_1. As t_1 increases, the inverter current drops resulting in lower power. With only turn-off and conduction losses, a trade-off between the switching and conduction losses is necessary. Using modern IGBT modules, conduction losses are equal to turn-off

InductEV, Inc.
Exhibit 1010
Page 330

losses at switching frequencies around 20kHz. With such devices, this would be the best practical operating frequency to maximize the inverter's efficiency.

8-2.2 AN ANALYTICAL PROCEDURE FOR SYSTEM DESIGN

To facilitate analysis and design of the system, a four-step process is followed:

Step1: Firstly an inverter model is developed in which the resonant tank (the electromagnetic structure, the primary and secondary compensations as well as the load) is modelled as a sinusoidal voltage source. With this simplification, the inverter current waveform as well as the inverter output power can be determined as a function of the resonant tank voltage.

Step 2: Once the inverter current waveform is known, the fundamental component of the inverter current is calculated. Of particular importance is the phase relationship between the inverter current and the resonant tank voltage.

Step 3: Next the impedance model developed in Chapter 3 is used to model the resonant tank (the electromagnetic structure, the primary and secondary compensations as well as the load). If all parameters are known, the model can be used to calculate the power and phase relationships of the resonant tank.

Step 4: Finally the two models are combined, and the steady state operating point is determined using power flow balance between the inverter and the resonant tank.

8-3 CAPABILITY OF THE INVERTER

The output power of the inverter can be calculated from the output voltage (v_i) and current (i_i). The amplitude of the rectangular inverter output voltage equals the dc bus voltage (V_d), while the pulse width is controllable by the switching instants t_1 and t_2. The waveform of the inverter output current is dependent on not only the switching instants and the dc bus voltage, but also the resonant tank voltage (v_p) and the series inductance (L_m). An inverter model is developed in this section to investigate influences of these parameters on the capability of the inverter.

8-3.1 THE INVERTER MODEL

In the inverter model shown in Figure 8-4, all primary and secondary resonant tank components are replaced by a single sinusoidal voltage source v_p. This is a valid simplification for high Q resonant systems, where the resonant tank voltages are very close to sinusoidal.

InductEV, Inc.
Exhibit 1010
Page 331

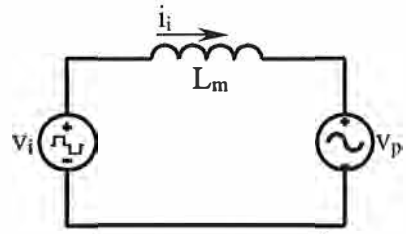

Fig. 8-4. Simplified model of the LCL resonant inverter.

The resonant tank voltage is given by:

$$v_p(t) = \hat{V}_p \sin \omega t \tag{8-1}$$

The inverter voltage depends on the states of the switches, and is equal to:

$$v_i(t) = \begin{cases} v_p(t), & 0 < t < t_1 \\ V_d, & t_1 < t < t_2 \\ 0, & t_2 < t < t_3 \\ v_p(t), & t_3 < t < T/2 \end{cases} \tag{8-2}$$

With this inverter model, the inverter current (i_i) can be determined from:

$$v_i(t) - v_p(t) = L_m \frac{di_i(t)}{dt} \tag{8-3}$$

During the time interval from t_1 to t_2, the inverter current solved from (8-3) is:

$$i_i(t) = \frac{V_d}{L_m}(t - t_1) + \frac{\hat{V}_p}{\omega L_m}[\cos \omega t - \cos \omega t_1] \qquad t_1 < t < t_2 \tag{8-4}$$

During the freewheeling period after t_2, the inverter current solved from (8-3) is:

$$i_i(t) = \frac{V_d}{L_m}(t_2 - t_1) + \frac{\hat{V}_p}{\omega L_m}[\cos \omega t - \cos \omega t_1] \qquad t_2 < t < t_3 \tag{8-5}$$

Since the inverter current drops to zero at t_3, the time t_2 can be expressed in terms of t_1 and t_3:

$$t_2 = t_1 + \frac{\hat{V}_p}{\omega V_d}[\cos \omega t_1 - \cos \omega t_3] \tag{8-6}$$

To ensure discontinuous current mode operation, t_3 has to be less than T/2. The maximum value of t_2 is thus:

$$t_{2,\max} = t_1 + \frac{\hat{V}_p}{\omega V_d}[\cos \omega t_1 + 1] \tag{8-7}$$

8-3.2 WAVEFORM OF THE INVERTER CURRENT

For a general analysis of the waveform of the inverter current, the resonant tank voltage is normalized with respect to the dc voltage as:

InductEV, Inc.
Exhibit 1010
Page 332

$$V_{pn} = \frac{\hat{V}_p}{V_d} \tag{8-8}$$

Time is normalized with respect to the period as:

$$t_n = \frac{t}{T} = \frac{\omega T}{2\pi} \tag{8-9}$$

The inverter current expressed in terms of these normalized parameters is then:

$$i_i(t_n) = \left(\frac{V_d}{\omega L_m}\right)\begin{cases} 0, & 0 < t_n < t_{1n} \\ 2\pi(t_n - t_{1n}) + V_{pn}[\cos(2\pi t_n) - \cos(2\pi t_{1n})], & t_{1n} < t_n < t_{2n} \\ 2\pi(t_{2n} - t_{1n}) + V_{pn}[\cos(2\pi t_n) - \cos(2\pi t_{1n})], & t_{2n} < t_n < t_{3n} \\ 0, & t_{3n} < t_n < 0.5 \end{cases} \tag{8-10}$$

where t_{2n} is derived from (8-6) as:

$$t_{2n} = t_{1n} + \frac{V_{pn}}{2\pi}[\cos(2\pi t_{1n}) - \cos(2\pi t_{3n})] \tag{8-11}$$

In the following analysis throughout this chapter, it is assumed that t_{2n} is controlled according to (8-11) using selections of t_{1n} and t_{3n}, and measurements of $\hat{V}_p$, V_d and ω.

The inverter current waveform is shown in Fig. 8-5 for selected V_{pn} assuming the switching instants are controlled to achieve maximum pulse width (here, t_{1n}=0, t_{3n}=0.5). In this figure and following similar figures, the maximum V_{pn} (defined as $V_{pn,max}$) is determined using (8-11) at the condition that t_{2n} equals t_{3n}. Discontinuous current operation is impossible with higher V_{pn}.

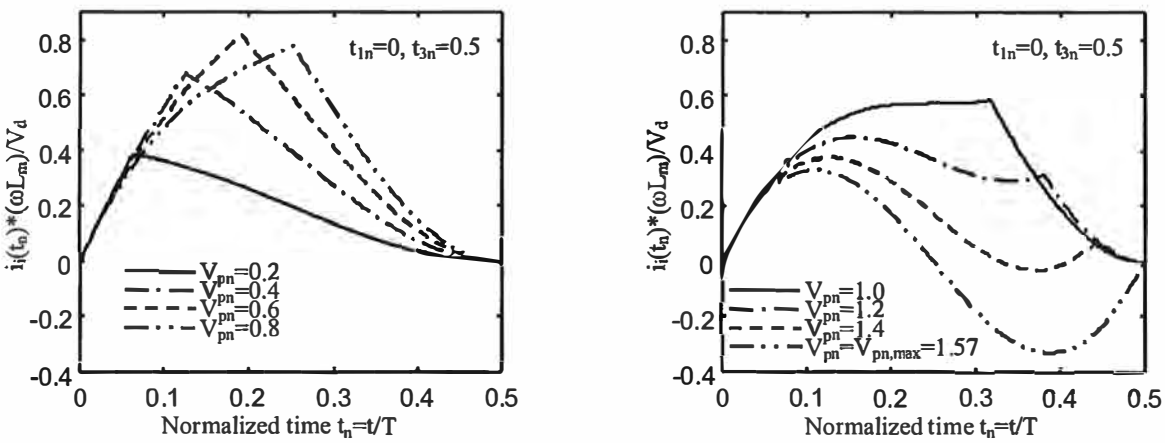

Fig. 8-5. Influences of varying V_{pn} on the inverter current waveform assuming maximum pulse width by setting t_{1n}=0, t_{3n}=0.5.

The waveform of the inverter current is a strong function of the resonant tank voltage. To ensure maximum power delivery, it is desirable to maximize the average current while minimizing peak current. This can be achieved when V_{pn} is close to unity. At this operating condition, the inverter

InductEV, Inc.
Exhibit 1010
Page 333

current waveform is close to a trapezoid.

The effect of increasing t_{1n} on the inverter current waveform is shown in Fig. 8-6 assuming maximum t_{3n} of 0.5. The average inverter current decreases as t_{1n} is increased, and becomes negative with high resonant tank voltage resulting in negative power flow that while possible theoretically is in practice not possible with an ICPT system as the pickups always consume power.

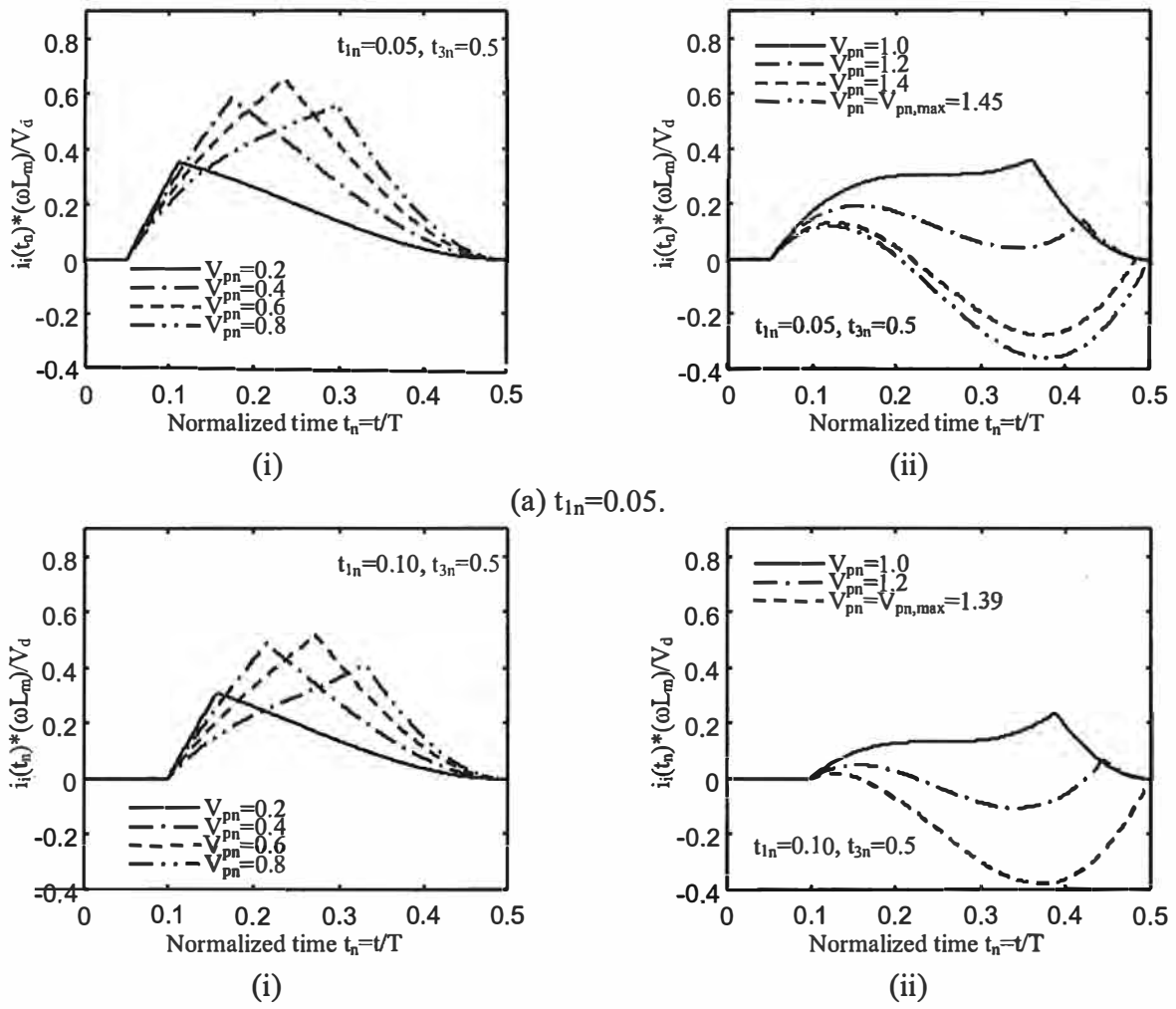

(a) t_{1n}=0.05.

(b) t_{1n}=0.10.

Fig. 8-6. Influences of V_{pn} and t_{1n} on the inverter current waveform (t_{3n} = 0.5).

The effect of decreasing t_{3n} on the inverter current waveform is shown in Fig. 8-7 assuming minimum t_{1n} of zero. The average inverter current reduces with decreasing t_{3n}. However, the sensitivity of the average current to decreases in t_{3n} is much lower than that seen with increases in t_{1n} (as seen in Fig. 8-6). Moreover, the average inverter current is positive across the whole range of possible resonant tank voltages ensuring positive power flow.

InductEV, Inc.
Exhibit 1010
Page 334

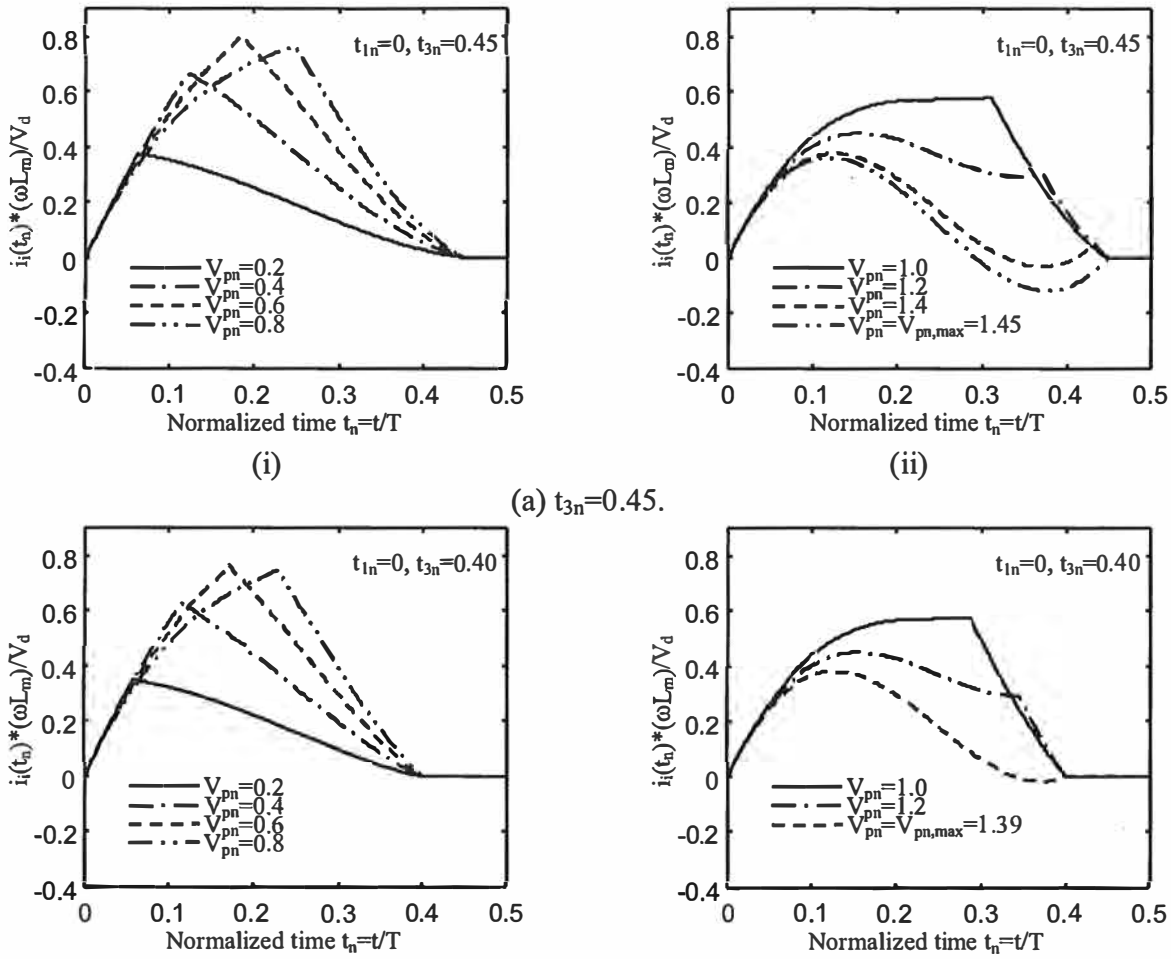

Fig. 8-7. Influences of V_{pn} and t_{3n} on the inverter current waveform (t_{1n} = zero).

8-3.3 INVERTER POWER DELIVERY CAPABILITY

The average power supplied by the inverter is equal to:

$$P_i = \frac{2}{T}\int_0^{T/2} v_i(t)i_i(t)dt \tag{8-12}$$

Before t_1 and after t_3, the inverter current is zero and the inverter supplies no power. During the freewheeling period from t_2 to t_3, the inverter voltage is zero, and again the inverter supplies no power. Power is only supplied by the inverter from t_1 to t_2, when the inverter voltage is equal to the dc bus voltage V_d. Equation (8-12) can thus be rewritten as:

$$P_i = \frac{2V_d}{T}\int_{t_1}^{t_2} i_i(t)dt \tag{8-13}$$

Substituting (8-4) into (8-13) results in:

$$P_i = \frac{V_d}{2\pi\omega L_m}\left\{V_d(\omega t_2 - \omega t_1)^2 + 2\hat{V}_p\left[\sin\omega t_2 - \sin\omega t_1 - (\omega t_2 - \omega t_1)\cos\omega t_1\right]\right\} \tag{8-14}$$

This equation shows that the inverter power can be controlled by varying t_1 and t_2.

InductEV, Inc.
Exhibit 1010
Page 335

In terms of the normalized primary resonant tank voltage given in (8-8) and the normalized time given in (8-9), the inverter power delivery capability given in (8-14) can be expressed as:

$$P_i = \left(\frac{V_d^2}{\pi\omega L_m}\right)\left\{2\pi^2(t_{2n}-t_{1n})^2 + V_{pn}\left[\sin(2\pi t_{2n}) - \sin(2\pi t_{1n}) - 2\pi(t_{2n}-t_{1n})\cos(2\pi t_{1n})\right]\right\} \tag{8-15}$$

where t_{2n} is a function of V_{pn}, t_{1n} and t_{3n} as given by (8-11).

8-3.4 FUNDAMENTAL COMPONENT OF THE INVERTER CURRENT

In this section, the fundamental inverter current is calculated to determine the phase relationship between the inverter current and the resonant tank voltage. Using Fourier analysis, the inverter current can be expressed as the sum of its Fourier components:

$$i_i(t) = \sum_{h=odd}\{A_h\cos(h\omega t) + B_h\sin(h\omega t)\} \tag{8-16}$$

where

$$A_h = \frac{4}{T}\int_0^{T/2} i_i(t)\cos(h\omega t)dt$$

$$B_h = \frac{4}{T}\int_0^{T/2} i_i(t)\sin(h\omega t)dt$$

Substituting (8-4) and (8-5) into (8-16), the fundamental component of the inverter current is:

$$i_{i1}(t) = A_1\cos\omega t + B_1\sin\omega t = C_1\sin(\omega t + \Phi_1) \tag{8-17}$$

where

$$A_1 = \frac{2}{\pi\omega L_m}\left\{\begin{array}{l} V_d\left[(\omega t_2 - \omega t_1)\sin(\omega t_3) + \cos(\omega t_2) - \cos(\omega t_1)\right] \\ +\hat{V}_p\left[\begin{array}{l}\cos(\omega t_1)\sin(\omega t_1) - \cos(\omega t_1)\sin(\omega t_3) \\ +\dfrac{\omega t_3 - \omega t_1}{2} + \dfrac{\sin(2\omega t_3) - \sin(2\omega t_1)}{4}\end{array}\right]\end{array}\right\}$$

$$B_1 = \frac{2}{\pi\omega L_m}\left\{\begin{array}{l} V_d\left[(\omega t_1 - \omega t_2)\cos(\omega t_3) + \sin(\omega t_2) - \sin(\omega t_1)\right] \\ +\hat{V}_p\left[\begin{array}{l}\cos(\omega t_1)\cos(\omega t_3) - \cos^2(\omega t_1) \\ +\dfrac{\sin^2(\omega t_3) - \sin^2(\omega t_1)}{2}\end{array}\right]\end{array}\right\}$$

$$C_1 = \sqrt{A_1^2 + B_1^2}$$

$$\Phi_1 = \tan^{-1}(A_1/B_1)$$

The phase angle Φ_1 is the angle between the resonant tank voltage and the fundamental of the inverter current, and gives a good indication of how well the inverter matches the resonant tank.

InductEV, Inc.
Exhibit 1010
Page 336

In terms of the normalized resonant tank voltage given in (8-8) and the normalized time given in (8-9), the phase angle of the fundamental inverter current derived in (8-17) can be expressed as:

$$\Phi_1 = \tan^{-1}\frac{\begin{bmatrix}\cos(2\pi t_{2n})-\cos(2\pi t_{1n})\\+2\pi(t_{2n}-t_{1n})\sin(2\pi t_{3n})\end{bmatrix}+V_{pn}\begin{bmatrix}\cos(2\pi t_{1n})\sin(2\pi t_{1n})-\cos(2\pi t_{1n})\sin(2\pi t_{3n})\\+\pi(t_{3n}-t_{1n})+\dfrac{\sin(4\pi t_{3n})-\sin(4\pi t_{1n})}{4}\end{bmatrix}}{\begin{bmatrix}\sin(2\pi t_{2n})-\sin(2\pi t_{1n})\\-2\pi(t_{2n}-t_{1n})\cos(2\pi t_{3n})\end{bmatrix}+V_{pn}\begin{bmatrix}\cos(2\pi t_{1n})\cos(2\pi t_{3n})-\cos^2(2\pi t_{1n})\\+\dfrac{\sin^2(2\pi t_{3n})-\sin^2(2\pi t_{1n})}{2}\end{bmatrix}} \tag{8-18}$$

where t_{2n} is a function of V_{pn}, t_{1n} and t_{3n} as given by (8-11).

The phase angle Φ_1 is a function t_{1n}, t_{3n} and V_{pn}. Importantly, it is independent of the frequency and will be used later to determine the steady state operating frequency.

The effect of increasing t_{1n} on the phase angle Φ_1 is shown in Fig. 8-8 assuming maximum t_{3n} of 0.5. In each case, there exists a maximum V_{pn} where the phase angle is either 90° or –90°. Here, the fundamental inverter current is zero and no power is transferred into the resonant tank. Further increases in V_{pn} would theoretically result in negative power flow. This is practically impossible with ICPT systems and therefore is not considered.

With t_{1n} controlled at zero, the minimum phase angle is about 10° when V_{pn} is slightly above unity. As noted in section 8-3.2, maximum inverter power is achieved when V_{pn} is near unity. It is thus desirable to make the phase angle in this range close to zero to ensure a suitable matching between the inverter and the resonant tank, which is designed to transfer maximum power with zero phase angle of the resonant tank impedance (as noted in Chapter 5). This can be achieved by increasing t_{1n} to around 0.04.

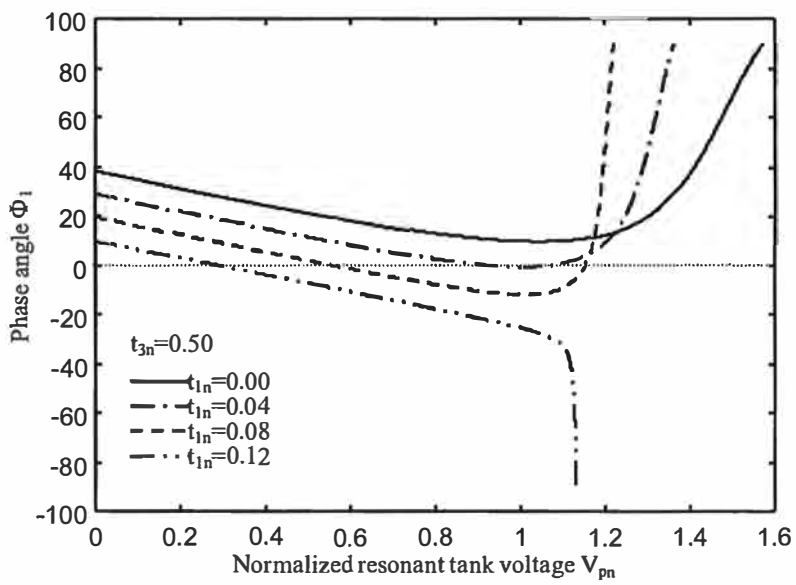

Fig. 8-8. Influences of increasing t_{1n} on the inverter current phase relationship assuming maximum t_{3n} of 0.5.

InductEV, Inc.
Exhibit 1010
Page 337

The effect of decreasing t_{3n} on the phase angle Φ_1 is shown in Fig. 8-9 assuming minimum t_{1n} of zero. Decreasing t_{3n} results in an increasing phase angle between the inverter current and the resonant tank voltage. Consequently, in the rest of this chapter it is assumed that t_{2n} is controlled using (8-11) to force t_{3n} to be 0.5.

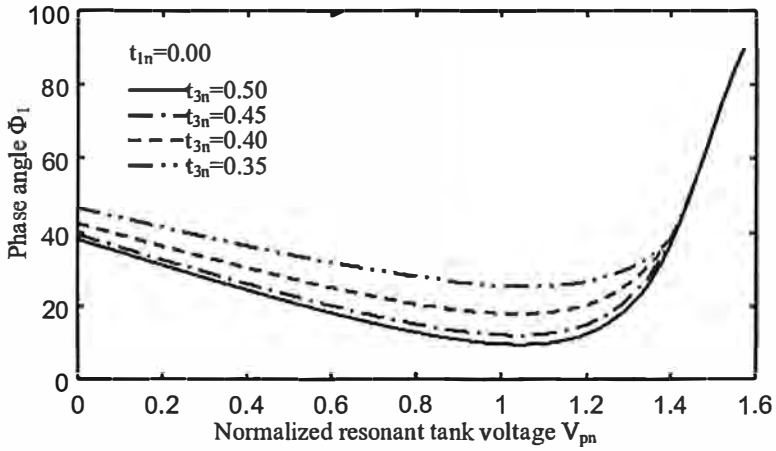

Fig. 8-9. Influences of decreasing t_{3n} on the inverter current phase relationship assuming minimum t_{1n} of zero.

8-4 CAPABILITY OF THE RESONANT TANK

The electromagnetic structure, the primary and secondary compensations as well as the load are now considered in more detail using the contact-less electric vehicle battery charger (described in section 3-11 and investigated in sections 4-6 and 5-6). This example is designed using the design methodology proposed in chapter 4 and the tuning scheme suggested in Chapter 5. It is assumed in this design that the primary current is controlled constant, the secondary pickup is tuned to resonate at the nominal frequency, and the primary is tuned to have unity DPF at rated load. However, when matching the inverter into the resonant tank, these ideal operating conditions may be not available due to non-linear behaviour of the inverter. This is investigated in this section to determine influences of the inverter switching control on the capability of the resonant tank.

8-4.1 THE RESONANT TANK MODEL

The total impedance (Z_t) of the resonant tank circuit can now be calculated using the load model developed in section 3-10.1. For PP topology, it is more convenient to express this in terms of an admittance as:

InductEV, Inc.
Exhibit 1010
Page 338

$$Y_t = j\omega C_p + \cfrac{1}{j\omega L_p + \cfrac{\omega^2 M^2}{j\omega L_s + \cfrac{1}{j\omega C_s + \cfrac{1}{R}}}} \tag{8-19}$$

The phase angle of the resonant tank admittance is determined as:

$$\angle Y_t = \tan^{-1}\left(\frac{\operatorname{Im} Y_t}{\operatorname{Re} Y_t}\right) \tag{8-20}$$

where the 'Re Y_t' and 'Im Y_t' represents the real and imaginary components of the resonant tank admittance.

With given electromagnetic structure (L_p, L_s, M), primary and secondary compensations (C_p, C_s) as well as load (R), the resonant tank admittance and its phase angle are functions of the operating frequency.

8-4.2 OPERATING FREQUENCY

The phase angle of the resonant tank admittance at rated load is shown in Fig. 8-10 as a function of the normalized frequency u (ω/ω_0). As expected, the phase angle is zero at u of unity.

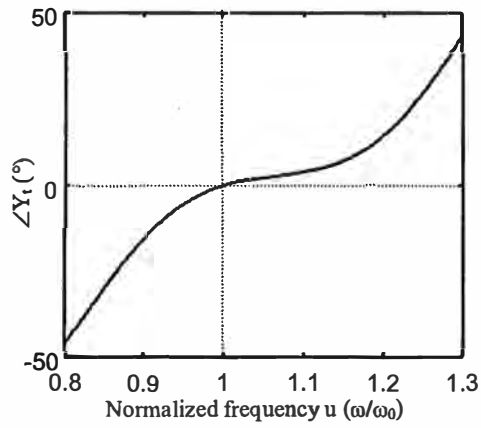

Fig. 8-10. Phase angle of the resonant tank admittance at rated load.

As noted in section 8-3.4, the phase angle of the fundamental inverter current is independent of the operating frequency. This enables the steady state operating frequency to be determined by matching the inverter model to the resonant tank model. At steady state, the phase angle of the primary resonant tank admittance must equal the phase angle of the fundamental inverter current. With the phase angle calculated based on selections of t_{1n}, t_{3n} and known V_{pn} using the inverter model, the operating frequency can be determined using the resonant tank model as a function of these same parameters. Influences of increasing t_{1n} on the operating frequency are shown in Fig. 8-11 assuming maximum t_{3n} of 0.5. For selected t_{1n} and t_{3n}, the phase angle of the fundamental inverter current is calculated as a

InductEV, Inc.
Exhibit 1010
Page 339

function of V_{pn} (Fig. 8-8). The operating frequency is then determined using the calculated phase angle (The dependence between the phase angle and the operating frequency is shown in Fig. 8-10).

With maximum inverter pulse width (t_{1n}=0,t_{3n}=0.5), the operating frequency is significantly above ω_0 across the whole range of resonant tank voltages. Here, the operating frequency is detuned from the designed value (ω_0) by at least 18%.

With t_{1n} controlled near 0.04, the operating frequency is close to ω_0 when V_{pn} is near unity. This region arises when the phase angle is close to zero as noted in section 8-3.4, and is desirable as this minimizes pickup detuning effect. Here, the inverter is well matched to the resonant tank.

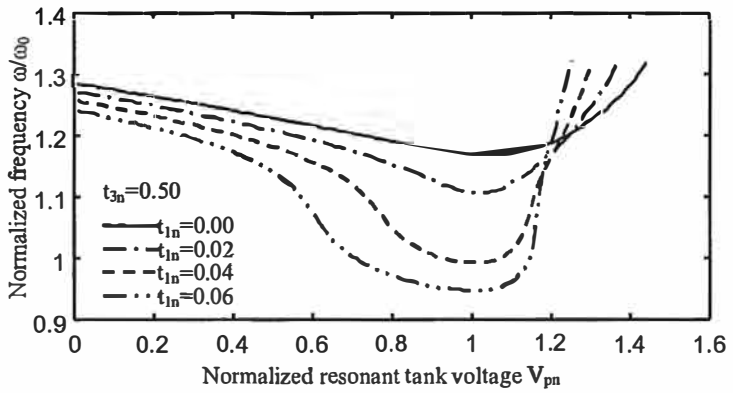

Fig. 8-11. Influences of increasing t_{1n} on the operating frequency assuming maximum t_{3n} of 0.5 at rated load.

8-4.3 POWER ABSORPTION CAPABILITY

At steady state, the power delivered by the inverter is completely absorbed by the resonant tank. The power transferred into the resonant tank can be calculated as:

$$P_t = (\mathrm{Re}\,Y_t)\frac{\hat{V}_p^2}{2} \tag{8-21}$$

It can be expressed in terms of the normalized resonant tank voltage as:

$$P_t = (\mathrm{Re}\,Y_t)\frac{V_d^2 V_{pn}^2}{2} \tag{8-22}$$

The power absorption capability of the resonant tank is thus proportional to the real component of the resonant tank admittance (the resonant tank conductance). The resonant tank conductance at rated load is shown in Fig. 8-12 as a function of the normalized operating frequency. It reaches a maximum at a frequency slightly higher than the secondary resonant frequency. Assuming a constant resonant tank voltage, maximum power can be achieved at this operating point, where the resonant tank runs at a small leading phase angle.

As noted in section 8-4.2, the operating frequency is dependent on selections of t_{1n} and t_{3n}, and the

InductEV, Inc.
Exhibit 1010
Page 340

resonant tank voltage (V_{pn}). Since the resonant tank conductance (Re Y_t) is a function of the frequency, both the resonant tank conductance and power absorption capability are dependent on these parameters. Influences of increasing t_{1n} on the resonant tank conductance and power absorption capability are shown in Fig. 8-13 and 8-14 for rated load (R=6Ω) assuming maximum t_{3n} of 0.5. For selected t_{1n} and t_{3n}, the operating frequency can be calculated as a function of V_{pn} (Fig. 8-11). The resonant tank conductance is then determined using the calculated operating frequency (The dependence between these two parameters is shown in Fig. 8-12). Using the determined resonant tank conductance, the power absorption capability of the resonant tank is then calculated by (8-22). It is divided by the square of the dc voltage to ensure the analysis remains independent of the choice of dc voltage. Once again, a t_{1n} of about 0.04 is most desirable because here the resonant tank power absorption capability is maximized.

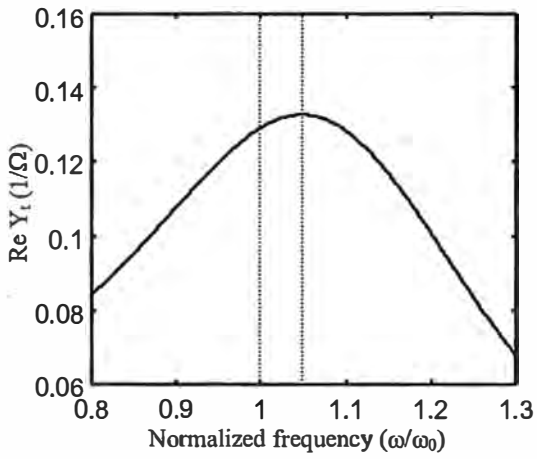

Fig. 8-12. Resonant tank conductance at rated load.

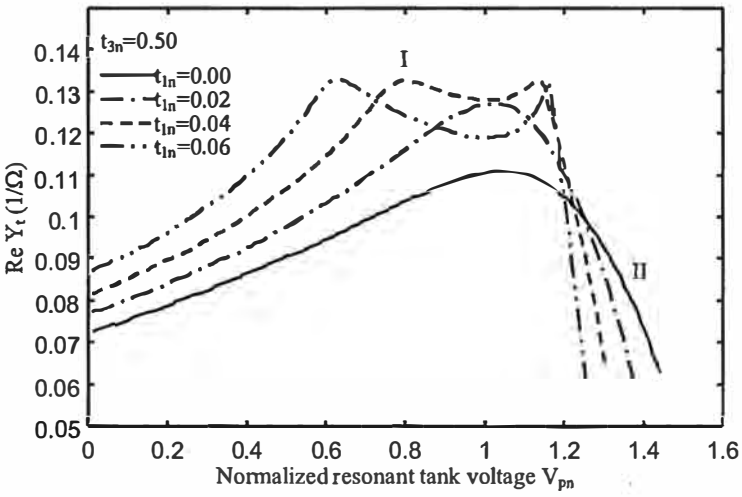

Fig. 8-13. Effects of t_{1n} on the resonant tank conductance at rated load.

InductEV, Inc.
Exhibit 1010
Page 341

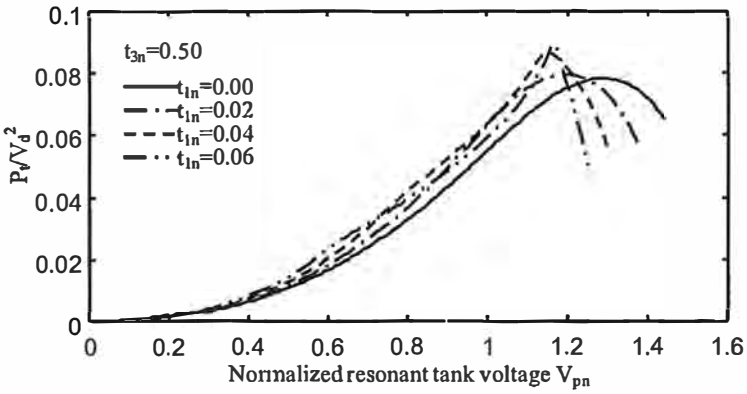

Fig. 8-14. Influences of t_{1n} on resonant tank power absorption capability at rated load.

8-5 STEADY STATE POWER FLOW ANALYSIS

The balance in power flow between the inverter and resonant tank is used in this section to develop an analytical procedure to determine suitable switching instant (t_{1n}) and series inductance (L_m) for maximum power transfer at rated load using the example discussed in section 8-4 for contact-less electric vehicle battery charging. The resulting design is then investigated under light load.

8-5.1 AN ANALYTICAL PROCEDURE FOR STEADY STATE ANALYSIS

The analytical procedure proposed for the determination of the steady state operation is shown in Fig. 8-15. This procedure is iterated in the next section for different values of t_{1n} and L_m in order to determine suitable designs for maximum power transfer.

Under steady state conditions it is assumed that the controller keeps the parameters t_{1n} and t_{3n} fixed. The steady state analysis thus starts by specifying selections of t_{1n} and t_{3n}, with t_{2n} calculated using (8-11). The phase angle then becomes a function of V_{pn} alone (as noted in section 8-3.4). The operating frequency, determined by matching the phase of the inverter current to the phase of the impedance of the resonant tank, is only a function of V_{pn} (as noted in section 8-4.2). Consequently, both the power delivery capability of the inverter (as noted in section 8-3.3) and the power absorption capability of the resonant tank (as noted in section 8-4.3) also become functions of V_{pn} allowing V_{pn} to be determined using the power flow balance between the inverter and the resonant tank. This enables the steady state operation to be identified.

8-5.2 THE SWITCHING INSTANTS AND THE SERIES INDUCTANCE

The power delivery characteristics of the inverter are very different to the power absorption characteristics of the resonant tank, and the inverter needs to be matched to the resonant tank for

InductEV, Inc.
Exhibit 1010
Page 342

efficient power transfer. This can be done by a correct choice of the series inductor L_m and a proper control of the switching instant t_{1n} assuming maximum t_{3n} of 0.5.

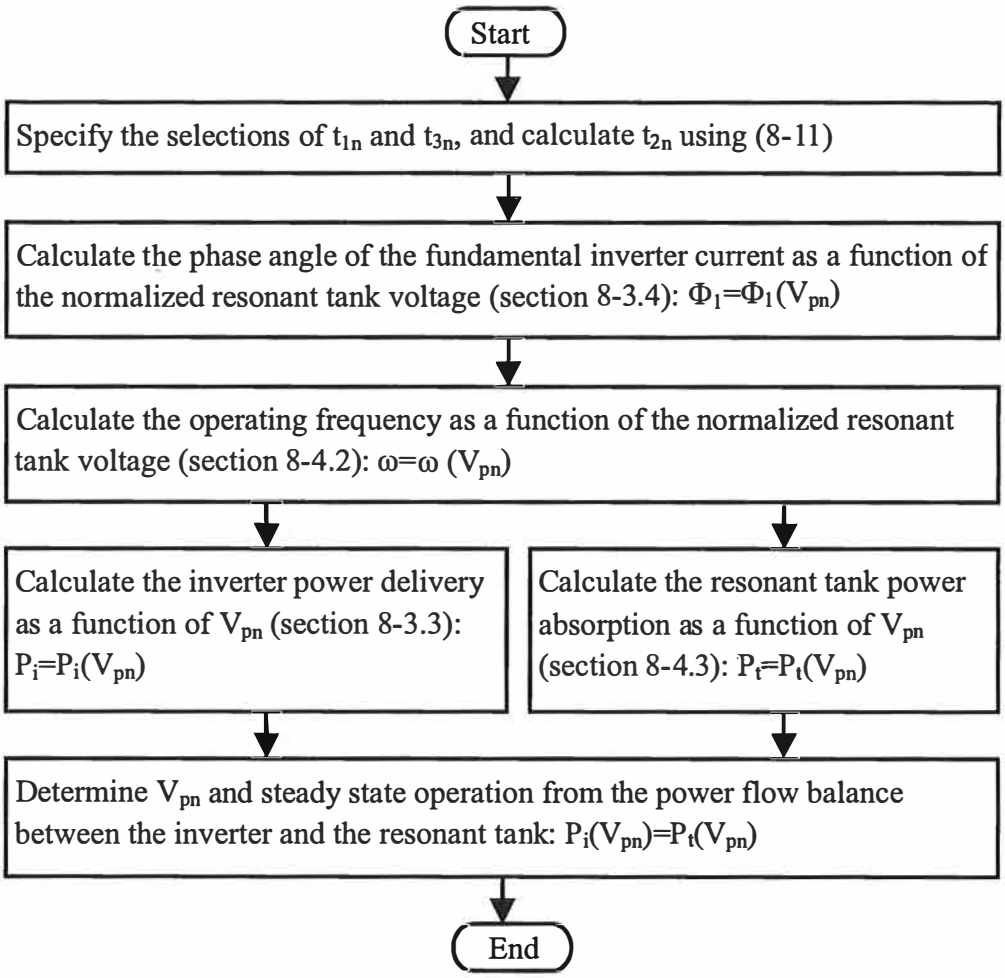

Fig. 8-15. An analytical procedure for the determination of steady state operation.

By plotting the inverter power for different values of L_m against the resonant tank power, a good choice of L_m can be made. This is shown in Fig. 8-16 (a) and (b) with t_{1n} chosen as 0.00 and 0.04 respectively. In this figure, both the inverter and resonant tank power are divided by the square of the dc voltage (V_d) enabling an analysis independent of V_d.

It can be seen that for large resonant tank voltages the inverter limits the power transfer, while for low resonant tank voltages the resonant tank limits the power transfer. A good choice for L_m is where the crossover point is at the maximum power absorption capability of the resonant tank. The effect of the series inductor L_m can be seen clearly, with the inverter power delivery increasing as L_m is made smaller. The price paid for using a smaller series inductor, however, is an increase in the inverter current, which directly increases the required VA rating of the inverter. From an inverter perspective, the largest possible value of L_m is desirable. From Fig. 8-16 it can be seen that both the inverter power delivery and the resonant tank power absorption depend on the choice of t_{1n}. Consequently, the

InductEV, Inc.
Exhibit 1010
Page 343

optimum value of L_m is also dependent on t_{1n}. With t_{1n} equal to 0.00, the optimum L_m is about 19μH. The optimum L_m decreases to about 12μH when t_{1n} is increased to 0.04.

Various maximum power points for different values of t_{1n} are compared in Table 8-1 along with the optimum series inductance L_m. In this table the dc bus voltage V_d is set at 130V in order to compare the results experimentally as discussed in section 8-6.

As t_{1n} is increased, the maximum power initially increases and the primary current reduces as the operating frequency moves closer to the secondary resonant frequency. However, the required series inductance L_m also becomes smaller as t_{1n} is increased, causing the peak inverter current i_i to increase. As t_{1n} is increased further to 0.06, very little power gain is achieved, but the inverter current increases by more than 20%. A further increase in t_{1n} results in a reduced power transfer capability but a much larger inverter current. For this application t_{1n} should be controlled close to 0.04 in order to maximize the power and minimize the primary current, while still keeping an acceptable peak inverter current level. At this condition, the optimal series inductance is 12μH.

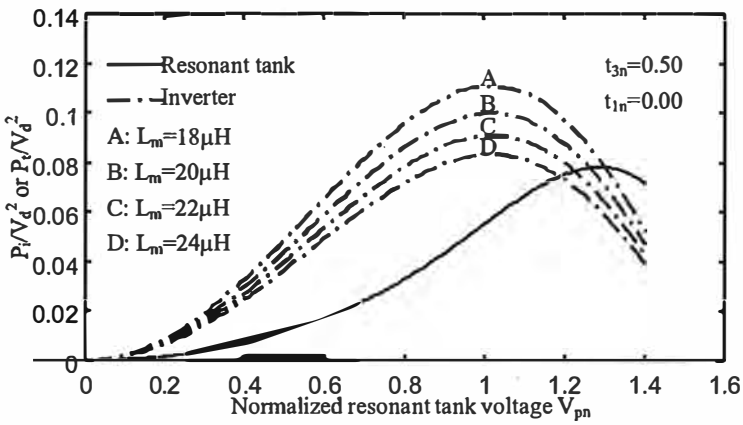

(a) t_{1n}=0.00.

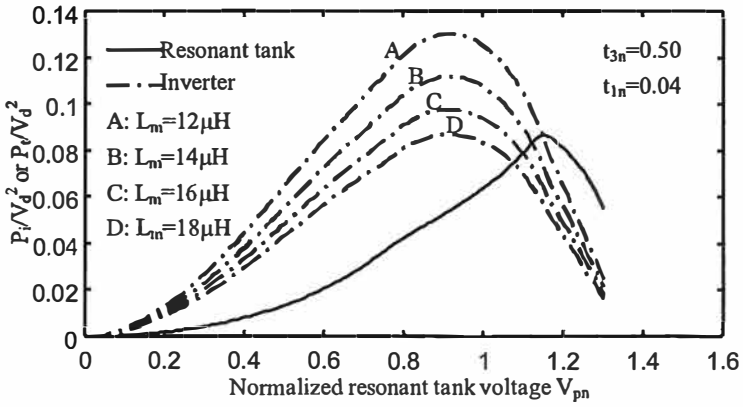

(b) t_{1n}=0.04.

Fig. 8-16. Inverter and resonant tank power flow balance at rated load.

InductEV, Inc.
Exhibit 1010
Page 344

TABLE 8-1
STEADY STATE OPERATIONS FOR MAXIMUM POWER WITH SELECTIONS OF t_{1n}

V_d	130V				
R	6Ω				
t_{3n}	0.5				
t_{1n}	0.00	0.02	0.04	0.06	0.08
L_m	19μH	16μH	12μH	6.5μH	3.2μH
$\hat{V}_p$	166.4V	154.8V	149.1V	151.3V	150.7V
P	1323W	1342W	1467W	1518W	1507W
I_p	38.5A	36.2A	34.1A	34.8A	33.9A
Peak i_i	18.8A	18.9A	21.1A	25.9A	38.5A
f	24.0kHz	23.0kHz	21.1kHz	20.9kHz	20.5kHz
Φ_1	17.7°	9.1°	3.1°	1.8°	2.1°

8-5.3 BEHAVIOUR AT LIGHT LOAD

The above analysis and design assumed operation at rated load. An identical approach can be used to investigate the behaviour of the system at other loading conditions. In this section, various steady state operations under light load are compared against rated load in Table 8-2 assuming t_{1n} and t_{3n} are controlled at the optimum values determined under rated load. The variation of the primary current at reduced load is notably small, which is a desirable characteristic for ICPT systems.

TABLE 8-2
SYSTEM BEHAVIOUR AT LIGHT LOAD

V_d	130V			
t_{1n}	0.04			
t_{3n}	0.5			
L_m	12μH			
R	6Ω	4Ω	2Ω	0Ω
$\hat{V}_p$	149.1V	158.5V	167.7V	177.1V
P	1467W	1006W	541W	0W
I_p	34.1A	34.9A	34.9A	39.5A
f	21.1kHz	22.5kHz	23.2kHz	21.7kHz

Inverter current waveforms are compared for different loading conditions in Fig. 8-17. As the load reduces, the current that needs to be turned off decreases. At loads of about 3Ω or less, zero turn-off losses can be achieved by turning off the switches while the current is flowing through the freewheeling diodes.

With decreasing load, the secondary harmonic gradually dominates the waveform of the inverter current. In order to reduce conduction losses under light load, the secondary harmonic can be minimized by reducing the duty cycle of the inverter (increasing t_{1n} and reducing t_{3n}).

InductEV, Inc.
Exhibit 1010
Page 345

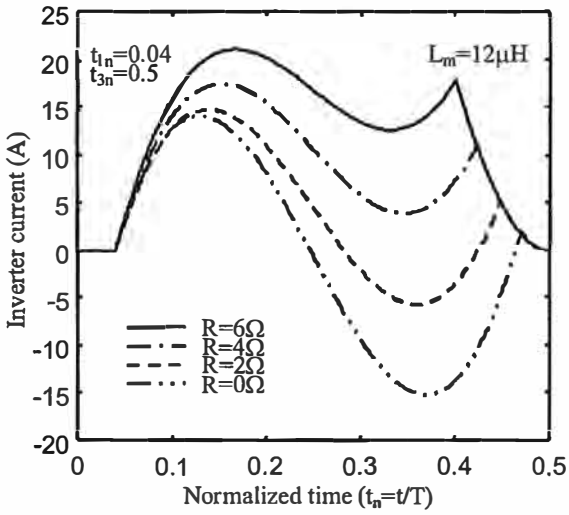

Fig. 8-17. Inverter current waveforms at light loads.

8-6 VERIFICATION

The developed theory was compared with experimental results taken on a system with the dc bus voltage V_d set at 130V. At this voltage the primary current is much lower than the rated current of 150A, and the power levels need to be scaled down correspondingly. SEMIKRON IGBT modules SKM150GB125D driven by SEMIKRON IGBT drivers SKHI22B are used in the test system. This IGBT module has low turn-off losses but high conduction losses, for the chosen example conduction losses are higher than turn-off losses. By choosing an IGBT with a lower on-state voltage, on-state losses can be traded off against switching losses.

The calculated and measured waveforms of the inverter current and the resonant tank voltage at steady state are shown in Fig. 8-18. The inverter is switched so that t_{1n} is equal to 0.04 and t_{3n} slightly less than 0.5. This ensures that the inverter current drops back to zero before the start of the next negative half cycle. The series inductor of 15μH is slightly larger than the optimal theoretical value of 12μH.

As shown, the form of the measured waveforms is well predicted. The magnitude of the measured resonant tank voltage is slightly smaller but close to the theoretical value, while the magnitude of the measured inverter current is a little bit larger. The difference is mainly due to the power losses within the system. The developed theory assumes the power drawn from the source is completely transferred to the load. Practically, the power drawn from the source must be higher than the power transferred to the load, mainly because of the conduction and switching losses of the inverter as well as the copper and core losses of the electromagnetic structure.

InductEV, Inc.
Exhibit 1010
Page 346

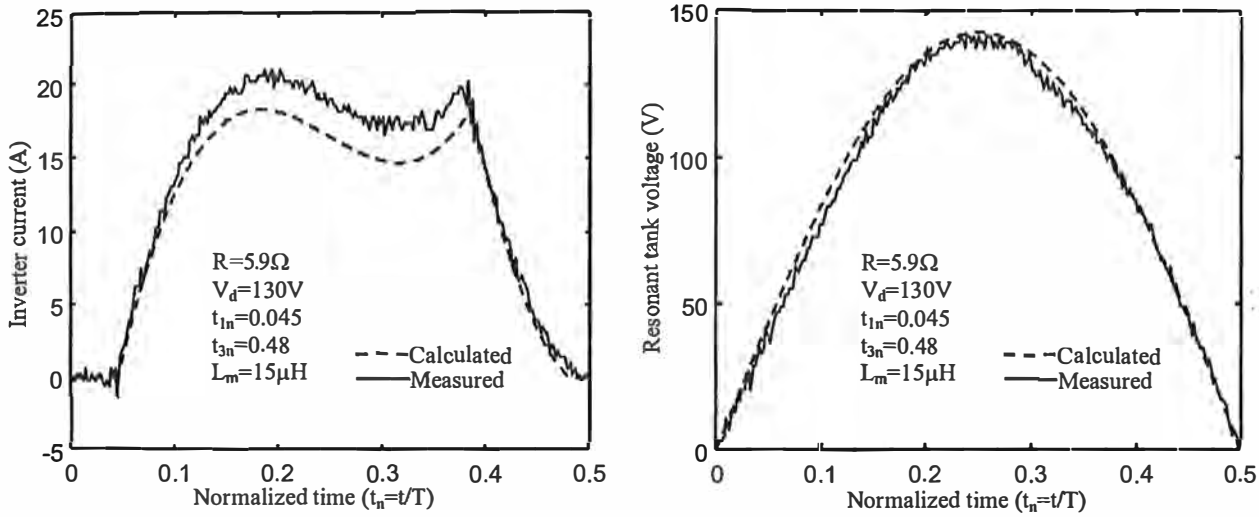

(a) Inverter current. (b) Resonant tank voltage.

Fig. 8-18. Calculated and measured steady state operation.

The measured operating frequency, primary current, and input and output powers are given in Table 8-3. These results compare well with the theoretical calculations in Table 8-1 despite the loss-less assumption of the analytical model.

TABLE 8-3
MEASURED FREQUENCY, PRIMARY CURRENT AND POWER

	Measurements	Calculations in Table 8-1
Frequency	20.9kHz	21.1kHz
Primary current	31.5A	34.1A
Input power to DC link	1485W	N/A
Output power	1275W	1467W
Efficiency	85.9%	N/A

8-7 CONCLUSIONS

In this chapter an LCL resonant inverter was investigated for ICPT applications using a variable-frequency controller operating in discontinuous current mode. This control philosophy reduces the required inverter VA rating, but results in a complex design. A feasible design approach is to derive the steady state operation using a power flow balance analysis between the inverter and the resonant tank.

The non-linear characteristics of the inverter were described using a differential equation model, while the resonant tank was modelled using the impedance model developed in Chapter 3. The theory

InductEV, Inc.
Exhibit 1010
Page 347

predicted the inverter operating point and enabled the optimum value of the series inductance and switching instants to be found. The system exhibits highly non-linear characteristics, requiring special care for controller design. The theoretical analysis and design considerations were confirmed using a contact-less electric vehicle battery charger.

REFERENCES

[1]. S. Dieckerhoff, M. J. Ruan, R. W. De Doncker, "Design of an IGBT-based LCL-resonant inverter for high-frequency induction heating," in Proc. *IEEE Industry Applications Society Annual Meeting*, vol. 3, 1999, pp. 2039-2045.

[2]. T. Bieler, M. Perrottet, V. Nguyen, and Y. Perriard, "Contactless power and information transmission," in Proc. *Industry Applications Society Annual Meeting, 2001,* vol. 1, pp. 83-88.

[3]. R. Laouamer, M. Brunello, J. P. Ferrieux, O. Normand, N. Buchheit, "A multi-resonant converter for non-contact charging with electromagnetic coupling," in Proc. *International Conference on Industrial Electronics, Control and Instrumentation*, vol. 2, 1997, pp. 792-797.

[4]. H. Abe, H. Sakamoto, and K. Harada, "A noncontact charger using a resonant converter with parallel capacitor of the secondary coil." *IEEE Transactions on Industry Applications,* vol. 36, pp 444-451, Mar./Apr. 2000.

[5]. Gyu Bum Joun, B. H. Cho, "An energy transmission system for an artificial heart using leakage inductance compensation of transcutaneous transformer," *IEEE Transactions on Power Electronics,* vol. 13, pp. 1013-1022, Nov. 1998.

[6]. J. T. Boys, G. A. Covic, A. W. Green, "Stability and control of inductively coupled power transfer systems," *IEE Proceedings-Electric Power Applications*, vol. 147, pp. 37-43, Jan. 2000.

[7]. J. G. Hayes, M. G. Egan, J. M. D. Murphy, S. E. Schulz, J. T. Hall, "Wide-load-range resonant converter supplying the SAE J-1773 electric vehicle inductive charging interface," *IEEE Transactions on Industry Applications*, vol. 35, pp. 884-895, July-Aug. 1999.

[8]. A. P. Hu, *Selected resonant converters for IPT power supplies*, PhD thesis, The Electrical and Electronics Engineering Department, The University of Auckland, Auckland, New Zealand, 2001, pp. 151-167.

InductEV, Inc.
Exhibit 1010
Page 348

InductEV, Inc.
Exhibit 1010
Page 349

CHAPTER 9

CONCLUSIONS AND FUTURE WORK

9-1 Conclusions
9-2 Future work

9-1 CONCLUSIONS

This thesis investigated the interactions between the primary power supply and the secondary pickups of ICPT systems. The influences of these interactions on the power transfer capability, the DPF, and the operating frequency were quantified for both variable and fixed frequency systems in terms of four fundamental design parameters: the normalized frequency ($u=\omega/\omega_0$), the primary and secondary quality factors (Q_p and Q_s), and the magnetic coupling coefficient (k).

The effect of the secondary loading on the primary was shown to increase with increasing k or Q_s, and is also highly sensitive to u. Notably, k, Q_p and Q_s were shown to be inter-related. Q_p decreases with increases in k or Q_s. When $Q_p >> Q_s$, the loading effects of the secondary on the primary are negligible, and the primary and secondary resonant designs can be considered independently. When Q_p is close to Q_s, the secondary loading significantly affects the primary resonance, and needs to be considered carefully to ensure power transfer capability and system stability.

Several new primary tuning schemes were proposed to improve the DPF of the power supply and the power transfer capability of the pickup by considering the interactions between the primary and secondary. These schemes enable the design of ICPT systems with smaller size, less weight, lower cost, greater power and better efficiency. The theory was verified using a contact-less electric vehicle battery charging system driven from an LCL resonant inverter operating under discontinuous current mode.

9-1.1 VARIABLE-FREQUENCY SYSTEMS

As discussed in Chapter 4 and 5, variable-frequency systems allow the operating frequency to vary so that the power supply operates with unity DPF. The amount of frequency variation depends on the loading effect of the secondary on the primary. Frequency variation is negligible in loosely coupled systems as the secondary loading effects are small. Here, with the primary and secondary resonant

InductEV, Inc.
Exhibit 1010
Page 350

circuits designed independently, the pickup can operate close to the designed frequency ensuring maximum power transfer. In well-coupled systems, where the secondary loading effects are more significant, it was found that this design approach also works well, providing that both the primary and secondary are series-compensated (the SS topology). However, when either the primary or the secondary is parallel compensated (the SP, PP and PS topologies), the operating frequency shifts significantly away from the pickup tuned frequency due to secondary loading effects. As a result, the pickup power transfer capability is substantially reduced.

In Chapter 5, a modified primary tuning scheme was proposed to minimize pickup frequency detuning effects for variable frequency systems in order to improve their power transfer capability. The primary compensation capacitance (C_p) is selected to compensate not only the primary self-inductance but also the reflected impedance (the loading effect) of the pickup. The necessary C_p was shown to depend on the choice of the compensation topology. With a parallel-compensated primary (the PP and PS topologies), the necessary change in C_p depends on Q_s. Consequently, here C_p was chosen for rated power, and while pickup frequency detuning effects under light load are unavoidable, rated power delivery is not affected.

Design criteria were also developed to ensure bifurcation could be avoided. These bifurcation criteria were found to be topology dependent, and can either be expressed in terms of Q_p and Q_s, or k and Q_s. With a high Q_s, the bifurcation criteria of all four topologies can be simply stated as $Q_p>Q_s$. When considered in terms of k, the maximum allowable Q_s before bifurcation decreases as k increases. For loosely coupled systems with a k of 0.1, the maximum allowable Q_s is about 10 in all four topologies. For well-coupled systems with a k of 0.6, the maximum allowable Q_s varies slightly between the topologies but is typically less than 2.

In Chapter 7, the sensitivity of the power transfer capability and the operating frequency to variations in the resonant parameters (C_p, C_s, L_p, L_s and M) were compared for both loosely coupled and well-coupled systems designed using both the original and modified tuning schemes. It was found that the original and modified tunings have similar sensitivities.

In Chapter 8, an LCL resonant inverter under discontinuous current mode was investigated. The modified tuning scheme proposed in chapter 5 was used in the system design. The selected control philosophy was shown to reduce the required VA rating of the power supply as well as turn-on losses, but required a complex design procedure. A feasible design methodology was prescribed by deriving the steady state operation of the inverter and ICPT system using a power flow balance analysis between the inverter and the resonant tank. An impedance model was used to analyse the resonant tank, while the inverter was modelled using differential equations. This approach was verified using a contact-less electric vehicle battery charging systems.

InductEV, Inc.
Exhibit 1010
Page 351

9-1.2 FIXED-FREQUENCY SYSTEMS

If a fixed-frequency controller is used in the primary, power transfer capability of the pickup can be assured providing the primary current is controlled constant. However, the DPF of the power supply is affected by the loading effects of the secondary on the primary.

In Chapter 6, a modified tuning scheme is proposed for fixed-frequency systems that aim to achieve load independent unity DPF. With series-compensated primary systems (the SS and SP topologies), load independent unity DPF is achieved when operating at ω_0. This in turn ensures maximum power transfer capability at the pickup.

In parallel-tuned primary systems (the PP and PS topologies), unity DPF is achievable only at rated load when operating at ω_0. At light load, the DPF can be very low. Load independent unity DPF is desirable, but can only be achieved if the operating frequency is deliberately raised above ω_0. This affects the power transfer capability and the required secondary VA rating of the pickup. It was found that rated power can be achieved with this modified tuning scheme for the majority of ICPT systems, which are either loosely coupled systems with reasonable Q_s or well-coupled systems with low Q_s. Furthermore, when delivering rated power, the required secondary VA rating for the PP topology increases slightly, but for the PS topology will be smaller. This arises from the fact that a series tuned pickup transfers maximum power at a frequency above ω_0, while a parallel tuned pickup transfers maximum power at ω_0.

In Chapter 7, the sensitivity of the DPF and the power transfer capability to variations in the resonant parameters (C_p, C_s, L_p, L_s and M) were compared for both loosely coupled and well coupled systems designed using either the original tuning scheme or the modified tuning scheme detailed in Chapter 6. Overall, the original and modified tunings have comparable sensitivities. The one exception arises in the tuning scheme for load independent unity DPF. Here, the DPF at light load is less sensitive to variations in all parameters considered, but the power transfer capability is more sensitive to variations in C_s. As shown here, C_s must be chosen to have good thermal and lifetime stability.

9-2 FUTURE WORK

The work of this thesis focused on single pickup applications and assumed the load to be linear and resistive. The thesis work may be extended to analyse and design multiple pickup systems, and also to investigate non-linear phenomena.

InductEV, Inc.
Exhibit 1010
Page 352

Multiple pickup applications: In many practical ICPT systems a common power supply transfers power to more than one secondary pickup. Optimal design of such systems needs to consider the loading effects of all pickups together.

Assuming all pickups have identical design and load, the secondary load impedance (Z_s) developed in section 3-4 is the same for each pickup, and the total reflected impedance from all pickups can be derived using (3-17) as:

$$Z_r = \sum_{i=1}^{n} Z_{ri} = n\frac{\omega^2 M^2}{Z_s} \tag{9-1}$$

where n is the number of pickups.

This is equivalent to the reflected impedance of a single identical pickup with an equivalent mutual inductance of:

$$M_n = \sqrt{n}M \tag{9-2}$$

The equivalent coupling coefficient is then:

$$k_n = \sqrt{n}k \tag{9-3}$$

With the above definition of 'equivalent mutual inductance' and 'equivalent coupling coefficient', the analyses and design considerations presented in this thesis for single pickup applications are also applicable for multiple pickup systems.

In practice, the design of each pickup can be different, and the loading condition on each pickup is almost always different. In this case, the equivalent magnetic coupling model could be extended to include a stochastic model to represent the secondary loads on the primary.

Non-linear phenomena: An ICPT system essentially consists of multiple power converters (the primary power supply and various pickup regulators) with mutual interactions via electromagnetic coupling. These power converters employ both semiconductor switches and reactive components. The switches control the power flow around the circuit, while the reactive components store energy. The circuits are non-linear, time varying dynamic systems. Practical switches and reactive components also have unwanted non-linear characteristics. The control circuits often have non-linear components. ICPT systems are therefore difficult to analyse, and full of unusual phenomena.

Fundamental circuit analysis of a power converter typically results in a non-linear time-varying model in terms of state-space variables. They are generally awkward to work with, and a simplified model is often required. A conventional approach is to take an average over a switching cycle such as that applied using state-space averaging. The aim is to replace the non-linear time-varying dynamic model by a linear time-invariant one. This is easy to understand and straightforward to implement. However, all information within a cycle is lost.

InductEV, Inc.
Exhibit 1010
Page 353

Considerable effort has gone into extending the basic state-space averaging process. One such extension is generalized state-space averaging. Here, the state-space variables are described within a sliding window moving with time. The order of the model can be arbitrarily determined according to system characteristics and the required accuracy. This approach has been used to model selected ICPT power converters successfully [1][2].

An alternative approach is to use discrete non-linear modelling such as a sampled-data model [3]. Here, the state-space variables are observed discretely at specific instants of time. With this model, the non-linear phenomena can be observed using conventional non-linear dynamic theory developed by mathematicians and physicists.

Advancement in the research of the non-linear phenomenon is useful in identifying the transient behaviour of ICPT systems, and could enable a variable-frequency system to operate in the bifurcation region, and as such significantly increase the power transfer capability.

REFERENCES

[1]. A. W. Green, "Modelling a push-pull parallel resonant convertor using generalised state-space averaging," *IEE Proc. Electric Power Applications*, vol. 140, pp. 350-356, Nov. 1993.

[2]. A. P. Hu, *Selected resonant converters for IPT power supplies*, PhD thesis, The Electrical and Electronics Engineering Department, The University of Auckland, Auckland, New Zealand, 2001, pp. 151-167.

[3]. S. Banerjee, G. C. Verghese, *Nonlinear phenomenon in power electronics – bifurcation, chaos, control and applications*, IEEE Press, NJ, 2001.

InductEV, Inc.
Exhibit 1010
Page 354

InductEV, Inc.
Exhibit 1010
Page 355

APPENDICES

A. Primary voltage and current gains
B. Reactive and real powers of the pickup coil
C. Quantified secondary current
D. Normalized reflected impedance of compensated pickup
E. Quantified impedance of the primary coil
F. Normalized reactance of the primary capacitance for systems with compensated pickup
G. Normalized impedance functions for systems with uncompensated pickup
H. Primary tuning for unity DPF at ω_0
I. Primary tuning for load independent unity DPF
J. Maximum allowable alternating voltage and current in capacitors

A. PRIMARY VOLTAGE AND CURRENT GAINS

In this section, the primary voltage and current gains are quantified in terms of the primary and secondary quality factors for series and parallel-compensated primary systems.

Series-compensated primary: When the primary is series compensated, the primary current (I_p) flows through the primary capacitor (C_p) and the primary winding (L_p).

The voltage across the primary winding is:

$$V_p = Z_p I_p = (j\omega L_p + Z_r) I_p = \left(j\omega L_p + \frac{\omega^2 M^2}{Z_s} \right) I_p \tag{A-1}$$

where Z_s is given by (3-7) for series and parallel compensated secondary systems.

Substituting (2-1) into (A-1) results in:

$$V_p = j\omega L_p I_p \left(1 - \frac{jk^2 \omega L_s}{Z_s} \right) \tag{A-2}$$

At ω_0, L_s is in resonance with C_s (i.e. $\omega_0 L_s = 1/(\omega_0 C_s)$) so that:

$$\frac{\omega_0 L_s}{Z_s} = \begin{cases} \dfrac{\omega_0 L_s}{j\omega_0 L_s + \dfrac{1}{j\omega_0 C_s} + R} = Q_{s0} & \text{series secondary} \\[2ex] \dfrac{\omega_0 L_s}{j\omega_0 L_s + \dfrac{1}{j\omega_0 C_s + \dfrac{1}{R}}} = -j + Q_{s0} & \text{parallel secondary} \end{cases} \tag{A-3}$$

InductEV, Inc.
Exhibit 1010
Page 356

where Q_{s0} is the secondary quality factor at ω_0 as given by (2-23).

Substituting (A-3) into (A-2), the result is:

$$V_{p0} = \begin{cases} j\omega_0 L_p I_p \left(1 - jk^2 Q_{s0}\right) & \text{series secondary} \\ j\omega_0 L_p I_p \left(1 - k^2 - jk^2 Q_{s0}\right) & \text{parallel secondary} \end{cases} \tag{A-4}$$

Substituting the primary quality factor (Q_{p0}) at ω_0 as given in (2-29) into (A-4) results in:

$$V_{p0} = \begin{cases} j\omega_0 L_p I_p \left(\dfrac{Q_{p0} - j}{Q_{p0}}\right) & \text{series secondary} \\ j\omega_0 L_p I_p \left(\dfrac{Q_{p0} Q_{s0} - jQ_{s0}}{1 + Q_{p0} Q_{s0}}\right) & \text{parallel secondary} \end{cases} \tag{A-5}$$

The inverter output voltage can be calculated as:

$$V_i = \left(\frac{1}{j\omega C_p}\right) I_p + V_p \tag{A-6}$$

At ω_0, L_p is in resonance with C_p so that:

$$V_{i0} = \left(\frac{1}{j\omega_0 C_p}\right) I_p + V_{p0} = -j\omega_0 L_p I_p + V_{p0} \tag{A-7}$$

Substituting (A-5) into (A-7) results in:

$$V_{i0} = \begin{cases} j\omega_0 L_p I_p \left(\dfrac{-j}{Q_{p0}}\right) & \text{series secondary} \\ j\omega_0 L_p I_p \left(\dfrac{-1 - jQ_{s0}}{1 + Q_{p0} Q_{s0}}\right) & \text{parallel secondary} \end{cases} \tag{A-8}$$

The voltage gain (ratio of the voltage across the primary coil to the inverter output voltage) at ω_0 derived from (A-5) and (A-8) is:

$$V_{GAIN} = \begin{cases} \sqrt{1 + Q_{p0}^2} & \text{series secondary} \\ \sqrt{\dfrac{Q_{s0}^2 \left(1 + Q_{p0}^2\right)}{1 + Q_{s0}^2}} & \text{parallel secondary} \end{cases} \tag{A-9}$$

Parallel-compensated primary: When the primary is parallel compensated, the inverter output voltage (V_i) is identical to the primary voltage (V_p).

The inverter output current can be calculated as:

$$I_i = j\omega C_p V_p + I_p \tag{A-10}$$

At ω_0, L_p is in resonance with C_p so that:

InductEV, Inc.
Exhibit 1010
Page 357

$$I_{i0} = j\omega_0 C_p V_{p0} + I_p = \frac{jV_{p0}}{\omega_0 L_p} + I_p \tag{A-11}$$

Substituting (A-5) into (A-11) results in:

$$I_{i0} = \begin{cases} I_p\left(\dfrac{j}{Q_{p0}}\right) & \text{series secondary} \\ I_p\left(\dfrac{1+jQ_{s0}}{1+Q_{p0}Q_{s0}}\right) & \text{parallel secondary} \end{cases} \tag{A-12}$$

The current gain (ratio of the current flowing through the primary coil to the inverter output current) at ω_0 derived from (A-12) is:

$$I_{GAIN} = \begin{cases} Q_{p0} & \text{series secondary} \\ \sqrt{\dfrac{(1+Q_{p0}Q_{s0})^2}{1+Q_{s0}^2}} & \text{parallel secondary} \end{cases} \tag{A-13}$$

B. REACTIVE AND REAL POWERS OF THE PICKUP COIL

The reactive and real powers associated with the pickup coil are calculated in this section for series and parallel-compensated secondary systems.

The apparent power (complex power) of the pickup coil can be calculated using the secondary voltage and current as:

$$S_s = I_s V_s \tag{B-1}$$

Series-compensated secondary: In a series-compensated pickup, the secondary voltage can be determined as:

$$V_s = I_s\left(\frac{1}{j\omega C_s} + R\right) \tag{B-2}$$

Substituting (B-2) into (B-1), the result is:

$$S_s = I_s^2\left(\frac{1}{j\omega C_s} + R\right) = I_s^2 R + \frac{I_s^2}{j\omega C_s} \tag{B-3}$$

As shown, the reactive power of the pickup coil equals the reactive power of the secondary compensation capacitor (C_s), while the real power transferred by the pickup coil equals the power going to the load (R).

Parallel-compensated secondary: In a parallel-compensated pickup, the secondary current can be

InductEV, Inc.
Exhibit 1010
Page 358

determined as:

$$I_s = V_s\left(j\omega C_s + \frac{1}{R}\right) \tag{B-4}$$

Substituting (B-4) into (B-1), the result is:

$$S_s = V_s^2\left(j\omega C_s + \frac{1}{R}\right) = \frac{V_s^2}{R} + V_s^2\left(j\omega C_s\right) \tag{B-5}$$

The reactive power of the pickup coil again equals the reactive power of the secondary compensation capacitor, while the real power transferred by the pickup coil equals the power going to the load.

C. QUANTIFIED SECONDARY CURRENT

The secondary current is quantified in this section in terms of the short circuit current (I_{sc}), the normalized frequency ($u=\omega/\omega_0$), and the secondary quality factor (Q_{s0}) at ω_0.

Substituting (3-7) into (3-31) results in:

$$\frac{I_s}{I_{sc}} = \frac{j\omega L_s}{Z_s} = \begin{cases} \dfrac{j\omega L_s}{j\omega L_s + \dfrac{1}{j\omega C_s} + R} & \text{series secondary} \\[2ex] \dfrac{j\omega L_s}{j\omega L_s + \dfrac{1}{j\omega C_s + \dfrac{1}{R}}} & \text{parallel secondary} \end{cases} \tag{C-1}$$

Substituting the normalized frequency defined by (3-29) into (C-1) results in:

$$\frac{I_s}{I_{sc}} = \begin{cases} \dfrac{ju\omega_0 L_s}{ju\omega_0 L_s + \dfrac{1}{ju\omega_0 C_s} + R} & \text{series secondary} \\[2ex] \dfrac{ju\omega_0 L_s}{ju\omega_0 L_s + \dfrac{1}{ju\omega_0 C_s + \dfrac{1}{R}}} & \text{parallel secondary} \end{cases} \tag{C-2}$$

Substituting (2-23) into (C-2) results in:

$$\frac{I_s}{I_{sc}} = \begin{cases} \dfrac{Q_{s0}^2 u^2\left(u^2-1\right) + jQ_{s0}u^3}{u^2 + Q_{s0}^2\left(u^2-1\right)^2} & \text{series secondary} \\[2ex] \dfrac{Q_{s0}^2 u^2\left(u^2-1\right) + u^2 + jQ_{s0}u}{u^2 + Q_{s0}^2\left(u^2-1\right)^2} & \text{parallel secondary} \end{cases} \tag{C-3}$$

The ratio of the secondary current to the short circuit current derived from (C-3) is:

InductEV, Inc.
Exhibit 1010
Page 359

$$\left|\frac{I_s}{I_{sc}}\right| = \begin{cases} \dfrac{\sqrt{Q_{s0}^4 u^4 \left(u^2-1\right)^2 + Q_{s0}^2 u^6}}{u^2 + Q_{s0}^2\left(u^2-1\right)^2} & \text{series secondary} \\ \dfrac{\sqrt{\left[Q_{s0}^2 u^2\left(u^2-1\right)+u^2\right]^2 + Q_{s0}^2 u^2}}{u^2 + Q_{s0}^2\left(u^2-1\right)^2} & \text{parallel secondary} \end{cases} \tag{C-4}$$

D. NORMALIZED REFLECTED IMPEDANCE OF COMPENSATED PICKUP

Dividing (3-18)&(3-19) by (3-26) results in:

$$\mathrm{Re}\,Z_{rn} = \frac{\mathrm{Re}\,Z_r}{\mathrm{Re}\,Z_{r0}} = \begin{cases} \dfrac{\omega^4 C_s^2 R^2}{\omega_0^2\left(\omega^2 C_s L_s - 1\right)^2 + \omega^2\omega_0^2 C_s^2 R^2} & \text{series secondary} \\ \dfrac{\omega^2 L_s^2}{R^2\left(\omega^2 C_s L_s - 1\right)^2 + \omega^2 L_s^2} & \text{parallel secondary} \end{cases} \tag{D-1}$$

and

$$\mathrm{Im}\,Z_{rn} = \frac{\mathrm{Im}\,Z_r}{\mathrm{Re}\,Z_{r0}} = \begin{cases} \dfrac{-\omega^3 C_s\left(\omega^2 C_s L_s - 1\right)R}{\omega_0^2\left(\omega^2 C_s L_s - 1\right)^2 + \omega^2\omega_0^2 C_s^2 R^2} & \text{series secondary} \\ \dfrac{-\omega^3\left[C_s R^2\left(\omega^2 C_s L_s - 1\right) + L_s\right]L_s^2}{R^3\left(\omega^2 C_s L_s - 1\right)^2 + \omega^2 L_s^2 R} & \text{parallel secondary} \end{cases} \tag{D-2}$$

Substituting (3-29) into (D-1)&(D-2) results in:

$$\mathrm{Re}\,Z_{rn} = \frac{\mathrm{Re}\,Z_r}{\mathrm{Re}\,Z_{r0}} = \begin{cases} \dfrac{u^4}{\left(\dfrac{u^2\omega_0 L_s}{R} - \dfrac{1}{\omega_0 C_s R}\right)^2 + u^2} & \text{series secondary} \\ \dfrac{u^2}{\left(u^2\omega_0 C_s R - \dfrac{R}{\omega_0 L_s}\right)^2 + u^2} & \text{parallel secondary} \end{cases} \tag{D-3}$$

and

$$\mathrm{Im}\,Z_{rn} = \frac{\mathrm{Im}\,Z_r}{\mathrm{Re}\,Z_{r0}} = \begin{cases} \dfrac{-u^3\left(\dfrac{u^2\omega_0 L_s}{R} - \dfrac{1}{\omega_0 C_s R}\right)}{\left(\dfrac{u^2\omega_0 L_s}{R} - \dfrac{1}{\omega_0 C_s R}\right)^2 + u^2} & \text{series secondary} \\ \dfrac{-u^3\left[u^2\left(\omega_0 C_s R\right)^2\left(\dfrac{\omega_0 L_s}{R}\right) - \omega_0 C_s R + \dfrac{\omega_0 L_s}{R}\right]}{\left(u^2\omega_0 C_s R - \dfrac{R}{\omega_0 L_s}\right)^2 + u^2} & \text{parallel secondary} \end{cases} \tag{D-4}$$

The normalized reflected resistance and reactance given in (D-3) and (D-4) can be represented as

InductEV, Inc.
Exhibit 1010
Page 360

functions of Q_{s0} and u by:

$$\mathrm{Re}Z_{rn} = \frac{\mathrm{Re}Z_r}{\mathrm{Re}Z_{r0}} = \begin{cases} \dfrac{u^4}{\left(u^2-1\right)^2 Q_{s0}^2 + u^2} & \text{series secondary} \\ \dfrac{u^2}{\left(u^2-1\right)^2 Q_{s0}^2 + u^2} & \text{parallel secondary} \end{cases} \tag{D-5}$$

and

$$\mathrm{Im}Z_{rn} = \frac{\mathrm{Im}Z_r}{\mathrm{Re}Z_{r0}} = \begin{cases} \dfrac{-u^3\left(u^2-1\right)Q_{s0}}{\left(u^2-1\right)^2 Q_{s0}^2 + u^2} & \text{series secondary} \\ \dfrac{-u^3\left[\left(u^2-1\right)Q_{s0} + \dfrac{1}{Q_{s0}}\right]}{\left(u^2-1\right)^2 Q_{s0}^2 + u^2} & \text{parallel secondary} \end{cases} \tag{D-6}$$

E. QUANTIFIED IMPEDANCE OF THE PRIMARY COIL

Substituting (C-3) into (3-41) results in:

$$\frac{Z_p}{j\omega_0 L_p} = \begin{cases} \dfrac{u\left\{u^2 + Q_s^2\left(u^2-1\right)\left[u^2\left(1-k^2\right)-1\right]\right\} - jk^2 Q_s u^4}{u^2 + Q_s^2\left(u^2-1\right)^2} & \text{series secondary} \\ \dfrac{u\left\{u^2\left(1-k^2\right) + Q_s^2\left(u^2-1\right)\left[u^2\left(1-k^2\right)-1\right]\right\} - jk^2 Q_s u^2}{u^2 + Q_s^2\left(u^2-1\right)^2} & \text{parallel secondary} \end{cases} \tag{E-1}$$

The impedance of the primary coil thus can be quantified in terms of the primary self-inductance ($\omega_0 L_p$) at ω_0 as well as u and Q_{s0} as:

$$\left|\frac{Z_p}{j\omega_0 L_p}\right| = \begin{cases} \dfrac{\sqrt{k^4 Q_s^2 u^8 + u^2\left\{u^2 + Q_s^2\left(u^2-1\right)\left[u^2\left(1-k^2\right)-1\right]\right\}^2}}{u^2 + Q_s^2\left(u^2-1\right)^2} & \text{series secondary} \\ \dfrac{\sqrt{k^4 Q_s^2 u^4 + u^2\left\{u^2\left(1-k^2\right) + Q_s^2\left(u^2-1\right)\left[u^2\left(1-k^2\right)-1\right]\right\}^2}}{u^2 + Q_s^2\left(u^2-1\right)^2} & \text{parallel secondary} \end{cases} \tag{E-2}$$

F. NORMALIZED REACTANCE OF THE PRIMARY CAPACITANCE FOR SYSTEMS WITH COMPENSATED PICKUP

The normalized reactance of the primary compensation capacitance (C_p) can be calculated using (3-26) as:

$$\frac{1}{\omega C_p(\mathrm{Re}Z_{r0})} = \begin{cases} \dfrac{R}{\omega C_p \omega_0^2 M^2} & \text{series secondary} \\ \dfrac{L_s^2}{\omega C_p M^2 R} & \text{parallel secondary} \end{cases} \tag{F-1}$$

InductEV, Inc.
Exhibit 1010
Page 361

Substituting (3-29) into (F-1) results in:

$$\frac{1}{\omega C_p(\mathrm{Re}\,Z_{r0})}=\begin{cases}\dfrac{R}{uC_p\omega_0^3M^2} & \text{series secondary}\\[2ex] \dfrac{L_s^2}{u\omega_0C_pM^2R} & \text{parallel secondary}\end{cases} \tag{F-2}$$

Substituting (2-1) into (F-2) results in:

$$\frac{1}{\omega C_p(\mathrm{Re}\,Z_{r0})}=\begin{cases}\dfrac{R}{uk^2C_p\omega_0^3L_pL_s} & \text{series secondary}\\[2ex] \dfrac{L_s}{u\omega_0k^2C_pL_pR} & \text{parallel secondary}\end{cases} \tag{F-3}$$

Substituting (2-28) into (F-3) results in:

$$\frac{1}{\omega C_p(\mathrm{Re}\,Z_{r0})}=\begin{cases}\dfrac{R}{uk^2\omega_0L_s} & \text{series secondary}\\[2ex] \dfrac{\omega_0L_s}{uk^2R} & \text{parallel secondary}\end{cases} \tag{F-4}$$

In terms of Q_{s0}, (F-4) can represented as:

$$\frac{1}{\omega C_p(\mathrm{Re}\,Z_{r0})}=\frac{1}{uk^2Q_{s0}} \tag{F-5}$$

As shown, the normalized reactance of the primary capacitance is a function of u, Q_{s0}, and k.

Substituting (2-29) into (F-5), the normalized reactance of the primary compensation capacitance becomes a function of u, Q_{p0} and Q_{s0} given by:

$$\frac{1}{\omega C_p(\mathrm{Re}\,Z_{r0})}=\begin{cases}\dfrac{Q_{p0}}{u} & \text{series secondary}\\[2ex] \left(\dfrac{1}{u}\right)\left(Q_{p0}+\dfrac{1}{Q_{s0}}\right) & \text{parallel secondary}\end{cases} \tag{F-6}$$

G. NORMALIZED IMPEDANCE FUNCTIONS FOR SYSTEMS WITH UNCOMPENSATED PICKUP

At the condition that ω_0L_s and R are equal, the secondary impedance Z_s can be expressed as:

$$Z_s=j\omega L_s+R=j\omega L_s+\omega_0L_s=L_s(\omega_0+j\omega) \tag{G-1}$$

Substituting (G-1) into (3-17), the reflected resistance and reactance can be derived as:

$$\mathrm{Re}\,Z_r=\frac{\omega_0\omega^2M^2}{(\omega_0^2+\omega^2)L_s} \tag{G-2}$$

and

InductEV, Inc.
Exhibit 1010
Page 362

$$\operatorname{Im} Z_r = \frac{-\omega^3 M^2}{\left(\omega_0^2 + \omega^2\right) L_s} \tag{G-3}$$

The reflected resistance and reactance at ω_0 are then:

$$\operatorname{Re} Z_{r0} = \frac{\omega_0 M^2}{2L_s} \tag{G-4}$$

and

$$\operatorname{Im} Z_{r0} = \frac{-\omega_0 M^2}{2L_s} \tag{G-5}$$

The normalized reflected resistance and reactance defined in (3-33) are then:

$$\operatorname{Re} Z_{rn} = \frac{\operatorname{Re} Z_r}{\operatorname{Re} Z_{r0}} = \frac{2u^2}{1+u^2} \tag{G-6}$$

and

$$\operatorname{Im} Z_{rn} = \frac{\operatorname{Im} Z_r}{\operatorname{Re} Z_{r0}} = \frac{-2u^3}{1+u^2} \tag{G-7}$$

The normalized reactance of the self-inductance (L_p) of the primary coil can be calculated as:

$$\frac{\omega L_p}{\operatorname{Re} Z_{r0}} = \frac{2\omega L_p L_s}{\omega_0 M^2} \tag{G-8}$$

Substituting (2-1)&(3-29) into (G-8), the result is:

$$\frac{\omega L_p}{\operatorname{Re} Z_{r0}} = \frac{2u}{k^2} \tag{G-9}$$

The normalized reactance of the primary compensation capacitance (C_p) can be calculated as:

$$\frac{1}{\omega C_p \left(\operatorname{Re} Z_{r0}\right)} = \frac{2L_s}{\omega \omega_0 C_p M^2} \tag{G-10}$$

Substituting (2-28) into (G-10) results in:

$$\frac{1}{\omega C_p \left(\operatorname{Re} Z_{r0}\right)} = \frac{2\omega_0 L_p L_s}{\omega M^2} \tag{G-11}$$

Substituting (2-1)&(3-29) into (G-11), the result is:

$$\frac{1}{\omega C_p \left(\operatorname{Re} Z_{r0}\right)} = \frac{2}{uk^2} \tag{G-12}$$

H. PRIMARY TUNING FOR UNITY DPF AT ω_0

In this section, the required C_p is calculated for each topology to achieve unity DPF when operating

InductEV, Inc.
Exhibit 1010
Page 363

at ω_0.

SS topology: Substituting (3-52) into (5-1) results in:

$$\omega_0 L_p - \frac{1}{\omega_0 C_p} + \operatorname{Im} Z_{r0} = 0 \tag{H-1}$$

Substituting (3-27) into (H-1) results in:

$$\omega_0 L_p - \frac{1}{\omega_0 C_p} = 0 \tag{H-2}$$

The required C_p determined from (H-2) is:

$$C_p = \frac{1}{\omega_0^2 L_p} \tag{H-3}$$

Substituting (2-22) into (H-3) results in:

$$C_p = \frac{C_s L_s}{L_p} \tag{H-4}$$

SP topology: Equation (H-1) is also valid for the SP topology. Substituting (3-27) into (H-1) results in:

$$\omega_0 L_p - \frac{1}{\omega_0 C_p} - \frac{\omega_0 M^2}{L_s} = 0 \tag{H-5}$$

The required C_p determined from (H-5) is:

$$C_p = \frac{1}{\omega_0^2 \left(L_p - \frac{M^2}{L_s} \right)} \tag{H-6}$$

Substituting (2-22) into (H-6) results in:

$$C_p = \frac{C_s L_s}{L_p - \frac{M^2}{L_s}} \tag{H-7}$$

Substituting (2-1) into (H-7) results in:

$$C_p = \left(\frac{C_s L_s}{L_p} \right) \left(\frac{1}{1 - k^2} \right) \tag{H-8}$$

PP topology: Substituting (3-52) into (5-1) results in:

$$\omega_0 C_p - \frac{\omega_0 L_p + \operatorname{Im} Z_{r0}}{(\operatorname{Re} Z_{r0})^2 + (\omega_0 L_p + \operatorname{Im} Z_{r0})^2} = 0 \tag{H-9}$$

InductEV, Inc.
Exhibit 1010
Page 364

Substituting (3-26)&(3-27) into (H-9) results in:

$$\omega_0 C_p - \frac{\omega_0 L_p - \frac{\omega_0 M^2}{L_s}}{\left(\frac{M^2 R}{L_s^2}\right)^2 + \left(\omega_0 L_p - \frac{\omega_0 M^2}{L_s}\right)^2} = 0 \tag{H-10}$$

The required C_p determined from (H-10) is:

$$C_p = \frac{L_p - \frac{M^2}{L_s}}{\left(\frac{M^2 R}{L_s^2}\right)^2 + \omega_0^2\left(L_p - \frac{M^2}{L_s}\right)^2} \tag{H-11}$$

Substituting (2-22) into (H-11) results in:

$$C_p = \frac{L_p - \frac{M^2}{L_s}}{\left(\frac{M^2 R}{L_s^2}\right)^2 + \left(\frac{1}{C_s L_s}\right)\left(L_p - \frac{M^2}{L_s}\right)^2} \tag{H-12}$$

Substituting (2-1)&(2-23) into (H-12) results in:

$$C_p = \left(\frac{C_s L_s}{L_p}\right)\left(\frac{1-k^2}{Q_{s0}^2 k^4 + \left(1-k^2\right)^2}\right) \tag{H-13}$$

PS topology: Equation (H-9) is also valid for the PS topology. Substituting (3-26)&(3-27) into (H-9) results in:

$$\omega_0 C_p - \frac{\omega_0 L_p}{\left(\frac{\omega_0^2 M^2}{R}\right)^2 + \left(\omega_0 L_p\right)^2} = 0 \tag{H-14}$$

The required C_p determined from (H-14) is:

$$C_p = \frac{L_p}{\left(\frac{\omega_0^2 M^2}{R}\right)^2 + \omega_0^2 L_p^2} \tag{H-15}$$

Substituting (2-22) into (H-15) results in:

$$C_p = \frac{L_p}{\left(\frac{M^2}{C_s L_s R}\right)^2 + \frac{L_p^2}{C_s L_s}} \tag{H-16}$$

Substituting (2-1)&(2-23) into (H-16) results in:

InductEV, Inc.
Exhibit 1010
Page 365

$$C_p = \left(\frac{C_s L_s}{L_p}\right)\left(\frac{1}{Q_{s0}^2 k^4 + 1}\right) \tag{H-17}$$

As a summary of the above analysis, the necessary primary compensation capacitance for each topology is:

$$C_p = \begin{cases} \dfrac{C_s L_s}{L_p} & \text{SS topology} \\ \dfrac{C_s L_s}{L_p}\left(\dfrac{1}{1-k^2}\right) & \text{SP topology} \\ \dfrac{C_s L_s}{L_p}\left(\dfrac{1-k^2}{Q_{s0}^2 k^4 + (1-k^2)^2}\right) & \text{PP topology} \\ \dfrac{C_s L_s}{L_p}\left(\dfrac{1}{Q_{s0}^2 k^4 + 1}\right) & \text{PS topology} \end{cases} \tag{H-18}$$

Substituting (H-18) into (F-3) results in:

$$\frac{1}{\omega C_p (\mathrm{Re}\, Z_{r0})} = \begin{cases} \dfrac{R}{uk^2 \omega_0 L_s} & \text{SS topology} \\ \left(\dfrac{\omega_0 L_s}{uk^2 R}\right)(1-k^2) & \text{SP topology} \\ \left(\dfrac{\omega_0 L_s}{uk^2 R}\right)\left(\dfrac{Q_{s0}^2 k^4 + (1-k^2)^2}{1-k^2}\right) & \text{PP topology} \\ \left(\dfrac{R}{uk^2 \omega_0 L_s}\right)(Q_{s0}^2 k^4 + 1) & \text{PS topology} \end{cases} \tag{H-19}$$

Substituting (2-23) into (H-19) results in:

$$\frac{1}{\omega C_p (\mathrm{Re}\, Z_{r0})} = \begin{cases} \dfrac{1}{uk^2 Q_{s0}} & \text{SS topology} \\ \left(\dfrac{1}{uk^2 Q_{s0}}\right)(1-k^2) & \text{SP topology} \\ \left(\dfrac{1}{uk^2 Q_{s0}}\right)\left(\dfrac{Q_{s0}^2 k^4 + (1-k^2)^2}{1-k^2}\right) & \text{PP topology} \\ \left(\dfrac{1}{uk^2 Q_{s0}}\right)(Q_{s0}^2 k^4 + 1) & \text{PS topology} \end{cases} \tag{H-20}$$

Substituting (2-29) into (H-20), the normalized reactance of the primary compensation capacitance is found to be a function of u, and Q_{p0} given by:

InductEV, Inc.
Exhibit 1010
Page 366

$$\frac{1}{\omega C_p(\mathrm{Re}\,Z_{r0})}=\begin{cases}\dfrac{Q_{p0}}{u} & \text{series primary (SS\&SP topologies)}\\[2ex] \dfrac{1+Q_{p0}^2}{uQ_{p0}} & \text{parallel primary (PP\&PS topologies)}\end{cases} \tag{H-21}$$

I. PRIMARY TUNING FOR LOAD INDEPENDENT UNITY DPF

In this section, the required C_p and operating frequency are calculated for each topology to achieve unity DPF for all loading conditions.

SS Topology: As C_p determined in (H-4) is independent of Q_{s0}, this choice enables the SS topology to achieve unity DPF for all loading conditions by operating at ω_0.

SP Topology: Since C_p determined in (H-8) is also independent of Q_{s0}, this choice similarly enables the SP topology to achieve load independent unity DPF by operating at ω_0.

PP topology: With a parallel-compensated secondary, the impedance of the primary coil given by (3-39) can be expressed in the form of admittance as:

$$\frac{1}{Z_p}=\frac{R(1-\omega^2C_sL_s)+j\omega L_s}{-\omega^2(L_pL_s-M^2)+jR\omega[L_p-\omega^2C_s(L_pL_s-M^2)]} \tag{I-1}$$

If the operating frequency is:

$$\omega=\frac{\omega_0}{\sqrt{1-k^2}} \tag{I-2}$$

it can be shown using (2-1) and (2-22) that the following equation is true:

$$L_p-\omega^2C_s(L_pL_s-M^2)=0 \tag{I-3}$$

The equation (I-3) can be rearranged to:

$$\omega^2C_s=\frac{L_p}{L_pL_s-M^2} \tag{I-4}$$

Substituting (I-3) and (I-4) into (I-1), the result is:

$$\frac{1}{Z_p}=\frac{1}{j\omega\left(L_p-\dfrac{M^2}{L_s}\right)}+\frac{M^2R}{\omega^2(L_pL_s-M^2)^2} \tag{I-5}$$

Substituting (I-5) into (3-52) results in:

InductEV, Inc.
Exhibit 1010
Page 367

$$Y_t = \frac{1}{Z_t} = j\omega C_p + \frac{1}{Z_p} = j\omega C_p + \frac{1}{j\omega\left(L_p - \frac{M^2}{L_s}\right)} + \frac{M^2 R}{\omega^2\left(L_p L_s - M^2\right)^2} \tag{I-6}$$

If C_p is selected to be:

$$C_p = \frac{1}{\omega^2\left(L_p - \frac{M^2}{L_s}\right)} \tag{I-7}$$

the equation (I-6) can be simplified to:

$$Y_t = \frac{M^2 R}{\omega^2\left(L_p L_s - M^2\right)^2} \tag{I-8}$$

As shown the load admittance is a conductance for all loading conditions, and as such assures load independent unity DPF.

Substituting (I-2), (2-1) and (2-22) into (I-7), the required C_p can be calculated as:

$$C_p = \frac{C_s L_s}{L_p} \tag{I-9}$$

PS Topology: With a series-compensated secondary, the impedance of the primary coil given by (3-39) can be expressed in the form of admittance as:

$$\frac{1}{Z_p} = \frac{1 - \omega^2 C_s L_s + j\omega C_s R}{-R\omega^2 L_p C_s + j\omega\left[L_p - \omega^2 C_s\left(L_p L_s - M^2\right)\right]} \tag{I-10}$$

At the operating frequency given in (I-2), (I-3) and (I-4) are valid. Substituting (I-3) and (I-4) into (I-10) results in:

$$\frac{1}{Z_p} = \frac{1}{j\omega L_p} + \frac{M^2}{L_p^2 R} \tag{I-11}$$

Substituting (I-11) into (3-52), the load admittance is calculated as:

$$Y_t = \frac{1}{Z_t} = j\omega C_p + \frac{1}{Z_p} = j\omega C_p + \frac{1}{j\omega L_p} + \frac{M^2}{L_p^2 R} \tag{I-12}$$

If C_p is selected to be:

$$C_p = \frac{1}{\omega^2 L_p} \tag{I-13}$$

the equation (I-12) can be simplified to:

$$Y_t = \frac{M^2}{L_p^2 R} \tag{I-14}$$

The load admittance again is a conductance for all loading conditions and as such assures load

InductEV, Inc.
Exhibit 1010
Page 368

independent unity DPF.

Substituting (I-2), (2-1) and (2-22) into (I-13), the required C_p can be calculated as:

$$C_p = \left(\frac{C_s L_s}{L_p}\right)\left(1-k^2\right) \tag{I-15}$$

As a summary of the above analysis, the necessary operating frequency and C_p to achieve load independent unity DPF for each topology are:

$$\omega = \begin{cases} \omega_0 & \text{series primary (SS\&SP topologies)} \\ \dfrac{\omega_0}{\sqrt{1-k^2}} & \text{parallel primary (PP\&PS topologies)} \end{cases} \tag{I-16}$$

and

$$C_p = \begin{cases} \dfrac{C_s L_s}{L_p} & \text{SS topology} \\ \dfrac{C_s L_s}{L_p}\left(\dfrac{1}{1-k^2}\right) & \text{SP topology} \\ \dfrac{C_s L_s}{L_p} & \text{PP topology} \\ \dfrac{C_s L_s}{L_p}\left(1-k^2\right) & \text{PS topology} \end{cases} \tag{I-17}$$

J. MAXIMUM ALLOWABLE ALTERNATING VOLTAGE AND CURRENT IN CAPACITORS

In this section, the maximum allowable alternating voltage and current of a capacitor characterised in Fig. 7-1 into three regions labelled as 'I', 'II' and 'III' are discussed in detail.

Region I: Below f_1, the applied alternating voltage should not exceed the rated ac voltage $V_{ac,rated}$ of the capacitor and the maximum allowable alternating current is given by:

$$I_{ac,\max} = \omega C V_{ac,\max} = 2\pi f C V_{ac,rated} \tag{J-1}$$

where C is the capacitance of the capacitor.

Region II: Between f_1 and f_2, the power loss of the capacitor should not exceed its thermal power transfer capability. The power loss in the capacitor is the product of the apparent power and the dissipation factor (tan δ), and is given by:

InductEV, Inc.
Exhibit 1010
Page 369

$$P_{loss} = V_{ac}^2 \omega C \tan\delta = V_{ac}^2 2\pi f C \tan\delta \tag{J-2}$$

The thermal power transfer of the capacitor is:

$$P_{thermal} = \alpha A \Delta T \tag{J-3}$$

where 'α' is the heat transfer coefficient, 'A' is the surface area, and 'ΔT' is the temperature gradient from the surface to the ambient.

The maximum permissible alternating voltage and current can be determined by equating (J-2) and (J-3). The results are:

$$V_{ac,\max} = \sqrt{\frac{\alpha A \Delta T_{\max}}{2\pi f C \tan\delta}} \tag{J-4}$$

and

$$I_{ac,\max} = \omega C V_{ac,\max} = \sqrt{\frac{2\pi f C \alpha A \Delta T_{\max}}{\tan\delta}} \tag{J-5}$$

In this frequency range, the dissipation factor (tan δ) typically increases at a rate less than the frequency. As a result, the maximum allowable alternating voltage decreases with increasing frequency, while the maximum allowable alternating current increases.

At f_1, the maximum permissible alternating voltage ($V_{ac,\max}$) calculated using (J-4) equals the rated ac voltage $V_{ac,rated}$. The frequency f_1 thus can be determined as:

$$f_1 = \frac{\alpha A \Delta T_{\max}}{V_{ac,rated}^2 2\pi C \tan\delta} \tag{J-6}$$

Region III: Above f_2, the applied alternating current should not exceed the rated ac current $I_{ac,rated}$ of the capacitor, and the maximum permissible alternating voltage is given by:

$$V_{ac,\max} = \frac{I_{ac,rated}}{\omega C} = \frac{I_{ac,rated}}{2\pi f C} \tag{J-7}$$

At f_2, the maximum permissible alternating current ($I_{ac,\max}$) calculated using (J-5) equals the rated ac current $I_{ac,rated}$. The frequency f_2 thus can be determined as:

$$f_2 = \frac{I_{ac,rated}^2 \tan\delta}{2\pi C \alpha A \Delta T_{\max}} \tag{J-8}$$

InductEV, Inc.
Exhibit 1010
Page 370

APPENDIX A

Ingrid Hsieh-Yee

Professor Emerita
Dept. of Library and Information Science
Catholic University of America
Washington, D.C. 20064
E-mail: hsiehyee@cua.edu

Education

Ph.D. 1990. Library and Information Studies, University of Wisconsin-Madison
Minors: Sociology and Psychology

M.A. 1984. Library and Information Studies, University of Wisconsin-Madison.

M.A. 1983. Comparative Literature, University of Wisconsin-Madison.

B.A. 1980. Foreign Languages and Literature, National Taiwan University.

Work Experience

Professor, School/Dept. of Library and Information Science, Catholic University of America, 1990-2022 (Assistant Professor, 1990-1996; Associate Professor, 1997-2004; Professor 2004-2022; Professor Emerita 2022)

Co-Chair, Dept. of Library and Information Science, Catholic University of America, June 2015-August 2016.

Acting Dean, School of Library and Information Science, Catholic University of America, January 2010-June 2012.

Cataloger, Dept. of Legislative Reference Library, Annapolis, Maryland, 1989-1990.

Lecturer, School of Library and Information Studies, University of Wisconsin-Madison, 1988.

Teaching Assistant, School of Library and Information Studies, University of Wisconsin-Madison, 1986-1988.

Cataloger, Health Sciences Library, University of Wisconsin-Madison, 1984-1986.

Areas of Teaching and Research Interests

Information Organization and Access; Metadata; Cataloging & Classification; Information Architecture; Information Retrieval; Digital Collections; Social Media; Scholarly

Communication; Information Behavior; Health Informatics; Human Computer Interaction; Usability Studies

Grants & Honors

Cultural Heritage Information Management Project. IMLS grant. Amount: $498,741. Period: Aug. 2012 to July 2015. Co-PI with Dr. Youngok Choi.

D.C. Health Information Technology (HIT4): Building Capacity & Providing Access in Our Nation's Capital. Dept. of Labor H2B Training Grant. Grant amount: $4,175,500. Grant period: Nov. 2011 to Dec. 2015. Partner with the Metropolitan School of Professional Studies of the Catholic University of America, Children's National Medical Center, D.C. Department of Employment Services, Holy Cross Hospital, Howard University, Center for Urban Progress, Providence Hospital, and Sibley Memorial Hospital.

Capital Health Careers Project. Department of Labor Healthcare Sector and Other High Growth and Emerging Industries Grant. Grant amount: $4,953,999. Grant period: March 2010 – February 2013. Awarded to a group of healthcare organizations and educational institutions in Washington, D.C. Providence Health Foundation of Providence Hospital (Lead institution). Part of the grant supported the development of a Master's degree program in Information Technology with a concentration in Health Information Technology offered by the School of Library and Information Science.

The Washington D.C. School Librarians Project. IMLS grant. Grant amount: $412,660. Grant period: Aug. 2007 – June 2011. The School partnered with the District of Columbia Public Schools (DCPS) and the District of Columbia Library Association to educate and mentor school media specialists for the DCPS system. PI, Jan. 2010 to June 2011.

SIG Member of the Year, American Society for Information Science and Technology (2009).

Most Outstanding Paper of *OCLC Systems & Services* (2001).

ALISE Research Grant (2001).

Most Outstanding Paper of *OCLC Systems & Services* (2000).

Research Grant from ERIC (1999-2000).

Best Research Paper Award; Association for Library and Information Science Education (1998).

Research Grants, Catholic University of America. 1991, 1992, 1993, 1996, 1998, 1999, 2004, 2005, 2006, 2007, 2013-14.

Cooperative Faculty Research Grant, Consortium of Universities in the Washington Metropolitan Area (1993-1994).

Cooperative Research Grant, Council on Library Resources (1993-1994).

Journal of the American Society for Information Science Best Paper Award (1993).

ASIS/ISI Information Science Doctoral Dissertation Scholarship (1989).

HEA Title IIB Fellowship (Dept. of Education) (1989)

Chinese-American Librarians Association Scholarship (1987).

Beta Phi Mu (1985).

Vilas Fellowship, University of Wisconsin-Madison. 1984

Publications

Hsieh-Yee, I. (2021). Can We Trust Social Media? *Internet Reference Services Quarterly*, 1-15. Published online: 28 July, 2021. 10.1080/10875301.2021.1947433.

Bailey, T., & Hsieh-Yee, I. (2020). Combating the Sharing of False Information: History, Framework & Literacy Strategies, *Internet Reference Services Quarterly*, 24 (1-2), 9-30.

Choi, Y., and Hsieh-Yee, I. (2010). Finding Images in an OPAC: Analysis of User Queries, Subject Headings, and Description Notes. *Canadian Journal of Information and Library Science,* 34(3): 271 – 295.

Hsieh-Yee, I. (2008). Educating Cataloging Professionals in a Changing Information Environment. *Journal of Education for Library and Information Science,* 46(2): 93-106.

Vellucci, S. L., Hsieh-Yee, I., and Moen, W.E. (2007). The Metadata Education and Research Information Commons (MERIC): A Collaborative Teaching and Research Initiative. *Education for Information,* 25(3&4): 169-178.

NISO Framework for Guidelines for Building Good Digital Collections. 3rd ed. Baltimore, MD: National Information Standards Organization, 2007. Also available online: http://www.niso.org/framework/framework3.pdf (NISO Working Group members: Priscilla Caplan (chair), Grace Agnew, Murtha Baca, Tony Gill, Carl Fleischhauer, Ingrid Hsieh-Yee, Jill Koelling, and Christie Stephenson.)

Choi, Y., Hsieh-Yee, I., and Kules, B. (2007). Retrieval Effectiveness of TOC and LCSH. *Proceedings of the Joint Conference on Digital Libraries*, pp. 233-234.

Vellucci, S., and Hsieh-Yee, I. (2007). They Didn't Teach Me That in Library School! Building

a Digital Teaching Commons to Enhance Metadata Teaching, Learning and Research. *Proceedings of the National Conference of the Association of College and Research Libraries, Baltimore, MD*, pp. 26-31.

Mitchell, Vanessa, and Ingrid Hsieh-Yee. (2007). Converting Ulrich's Subject Headings to FAST Headings: A Feasibility Study. *Cataloging & Classification Quarterly,* 45(1): 59-85.

Hsieh-Yee, I., Tang, R., and Zhang, S. (2007). User Perceptions of a Federated Search System. *IEEE Technical Committee on Digital Libraries Bulletin,* Summer 3(2) (URL = http://www.ieee-tcdl.org).

Tang, R., Hsieh-Yee, I., and Zhang, S. (2007). User Perceptions of MetaLib Combined Search: An Investigation of How Users Make Sense of Federated Searching." *Internet Reference Services Quarterly,* 12(12): 211-236.

Hsieh-Yee, I., Tang, R., and Zhang, S. (2006). User Perceptions of a Federated Search System. *Proceedings of the Joint Conference on Digital Libraries*, *June 11-15, 2006, Chapel Hill*, p. 338.

Hsieh-Yee, I. (2006). *Organizing Audiovisual and Electronic Resources for Access: A Cataloging Guide*. 2nd ed. Westport, Conn.: Libraries Unlimited.

NISO A Framework of Guidance for Building Good Digital Collections. 2nd ed. Bethesda, MD: National Information Standards Organization, 2004. Framework Advisory Group: Grace Agnew, Liz Bishoff, Priscilla Caplan (Chair), Rebecca Gunther and Ingrid Hsieh-Yee.

Hsieh-Yee, I. (2004). Cataloging and Metadata Education in North American LIS Programs. *Library Resources & Technical Services,* 48(1): 59-68.

Hsieh-Yee, I. (2004). Cataloging and Metadata Education. In Gary E. Gorman (Ed.), *International Yearbook of Library and Information Management 2003: Metadata Applications and Management*, (pp.204-234). London: Facet Publishing.

Yee, P. L., Hsieh-Yee, I., Pierce, G.R., Grome, R., and Schantz, L. (2004). Self-Evaluative Intrusive Thoughts Impede Successful Searching on the Internet. *Computers in Human Behavior,* 20(1): 85-101.

Hsieh-Yee, I. (2003). Cataloging and Metadata Education: A Proposal for Preparing Cataloging Professionals of the 21st Century. A report submitted to the ALCTS-Education Task Force in response to Action Item 5.1 of the *Bibliographic control of Web Resources: A Library of Congress Action Plan*. Approved by the Association for Library Collections and Technical Services. Web version available since April 2003 at http://lcweb.loc.gov/catdir/bibcontrol/CatalogingandMetadataEducation.pdf.

Hsieh-Yee, I. (2002). Cataloging and Metadata Education: Asserting a Central Role in Information Organization. *Cataloging & Classification Quarterly* 34(½): 203-222.

Hsieh-Yee, I., and Smith, M. (2001). The CORC Experience: Survey of Founding Libraries, Part I. *OCLC Systems & Services,* 17: 133-140. (Received "The Most Outstanding Paper of OCLC Systems & Services in 2001" award.)

Hsieh-Yee, I., and Smith, M. (2001). The CORC Experience: Survey of Founding Libraries, Part II, Automated Tools and Usage. *OCLC Systems & Services,* 17: 166-177. (Received "The Most Outstanding Paper of OCLC Systems & Services in 2001" award.)

Hsieh-Yee, I. (2001). ERIC User Services: Changes and Evaluation for the Future. *Government Information Quarterly,* 18: 31-42.

Hsieh-Yee, Ingrid. (2001). Research on Web Search Behavior. *Library and Information Science Research,* 23: 167-185.

Logan, E., and Hsieh-Yee, I. (2001). Library and Information Science Education in the Nineties. *Annual Review of Information Science and Technology,* 35: 425-477.

Hsieh-Yee, I. (Ed.) (2001). *Library and Information Science Research*, 23 (2). A special issue in honor of the retirement of Douglas L. Zweizig.

Hsieh-Yee, I. (2000). *ERIC User Services: Evaluation in a Decentralized Environment*. Washington, D.C.: Dept. of Education.

Hsieh-Yee, Ingrid. (2000). *Organizing Audiovisual and Electronic Resources for Access: A Cataloging Guide*. Littleton, CO: Libraries Unlimited.

Hsieh-Yee, I. (2000). Organizing Internet Resources: Teaching Cataloging Standards and Beyond. *OCLC Systems & Services,* 16: 130-143. (Received "The Most Outstanding Paper of OCLC Systems & Services in 2000" award.)

Hsieh-Yee, I. (1998). The Retrieval Power of Selected Search Engines: How Well Do They Address General Reference Questions and Subject Questions? *Reference Librarian,* 60: 27-47.

Hsieh-Yee, I. (1998). Search Tactics of Web Users in Searching for Texts, Graphics, Known Items and Subjects: A Search Simulation Study. *Reference Librarian,* 60: 61-85. (Received the 1997 Best ALISE Research Paper Award.)

Hsieh-Yee, I. (1997). Access to OCLC and Internet Resources: LIS Educators' Views and Teaching Practices. *RQ,* 36: 569-86.

Hsieh-Yee, I. (1997). Teaching Online and CD-ROM Resources: LIS Educators' Views and Practices. *Journal of Education for Library and Information Science,* 38: 14-34.

Hsieh-Yee, I. (1996). The Cataloging Practices of Special Libraries and Their Relationship with OCLC. *Special Libraries,* 87: 10-20.

Hsieh-Yee, I. (1996). Modifying Cataloging Practice and OCLC Infrastructure for Effective Organization of Internet Resources. In *Proceedings of the OCLC Internet Cataloging Colloquium*. [Online]. Available: http://www.oclc.org/oclc/man/colloq/hsieh.htm

Hsieh-Yee, I. (1996). Student Use of Online Catalogs and Other Information Channels. *College & Research Libraries,* 57: 161-175.

Hsieh-Yee, I. (1995). Ten entries in James S. C. Hu (Ed.), *Encyclopedia of Library & Information Science*, 913, 1028-29, 1036, 1037, 1145-46, 1514, 1575, 1763-64, 2216-27, 2378-79. Taipei, Taiwan: Sino-American Publishing. (Topics include "Advanced Technology/Libraries," "Information Ethics," "Instruction on Cataloging and Classification," "Instruction on Reference Services.")

Hsieh-Yee, I. (1993). Effects of Search Experience and Subject Knowledge on Online Search Behavior: Measuring the Search Tactics of Novice and Experienced Searchers. *Journal of the American Society for Information Science,* 44: 161-174. (Received the 1993 Best JASIS Paper Award.)

Works in Progress

Hsieh-Yee, I. Actionable lessons for debunking false information: A comparative analysis of literacy lessons in communication and library and information science

Hsieh-Yee, I. Representing diverse voices and communities in cataloging and indexing: The evolution of controlled vocabularies

Hsieh-Yee, I. Information Organization and Retrieval in Practice (a monograph scheduled for completion and publication in 2023)

Presentations

Bailey, T. & Hsieh-Yee, I. (February 2020). The Phenomena of Sharing Misinformation and the Need for Information Literacy. Presented at the 2020 Bridging the Spectrum Symposium, Washington, D.C., February 14, 2020.

Hsieh-Yee, I. and Fragan-Fly, J. (May 2018) Trends, Design & Strategies for Digital Scholarship Services. Presented at the 2018 Maryland/Delaware Library Association Conference, Cambridge, MD.

Hsieh-Yee, I. (February, 2018) Research Data Management: What It Takes to Succeed. Presented at the 10th Bridging the Spectrum Symposium, Washington, D.C.

Hsieh-Yee, I. (February, 2017) *Research Data Management: New Competencies and Opportunities for Information Professionals*. Presented at the 9th Bridging the Spectrum Symposium, Washington, D.C.

Hsieh-Yee, I. and Lawton, P. (February, 2017) *Enhancing Catholic Portal Searches with User Terms and LCSH*. Presented at the 9th Bridging the Spectrum Symposium, Washington, D.C.

Hsieh-Yee, I. (2016, October) *Visualizing Data for Information*. Presented at the 2016 Virginia Library Association Conference, Hot Springs, VA.

Hsieh-Yee, I. (2016, August) *Religious Materials Toolbox for Archivists: Solutions to Problems Facing the Profession*. Presented at Archives * Records 2016, Atlanta, GA.

Hsieh-Yee, I. and Lawton, P. (2016, March) *Enhancing Retrieval of Catholic Materials with LCSH Knowledge Structure*. Presented at the 2016 Catholic Library Association Conference, San Diego, CA.

Fagan-Fry, J. and Hsieh-Yee, I. (2016, February) *Approaches to Digital Scholarship at Top Universities around the World: Scholarly Publishing in the Digital Age.* Presented at the 8th Bridging the Spectrum Symposium, Washington, D.C.

Hsieh-Yee and Fagan-Fry, J. (2016, January) *Innovative Services for Digital Scholarship at Top 100 Research Libraries of the World*. Poster presented at the 2016 Annual Conference of the Association for Library and Information Science Education, Boston, Mass.

Hsieh-Yee, I. and Lawton, P. (2015, June). *Crowdsourcing terms for CRRA portal themes.* Poster presented at the third CRRA symposium and annual meeting, Bringing the created toward the Creator: Liturgical art and design since Vatican II. Catholic Theological Union, Chicago, Illinois.

Hsieh-Yee, I. and Lawton, P. (2015, February). *Crowdsourcing terms for thematic exploration in the Catholic Portal.* Poster presented at the 7th Annual Bridging the Spectrum Symposium, Washington, D.C.

Hsieh-Yee, I., James, R., and Fagan-Fry, J. (2015, February). *Support for digital scholarship at top university libraries of the world*. Poster presented at the 7th Annual Bridging the Spectrum Symposium, Washington, D.C.

Hsieh-Yee, I., Zhang, S., Lin, K., and Cherry, S. (2015, February). *Thus said the end users: Summon experience and support for research workflows*. Poster presented at the 7th Annual Bridging the Spectrum Symposium, Washington, D.C.

Yontz, E., Hsieh-Yee, I., & Houston, S. (2015, February). *Healthy Heroes Summer Reading Club: Developing healthy youth at public libraries.* 11th Annual Jean Mills Health Symposium, Greenville, North Carolina.

Yontz, E., Hsieh-Yee, I., and Houston, S. (2015, January). *Healthy youth and libraries: A pilot study.* Association for Library & Information Science Education (ALISE) Annual Conference, Chicago, Illinois.

Hsieh-Yee, I. (2014, May). *Linking CRRA resources to portal themes via authority files*. Presented at the Catholic Research Resources Alliance 2014 Membership Meeting, Marquette, WI.

Hsieh-Yee, I. (2014, April). *Enhancing subject access to CRRA resources*. Presented at the 2014 Catholic Library Association Conference, Pittsburgh, PA.

Hsieh-Yee, I. (2014, January). *Health Information Technology Program: Educational entrepreneurship in action*. Presented at the 2014 annual Conference of the Association for Library and Information Science Education, Philadelphia, PA

Hsieh-Yee, I., Zhang, S., Lin, K., and Cherry, S. (2014, January). *Discovering information through Summon: An analysis of user search strategies and search success*. Paper presented at the 6th Bridging the Spectrum Symposium, Washington, D.C.

Hsieh-Yee, I. (2012, December). *National Digital Stewardship Alliance and SLIS at CUA: An Educational Partnership*. Paper presented at Best Practices Exchange: Acquiring, Preserving, and Providing Access to Government Information in the Digital Era, Annapolis, MD

Choi, Y. and Hsieh-Yee, I. (2010, January). *Finding Images in an OPAC: Analysis of User Queries, Subject Headings, and Description Notes*. Paper presented at 2nd Annual Bridging the Spectrum Symposium, Catholic University of America, Washington, D.C.

Hsieh-Yee, I. and Coogan, J. (2010, January). *Google Scholar vs. Academic Search Premier: What Libraries and Searchers Need to Know*. Paper presented at 2nd Annual Bridging the Spectrum Symposium, Catholic University of America, Washington, D.C.

Hsieh-Yee, I. (2009, November). *Information Science Education: An LIS School's Perspective*. Paper presented at Annual Meeting of the American Society for Information Science and Technology, Vancouver, British Columbia, Canada.

Hsieh-Yee, I., Menard, E., Ya-Ning Chen, A., Shu-Jiun Chen, S., Kalfatovic, M. R., Wisser. K. M. (2009, November). *Information Organization in Libraries, Archives and Museums: Converging Practices and Collaboration Opportunities*. Presented at Annual Meeting of the American Society for Information Science and Technology, Vancouver, British Columbia, Canada. (Organizer and moderator of this panel.)

Hsieh-Yee, I. and Coogan, J. (2009, July). *Catching up to Google Scholar: The Retrieval Power of Academic Search Premier and Google Scholar*. Poster presented at American Library Association Conference, Chicago, Illinois.

Hsieh-Yee, I., with the CUA Scholarly Communications Project Team. (2009, January). *Digital Scholarship@CUA: Developing an Institutional Repository for CUA*. Poster presented at 1st Annual Bridging the Spectrum Symposium, Catholic University of America, Washington, D.C.

Wise, M., Cylke, K., and Hsieh-Yee, I. (2009, January). *Digital Talking Books: Meeting the Needs of the Blind and the Handicapped*. Paper presented at the Bridging the Spectrum Symposium, Catholic University of America, Washington, D.C.

Hsieh-Yee, I. (2009, January). *User Expectations of MERIC*. Presented at the Information Organization Competencies for the 21st Century Discussion Session of the 2009 Conference of the Association for Library and Information Science Education, Denver, Colorado.

Choi, Y., and Hsieh-Yee, I. (2008,November). *Subject Access for Images in an OPAC.* Annual Meeting of the American Society for Information Science and Technology, Columbus, Ohio. (Also co-organized a panel on Retrieving and Using Visual Resources: Challenges and Opportunities for Research and Education.)

Hsieh-Yee, I. (2008, June). *Educating Cataloging Professionals in a Changing Information Environment*. National Taiwan University, Taipei, Taiwan.

Vellucci, S. L., Moen, W.E., Hsieh-Yee, I., Marson, B., and Wisser, K. (2008, January) *Building a Metadata Education and Research Community through MERIC (Metadata Education and Research Information Commons): Demo and Stakeholder Input*. A panel presented at the 2008 Conference of the Association for Library and Information Science Education, Philadelphia, Pennsylvania.

Hsieh-Yee, I., Choi,Y. and Kules, B. (2007, October). *Searching for Books and Images in OPAC: Effects of LCSH, TOC and Subject Domains.* A poster presented at the American Society for Information Science and Technology Annual Meeting, Milwaukee, Wisconsin.

Hsieh-Yee, I. and Coogan, J. (2007, August) *Google Scholar vs. Academic Search Premier: A Comparative Analysis.* Presented to the Faculty and Staff of the University of the District

of Columbia.

Hsieh-Yee, I. and Coogan, J. (2007, June). *Google Scholar vs. Academic Search Premier: A Comparative Analysis*. Presented to the Washington Research Library Consortium Community, Catholic University of America, Washington, D.C.

Hsieh-Yee, I., Choi, Y., and Kules, B.. (2007, June). *What Users Need for Subject Access: Table of Contents or Subject Headings?* A poster presented at the 2007 American Library Association Annual Conference, Washington, D.C., June 2007.

Choi, Y., Hsieh-Yee, I., and Kules, B. (2007, June). *Retrieval Effectiveness of TOC and LCSH.* A paper presented at the Joint Conference on Digital Libraries 2007, Vancouver, Canada.

Vellucci, S. L., Hsieh-Yee, I., and Moen, W.E. (2007, May). *If We Build It, Will They Come? Building a Community of Practice for Metadata Stakeholders.* A poster presented at the Rutgers University Research Day, Bridgeton, New Jersey.

Hsieh-Yee, I. (2007, May). *Federated Searching: User Experience & Perceptions.* International Conference on Information Organization & Retrieval, National Taiwan University, Taipei, Taiwan.

Hsieh-Yee, I. (2007, May). *Search Performance of Google Scholar and Academic Search Premier.* International Conference on Information Organization & Retrieval, National Taiwan University, Taipei, Taiwan.

Hsieh-Yee, I. (2007, May) *MERIC: Building a Digital Commons for Metadata Education & Research.* International Conference on Information Organization & Retrieval, National Taiwan University, Taipei, Taiwan.

Hsieh-Yee, I., and Coogan, J. (2007, March/April). *A Comparative Analysis of Google Scholar and Academic Search Premier.* Poster presented at the Association of College & Research Libraries 13th National Conference, Baltimore, Maryland.

Vellucci, S. L. and Hsieh-Yee, I. (2007, March/April) *They Didn't Teach Me That in Library School! Building a Digital Teaching Commons to Enhance Metadata Teaching, Learning and Research*. On-site presentation and Webcast by Elluminate. A contributed paper presented at the Association of College & Research Libraries 13th National Conference, Baltimore, Maryland. The acceptance rate for contributed paper was 20%. This paper was one of 10 conference papers chosen for live webcast during the conference.

Moen, W., Hsieh-Yee, I. and Vellucci, S.L. (2007, January) *A DSpace Foundation for a Teaching & Research Commons: The Metadata Education and Research Information Commons.* A poster session presented at the Open Repositories Conference 2007, San Antonio, Texas.

Tang, R., Hsieh-Yee, I., and Zhang, S. (2006, November) *User Perception of MetaLib Combined Search*. Paper presented at the Annual Meeting of the American Society for Information Science and Technology, Austin, Texas, Nov. 2006.

Hsieh-Yee, I. (2006, November). *Federated Searching: User Perceptions, System Design, and Library Instructions.* Paper presented at the Annual Meeting of the American Society for Information Science and Technology, Austin, Texas. (Panel organizer, moderator, presenter).

Hsieh-Yee, I. (2006, November). *Building a Digital Teaching Commons to Enhance Teaching and Learning: The MERIC Experience and Challenges.* Paper presented at the Annual Meeting of the American Society for Information Science and Technology, Austin, Texas. (Panel organizer, moderator, presenter)

Hsieh-Yee, I. (2006, September). *Search Performance of Google Scholar and Academic Search Premier.* Paper presented at the ERIC Publishers Meeting, Washington, D.C.

Hsieh-Yee, I., Zhang, S., and Rong Tang, R. (2006, June). *User Perceptions of a Federated Search System*. Poster presented at Joint Conference on Digital Libraries, Chapel Hill, North Carolina.

Hsieh-Yee, I. and Zhang, S. (2006, June). *Preparing Users for Federated Search: Implications of a MetaLib User Perceptions Study.* Paper presented at the 2006 Ex Libris User Groups of North America Conference, Knoxville, Tennessee.

Hsieh-Yee, I. (2006, January). *MERIC Organizations and Navigation*. Paper presented at the 2006 ALISE Annual Conference, San Antonio, Texas.

Hsieh-Yee, I. (2006, January). *Metadata and Cataloging Education: Recommended Competencies.* Paper presented at the 2006 ALISE Annual Conference, San Antonio, Texas.

Hsieh-Yee, I. (2005, November). *Digital Library Evaluation: Progress & Next Steps.* Presentation at the Annual Meeting of the American Society for Information Science & Technology, Charlotte, North Carolina.

Hsieh-Yee, I. (2005, August). *Providing Access to Digital Content: Issues for DL Managers.* Presentation at MDK12 Digital Library Steering Committee Meeting, Columbia, Maryland.

Hsieh-Yee, I. (2005, April). *Enhancing Teaching and Learning: The Role of School Library Media Specialists.* Presentation at Meeting of the Baltimore County Public School System School Media Specialists, Baltimore, Maryland.

Hsieh-Yee, I. (2005, January). *Subject Access and Users: Insights & Inspirations from Marcia J. Bates.* Paper presented at the Historical Perspectives SIG, 2005 Conference of the Association for Library and Information Science Education, Boston, Massachusetts.

Hsieh-Yee, I. (2005, January). *Electronic Resource Management: Practice, Employer Expectations, & CE Interests.* Paper presented at Technical Services Education SIG, 2005 Conference of the Association for Library and Information Science Education, Boston, Massachusetts.

Hsieh-Yee, I. (2004, October). *Library Professionals for the Digital Age: Competencies & Preparation.* Paper presented at Bibliographic Access Management Team meeting, Library of Congress, Washington, D.C.

Hsieh-Yee, I. (2004, January). *Cataloging and metadata expertise for the digital era.* Presented at Preparing 21st Century Cataloging and Metadata Professionals: A Workshop for Educators and Trainers, San Diego and sponsored by ALCTS, ALISE, LC, and OCLC.

Hsieh-Yee, I. (2004, January). *Educating catalogers for the digital era.* Paper presented at the Technical Services SIG, 2004 Conference of the Association for Library and Information Science Education, San Diego.

Hsieh-Yee, I. (2003, July). *Cataloging Education for the 21st Century.* A presentation at the Library of Congress, Washington, D.C.

Hsieh-Yee, I. (2002, January) *Metadata Education and Research Priorities: A Delphi Study of Metadata Experts.* Presentation at the 2002 Conference of the Association for Library and Information Science Education, New Orleans.

Hsieh-Yee, I. (2001, November). *A Delphi Study of Metadata: Preliminary Findings.* Poster session at the 2001 Annual Meeting of the American Society for Information Science & Technology, Washington, D.C.

Hsieh-Yee, I. (2001, June). *Resources on Asian American Children: Analysis of Retrieval by Search Engines and WorldCat.* Presentation at the National Conference on Asian Pacific American Librarians, San Francisco.

Hsieh-Yee, I. (2001, January). *Delphi Study on Metadata: Project Design.* Presentation at Research Awards Session, Association for Library & Information Science Education, Washington, D.C.

Hsieh-Yee, I. (2000, May). *Web Search Behavior Research: Progress and Implications.* Presentation at the Symposium on Evaluating Library and Information Science Research, University of Wisconsin-Madison, Madison, Wisconsin.

Hsieh-Yee, I. (2000, March). *ERIC User Services: Evaluation in a Decentralized Environment.* Presentation at the National ERIC Joint Directors/Technical Meeting, Arlington, Virginia.

Hsieh-Yee, I. (2000, January). *Enhancing Learning with Web Technology.* Presentation at Faculty Conversations, Catholic University of America, Washington, D.C.

Hsieh-Yee, I. (2000, January). *From Surrogates to Objects: CUA's Approaches to Organizing Electronic Resources.* Paper presentation at the Annual Conference of the Association for Library and Information Science Education, San Antonio, Texas.

Yee, P., and Hsieh-Yee, I. (1997, November). *Individual Differences in Search Behavior on the WWW.* A poster session presented at the 38th Annual Meeting of the Psychonomic Society, Philadelphia, Pennsylvania.

Hsieh-Yee, I. (1997, April). *Research + Marketing + Preparation = Job!* Presented at the "Workshop on Resume and Interview Techniques," Special Libraries Association, Student Chapter, Catholic University of America, Washington, D.C.

Hsieh-Yee, I. (1997, February). *Creating CyberCatalogers: Education and Training.* Presentation at ALA's Midwinter Meeting, Washington, D.C.

Hsieh-Yee, I. (1997, February). *Search Tactics of Web Users in Searching for Texts, Graphics, Known Items and Subjects: A Search Simulation Study.* Presented at the Conference of the Association for Library and Information Science Education, Washington, D.C.

Hsieh-Yee, Ingrid. "Beginning Your Special Library/Information Center Career." Presented at SLA's "Career Day," Jan. 11, 1997, Catholic University of America.

Hsieh-Yee, I. (1996, September). *The Roles of Library and Information Scientists in Managing Electronic Information.* Presentation at Hamilton College, Clinton, New York.

Hsieh-Yee, I. (1996, May). *The Future of Cataloging as a Profession.* Presented at "The Cataloging Forum, Library of Congress, Washington, D.C.

Hsieh-Yee, I. (1994, October). *The Impact of the Internet on OPACs.* Presented at the Third Workshop on User Interfaces for OPACs, Library of Congress, Washington, D.C.

Reports

Hsieh-Yee, I., with Knowledge Management Competencies and Performance Action Group of the Federal Knowledge Management Initiative. "From Knowledge Management Competencies to Improved Organizational Performance." April 9, 2009.

Hsieh-Yee, I., with Knowledge Practices Action Group of the Federal Knowledge Management Initiative. "KM Practice in Government Agencies: Findings and Recommendations." April 9, 2009.

Hsieh-Yee, I. "Delphi Study on Metadata." 2001. Three quarterly reports submitted to the Association for Library and Information Science Education.

Hsieh-Yee, I. "College Students' Information Channels: Patterns of Use and Possible Factors in Channel Selection." 1995. Submitted to the Catholic University of America.

Hsieh-Yee, I. "The Information-Seeking Patterns of Scholars and Their Use of an Online Information System." 1994. Submitted to the Council on Library Resources.

Book Reviews

Review of *The Measurement and Evaluation of Library Services*, by Sharon L. Baker and F. Wilfrid Lancaster. *Information Processing and Management* 30 (1994): 450-52.

Review of *Subject Access to Films and Videos, by Sheila S. Intner and William E. Studwell; and Cataloging Unpublished Nonprint Materials*, by Verna Urbanski with Bao Chu Chang and Bernard L. Karon. *Information Processing and Management* 30 (1994): 449-50.

Review of *Automated Information Retrieval in Libraries: A Management Handbook*, by Vicki Anders. *Journal of Library and Information Science* 19 (1993): 98-100.

Review of *Full Text Databases*, by Carol Tenopir and Jung Soon Ro. *Information Processing and Management* 28 (1992): 667-68.

Review of *Descriptive Cataloging for the AACR2R And USMARC: A How-to-Do It Workbook*, by Larry Millsap and Terry Ellen Ferl. *Information Processing and Management* 28 (1992): 809-11.

Review of *MARC Manual: Understanding and Using MARC Records*, by Deborah J. Byrne. *Information Processing and Management* 28 (1992): 537-38.

Service

Professional Associations and Societies

- Library of Congress. RDA Training Program for the Profession. Co-authored with Tim Carlton. 2013-2014.
- 2014 Digital Preservation Outreach & Education Survey. Contributed to the design of the survey, 2014.
- National Digital Stewardship Alliance. Outreach Committee. 2011-2014.
- National Digital Stewardship Residency Program. Advisory Group, 2012-2013.
- FEDLINK Health Information Technology Advisory Council, 2011-2015.

- 2012 Joint Conference on Digital Libraries. Program Planning Committee, Pre-Conference Proposals Review Committee, 2012
- Catholic Research Resources Alliance. Five-Year Strategic Plan Task Force, 2011-2012
- Institute of Museum and Library Services. Grant reviewer. 2004, 2005, 2010.

- Association for Library and Information Science Education.
  * ALISE Bodan Wynar Research Paper Award Committee, 2015, 2016, 2017
  * ALISE Eugene Garfield Dissertation Award Competition, Jury, 2013, 2014
  * ALISE Research Grant Competition Committee. Chair, 2012
  * Pratt-Severn Faculty Innovation Award. Chair, 2009, 2010
  * ALISE Doctoral Poster Jury, 2012
  * "Information Organization Competencies for the 21st Century" Discussion session leader. 2009 Conference of the Association for Library and Information Science Education.
  * Assisted Technical Services SIG Convener in organizing a program, ""Building a Metadata Education and Research Community through MERIC (Metadata Education and Research Information Commons): Demo and Stakeholder Input" for the 2008 ALISE conference.
  * Association for Library Collections and Technical Services/Association for Library and Information Science Education (ALCTS/ALISE) Metadata Education and Research Information Center (MERIC) Advisory Board, Co-Chair (with Sherry Vellucci), 2005-2007. Chair, 2008-2009 (leading the effort to build MERIC, a repository and collaborative space for metadata educators, practitioners, and researchers)
  * Technical Services SIG, Convener, 2004-2005. Organized a program on "Electronic Resources Management: Current Practices, Employer Expectations, and Teaching Strategies" for the 2005 conference in Boston, Massachusetts.
  * Technical Services SIG, Convener, 2003-2004. Organized a program on "Organizing Information with Metadata: Desired Competencies and Teaching Innovations" for the 2004 conference.
  * Technical Services SIG, Convener, 1999-2000. Organized a program on "Teaching the Organization of Electronic Resources" for the 2000 conference.
  * Curriculum SIG, Co-convener (with Sibyl Moses), 1996-97. Organized a program on "Government Information Policy" for the 1997 conference.

- American Society for Information Science & Technology.
  * Reviewer, Conference program panel submissions and poster submissions, 2005, 2006, 2007, 2009, 2011, 2012, 2013, 2014, 2015, 2016, 2017
  * Nomination Committee, 2009-2011
  * Information Science Education Special Interest Group. American Society for Information Science and Technology. Chair-Elect, 2007-2008. Chair 2008-2009.
  * Committee on Information Science Education. 1999-2006.
  * Committee on Information Science Education. Organizing Committee for an orientation program for students at ASIS annual meetings, 1999-2001
  * Committee on Information Science Education. Sub-committee on Student Welfare (focusing on issues related to master's education), 1998-2001

* SIG ED. Organizing Committee for the "Seminar on Research and Career Development" for junior researchers. 1995-96 (chair), 1997-2001
* ISI Doctoral Dissertation Proposal Scholarship Jury, 1997; 2001, 2002
* Pratt-Severn Best Student Research Paper Award Jury. Chair. 1997
* 1998 Midyear Meeting (referee of contributed papers), 1997
* Organizer and moderator of the ASIS Doctoral Forum and the Doctoral Research Seminar 1994-1995
* SIG Human Computer Interaction. Chair-Elect, Chair, 1993-1995
* Doctoral Forum Award Jury, 1995
* Best Student Paper Award Jury, 1995

- American Library Association.
  * Committee on Accreditation, External Review Panelist, 2009- (site visiting team 2013-2014; site visiting team 2016-2017)
  * Association for Library Collections and Technical Services Task Force on Competencies and Education for a Career in Cataloging, member, 2008-2009
  * Facilitator for "What They Don't Teach in Library School: Competencies, Education and Employer Expectations for a Career in Cataloging," an Association for Library Collections and Technical Services Preconference, June 22, 2007 in Washington, D.C. Also a local liaison for bringing this program to the Catholic University of America.
  * Facilitator for a discussion on "Effect of Electronic Resources on Technical Services" at ALA's Midwinter Meeting held in Feb. 1997 in Washington, D.C.
  * International Relations Committee, Subcommittee Task Force for IFLA and China, 1994-1997

- Virginia Association of School Librarians. Scholarships and Awards Committee. 2010-2012

- Federal Knowledge Management Initiative, Knowledge Management Practices Action Group. Member. 2009 (leading the effort to build a knowledge management repository)
- Federal Knowledge Management Initiative, Knowledge Management Competencies & Learning Action Group. Member. 2009 (developing an action plan for helping government knowledge workers and government agencies to develop knowledge management competencies)
- National Center for Education Statistics. Technical Review Panel. 2008.
- External evaluator for a case of promotion to full professorship. University of Tennessee. 2008.
- National Information Standards Organization (NISO). Advisory Board, Revision of "IMLS Framework of Guidance for Building Good Digital Collections," 2004, 2007.
- Library of Congress, Bibliographic Control of Web Resources: A Library of Congress Action Plan. Principal Investigator of Action Item 5.1, focusing on cataloging and metadata education for students and new librarians, 2002-2003. (worked with the Association for Library Collections and Technical Services, Education Task Force)

- Chinese American Librarians Association
  * Chinese American Librarians Association Outstanding Library Leadership Award in Memory of Dr. Margaret Chang Fung, Award Committee, 2016-2017
  * Achievement Award Jury, 2000-2001
  * CALA Goal 2000 Task Force, 1997
  * Scholarship Committee, 1995, 1996-1997 (chair)
  * Board of Directors, 1994-1997
  * Publication Committee, 1993-1995
  * International Relations Committee, 1993-1996

- Sailor[SM] Assessment Advisory Group (An impact study of Sailor, Maryland's Public Information Network), 1995

- Editorial boards
  Journal of Library & Information Science. Editorial Board, 2012-
  Chinese American Librarians Association, *Occasional Papers Series*. Editorial Board, 2009-2016.
  Library Quarterly. Editorial Board, 2003-2008
  Bulletin of the Medical Library Association, 1994-97
  Newsletter editor for the Chinese American Librarians Association, 1989-92

- Referee for the following journals
  Information Processing and Management
  Journal of Digital Information
  Journal of Education for Library and Information Science
  Journal of Information Science
  Journal of Library & Information Science
  Journal of Library Metadata
  Journal of the American Society for Information Science & Technology
  Library and Information Science Research
  Library Quarterly

- Expert reviewer, "Digital Library" course, Evaluation module, University of North Carolina, Chapel Hill, 2007-2008.
- Expert reviewer, "Information Organization" course, University of Michigan, Ann Arbor. 2007.

Catholic University of America

- Academic Senate Committee on Appointments and Promotions, 2005-2008
- Academic Senate Committee on Committees and Rules, 2009-2012, 2019-2022
- Academic Senate representative (for School of Arts & Sciences), 2017-2020

- Academic Senate representative (for School of Library & Information Science) 2003-2012
- Academic Senate Library Committee, Interim Chair (2007), Member, 2008-2012
- Academic Senate Committee on Computing, 1995-2003

- President's Administrative Council, 2010-2012
- Deans' Council, 2010-2012
- Academic Leadership Group, 2010-2012
- Graduate Board, 2010-2012

- School of Arts & Sciences, Committee on Appointments and Promotions, 2015-2019
- School of Arts & Sciences, Academic Council, 2015-2016.
- School of Arts & Sciences, Ordinary Professor Group, 2013-
- Doctoral Dissertation Defense Committee, Chair, Dept. of Psychology, 2016, 2017, 2018, 2019, 2020, 2021, 2022
- Doctoral Dissertation Defense Committee, Chair, Dept. of Education, 2014, 2015, 2017, 2018, 2019
- Doctoral Dissertation Defense Committee, Chair, National Catholic School of Social Services, 2019, 2020, 2021
- Doctoral Dissertation Defense Committee, Chair, School of Nursing, 2006, 2008
- CUA Scholarly Communication Project Team, Member (2007), Chair, 2008-2009
- Dean Search Committee, 1992-1994, 1998-1999, 2002-2003, 2006-2007
- Fulbright Review Panel, 2006
- CUA Service Learning Advisory Board, 2001-2002
- CUA Faculty Conversations on Enhancing Teaching and Learning through Technology, Planning Group, 1999-2001
- CUA Initiative on Technology and Teaching, 1998-2001

Dept. of Library and Information Science

- Admissions Committee, 2007-2009, Chair 2010-2012, Member 2013-2015, Member 2018-2022
- Appointments and Promotions Committee, 1991-2022
- Student advisement, 1990-2022
- 4+1 Bachelor to Master program, Program Advisor, 2014-2022
- LIS Minor, Advisor, 2017-2022
- Curriculum Committee, 2020-21 (Member), 2021-2022 (Chair)
- Scholarship & Awards Committee, 2016-2018, 2020-21
- Comprehensive examination editor, 2020-21
- Symposium, Colloquium, Lecture Series Committee, May 2018-May 2020 (Chair)
- Symposium and Colloquium Committee, fall 2016-May 2018
- Bridging the Spectrum Symposium session moderator, 2018, 2019, 2020, 2021

- Organization of Information Core Course Outcomes Assessment, 2019, 2020
- The Information Professions in Society Core Course Outcomes Assessment, 2019, 2020
- Community Services Librarianship, Course of Study Review and Revision, 2020
- Organization of Information, Course of Study Review and Revision, 2019
- Organization of Information, Competency and Course Offerings Review, 2018-2019
- Accreditation presentation, Chair, June 2015-August 2016
- Interim Co-Chair, June 2015-August 2016.
- Blended/OWL Learning Committee, spring 2016-2018
- Technology Committee, fall 2016-2017
- Comprehensive examination editor, 2016-2017, reader (every year since 1990)
- LIS Advisory Board, 2015-2016 (chair); fall 2016- May 2018 (member)
- Committee on Planning and Assessment, 2015-2016 (chair)
- Senior Faculty Committee, 2014-2016.
- Accreditation Steering Committee, 2014-2016 (Chair, 2015-2016)
- Accreditation Students Standard Committee, co-chair, 2014-2016
- Accreditation Mission, Goals, and Objectives Standard Committee, co-chair, 2014-2016
- Accreditation Curriculum Standard, member 2014-2-16
- Accreditation Administration and Finance Standard, member 2014-2016
- Cultural Heritage Information Management Project (IMLS-funded), Co-PI, 2012-2015
- Cultural Heritage Information Management Forum (scheduled for June 2015), Co-Organizer, 2013-2015
- Health Information Technology Interim Review Committee, 2015 (chair)
- Health Sciences Librarianship Advisory Group, 2015- (chair)
- Comprehensive examination editors, 2013-2014, 2016-2017
- National Digital Stewardship Alliance liaison, 2011-2014
- Advisory Board, Chair 2010-2012
- Academic Honesty Committee, Chair, 2008-2012
- Blended Learning Committee, 2010-2012
- Colloquium Committee, 2010-2012
- Comprehensive Examination Administration, 2010-2012
- Cultural Heritage Information Management Advisory Committee, 2010-2012 (chair), 2013-
- Curriculum Committee, 1991-2003, 2007-2009, Chair 2010-2012, member 2013-
- Curriculum Subcommittee on Comprehensive Examination, Chair 2009-2012
- Health Information Technology Advisory Board, Chair 2010-2012. Member 2013-
- Health Sciences Advisory Committee, 2009, Chair 2010-2012. Member 2013-
- HIT Expert Forum, Chair 2012. Member 2013-2015
- Health Information Technology Student Group Advisor, 2011-2012
- State Council for Higher Education of Virginia, SLIS Representative, 2010-2012
- Symposium Planning Committee, 2010-2012
- Website Management Team, Chair, 2010-2012
- Urban School Librarianship Project (IMLS-Funded), PI, 2007-2011 (chair, 2010-11)

- Failing Grades Committee, 1995-1997 (chair), 2000-2001 (chair), 2004-2005 (chair), 2007 (chair)-2011
- Faculty Search Committee, 1994-1998, 2002-2004, 2006 (chair), Fall 2007-2009, Chair fall 2009-2012
- Recruitment Committee, Chair 2010-2012
- Strategic Planning Committee, Chair 2010-2012
- Technology Committee, 2010-2012
- Accreditation Advisory Committee, 2007-2009
- Accreditation Coordinating Committee, 2007-2009
- Accreditation Steering Committee, 2007-2009
- SLIS Advisory Group, 2007-2009
- Accreditation Curriculum Standard Committee, Co-chair, 2007-2009
- Accreditation Faculty Standard Committee, Co-chair, 2007-2009
- LSC 551 Information Organization Review Team, Co-chair, 2008-2009, 2015-2016.
- Curriculum Subcommittee on Portfolios, 2009
- LSC 555 Information Systems in Libraries and Information Centers Review Team, contributor, 2008-2009
- Redesign of LSC 730 Use and Users of Libraries and Information. 2009-
- Development of a metadata institute that was taught as LSC 715 Organization of Internet Resources in 2008. The institute is being revised and will be offered in 2010 under a new course title.
- Development of lesson plans, assignments, and evaluation rubrics for LSC 606, Cataloging and Classification, for the School's NCATE accreditation. 2008
- Howard and Mathilde Rovelstad Scholarship Committee, Chair, 2004-2007
- Assistant Dean Search Committee, Chair, Fall 2007
- Liaison to the Association for Library Collections and Technical Services to bring its preconference program, Cataloging Education and Employer Expectations, to CUA during the 2007 American Library Association Annual Meeting in Washington, D.C.
- Organizer of the colloquium presentation and reception for Tamar Sadeh of Ex Libris on PRIMO June 2007
- Practicum review and design (work with potential supervisors, such as the American Indian Museum internship description revision) 2006-
- Comprehensive examinations (edits, proctoring, and grading), 1990-
- SLIS Web site redesign: Comments and suggestions. Fall 2007
- Conducted surveys of current students and alumni in preparation for the 2005 re-accreditation, 2004-2005
- Technology Committee, 1992-1999 (chair, 1996-1998), 2002-2003 (member)
- Colloquia Committee 1997-1999, 2002-2003.
- Advisor of the CUA Student Chapter of the American Society for Information Science and Technology, 2002-2003
- Visiting Professor Search Committee, 1999, 2000, 2001
- Leader, Participation in the CORC experiment, 1999-2000
- Advisor of the Special Libraries Association Student Chapter, 1993-1999; the group was recognized for outstanding leadership by SLA in 1999.

- COA planning Committee, Task Force on Electronic Presentation of SLIS Reports (team leader) 1997-1998
- COA Planning Committee, Subcommittee on Technology 1996-1998
- NLM practicum coordinator, 1997-1998
- Computer Literacy Workshops: Assisted with the development and evaluation of the workshops, 1996-1998
- Leader, Participation in the InterCat project, 1995-1997

APPENDIX B

MARC 21 Reference Materials

Part VII: A Summary of Commonly Used MARC 21 Fields
Part VIII: A List of Other Fields Often Seen in MARC Records
Part IX: The Leader
Part X: Field 008 for Books

Part VII:

A Summary of Commonly Used MARC 21 Fields

This is a summary of the MARC 21 tags used most frequently by libraries in entering their own bibliographic records. For full listings of all MARC 21 tags, indicators, and subfield codes, see *MARC 21 Format for Bibliographic Data*.

In the explanations on these pages:

Tags -- The tags (3-digit numbers) are followed by the names of the fields they represent. In this summary, and in the *MARC 21 Format for Bibliographic Data*, if a tag can appear more than once in one bibliographic record, it is labeled repeatable (R). If it can only be used once, it is labeled non-repeatable (NR). For example, a catalog record can have several subjects, so the tags for subject added entries (6XX) are labeled repeatable (R).

Indicators -- The use of indicators is explained in fields where they are used. Indicators are one-digit numbers. Beginning with the 010 field, in every field -- following the tag -- are two character positions, one for Indicator 1 and one for Indicator 2. The indicators are not actually defined in all fields, however. And it is possible that a 2nd indicator will be used, while the 1st indicator remains undefined (or vice versa). When an indicator is undefined, the character position will be represented by the character # (for blank space).

Subfield codes -- All the data in each field (beginning with the 010 field) is divided into subfields, each of which is preceded by a delimiter-subfield code combination. The most common subfield codes used with each tag are shown. Each subfield code is preceded by the character $, signifying a delimiter. The name of the subfield follows the code.

In general, every field MUST have a subfield 'a' (**$a**). One exception that is often seen is in Field 020 (ISBN), when the ISBN information (subfield **$a**) is unavailable but the price (subfield **$c**) is known. Some subfields are repeatable. In this summary, repeatability is noted for only the more common repeatable subfields.

Examples: Examples follow the explanation for each field. For clarity, one space has been placed between the tag and the first indicator, one space has been placed between the second indicator and the first delimiter- subfield code, and one space has been inserted between the delimiter-subfield code and the subfield data.

010 Library of Congress Control Number -- (LCCN)
(NR, or Not Repeatable
Indicators undefined.

InductEV, Inc.
Exhibit 1010
Page 395

Subfield used most often:

$a -- Library of Congress control number

```
Example:    010 ##  $a ###86000988#
```

020 International Standard Book Number -- (ISBN)
(R, or Repeatable)

Indicators undefined.

Subfields used most often:

$a -- International Standard Book Number
$c -- Terms of availability (often a price)
$z -- Cancelled/invalid ISBN (R)

```
Example:    020 ##  $a 0877547637
```

040 Cataloging source -- (NR)

Indicators undefined.

Subfields used most often:

$a -- Original cataloging agency
$c -- Transcribing agency
$d -- Modifying agency (R)

```
Example:    040 ## $a DLC
                   $c DLC
                   $d gwhs
```

100 Main entry -- Personal name -- (primary author)
(NR; there can be only one main entry)

Indicator 1: Type of personal name entry element

0 -- Forename
1 -- Surname (this is the most common form)
3 -- Family name

Indicator 2 undefined.

Indicator 2 became obsolete in 1990. Older records may display 0 or 1

Subfields used most often:

$a -- Personal name
$b -- Numeration
$c -- Titles and other words associated with a name (R)
$q -- Fuller form of name
$d -- Dates associated with a name (generally, year of birth)

```
Example:    100 1# $a Gregory, Ruth W.
```

InductEV, Inc.
Exhibit 1010
Page 396

```
                          $q (Ruth Wilhelme),
                          $d 1910-
```

130 Main entry -- Uniform title -- (NR)

Indicator 1: Nonfiling characters

0-9 -- Number of nonfiling characters present (for initial articles, including spaces)

Indicator 2 undefined.

Indicator 2 became obsolete in 1990. (See 100 above.)

Subfields used most often:

$a -- Uniform title
$p -- Name of part/section of a work (R)
$l -- Language of a work
$s -- Version
$f -- Date of a work

```
Example:    130 0# $a Bible.
                   $p O.T.
                   $p Psalms.
```

240 Uniform title (NR)

Indicator 1: Uniform title printed or displayed

0 -- Not printed or displayed
1 -- Printed or displayed (most common)

Indicator 2: Nonfiling characters

0-9 -- Number of nonfiling characters present (for initial articles, including spaces)

Subfields used most often:

$a -- Uniform title
$l -- Language of a work
$f -- Date of a work

```
Example:    240 10 $a Ile mystérieuse.
                   $l English.
                   $f 1978
```

245 Title Statement (NR)

Indicator 1: Title added entry

(Should the title be indexed as a title added entry?)

0 -- No title added entry

(indicates a title main entry; i.e. no author is given)

1 -- Title added entry

(the proper indicator when an author given in 1XX; the most common situation)

Indicator 2: Nonfiling characters

InductEV, Inc.
Exhibit 1010
Page 397

0-9 -- Number of nonfiling characters present, including spaces; usually set at zero, except when the title begins with an article; e.g., for *The robe*, the second indicator would be set to 4. The letters *T*, *h*, *e*, and the space following them are then ignored in alphabetizing titles. The record will be automatically filed under "*r*" -- for *Robe*.

Subfields used most often:

$a -- Title proper
$h -- Medium (often used for non-book media)
$p -- Name of part/section of a work (R)
$b -- Reminder of title (subtitles, etc.)
$c -- Remainder of title page transcription/Statement of responsibility

```
Example:    245 14 $a The DNA story :
                   $b a documentary history of gene
                      cloning /
                   $c James D. Watson, John Tooze.
```

246 Varying form of title (R)

Indicator 1: Note/title added entry controller
1 -- Note, title added entry
3 -- No note, title added entry

Indicator 2: Type of title
-- No information provided
0 -- Portion of title
1 -- Parallel title
4 -- Cover title
8 -- Spine title

Subfield used most often:
$a -- Title proper

```
Example:    246 3# $a Four corners power review
```

250 Edition statement (NR)

Indicators undefined.

Subfield used most often:
$a -- Edition statement

```
Example:    250 ## $a 6th ed.
```

260 Publication, distribution, etc. (Imprint) (R)

Indicator 1: Sequence of publishing statements
-- No information provided

Indicator 2: Undefined

InductEV, Inc.
Exhibit 1010
Page 398

Subfields used most often:

$a -- Place of publication, distribution, etc. (R)
$b -- Name of publisher, distributor, etc. (R)
$c -- Date of publication, distribution, etc. (R)

```
Example:    260 ## $a New York :
                   $b Chelsea House,
                   $c 1986.
```

300 Physical description (R)

Indicators undefined.
Subfields used most often:

$a -- Extent (number of pages) (R)
$b -- Other physical details (usually illustration information)
$c -- Dimensions (cm.) (R)
$e -- Accompanying material (for example, "teacher's guide" or "manual")

```
Example:    300 ## $a 139 p. :
                   $b ill. ;
                   $c 24 cm.
```

440 Series statement / Added entry--Title

This field was made obsolete in 2008 to simplify the series statement. See 490 and 830.

490 Series statement (No added entry is traced from field) (R)

Indicator 1: Specifies whether series is traced (whether an 8XX tag is also present)

0 -- Series not traced
1 -- Series traced (8XX is in record)

Indicator 2 undefined.
Subfield used most often:

$a -- Series statement (R)
$v -- Volume number (R)

```
Example:    490 1# $a Colonial American craftsmen
```

500 General note (R)

Indicators undefined.
Subfield used most often:

$a -- General note (Used when no specialized note field has been defined for the information. Examples: Notes regarding the index; the source of the title; variations in title; descriptions of the nature, form, or scope of the item.)

InductEV, Inc.
Exhibit 1010
Page 399

```
Example:    500 ##  $a Includes index.
```

504 Bibliography, etc. note (R)

Indicators undefined.

Subfield used most often:

$a -- Bibliography, etc. note

```
Example:    504 ## $a Includes bibliographical
                      references.
```

505 Formatted contents note (R)

Indicator 1: Type of contents note

0 -- Complete contents

1 -- Incomplete contents (used with multivolume set when some volumes are not yet published)

2 -- Partial contents

Indicator 2: Level of content designation

-- Basic

Subfield used most often:

$a -- Formatted contents note

```
Example:    505 0# $a Pride and prejudice -- Emma
                      -- Northanger Abbey.
```

520 Summary, etc. note (R)

Indicator 1: Display constant controller

-- Summary

1 -- Review

2 -- Scope and content

3 -- Abstract

Indicator 2 undefined

Subfields used most often

$a -- Summary, abstract, or annotation

$b -- Expansion of summary note

```
Example:    520 ## $a This basic guide to parliamentary
                      procedure tells how to conduct
                      and participate in a meeting
                      properly.
```

600 Subject added entry -- Personal name (R)

Indicator 1: Type of personal name entry element

0 -- Forename

InductEV, Inc.
Exhibit 1010
Page 400

1 -- Surname (this is the most common form)
3 -- Family name

Indicator 2: Subject heading system/thesaurus (identifies the specific list or file which was used)

0 -- Library of Congress Subject Headings
1 -- LC subject headings for children's literature
2 -- Medical Subject Headings
3 -- National Agricultural Library subject authority file
4 -- Source not specified
5 -- Canadian Subject Headings
6 -- Répertoire de vedettes-matière
7 -- Source specified in subfield $2

(Note regarding Sears subject headings: The MARC 21 format does not provide an assigned indicator for Sears subject headings. Therefore, an indicator of 7 is used, and the MARC defined code "sears" is placed in subfield $2.)

Subfields used most often:

$a -- Personal name (surname and forename)
$b -- Numeration
$c -- Titles and other words associated with a name (R)
$q -- Fuller form of name
$d -- Dates associated with a name (generally, year of birth)
$t -- Title of a work
$v -- Form subdivision (R)
$x -- General subdivision (R)
$y -- Chronological subdivision (R)
$z -- Geographic subdivision (R)
$2 -- Source of heading or term (used with 2nd indicator of 7)

```
Example:    600 10 $a Shakespeare, William,
                   $d 1564-1616
                   $x Comedies
                   $x Stage history.
```

```
Example:    600 10 $a Shakespeare, William,
                   $d 1564-1616
                   $x Knowledge
                   $z Rome
                   $v Congresses.
```

Notice that subfields $v, $x, and $z in the 600 field are repeatable. Subfields $v, $x, $y, and $z do not have to be in alphabetical order. They will be in the order prescribed by the instructions given by the subject heading system.

610 Subject added entry -- Corporate name (R)

*Indicator 1:*Type of corporate name entry element

InductEV, Inc.
Exhibit 1010
Page 401

0 -- Inverted name (not used with AACR2)
1 -- Jurisdiction name
2 -- Name in direct order

Indicator 2: Subject heading system/thesaurus.
See indicator 2 under 600

Subfields used most often:
$a -- Corporate name or jurisdiction name as entry element
$b -- Subordinate unit (R)
$v -- Form subdivision (R)
$x -- General subdivision (R)
$y -- Chronological subdivision (R)
$z -- Geographic subdivision (R)
$2 -- Source of heading or term (used with 2nd indicator of 7)

```
Example:    610 10 $a United States.
                   $b Army Air Forces
                   $v Biography.
```

650 Subject added entry -- Topical term (Most subject headings fit here.) (R)

Indicator 1: Level of subject
-- No information provided

Indicator 2: Subject heading system/thesaurus
(identifies the specific list or file which was used)
0 -- Library of Congress Subject Headings
1 -- LC subject headings for children's literature
2 -- Medical Subject Headings
3 -- National Agricultural Library subject authority file
4 -- Source not specified
5 -- Canadian Subject Headings
6 -- Répertoire de vedettes-matière
7 -- Source specified in subfield $2

Note regarding Sears subject headings: The MARC 21 format does not provide an assigned indicator for Sears subject headings. Therefore, an indicator of 7 is used, and the MARC defined code "sears" is placed in subfield $2.)

Subfields used most often:
$a -- Topical term
$v -- Form subdivision (R)
$x -- General subdivision (R)
$y -- Chronological subdivision (R)
$z -- Geographic subdivision (R)
$2 -- Source of heading or term used with 2nd indicator of 7)

```
Example:    650 #0 $a Theater
                   $z United States
                   $v Biography
                   $v Dictionaries.
```

Notice that subfields $v, $x, and $z in the 650 field are repeatable. Subfields $v, $x, $y, and $z do not have to be in alphabetical order. They will be in the order prescribed by the instructions given by the subject heading system.

651 Subject added entry -- Geographic name (R)

Indicator 1: undefined.

Indicator 2: Subject heading system/thesaurus.

See indicator 2 under 600

Subfields used most often:

$a -- Geographic name
$v -- Form subdivision (R)
$x -- General subdivision (R)
$y -- Chronological subdivision (R)
$z -- Geographic subdivision (R)
$2 -- Source of heading or term (used with 2nd indicator of 7)

```
Example:    651 #0 $a United States
                   $x History
                   $v Chronology.
```

Notice that subfields $v, $x, and $z in the 651 field are repeatable. Subfields $v, $x, $y, and $z do not have to be in alphabetical order. They will be in the order prescribed by the instructions given by the subject heading system.

700 Added entry -- Personal name (R)

Indicator 1: Type of personal name entry element

0 -- Forename
1 -- Surname (this is the most common form)
3 -- Family name

Indicator 2: Type of added entry

-- No information provided (most common; co-authors, editors, etc.)
2 -- Analytical entry (The values for Indicator 2 changed in 1994 with Format Integration, and older records may display additional values. An analytical entry involves an author/title of an item contained in a work.)

Subfields used most often:

$a -- Personal name
$b -- Numeration
$c -- Titles and other words associated with a name (R)
$q -- Fuller form of name
$d -- Dates associated with a name (generally, year of birth)
$e -- Relator term (such as ill.) (R)
$4 -- Relator code (R)

InductEV, Inc.
Exhibit 1010
Page 403

```
Example:    700 1# $a Baldridge, Letitia.
```

710 Added entry -- Corporate name (R)

Indicator 1: Type of corporate name entry element
- 0 -- Inverted name (not used with AACR2)
- 1 -- Jurisdiction name
- 2 -- Name in direct order

Indicator 2: Type of added entry.
- See Indicator 2 under 700
- # -- No information provided
- 2 -- Analytical entry

Subfields used most often:
- **$a** -- Corporate name or jurisdiction name as entry element
- **$b** -- Subordinate unit (R)

```
Example:    710 2# $a Sunburst Communications (Firm)
```

740 Added entry -- Uncontrolled related/analytical title (R)

Indicator 1: Nonfiling characters
- 0-9 -- Number of nonfiling characters present (for initial articles, including spaces)

*Indicator 2:*Type of added entry. See Indicator 2 under 700
- # -- No information provided
- 2 -- Analytical entry
- (This field was redefined in 1994 with Format Integration. Prior to 1994, the field was also used for variant titles, such as a different wording on a spine title. In records created since Format Integration, those variant tiles appear in a 246 field.)

Subfield used most often:
- **$a** -- Title

```
Example:    740 02 $a Uncle Vanya.
```

800 Series added entry -- Personal name (R)

Indicator 1: Type of personal name entry element
- 0 -- Forename
- 1 -- Surname
- 3 -- Family name

Indicator 2 undefined.

Subfields used most often:
- **$a** -- Personal name
- **$b** -- Numeration
- **$c** -- Titles and other words associated with a name (R)
- **$q** -- Fuller form of name

InductEV, Inc.
Exhibit 1010
Page 404

$d -- Dates associated with a name (generally, year of birth)
$t -- Title of a work (the series)
$v -- Volume number

```
Example:    800 1# $a Fisher, Leonard Everett.
                   $t Colonial American craftsmen.
```

830 Series added entry -- Uniform title (R)

Indicator 1 undefined.
Indicator 2: Nonfiling characters
0-9 -- Number of nonfiling characters present (for initial articles, including spaces)
Subfield used most often:
$a -- Uniform title
$v -- Volume number

```
Example:    830 #0 $a Railroads of America (Macmillan)
```

[Back to Top of Page]

Part VIII:

A List of Other Fields Often Seen in MARC Records

001	Control number
003	Control number identifier
005	Date and time of latest transaction
006	Fixed-length data elements -- additional material characteristics
007	Physical description fixed field
008	Fixed length data elements (See Part X)
022	International Standard Serial Number (ISSN)
037	Source of acquisition
041	Language code
043	Geographic area code
050	Library of Congress call number
060	National Library of Medicine call number
082	Dewey Decimal classification number (the one recommended by the Library of Congress; locally-assigned call numbers may appear elsewhere)
110	Main entry -- Corporate name (less frequent under AACR2 rules)
256	Computer file characteristics
263	Projected publication date (indicates a CIP -- Cataloging in Publication -- record)

InductEV, Inc.
Exhibit 1010
Page 405

306 Playing time
508 Creation/production credits note
510 Citation/references note (review sources)
511 Participant or performer note
521 Target audience note (first indicator: 0 = reading grade level, 1 = interest age level, 2 = interest grade level, 3 = special audience characteristics, 4 = motivation interest level)
530 Additional physical form available note
538 System details note
586 Awards note
656 Index term -- Occupation
730 Added entry -- Uniform title
852 Location
856 Electronic location and access
9XX Reserved for local use. (They are used by vendors, systems, or individual libraries to exchange additional data)

[Back to Top of Page]

Part IX:

The Leader

There are 24 positions in the Leader, numbered from 00 to 23. For fuller explanation, see the *MARC 21 Format for Bibliographic Data*.

00-04 Record length (calculated by the computer for each record)
05 Record status
- a = increase in encoding level
- c = corrected or revised
- d = deleted
- n = new
- p = increase in encoding from prepublication (previous CIP)

06 Type of record
- a = language material
- c = printed music
- d = manuscript music
- e = cartographic material
- f = manuscript cartographic material
- g = projected medium
- i = nonmusical sound recording
- j = musical sound recording
- k = 2-dimensional nonprojectable graphic
- m = computer file
- o = kit
- p = mixed materials
- r = 3-dimensional artifact or naturally occurring object
- t = manuscript language material

07 Bibliographic level
- a = monographic component part
- b = serial component part

InductEV, Inc.
Exhibit 1010
Page 406

c = collection
d = subunit
i = integrating resource
m = monograph/item
s = serial

08 Type of control
# = no specified type
a = archival

09 Character coding scheme
# = MARC-8
a = UCS/Unicode

10 Indicator count (always "2")

11 Subfield code count (always "2")

12-16 Base address of data (calculated by the computer for each record)

17 Encoding level
# = full level
1 = full level, material not examined
2 = less-than-full level, material not examined
3 = abbreviated level
4 = core level
5 = partial (preliminary) level
7 = minimal level
8 = prepublication level (CIP)
u = unknown
z = not applicable

18 Descriptive cataloging form
# = non-ISBD
a = AACR2
i = ISBD
u = unknown

19 Multipart resource record level
# = Not specified or not applicable
a = Set
b = Part with independent title
c = Part with dependent title

20 Length of the length-of-field portion (always "4")

21 Length of the starting-character-position portion (always "5")

22 Length of the implementation-defined portion (always "0")

23 Undefined (always "0")

[Back to Top of Page]

Part X:

Field 008 for Books

Field 008 is used for Fixed Length Data Elements ("Fixed Field Codes"). There are 40 character positions in field 008, numbered from 00-39. Undefined positions must contain either a blank (#) or a fill character (|). Positions 00-17 and 35-39 are defined the same way for all media.

InductEV, Inc.
Exhibit 1010
Page 407

The information shown here for positions 18-34 applies only to books. For explanation of all the positions below and for positions 18-34 for other media, see the *MARC 21 Format for Bibliographic Data*.

Note that field 008 has no indicators or subfield codes.

00-05 Date entered on file (YYMMDD),
where Y=year, M=month, and D=day

06 Type of date/publication status:
- b = no dates given; B.C. date involved
- e = detailed date
- s = single known date/probable date
- m = multiple dates
- r = reprint/reissue date (Date 1) and original date (Date 2)
- n = dates unknown
- q = questionable date
- t = publication date and copyright date
- | = no attempt to code

07-10 Date 1/beginning date of publication

11-14 Date 2/ending date of publication

Date fields contain the year(s) of publication. The type of date(s) in these elements are specified in fixed field element 06: Type of date/publication status. (For further details, see the field 008 description in the *MARC 21 Format for Bibliographic Data*.)

15-17 Place of publication, production, or execution
For example:
- pk# = Pakistan
- cau = California (US)

(For a full list of codes used in these positions, see the *MARC Code List for Countries*.)

18-21 Illustrations (up to 4 codes):
- # = no illustrations
- a = illustrations
- b = maps
- c = portraits
- d = charts
- e = plans
- f = plates
- g = music
- h = facsimiles
- i = coats of arms
- j = genealogical tables
- k = forms
- l = samples
- m = phonodisc, phonowire, etc.
- o = photographs
- p = illuminations
- | = no attempt to code

22 Target audience:
- # = unknown or not specified
- a = preschool

b = primary
c = pre-adolescent
d = adolescent
e = adult
f = specialized
g = general
j = juvenile
| = no attempt to code

23 Form of item:
# = none of the following
a = microfilm
b = microfiche
c = microopaque
d = large print
f = braille
r = regular print reproduction
s = electronic
| = no attempt to code

24-27 Nature of contents (up to 4):
# = no specified nature of contents
a = abstracts/summaries
b = bibliographies (is one or contains one)
c = catalogs
d = dictionaries
e = encyclopedias
f = handbooks
g = legal articles
i = indexes
j = patent document
k = discographies
l = legislation
m = theses
n = surveys of literature
o = reviews
p = programmed texts
q = filmographies
r = directories
s = statistics
t = technical reports
u = standards/specifications
v = legal cases and notes
w = law reports and digests
z = treaties
| = no attempt to code

28 Government publication:
# = not a government publication
i = international intergovernmental
f = federal/national
a = autonomous or semi-autonomous component
s = state, provincial, territorial, dependent, etc.
m = multistate
c = multilocal

InductEV, Inc.
Exhibit 1010
Page 409

l = local
z = other type of government publication
o = government publication -- level undetermined
u = unknown if item is government publication
| = no attempt to code

29 Conference publication:
0 = not a conference publication
1 = conference publication
| = no attempt to code

30 Festschrift:
0 = not a festschrift
1 = festschrift
| = no attempt to code

31 Index:
0 = no index
1 = index present
| = no attempt to code

32 Undefined (since 1990) (Earlier records may contain the values 0 or 1)
= Undefined
| = no attempt to code

33 Literary form:
0 = not fiction (not further specified)
1 = fiction (not further specified)
c = comic strips
d = dramas
e = essays
f = novels
h = humor, satires, etc.
i = letters
j = short stories
m = mixed forms
p = poetry
s = speeches
u = unknown
| = no attempt to code

34 Biography:
# = no biographical material
a = autobiography
b = individual biography
c = collective biography
d = contains biographical information
| = no attempt to code

35-37 Language:
A three-letter code. For example: eng fre ger spa rus ita

(For a full list of codes used in these positions, see the *MARC Code List for Languages*.)

38 Modified record:
# = not modified
x = missing characters (because of characters unavailable in MARC character set)
s = shortened
d = "dashed-on" information omitted

InductEV, Inc.
Exhibit 1010
Page 410

r = completely romanized/printed cards in script
o = completely romanized/printed cards romanized
| = no attempt to code

39 Cataloging source:
# = national bibliographic agency
c = cooperative cataloging program
d = other sources
u = unknown
| = no attempt to code

[Back to Top of Page]

[Back to Table of Contents] -- [Continue to Part 11]

Library of Congress

Library of Congress Help Desk (10/27/2009)

InductEV, Inc.
Exhibit 1010
Page 411